UNIVERSIDAD POLITÉCNICA DE MADRID

Escuela Técnica Superior de Ingeniería Agronómica, Alimentaria y de Biosistemas

Fine-tune regulatory mechanisms required for efficient defences to herbivores

DOCTORAL THESIS

Submitted for the degree of Doctor by:

Irene Rosa Díaz

Bachelor's in Food Science and Technology

Madrid, 2023

UNIVERSIDAD POLITÉCNICA DE MADRID
Escuela Técnica Superior de Ingeniería
Agronómica, Alimentaria y de Biosistemas

Doctoral Degree in Biotechnology and Genetic Resources of Plants and Associated Microorganisms

Fine-tune regulatory mechanisms required for efficient defenses to herbivores

DOCTORAL THESIS

Submitted for the degree of Doctor by:

Irene Rosa Díaz
Bachelor's in Food Science and Technology

Under the supervision of:
Dr. Isabel Díaz Rodríguez

Madrid, 2023

Title: Fine-tune regulatory mechanisms required for efficient defences to herbivores

Author: Irene Rosa Díaz

Doctoral Programme: Biotechnology and Genetic Resources of Plants and Associated Microorganisms

Thesis Supervision:

Dr. Isabel Díaz Rodríguez, PhD in Biological Sciences by Universidad Complutense de Madrid, Profesora Catedrática en la Universidad Politécnica de Madrid

External Reviewers:

Thesis Defense Committee:

Thesis Defense Date:

This thesis has been partially supported by the Spanish Ministry grant 'AYUDAS PARA CONTRATOS PREDOCTORALES PARA LA FORMACIÓN DE DOCTORES; PRE2018-083375,' as well as from the projects BIO2017-83472-R, PID2020-115219RB-100, and PDC2021-121055-I00.

A mi madre

A Olivia

ACKNOWLEDGEMENTS

This research was carried out at the 'Centro de Biotecnología y Genómica de Plantas, CBGP-UPM-INIA/CSIC' within the Molecular Interaction Plant-Pest group. The study received invaluable financial support from the Spanish Ministry grant 'AYUDAS PARA CONTRATOS PREDOCTORALES PARA LA FORMACIÓN DE DOCTORES; PRE2018-083375,' as well as from the projects BIO2017-83472-R, PID2020-115219RB-100, and PDC2021-121055-I00. We extend our heartfelt gratitude for this support, which made our research endeavours possible."

I would like to express my gratitude to The Sainsbury Laboratory at the University of Cambridge for welcoming me during a short stage, which was made possible by the support of PRE2018-083375 and further extended thanks to a fellowship from the Gatsby Charitable Foundation awarded to Alexander Jones.

My deepest appreciation goes to my supervisor, Professor Isabel Díaz, who not only guided me throughout this journey but also leads the Molecular Interaction Plant-Pest group. Under her mentorship, I had the privilege of being part of a vibrant and intellectually stimulating environment, engaging in insightful discussions.

AGRADECIMIENTOS

Tras cinco años de montaña rusa científica cierro esta etapa; ¡¡Por fin he escrito el libro!!

En primer lugar, quiero expresar mi profundo agradecimiento a Isabel Díaz por tu inquebrantable apoyo como mi directora de tesis. Tu acogida y confianza desde el principio han significado el mundo para mí. Aprecio enormemente todas las enriquecedoras discusiones científicas que hemos tenido, así como las sesiones de psicología y motivación que, sin duda, han sido cruciales para superar los desafíos. Bromas aparte, si alguna vez decides pasar la factura, de esas sesiones de psicólogo estaré dispuesta a hipotecarme por el resto de mi vida. Ser tu última tesis es un honor, y solo espero que el cierre de este capítulo haya sido tan "bueno" como la experiencia completa a tu lado. ¡Gracias por ser una guía excepcional y una fuente constante de inspiración!

También quiero agradecer a Estrella, por la generosidad y camaradería que compartimos en el laboratorio. Extrañaré nuestras comidas, momentos de complicidad, y, por supuesto, los cotilleos y salseos que hicieron más ameno el CBGP. Me siento agradecida por haber tenido a alguien tan dedicada y amable a mi lado. Sin duda, Espero encontrarme una "Estrella" en mi próximo destino. ¡Gracias por todo!

Por supuesto no puedo olvidarme de algunas que ya no están en el 121, pero que siempre lo estarán. Queridas Ana y Gara, no puedo evitar reflexionar sobre la travesía de mi tesis y darme cuenta de que, sin ustedes, este camino habría sido imposible. Ana, tus enseñanzas y apoyo fueron mi ancla en el laboratorio 121; realmente, creo que no habría sobrevivido sin ti. Siempre recordaré con cariño tus sabios consejos y la forma en que hiciste mi aprendizaje tan significativo. Aún te echo de menos y miro tu poyata con añoranza.

A ti, Gara, mi homóloga y compañera de innumerables horas compartidas en la poyata, quiero expresarte mi profundo agradecimiento. Los miles de millones de ácaros que pusimos juntas son solo un reflejo de la inmensa colaboración y camaradería que compartimos. Tu apoyo incondicional en cada paso del camino ha sido fundamental. Me

reconforta saber que, aunque estés en otro laboratorio "dos puertas" más allá, nuestra conexión persiste. Gracias por ser parte esencial de esta etapa crucial de mi vida académica.

A Marta Boter, quiero agradecerte sinceramente por llegar en un momento tan crucial de mi vida. Tu influencia ha sido transformadora, enseñándome a relativizar la ciencia y a valorar el conocimiento por sí mismo. Desde tu llegada, has sido un apoyo invaluable, y cada día contigo ha sido inspirador y un aprendizaje. Aprecio tu manera de hacer las cosas, incluso cuando "matas gatitos". Gracias por ser una guía excepcional y por enriquecer mi viaje científico de manera inigualable.

A "los chicos de Estrella"; Alejandro, Lucía y Álvaro habéis sido siempre un apoyo incondicional siempre yan colaboradores y dispuestos. Ahora el laboratorio queda en vuestras manos ¡cuidadlo! Alejandro, echaré de menos nuestras tertulias por la tas tardes. ¡Chicos! Gracias por hacer que cada día en el laboratorio sea memorable.

A René, mi más sincero agradecimiento por ser mi fuente inagotable de consejos científicos y compañía en tantas conversaciones enriquecedoras. Tu apoyo ha sido vital en innumerables situaciones, y valoro profundamente la sabiduría que compartes. Eres vital. De hecho, creo que si te vas (aunque sea de vacaciones…) el CBGP muere.

A Bruno "huevas", mi amigo por excelencia del CBGP. Aunque ha pasado tiempo desde que te marchaste, aún siento tu ausencia. La esperanza de volver a vivir en el mismo país pronto me llena de ilusión. Gracias por ser un amigo leal y hacer que los días en el trabajo fueran más divertidos y los jueves por Lavapiés muy significativos.

A Ana Cayuela, mi amiga de PhD fuera del CBGP. Doy las gracias por las innumerables cervezas compartidas y alitas de pollo, por los momentos de desahogo con los 'estoy hasta el XX'. ¡¡Recuerdo cuando nos quejábamos de no tener artículos y ahora parece que vamos a publicar juntas!!

I would also like to express my sincere gratitude to the team at SCLU, with special thanks to Xander for his unwavering support at all times. Jim, your guidance and introduction to the fascinating world of stomata-ABA have been invaluable. Marino, thank you for

making this "short" stage possible and providing insights into the other side of CB A heartfelt thanks to the Jones lab, particularly Annaliza and Bijun. Your contributions have been invaluable. Last but not least, a special acknowledgment to Aram. I will be eternally grateful for everything you have done, helping me not just survive but thrive during that summer.

Quiero agradecer a herramientas prácticas y divertidas que han marcado mi experiencia científica. En primer lugar, a Sci-hub, por hacer que el conocimiento sea accesible para todos, incluso para quienes pertenecemos a universidades con recursos limitados.

Además, mi agradecimiento a Rosendo y su canción "Flojos de pantalón". Cada placa de RT-qPCR en esta tesis se ha empezado a cargar con esa canción, ¡Gracias!

A personas que están ajenas a la ciencia pero que sin ellas hubiera sido imposible llegar hasta aquí. Victor, que encara que ja no estem junts, has sigut una part vital de la tesis. Gràcies ¡A las chicas! Vanesa y Karem. Porque sin vosotras no habría logrado llegar "medio cuerda" a esta etapa. Muchas gracias por estar siempre. Me gustaría disfrutaros más tiempo.

Por último, a la familia que ya tengo; en especial a mi madre.

Y a la familia que vamos a formar; Marton y Olivia.

ABSTRACT

Plants face challenges from both environmental factors and herbivorous pests, leading to significant yield losses. When detecting herbivores, plants activate specific immune responses through complex transcriptional reprogramming events, orchestrated by dynamic networks responsive to various signals.

In this comprehensive investigation, we have delved into the intricate mechanisms that plants employ to defend themselves against herbivorous pests, with a particular focus on two significant culprits: the highly polyphagous mite, *Tetranychus urticae*, the main arthropod target of our investigation, and the globally dispersed *Piers brassicae* butterfly caterpillars. Our research has been cantered on the model plant *Arabidopsis thaliana*, which is susceptible to both species and offers valuable tools for studying these defensive processes.

Our study has emphasized the crucial role of nitric oxide (NO) in plant defense against pests. NO serves as a signalling molecule, metabolic intermediate, and toxic oxidative product, contributing significantly to the plant's defense against insects and mites. This understanding has enhanced our insight into the plant's defensive strategies.

Furthermore, we have unravelled the intricate interplay of hormones, such as jasmonic acid (JA) and abscisic acid (ABA), in regulating defense responses. Our study has shed light on JA catabolism and its impact on plant defense, along with investigating the influence of ABA and stomatal behaviour in the face of *T. urticae* attacks. These findings have deepened the understanding of the hormonal regulation underlying plant resistance strategies.

Additionally, our research has explored the realm of post-transcriptional gene silencing, particularly driven by microRNAs and resistance (R) genes. By elucidating the role of the miR825-5p in regulating gene expression of target-Nucleotide-binding, Leucine-rich domains (NLRs), involved in the plant arthropod interplay and dissecting the molecular mechanisms behind, we have uncovered vital components of the plant's defense toolkit.

In summary, our comprehensive study not only has unveiled the molecular intricacies of plant defense against herbivorous pests but has also provided critical insights into potential strategies for enhancing plant resilience and agricultural pest management practices.

RESUMEN

Las plantas se enfrentan desafíos tanto de factores ambientales como de plagas. Al detectar herbívoros, las plantas activan respuestas inmunes específicas a través de eventos de reprogramación transcripcional complejos, orquestados por redes dinámicas sensibles a diversas señales.

En esta investigación, exploramos los mecanismos que las plantas emplean para defenderse contra dos las plagas: el ácaro altamente polífago *Tetranychus urticae,* el principal artrópodo diana de nuestra investigación, y las orugas de la mariposa *Pieris brassicae*. Nuestra investigación se ha centrado en la planta modelo *Arabidopsis thaliana*, que es susceptible a ambas especies y ofrece herramientas valiosas para estudiar estos procesos defensivos.

Nuestro estudio ha destacado el papel crucial del óxido nítrico (NO) en la defensa de las plantas contra las plagas. El NO actúa como molécula señalizadora, intermediario metabólico y producto oxidativo tóxico, contribuyendo significativamente a la defensa de la planta contra insectos y ácaros.

Además, hemos desentrañado la compleja interacción de hormonas, como el ácido jasmónico (JA) y el ácido abscísico (ABA), en la regulación de las respuestas defensivas. Nuestro estudio ha arrojado luz sobre el catabolismo del JA y su impacto en la defensa de la planta, junto con la influencia del ABA y el comportamiento estomático frente al ataque de *T. urticae*.

Adicionalmente, nuestra investigación ha explorado el ámbito del silenciamiento génico post-transcripcional, impulsado especialmente por microARNs y genes de resistencia (R), profundizando en el papel del miR825-5p como regulador de la expresión de genes diana Nucleotide-binding Leucine-rich domains (NLRs), implicados en la interacción planta-fitófago, y analizando los mecanismos moleculares que los sustentan.

En resumen, nuestro estudio llevado a cabo de forma exhaustiva no solo ha revelado las complejidades moleculares de la defensa de las plantas contra las plagas herbívoras, sino que también ha proporcionado conocimientos críticos sobre posibles estrategias para mejorar la resistencia de las plantas y las prácticas de manejo de plagas agrícolas.

INDEX

LIST OF FIGURES

Figure 11. The experimental setup systems utilized for spider mite plant experiments. A Plants infested individually by spider mites using a brush. **B, C** final experimental set up in hole Arabidopsis rosette. **D** experimental set up for detached leaf. **E** trays with water for the plants to prevent contamination between treatments.

Figure 12. Schematic overview of NO sources and pathways in a plant cell and a heatmap of NO-associated genes expressed in the subcellular locations of *A. thaliana* after spider mite feeding. The diagram shows the main sources and pathways of NO (black arrows) including both oxidative and reductive pathways, the main scavengers (pink arrows) including superoxide ion, GSH, and hemoglobins, and the main NO mechanisms of action (orange arrows). Discontinued lines represent the mechanisms not experimentally demonstrated. A heatmap showing transcriptomic data of NO-associated genes from *A. thaliana* at different infestation times (0.5, 1, 3, and 24 h) with *T. urticae* is comprised within bubbles, positioned over the subcellular compartment where genes are expressed according to SUBA predictions, with a score ≥0.5. IAA, indole-3-acetic acid; IBA, indole-3-butyric acid; GSH, glutathione; GSNO, S-nitrosoglutathione; GSNOR, S-nitrosoglutathione reductase; Hbs, hemoglobins; L-Arg, L-arginine; mETC, mitochondrial electron transport chain; NR, nitrate reductase; NO, nitric oxide; NOS-L, nitric oxide synthase-like; NOA, NO-associated protein; P-NO, nitrosylated protein; P-N-Tyr, nitrated protein; P-SNO, S-nitrosylated protein; PTMs, post-translational modifications; XOR, xanthine oxidoreductase.

Figure 13. Overview of the jasmonate pathway including the major molecular players involved in biosynthesis, signalling, and catabolism. Black font means the chemical compound, blue font means the enzymes involved, and green fonts shows the main metabolites, enzymes, and proteins, respectively, for each section of the pathway. Scheme extracted from Delgado et al., (2021).

Figure 14. Scheme of *JA* metabolism and expression of genes involved in the pathway, in Arabidopsis Col-0 at different *T. urticae* infestation times. Scheme of the JA metabolic pathway indicating genes encoding enzymes involved in each reaction. Differential expression of JA metabolism genes at 0.5, 1, 3 and 24 h after *T. urticae* infestation. 13-HOPT: 13-hydroperoxyliolenic acid; 12,13-EOT: 12,13-Epoxy-9-octadecenoic acid; 12-OPDA:12-oxo-phytodienoic acid; JA: Jasmonic acid; JA-Ile: JA-Isoleucine; Me-JA: methyl-JA; LOX: Lipoxygenase; AOS: Allene oxide synthase; AOC: Allene oxidase cyclase; OPR3: Cis-12-oxo-ohytodienoic acid reductase 3; JMT: JA methyl transferase; IAR3 and ILL6: amydohydrolases; JAR1: jasmonate resistant 1; CYP94B and CYP94C: JA-Ile oxidases; JAO: Jasmonic acid oxidase; ST2A: sulfotransferase 2A.

Figure 15. JAO2 gene expression in Arabidopsis Col-0. A, Correlation between RNAseq data and RTqPCR validation for *JAO2* gene in Arabidopsis Col-0 at 0.5, 1, 3 and 24 h post-infestation, expressed as Log2fold change, are mean of three biological replicates. r value indicates Pearson correlation between RNAseq and RTqPCR data**. B,** Relative expression level of *JAO2* gene in different tissues (1W-3W: 1-3 week rosettes, Sq: siliques, S: seeds, F: flowers, L: leaves stem and R: roots). Data are mean ± SE of three **B** replicates.

Figure 16. Plant damage, hydrogen peroxide and callose determination in jao2 and Col-0 Arabidopsis genotypes after *T. urticae* infestation and mite performance after feeding in these plants. A, Foliar damaged area was quantified in Col-0 and *jao2* mutants after 4 d of mite infestation. **B,** Callose deposition in leaves after 24 h of mite infestation. **C** Hydrogen peroxide expressed as DAB units, after 24 h of mite infestation. **D,** Effects of Arabidopsis genotypes on *T. urticae* fecundity measured 36 h after infestation with synchronized mite females. Data are mean ± SE of nine **A, B, C** and six **D** replicates. Different letter indicates significant differences (P<0.5, One way ANOVA followed by Tukey's multiple comparison test).

Figure 17. Expression of *JAO* genes in Arabidopsis Col-0 in response to *T. urticae* infestation and in *jao2*-2 mutant line. Correlation between RNAseq and RTqPCR data for *JAO1*; **A**, *JAO3*; **B** and *JAO4*; **C** genes in Arabidopsis Col-0 at 0.5, 1, 3 and 24 h after *T. urticae* infestation. Expression of *JAO1*; **D**, *JAO3*; **E** and *JAO4*; **F** genes in *jao2* mutant lines and Col-0 plants after 24h of mite infestation, by RTqPCR assays. Data, expressed as Log2 fold change. r value indicates Pearson correlation between RNAseq and RTqPCR data.

Data are mean of three biological replicates. Significant factors (SF) indicate whether the two independent factors, G (genotype) and T (mite treatment), and/or their interaction (TxG,I), were statistically significant. Different letter indicates significant differences (P<0.5, Two-way ANOVA followed by Tukey's multiple comparison test).

Figure 18. Plant damage, hydrogen peroxide and callose determination in *jaoT* and Col-0 Arabidopsis genotypes after *T. urticae* infestation and mite performance after feeding in these plants. A, Foliar damaged area was quantified in Col-0 and *jaoT* (jao2-1, jao3-1, jao4-2) mutant after 4 d of mite infestation. **B** Callose deposition in leaves after 24 h of mite infestation. **C,** Hydrogen peroxide expressed as DAB units, after 24 h of mite infestation. **D,** Effects of Arabidopsis genotypes on *T. urticae* fecundity measured 36 h after infestation with synchronized mite females, Data are mean ± SE of nine A, B, C and six **D** replicates. Different letter indicates significant differences (P<0.5, Two-way ANOVA followed by Tukey's multiple comparison test).

Figure 19. Expression of genes involved in JA/JA-Ile biosynthetic pathway in Arabidopsis *jao2* mutant line and Col-0 plants 24 h after mite infestation. Relative expression of genes involved in the JA biosynthetic pathway. *AOS*: Allene Oxide Synthase; **A**, *JAR1*: Jasmonic acid response 1; **B**, *MYC2*: MYC transcription factor; **C**. Data are mean of three biological replicates. Significant factors (SF) indicate whether the two independent factors, G (genotype) and T (mite treatment), and/or their interaction (TxG,I), were statistically significant. Different letter indicates significant differences (P<0.5, Two-way ANOVA followed by Tukey's multiple comparison test).

Figure 20. Quantification of hormones in Arabidopsis *jao2, jaoT* mutant lines and Col-0 after 24 h of *T. urticae* infestation. JA: Jasmonic Acid **A, B**, JA-Ile: Jasmonic-isoleucine acid **C, D**, SA: Salicylic Acid **E, F**. Values are normalized respect to internal standard area and sample fresh weight. Data are mean of three biological replicates. Significant factors (SF) indicate whether the two independent factors, G (genotype) and T (mite treatment), and/or their interaction (TxG,I), were statistically significant. Different letter indicates significant differences (P<0.5, Two-way ANOVA followed by Tukey's multiple comparison test).

Figure 21. Scheme of the JA catabolic pathway and quantification of JA/JA-Ile-derivatives in Arabidopsis *jao2-2, jaoT* mutant lines and Col-0 after 24 h of *T. urticae* infestation. Scheme of the JA catabolism indicating the genes encoding enzymes involved in each reaction. Quantification of JA-derivatives (12-OH-JA, 12-HSO4-JA, 12-COOH-JA, 12-OH-JA-Ile and 12-COOH-JA-Ile) expressed as normalized values (x102) respect to internal standard area and sample fresh weight, normalized peak area values. Values are mean ± SE of three biological replicates. C: control plants, M: mite infested plants. Compounds with differential significant levels respect to the control are highlighted in darker o weaker grey colour.

Figure 22. Quantification of indole glucosinolates and camalexin in Arabidopsis *jao2* mutant lines and Col-0 after *T. urticae* infestation. A, I3M, **B,** 4-MeO-I3M, **C,** 1-OH-I3M and **D,** camalexin quantified in *jao2-2* mutant lines and Col-0 plants 24 h after mite infestation. Data are expressed as normalized values respect to internal standard area and fresh sample weight (g), normalized peak area values. Values are normalized respect to internal standard area and sample fresh weight. Data are mean of three replicates. Significant factors (SF) indicate whether the two independent factors, G (genotype) and T (mite treatment), and/or their interaction (TxG,I), were statistically significant. ns: no statistically significant. Different letter indicates significant differences (P<0.5, Two-way ANOVA followed by Tukey's multiple comparison test).

Figure 23. Effects of mite infestation on stomata aperture, and on the leaf cell death when plants are incubated under light or dark conditions. A, Stomata aperture measured in Arabidopsis Col-0 detached leaves after 3, 8, 24 and 30 h of mite infestation. Results referred as width/length ratio. Significant factors (SF) indicate whether the two independent factors, R (infestation time) and C (mite treatment), and/or their interaction I (RxC) were statistically significant (Two-way ANOVA followed by Sidak's multiple comparison test, P<0.05). Numbers indicate significant differences between control and mite treatment at each point of infestation. Data are means ± SE of 10 biological replicates. **B**, Image of stomata closure

24 h after mite infestation. Bars = 8µm **C,** Cell death, measured in leaf discs by trypan blue staining after 16 h of mite infestation under dark and light conditions, is expressed in mm^2. t-Student test was accomplished to assess differences due to light treatments (P<0.05). Data are means ± SE of 15 biological replicates.

Figure 24. Quantification of hormone content in Arabidopsis Col-0 upon mite infestation. JA; **A**, JA-Ile; **B**, SA; **C** and ABA; **D** accumulation was quantified at 3, 8, 24 and 30 h after mite infestation. Values are expressed as ng of hormone per g of fresh weight (FW). Significant factors (SF) indicate whether the two independent factors, R (Infestation time) and C (mite treatment), and/or their interaction I (RxC) were statistically significant (Two-way ANOVA followed by Tukey's test, P<0.05). Asterisks and numbers indicate significant differences compare to control conditions. Data are means ± SE.

Figure 25. Stomata aperture after exogenous hormonal treatments. Stomata aperture measured at 3 h after spraying on the aerial part of the plant with 1 mM SA; **A**, 1 mM JA; **B** and 10 µM ABA; **C**. Results referred as width/length ratio. t-Student test was accomplished to assess differences due to hormone treatments (P<0.05) marked with one, two or three asterisks depending on significance. Data are means ± SE.

Figure 26. ABA accumulation at subcellular resolution level in leaf tissues of nuclear ABA-biosensor plants nls-ABACUS2-400n, after mite infestation. A, Projections of analysed images. Upper images correspond to nuclei expressing the biosensor and bottom images to FRET-processed results in detached leaves. **B**, Maximum Z- projections of the data quantified in A. Upper images correspond to nuclei expressing the biosensor and bottom images to Emission ratios. t-Student test was accomplished to assess differences due to control and mite conditions (P<0.05). Data are means ± SE of 8 biological replicates. **C,** Emission ratios of nlsABACUS2-400n biosensor in cells of Vascular Bundle, Bundle Sheath, Spongy Mesophyll, Pavement and Stomata type cells, after 24 h of mite infestation in detached leaves. Significant factors (SF) indicate whether the two independent factors, R (mite treatment) and C (nucleus type), and/or their interaction I (RxC) were statistically significant (Two-way ANOVA followed by Tukey's test, P<0.05). Data are means ± SE of 8 biological replicates. **D**, Increased levels of emission ratio in the different five cell types after infestation respect to non-infested ones.

Figure 27. Quantification of nuclei number in different cell type groups of nls-ABACUS2-400n plants after mite infestation. A Scheme of the leaf tissues and a mite feeding through stomata. **B** Total number detected nuclei in infested and control leaves. Total number of nuclei in different cell types: **C** Pavement, **D** Stomata, **E** Spongy mesophyll, **F** Bundle sheath and **G** Vascular bundle, after 24 h of mite infestation. Asterisks and numbers indicate significant differences between control and mite treatment (P<0.5, t-student test). Data are means ± SE of 8 biological replicates.

Figure 28. Plant damage and mite fecundity after mite infestation of *aba2-1* and *cyp707a1cyp701a3* and *pyr1pyl-112458, ost1-3* Arabidopsis mutants and Col-0 plants. A, Foliar damage quantified 4 d after mite infestation in whole plants in *aba2-1*, *cyp707a1cyp707a3* and Col-0 plants, and in **B,** *112458, ost1-3* and Col-0 plants. Data, expressed in mm^2. Effects on *T. urticae* fecundity measured 36 h after the infestation with synchronized mite females in detached leaves on **C**, *aba2-1 cyp707a1cyp707a3* and Col-0 plants, and in **D**, *112458, ost1-3* and Col-0 plants. Numbers indicate significant differences compare to Col-0 genotype. Data are means ± SE 10 biological replicates for Damage and 6 biological replicates for eggs. One-way ANOVA followed by Tukey's multiple comparisons test, P<0.05.

Figure 29. Redox status in the five Arabidopsis genotypes. A, Accumulation of H_2O_2 in detached leaves after 24 h of mite infestation, expressed as DAB units. Asterisks and numbers indicate significant differences compared to Col-0 genotype. Different letter indicates significant differences (P<0.5, One way ANOVA followed by Tukey's multiple comparison test). **B,** Pictures showing the H_2O_2 deposits during *T. urticae* feeding.

Figure 30. Effect of ABA pre-treatment of nls-ABACUS2-400n plants before mite infestation. Total emission ratio of biosensor signal **A**, stomata aperture is referred to width/length the width/length ratio **B**, damaged area expressed in mm_2 **C**, plant growth quantified in pixels **D** and infested Arabidopsis plant images ABA pre-treated and non-pre-treated **E**, of nls-ABACUS2-400n leaves either ABA-pre-treated for 3 h or non-pretreated, and then mite infested for 24h or in non-infested. A P<0.05 t-Student test was accomplished in all the panel. marked with one, two or three asterisks depending on significance. Data are means ± SE.

Figure 31. Effects of ABA (10 µM) and/or fussicoccin (1 µM) pre-treatments on stomata aperture and on Arabidopsis plant responses to mite infestation. A, Images of stomata behaviour in ABA and/or fusicoccin (FC) pre-treated plants. Bars = 8µm **B**, Stomata aperture in ABA and/or fusicoccin (FC) pre-treated plants after 24 h of mite infestation in detached leaves. Significant factors (SF) indicate whether the two independent factors, R (mite treatment) and C (Pre-treatment), and/or their interaction I (RxC) were statistically significant (Two-way ANOVA followed by Tukey's multiple comparison test, P<0.05). **C,** Plant damage in whole plant of ABA and/or fusicoccin (FC) pre-treated plants after 4 d of mite infestation. Numbers indicate significant differences compare to Mock treatment. One-way ANOVA followed by Tukey's multiple comparison test, P<0.05. Data are means ± SE of 8 biological replicates for the aperture and 9 biological replicates for damage.

Figure 32. Stomata density in *epf1epf2* mutant, *EPF2OE* over-expressing line and Col-0 plants, and determination of damage, stomata aperture and temperature in the three genotypes after mite infestation. A, Stomata density is expressed as mm^2 per detached leaves. (P<0.05). Numbers indicate significant differences compare to Col-0 genotype. Data are means ± SE 9 biological replicates. One-way ANOVA followed by Tukey's multiple comparisons test, P<0.05. **B,** Stomata pore aperture is referred to the width/length ratio in detached leaves. **C,** Temperature in ºC measured in whole plants. Significant factors (SF) indicate whether the two independent factors, R (mite treatment) and C (genotype), and/or their interaction I (RxC) were statistically significant (Two-way ANOVA followed by Tukey's multiple comparison test, P<0.05). Data are means ± SE of 8 biological replicates. **D,** Foliar damage in whole plant, expressed in mm^2, was quantified 4 d after mite infestation. t-Student test was accomplished. Data are means ± SE for 8 biological replicates **E,** Correlation between stomata density and damaged area for the three Arabidopsis genotypes.

Figure 33. The regulatory network of 22 nucleotides (nt)-long miRNAs and NBS-LRR mRNAs involved in production of phasiRNAs. The 22-nt miRNA guides AGO protein to cleave the target site on the NBS-LRR transcript, triggering dsRNA synthesis mediated by RDR6 (RNA-DEPENDENT RNA POLYMERASES 6) and SGS3 (SUPPRESSOR OF GENE SILENCING 3). dsRNA is subsequently processed by DCL4 (DICER-LIKE 4) and DRB4 (DOUBLE-STRANDED-RNA-BINDING PROTEIN 4) to generate a cluster of 21-nt phased siRNAs (phasiRNAs). These 21-nt phasiRNAs are loaded into AGO proteins, which in turn can lead to NBS-LRR mRNAs cleavage. On the other hand, these siRNAs will depress newer targets.

Figure 34. Expression of receptor genes in Arabidopsis Col-0 plants in response to *T. urticae* infestation at 0.5, 1, 3 and 24 h post-infestation. A PRR, NLR and TNL up-regulated genes at different mite infestation times detected in RNAseq data from Santamaria *et al*., 2021. Relative expression of *MRT1*; **B**, *MRT2*; **C** and miR825-5p and its primary form (PrimiR825); **D** at different infestation times. r value indicates Pearson correlation between RNAseq and qRTPCR data **B, C**. **D** Asterisks indicates significant differences for PrimiR825-5p or miR825-5p respect time 0 h (P<0.5, Two-way ANOVA followed by Tukey's multiple comparison test).

Figure 35. Hybridization energies of TNL genes putative targets of the miR825-5p. Hybridization energies of 6 TNL gene isoforms potential targets of miR825-5p using WM3 and default parameters on Araport11 tools. Extracted from López-Márquez *et al.,* 2021.

Figure 36. Gene expression profiles TNL genes putative targets of the miR825-5p at 0.5 h after *T. urticae* infestation. Relative expression levels of TNL genes in Col-0 Arabidopsis plants after 0.5 h of mite

infestation. TNL genes: *MRT1* isoforms, AT4G14370.1, AT4G14370.2 and AT4G14370.3; *MRT2*: AT5G41550; *MIST1*, AT5G38850.1, and AT4G08450.1; AT4G08450.2; AT1G63730.1; AT1G63740.1 and AT1G63740.1. Data are mean ± SE of three replicates. Asterisks indicates significant differences respect control plants (P<0.5, t- student test).

Figure 37. Expression profiles of TNL genes 0.5 h after *P. brassicae* infestation. Relative expression levels of TNL genes in Col-0 Arabidopsis plants after 0.5 h of *Pieris* larvae infestation. TNL genes: *MRT1* isoforms, AT4G14370.1, AT4G14370.2 and AT4G14370.3; *MRT2*: AT5G41550; *MIST1*, AT5G38850.1, and AT4G08450.1; AT4G08450.2; AT1G63730.1; AT1G63740.1 and AT1G63740.1. Data are mean ± SE of three replicates. Asterisks indicates significant differences respect control plants (P<0.5, t-student test).

Figure 38. Expression of and miR825-5p and its primary form (PrimiR825-2p) in Arabidopsis Col-0 plants in response to *P. brassicae* infestation at 0.5, 1, 3 and 24 h post-infestation. Data are mean ± SE of three replicates. Asterisks indicates significant differences for PrimiR825-5p or miR825-5p respect time 0 h (P<0.5, Two-way ANOVA followed by Tukey's multiple comparison test).

Figure 39. Plant damage, cell death after feeding on Col-0 and *mrt1* and *mrt2* mutant lines. A, B Foliar damage quantified in Col-0 and *mrt* mutant lines after 4 d of mite infestation. **C, D** Cell death quantified in Col-0 and *mrt* mutant lines after 24 h of mite infestation. Data are mean ± SE of nine **(A, B)** and ten **(C, D)** replicates. Different letter indicates significant differences (P<0.5, One way ANOVA followed by Tukey's multiple comparison test).

Figure 40. *T. urticae* mortality and fecundity after feeding on Col-0 and *mrt1* and *mrt2* mutant lines. A, B Mite mortality quantified in Col-0 and *mrt* mutant lines 24 h of mite infestation. **C, D** Cumulative number of mite eggs measured 36 h of infestation with synchronized mite females. Data are mean ± SE of six replicates. Different letter indicates significant differences (P<0.5, One way ANOVA followed by Tukey's multiple comparison test).

Figure 41. Plant damage, larvae weight after *P. brassicae* feeding on Col-0 and *mrt1* and *mrt2* single mutant lines. A Remaining leaf tissue area after 8 h of Pieris larvae feeding on Col-0 and *mrt1-mrt2* mutant lines. **B** Pieris larvae weight after 24 h of feeding on Col-0 and *mrt1-mrt2* mutant lines. Data are mean ± SE of twelve **(A)** and twenty-four **(B)** replicates. Different letter indicates significant differences (P<0.5, One way ANOVA followed by Tukey's multiple comparison test).

Figure 42. Plant damage and mite performance in *mrt1-mrt2*- double mutant and Col-0 Arabidopsis genotypes A Foliar damaged area was quantified in Col-0 and *mrt1-mrt2* double mutant after 4 d of mite infestation. **B** Effects of Arabidopsis genotypes on *T. urticae* fecundity measured 36 h after infestation with synchronised mite females. Data are mean ± SE of nine **(A)** and six **(B)** replicates. Different letter indicates significant differences (P<0.5, One way ANOVA followed by Tukey's multiple comparison test)

Figure 43. Plant damage, larvae weight after *P. brassicae* feeding on Col-0 and *mrt1-mrt2* double mutant lines. A Remaining leaf tissue area after 8 h of Pieris larvae feeding on Col-0 and *mrt1-mrt2 double mutant*. **B** *Pieris* larvae weight after 24 h of feeding on Col-0 and *mrt1-mrt2 double mutant* lines. Data are mean ± SE of twelve **A** and twenty-four **B** replicates. Different letter indicates significant differences (P<0.5, One way ANOVA followed by Tukey's multiple comparison test).

Figure 44. Gene expression analysis of *PR1*, *VSP2* in *mtr1-mrt2* double mutant after 24 h of *T. urticae* infestation. A; *PR1* and **B;** *VSP2* relative expression in *mtr1-mrt2* double. Data are means ± SE of three replicates. Significant factors (SF) indicate whether the two independent factors, G (genotype) and T (mite treatment), and/or their interaction (TxG,I) were statistically significant. Different letter indicates significant differences (P<0.5, Two-way ANOVA followed by Tukey's multiple comparison test).

Figure 45. Gene expression analysis of *PR1*, *VSP2* in *mtr1-mrt2* double mutant after 24 h of *P. brassicae* infestation. A; *PR1* and **B;** *VSP2* relative expression in *mtr1-mrt2* double. Data are means ± SE of three

replicates. Significant factors (SF) indicate whether the two independent factors, G (genotype) and T (mite treatment), and/or their interaction (TxG,I) were statistically significant. Different letter indicates significant differences (P<0.5, Two-way ANOVA followed by Tukey's multiple comparison test).

Figure 46. Gene expression analysis of *MIST1* in *mtr1-mrt2* double mutant after 24 h of *P. brassicae* infestation. Data are means ± SE of three replicates. Significant factors (SF) indicate whether the two independent factors, G (genotype) and T (mite treatment), and/or their interaction (TxG,I) were statistically significant.

Figure 47. Molecular characterization of miR825-5p lines from López-Márquez *et al.,* (2021) after *T. urticae* infestation. A Relative expression of miR825-5p after 0.5 h of infestation**. B** Cell death measured by Trypan blue after 24 h post infestation. Data are mean ± SE of three **A** and ten **B** replicates. **A** Asterisks indicates significant differences respect control plants differences (P<0.5, Two-way ANOVA followed by Tukey's multiple comparison test). **B** Asterisks indicates significant differences respect Col-0 plants (P<0.5, One way ANOVA followed by Tukey's multiple comparison test).

Figure 48. Molecular characterization of miR825-5p lines from López-Márquez *et al.,* (2021) after *T. urticae* infestation. Relative expression of *MRT1*, **A** and *MRT2*, **B** after 0.5 h of mite feeding. Data are mean ± SE of three replicates.

Figure 49. Plant damage, *T. urticae* fecundity after feeding on Col-0 and miR825-5p silencing and over-expressing lines. A Foliar damage quantified in Col-0 and miR825-5p silencing and over-expressing lines**.** after 4 d of mite infestation. **B** Cumulative number of mite eggs measured 36 h of infestation with synchronized mite females on Col-0 and miR825-5p silencing and over-expressing lines**.** Data are mean ± SE of nine **A** and six **B** replicates.

Figure 50. Plant damage, larvae weight after *P. brassicae* feeding on Col-0 and miR825-5p silencing and over-expressing lines. A Remaining leaf tissue area after 8 h of *Pieris* larvae feeding on Col-0 and miR825-5p silencing and over-expressing lines. **B** Pieris larvae weight after 24 h of feeding on Col-0 and miR825-5p silencing and over-expressing lines. Data are mean ± SE of twelve **A** and twenty-four **B** replicates.

Figure 51. Scheme of MRT1 and MRT2 gene fusions to the yellow fluorescent protein gene (YFP) and their mutated versions. Punctual mutations are indicted in Mut_MRT1 or Mut_MRT2 constructions.

Figure 52. Quantification of MRT1-YFP and MRT2-YFP fluorescence constructs in *N. benthamiana* plants expressing them alone or co-expressing with miRNAs. A Quantification of fluorescence emitted by *N. benthamiana* agroinfiltrated with Wt_MRT1-YFP or its mutated version Mut_MRT1-YFP, alone or combined with miR825-5p or miR319 at different expression times. **B** Quantification of fluorescence emitted by *N. benthamiana* agroinfiltrated with Wt_MRT2-YFP or its mutated version Mut_MRT2-YFP or alone or combined with miR825-5p or miR319, at different expression times. Data are means ± SE of 24 biological replicates. Statistics indicated in **Annexed tables 8 and 9** (P<0.5, Two-way ANOVA followed by Tukey's multiple comparison test).

Figure 53. Quantification of MRT1-YFP and MRT2-YFP fluorescence constructs in *N. benthamiana* plants co-expressing them alone or with phasiRNAs. A Quantification of fluorescence emitted by *N. benthamiana* agroinfiltrated with Wt_MRT1-YFP or its mutated version Mut_MRT1-YFP, alone or combined with miR319 or specific phasiRNAs at different expression times. **B** Quantification of fluorescence emitted by *N. benthamiana* agroinfiltrated with Wt_MRT2-YFP or its mutated version Mut_MRT2-YFP or alone or combined with miR319 or specific phasiRNAs, at different expression times. Data are means ± SE of 24 biological replicates. Statistics indicated in **Annexed tables 10 and 11** (P<0.5, Two-way ANOVA followed by Tukey's multiple comparison test.

Figure 54. A model depicting the crosstalk between various players and molecules identified thus far in the *T. urticae-A. thaliana* interaction. Specific mite elicitors/effectors are recognized by receptors (PRR

or NLR; TIRK, MRT1, MRT2, PP2-A5) that induce alterations in the membrane potential (Vm) and Ca2+ influx. Subsequently, reactive oxygen species (ROS) and nitrogen species (RNS) are triggered. Some ROS genes (and *TRXh5*) associated to ROS/RNS balance participate in the defense process, modulating somehow the hormonal signalling pathways, mainly through the JA/ABA ratios to finally induced appropriated plant defences and phenotypical changes in stomata. Among them, HCN and quinones mediated by the hydroxinitrile lyase enzyme (HNL) and cyanoalanine synthase of *T. urticae* (TuCAS), respectively. Finally, the glucosinolates (IGs) and other defensive metabolites are produced.

Annexed Figure 1. FRET-images processing. A Raw Confocal images after 24 h of mite infestation **B** FretCellType nucleus determination based on their shape. I. Pavement nuclei. II. Stomata nuclei III. Spongy mesophyll nuclei, IV. Bundle sheat nuclei, V. Vascular bundle nuclei.

Annexed Figure 2. Molecular characterization of Arabidopsis *jao2* mutant lines. **A** Scheme of the position of the T-DNA insertion (arrowhead) in the *JAO2* gene. **B** Expression levels of JAO2 gene in leaves of *jao2-1* and *jao2-2* mutant lines and Col-0 plants. Data are means ± SE of three replicates. **C** Plant phenotypes of j*ao2* and Col-0 rosettes 2 weeks after germination. **D** Determination of rosette area of jao2 lines. Different letter indicates significant differences **B, D** P<0.5, One way ANOVA followed by Tukey's multiple comparison test.

Annexed Figure 3. Expression levels of PR1 and MYC2 genes in the five Arabidopsis genotypes. PR1 gene **A, B** and MYC2 gene **C, D.** Gene expression levels were determined in aba2-1, cyp707a1cyp707a3, and in pyr1pyl-112458, ost1-3 and Col-0 whole plants. Values indicated as relative expression. Significant factors (SF) indicate whether the two independent factors, R (infestation time) and C (genotype), and/or their interaction I (RxC) were statistically significant (Two-way ANOVA followed by Tukey's multiple comparison test, P<0.05). Data are means ± SE of 3 pools of 6 biological replicates.

Annexed Figure 4. Effects of different ratios Fussicoccin/ABA on stomata aperture in Arabidopsis Col-0 plants. Stomata aperture of Arabidopsis detached leaves pre-treated with 10 µM ABA, 1 µM of fusicoccin (FC), or a combination of 10 µM ABA plus different concentrations (0.5, 1.0, and 5.0 µM) of FC. Numbers indicate significant differences compare to mock treatment. Data are means ± SE of 8 biological replicates.

Annexed Figure 5. miR825-5p binding side and the sequence characteristics. A miR825-5p binds Toll Interleukin domain in TNL proteins. **B** Alignment of the nucleotide sequences of TIR domain of MRT1 an MRT2**. C** Specific binding nucleotide sequences of miR825-5p for *MRT1* and *MRT2* genes.

Annexed Figure 6. Molecular characterization of Arabidopsis *mrt*- mutant lines. Scheme of the position of the T-DNA insertion (arrowhead) in **A**, *MRT1* and **B**, *MRT2* gene. Expression levels of **C**, *MRT1* and **D**, *MRT2* genes in leaves of *mrt*- mutant lines and Col-0 plants. Data are means ± SE of three replicates. Asterisks and numbers indicate significant differences compare to Col-0 genotype.

Annexed Figure 7. Gene expression analysis of MRT1, MRt2 and miR825-5p in mrt mutant lines after 0.5 h of *T. urticae* infestation. A MRT2 relative expression in mtr1-1 and mtr1-2 mutant lines. **B** MRT1 relative expression in mtr2-1 and mtr2-2 mutant lines. **C, D** relative expression of miR825-5p in mrt lines. Data are means ± SE of three replicates. Significant factors (SF) indicate whether the two independent factors, G (genotype) and T (mite treatment), and/or their interaction (TxG,I) were statistically significant. ns: no statistically significant.

Annexed Figure 8. DAPI/nuclei damage relation, H_2O_2 and membrane depolarization after *T. urticae* feeding 24 h in mrt1- and mrt2- single mutant plants. A, D DAPI staining overlapped in damaged zones after 24 h of mite infestation. **B, E** ROS production measured by DAB staining after 24 h of mite infestation. **C, F** Membrane depolarization measured by electric leakage after 24 h of mite infestation. Letters indicate significant differences compare to Col-0 genotype. (P<0.5, One way ANOVA followed by Tukey's multiple comparison test).

Annexed Figure 9. Molecular characterization of Arabidopsis *mrt1*-mrt2 mutant lines. **A** PCR assays of MRT1 and MRT2 genes in WT and mrt1-mrt2 double mutants' lines to show homozygous status. **B** Gene. expression levels of *MRT1* and *MRT2* in leaves of *mrt1-mrt2 double* mutant plants and Col-0 plants. Data are means ± SE of three replicates. Asterisks and numbers indicate significant differences compare to Col-0 genotype. **C** Phenotypes of 3 weeks-old wild-type and mrt1-mrt2 double mutant plants grown in soil. Bars = 0.5 cm.

Annexed Figure 10. Gene expression analysis R genes in *mrt1-mrt2* mutant lines. Relative expression of **A**; MIST1, **B**; AT4G08450, **C**; AT1G63740, **D**; AT1G63730 in *mrt1-mrt2* double mutant lines. Data are means ± SE of three replicates. Asterisks and numbers indicate significant differences compare to Col-0 genotype.

Annexed Figure 11. Expression levels of YFP in MRT1-YFP and MRT2-YFP in *N. benthamiana* plants. A Expression of fluorescence YFP protein emitted by *N. benthamiana* agroinfiltrated with Wt_MRT1-YFP or its mutated version Mut_MRT1-YFP, combined with miR825-5p at 36 h post agroinfiltration. **B** Expression of fluorescence YFP protein emitted by *N. benthamiana* agroinfiltrated with Wt_MRT2-YFP or its mutated version Mut_MRT2-YFP, combined with miR825-5p at 36 h post agroinfiltration. Asterisks and numbers indicate significant differences compare to Wt_MRT1 or Wt_MRT2 construction.

LIST OF TABLES

ACRONYMS

(W/V), weight in volume

.lif, Leica Image File

µg, microgram

ABA, Absicic Acid

BR, Brassinosteroids

CC, Coiled-Coil

CKs, Citokinines

CK, Cytokinin

cm, centimetres

CNLs, Coiled-coil Interleukin-1 receptor Resistance

Col-0, Columbia accession

Cys-SSH, Cysteine residues

d, day

DAB, 3,3'-Diaminobenzidine

DAMPs, Damage Associated Molecular Patterns

DAPI, 4',6-diamidino-2-phenylindole

DEGs, Differential Expressed Genes

DNA, Deoxyribonucleic Acid

eATP, extracellular Adenosine TriPhosphate

ET, Ethylene

ETI, Effector-Triggered Immunity

ETS, Effector Triggered Susceptibility

FC, Fusicoccin

FLIR, Forward Looking Infrared

GA, Gibberellic Acid

GFP, Green Fluorescent Protein

GO, Gene Ontology

h, hour

HAEs, Herbivore-Associated Elicitors

HAMPs, Herbivore-Associated Molecular Patterns

HIPVs, Herbivore-Induced Plant Volatiles

HNLRs, helper NLRs

IAA, Indole Acetic acid

ICS, Isochorismate Synthase

IDs, Integrated Domains

JA, Jasmonic Acid

JA-Ile, Jasmonic Isoleucine

LC/MS, Liquid chromatography–mass spectrometry

LED, Light-Emitting Diode

LRR, Leucine-Rich Repeat

m, minute

MAMPs, Microbe Associated Molecular Patterns

MAPK, Mitogen-Activated Protein Kinase

MeSA, Methyl Salicylate

miRNA, microRNAs

ml, millilitre

mm, millimetres

mM, millimolar

NAD, Nicotinamide Adenine Dinucleotide

NASC, European Arabidopsis stock centre

NBS, Nucleotide-binding Site

ng, nanogram

NLR, Nucleotide-binding Leucine-rich domains

NO, Nitric oxide

NRS, Nitrogen Reactive Species

nt, nucleotide

ºC, Celsius

OPDA, 12-Oxo-PhytoDienoic Acid

OS, Oral Secretions

PAL, Phenylalanine Ammonia-Lyase

PCR, Polymerase Chain Reaction

PDC, Programmed Cell Death

phasiRNAs, Phased secondary small interfering RNAs

PRR, Pattern Recognition Receptors

PTGS, posttranscriptional gene silencing

PTI, Pattern-Triggered Immunity

PTM, Post-Translational Modifications

RCS, Reactive Carbonyl Species

RLK, Receptor-Like Kinases

RNA, Ribonucleic Acid

RNS, Reactive Nitrogen Species

ROI, Region Of Interest

ROS, Reactive Oxygen Species

rpm, revolution per minute

RPW8, RPW8-like CC domain

RSS, Reactive Sulphur Species

RTqPCR, Real Time quantitative PCR

SA, Salicylic Acid

SAR, Systemic Acquire Resistance

SL, Strigolactone

sRNA, Small RNAs

TF, Transcription Factor

TIFF, Tag Image File Format

TIR, Toll Interleukin-1 receptor Resistance

TNL, TIR protein NLRs

UV, Ultraviolet

VM, Trans-membrane potential

WIR, Wound-Induced Resistance

WT, Wild type

YFP, Yellow Fluorescent Protein

1 INTRODUCTION AND OBJECTIVES

1.1 PHYTOPHAGOUS ARTHROPODS

Phytophagous arthropods represent a significant group of attackers for plants, exhibiting remarkable diversity, varied feeding modes, and a high capacity for adaptation (Erb & Reymond, 2019). Accordingly, the phenomenon of coevolution, denoting the reciprocal genetic adjustments, can manifest between plants and pests (Mithöfer & Boland, 2012; Dicke & van Loon, 2014).

The Arthropoda kingdom is the largest phylum in the animal kingdom, comprising about 84% of all known animal species, present in both terrestrial and aquatic environments. A defining characteristic of arthropods is their jointed exoskeleton made of chitin, along with segmented bodies bearing paired jointed appendages. The phylum is divided into four subphyla: Chelicerata (arachnids), Crustacea (crustaceans), Hexapoda (insects and springtails), and Myriapoda (millipedes and centipedes) **(Figure 1**).

Among the arthropods, only insects and mites (from the chelicerate group) are plant feeders and may be considered pests. Insects, found in the Hexapoda group, are the most abundant and are recognized by their three major body regions: head with mouthparts, eyes, and antennae; three-segmented thorax with legs and sometimes wings; and many-segmented abdomen housing digestive, excretory, and reproductive organs.

In the Chelicerate group, only a few families in the Acari subclass use living plants as a food source. The main phytophagous groups in this subclass are from the superfamilies Tetranychidea and Eriophyoidea (Vacante, 2016).

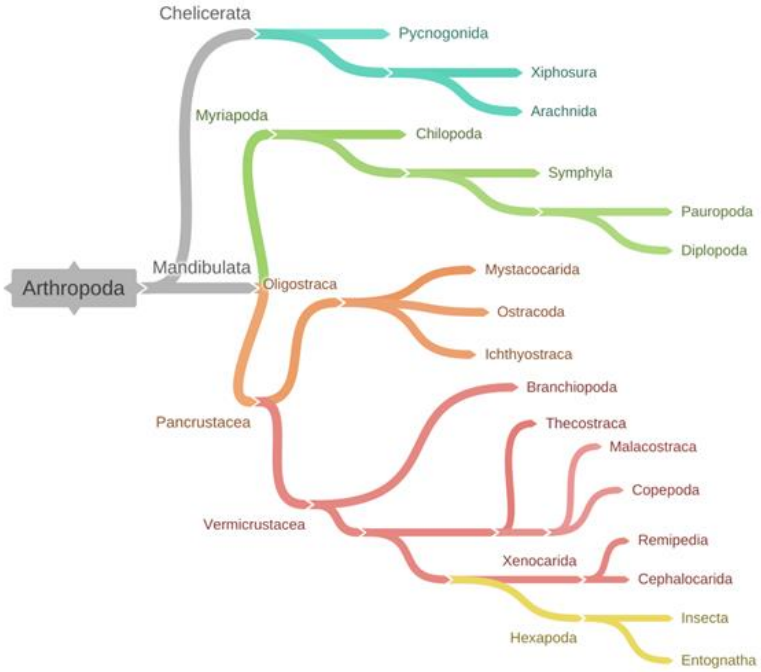

Figure 1. Consensus phylogeny of the major groups of Arthropoda. Based in GIGA Community of scientist.

1.1.1 THE GENERALIST *TETRANYCHUS URTICAE*

Tetranychus urticae Koch is commonly named as the two-spotted spider mite. It belongs the Arachnids class, and Tetranychidae subfamily. It is a small arthropod with 0.5 mm long and with two dark patches on the body. The colour of the patches can vary depending on the diet or the physiological stage. The life cycle is composed of the egg, the larva, two nymphal stages (protonymph and deutonymph) and the adults. Female *T. urticae* can produce over 100 eggs of varying sizes depending on the embryo's sex. This is due to the species' unique form of parthenogenesis called arrhenotoky, where unfertilized eggs develop into males, while diploid females originate from fertilized eggs (Macke *et al.*, 2011).

It is a very polyphagous pest with a worldwide distribution, it can feed from more than 1,100 documented plant species of which 150 are important agronomic crops. It is considered a serious threat for agriculture because it is an extremely polyphagous species but also because of its short life cycle, high offspring production and a remarkable ability to develop pesticide resistance (Santamaria *et al.*, 2020)

T. urticae mites have specialized mouthparts for feeding on plants, including an elongated and retractable cheliceral stylet connected to the pharynx and salivary glands. During feeding, they primarily target leaves by inserting the stylet between epidermal pavement cells or through stomatal openings without harming the epidermis (Bensoussan *et al.*, 2016). Subsequently, they use the retractable stylet to predigest the mesophyll cell content and extract its contents, leading to the loss of chlorophyll, reduced photosynthetic rates, and the formation of characteristic chlorotic lesions **(Figure 2)**. In severe infestations, this can result in leaf defoliation and crop losses. When food resources become scarce, *T. urticae* employs silk synthesis to migrate and colonize new plants. They create silk balls serving as aerial dispersal elements, carried by wind or animals, housing hundreds of mites (Clotuche *et al.*, 2011). The silk webbing also protects the colony from aggressions, aids mite movement, and acts as a pheromone substrate.

Nowadays, *T. urticae* is considered a serious threat to agriculture due to its polyphagous capacity, short life cycle, high offspring production, and remarkable ability to develop pesticide resistances.

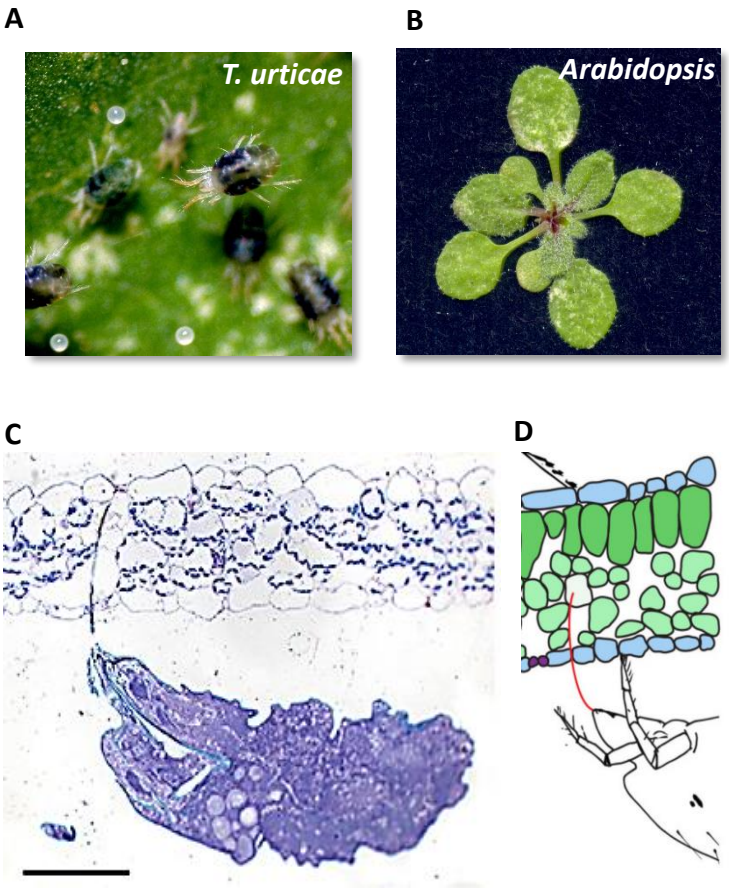

Figure 2. *Tetranychus urticae* feeding. A, *T. urticae* adults and eggs. Picture from Bensoussan *et al*., (2016) **B,** Chlorotic damage in Arabidopsis plants produced by *T. urticae* feeding **C,** Cross section of mite feeding on Arabidopsis leaf from Bensoussan et a., 2016. **D,** Scheme of mite feeding on a leaf cross section.

In addition, the genome of *T. urticae* has been sequenced (Grbić *et al.*, 2011) and there is a wide range genomic tools and protocols established for *T. urticae* (DeClerck & Steeves, 1988; Santamaria *et al.*, 2012; Suzuki *et al.*, 2017; Ojeda-Martinez *et al.*, 2020) make this specie as a model for the study of plant-mite interaction.

1.1.2THE SPECIALIST *PIERIS BRASSICAE*

Pieris brassicae, commonly known as the cabbage butterfly, is a specialist caterpillar feeder that primarily targets families like Brassicaceae. It is a lepidopteran insect of the Pieridae family. It has been identified as a significant pest for crops such as cabbage, cauliflower, broccoli, Brussels sprouts, among others (Sharma & Gupta, 2009).

The life cycle begins when females lay their eggs in batches, averaging 30-100 eggs. The eggs mature on the leaves until hatching, and the neonate larvae start feeding on the leaves. The larvae go through five instars before pupating, usually in a secluded area away from the host plant. During development, a single larva consumes 74-80 cm^2 of leaf area (Younas *et al.*, 2004), with increased chewing activity observed during the night **(Figure 3)**. The severity of insect pest incidence is greatly influenced by prevailing climatic conditions. Moreover, the management of *P. brassicae* through the application of hazardous pesticides has led to the development of resistance in this pest (Ullah *et al.*, 2016).

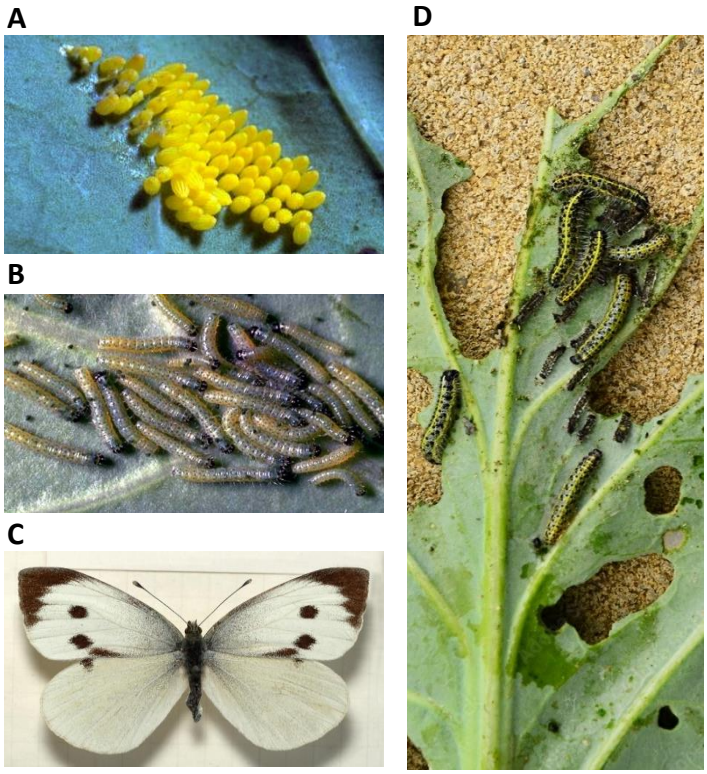

Figure 3. *Pieris brassicae* phenotype and life cycle. A, Eggs, **B,** Neonate larvae, **C,** adult butterfly, **D,** feeding mode of *P. brassicae*. Pictures from D. M Firake.

1.2 PLANT IMMUNITY AND HERBIVORES

To face the phytophagous feeders' plants, under the relentless pressure of intense evolutionary selection for more than 480 million years, plants have evolved sophisticated mechanisms to ensure their survival and optimize their fitness.

In this context, the most prevalent outcomes of specific plant-herbivore interactions are host tolerance and resistance. When an herbivore consumes plant tissue, two major defense mechanisms are triggered. Resistance refers to the host's capacity to curtail pathogen multiplication, whereas tolerance denotes the ability of the host to mitigate infection's impact on its fitness, irrespective of the level of pathogen multiplication. Tolerance is often attributed to the plant's vigor, growth, and ability to produce an acceptable yield (Pagán & García-Arenal, 2018).

Certain plant species have evolved tolerance to herbivory, displaying the ability to rapidly generate compensatory tissues, which can lead to increased reproductive success even under mild damage conditions (McNickle & Evans, 2018; Moustaka *et al.*, 2021). Conversely, other plants have developed traits that reduce herbivore consumption, showcasing a form of resistance (Santamaria *et al.*, 2017a, 2019).

These strategies are extensive and dynamic, involving a combination of constitutive and inducible defense responses. As a result, plants can rapidly enhance their resistance or tolerance to herbivore damage within a remarkably short timeframe, often within hours or minutes of the initial feeding by the herbivore.

1.2.1 CONSTITUTIVE DEFENCES

Plants possess constitutive defences that are present irrespective of herbivore attacks. These defences encompass both physical and chemical barriers that can operate independently or synergistically.

Physical barriers include external morphological features of plants that serve as hindrances to arthropod pests in terms of attachment, feeding, and oviposition. Notable examples of physical barriers include cell walls, spines, cuticles, petal hairs, waxes, and sclerophylly. Cuticle and trichome density are crucial traits in crop protection, preventing pest attachment to plant surfaces (Eigenbrode *et al.*, 1998; Tian *et al.*, 2012; Figueiredo *et al.*, 2013).

Abdelmaksoud *et al.*, 2020 provided evidence of reduced infestations of *Frankliniella occidentalis* thrips in strawberry cultivars with high densities of non-glandular trichomes. Additionally, non-glandular trichomes act as a physical deterrent, leading to significant reduction in oviposition by *T. urticae*, on raspberry genotypes with high leaf trichome densities (Karley *et al.*, 2016). Furthermore, the identification of underlying genetic markers suggests the potential utility of this trait in breeding for mite control (Graham *et al.*, 2014; Santamaria *et al.*, 2018a).

In addition to the structural adaptations observed in plants, certain species synthesize defensive metabolites as a crucial response to enhance defense mechanisms. Chemical defences can be categorized into primary metabolites mainly involved in plant growth, development, and reproduction, and secondary metabolites that serve as bioactive and specialized compounds involved in combating pests, attracting pollinators, and facilitating plant-plant interactions. Alterations in primary metabolism, such as carbohydrates and proteins, can not only impose growth limitations on phytophagous organisms but also generate precursors to produce defense-related compounds (Santamaria *et al.*, 2013; Zhou *et al.*, 2015).

Some examples of plant compounds that are toxic or impair gut function in arthropods include alkaloids (Zúñiga & Corcuera, 1986), benzoxazinoids (Ahmad *et al.*, 2011), glycosylates (Zhurov *et al.*, 2014; Santolamazza-Carbone *et al.*, 2016; Mao *et al.*, 2017), and terpenoids (Schmelz *et al.*, 2011).

Plant breeding typically avoids high levels of defensive compounds (Chen *et al.*, 2015) due to their negative impact on crop quality. However, targeted expression of defensive compounds in non-harvested plant organs, like gossypol in vegetative structures of cotton (Palle *et al.*, 2013), allows tissue-specific engineering of chemical resistance into crops. Assessing indirect effects on biocontrol by natural enemies is necessary (Ågren *et al.*, 2012).

Overall, while constitutive mechanisms offer the advantage of an immediate response to danger signals, they are limited in their ability to amplify the response. Moreover, these mechanisms require energy to remain functional, imposing constraints on the number that can be sustained within an organism (Paludan *et al.*, 2021).

1.2.2INDUCIBLE DEFENCES

Inducible defences in plants are activated only in the presence of attackers, relying on prompt and specific detection and recognition of herbivores (Wu & Baldwin, 2009; Santamaria *et al.*, 2018a). However, the deployment of these defensive mechanisms demands significant resource allocation, potentially leading to growth reduction due to decreased photosynthesis and a decline in overall energy reserves (Garcia *et al.*, 2021a)

The complex biochemical pathways underlying induced plant defense mechanisms (Walling, 2000) offer herbivores an alternative means to evade these defences, leading to detrimental effects on their fitness, survival, development, and reproductive capacity (Ament *et al.*, 2004). One example is the Kunitz trypsin inhibitor (KTI) family from Arabidopsis displayed inhibitory properties that may be involved in modulating the proteases responsible for the hydrolysis of dietary proteins in the spider mite *T. urticae* (Arnaiz *et al.*, 2018).

In addition, herbivores can manipulate these pathways to overcome plant defences (Zarate *et al.*, 2007) and employ stealthy feeding strategies (Walling, 2008). *T. urticae* displays variable ability to suppress induced defences in tomato plants, leading to lower defense levels. This suppression positively affects the fitness of non-suppressing mites on the same leaflet (Kant *et al.*, 2008). An additional instance involves the glucose oxidase found in caterpillar saliva, which diminishes induced defences (Musser *et al.*, 2005). Furthermore, attacks by Colorado potato beetles have been observed to suppress the transcription of genes encoding proteinase inhibitors (PI), which play a role in plant defense (Lawrence *et al.*, 2008).

The level of resistance maintained by a plant over time is influenced by various factors, including the speed and duration of the plant's response, the relationship between the amount of damage and the response, and whether the response varies with initial and repeated damage. In nature, plants can experience varying levels of damage and repeated attacks by herbivores throughout their lifetimes (Underwood, 2012).

This manipulation by herbivores can render attacked plants even more favourable resources for herbivores compared to non-damaged plants (Sarmento *et al.*, 2011). Other studies show that plants become more susceptible to attacks by herbivores after previous attacks by other species of herbivores (Sauge *et al.*, 2006; Poelman *et al.*, 2008) Specifically, it is important the production of herbivore-induced plant volatiles (HIPVs), and their role in tritrophic interactions. HIPVs can make the plant repellent to herbivores and/or more attractive to natural enemies of pests. In some cases, phytophagous can modulate HIPV production by the attacked plant, as demonstrated by Zhang & Li, 2019 in the case of *Bemisia tabaci,* an hemipteran which can manipulate the defense mechanisms of neighbouring plants to prepare them for an imminent attack.

Apart from the interactions within other herbivores, plants engage in concurrent associations with other organisms. One such interaction involves symbioses between plants and beneficial soil microorganisms, such as arbuscular mycorrhizal fungi. These fungi are recognized for promoting plant growth and aiding plants in coping with both biotic and abiotic stresses (Jung *et al.*, 2012). Notably, the lepidopteran *Spodoptera exigua* demonstrated reduced herbivore performance, potentially attributed to the effects of the nitrogen-mycorrhiza interaction on maize (Ramírez-Serrano *et al.*, 2022).

In conclusion, inducible defences in plants are a remarkable adaptation allowing for a tailored response. Herbivores have evolved complex biochemical pathways to evade these defences. The interaction between plants and herbivores involves specificity and intricate dynamics due to the co-evolution pressure. Overall, understanding these complex responses and its activation is vital for developing sustainable strategies for crop protection and ecosystem management **(Figure 4).**

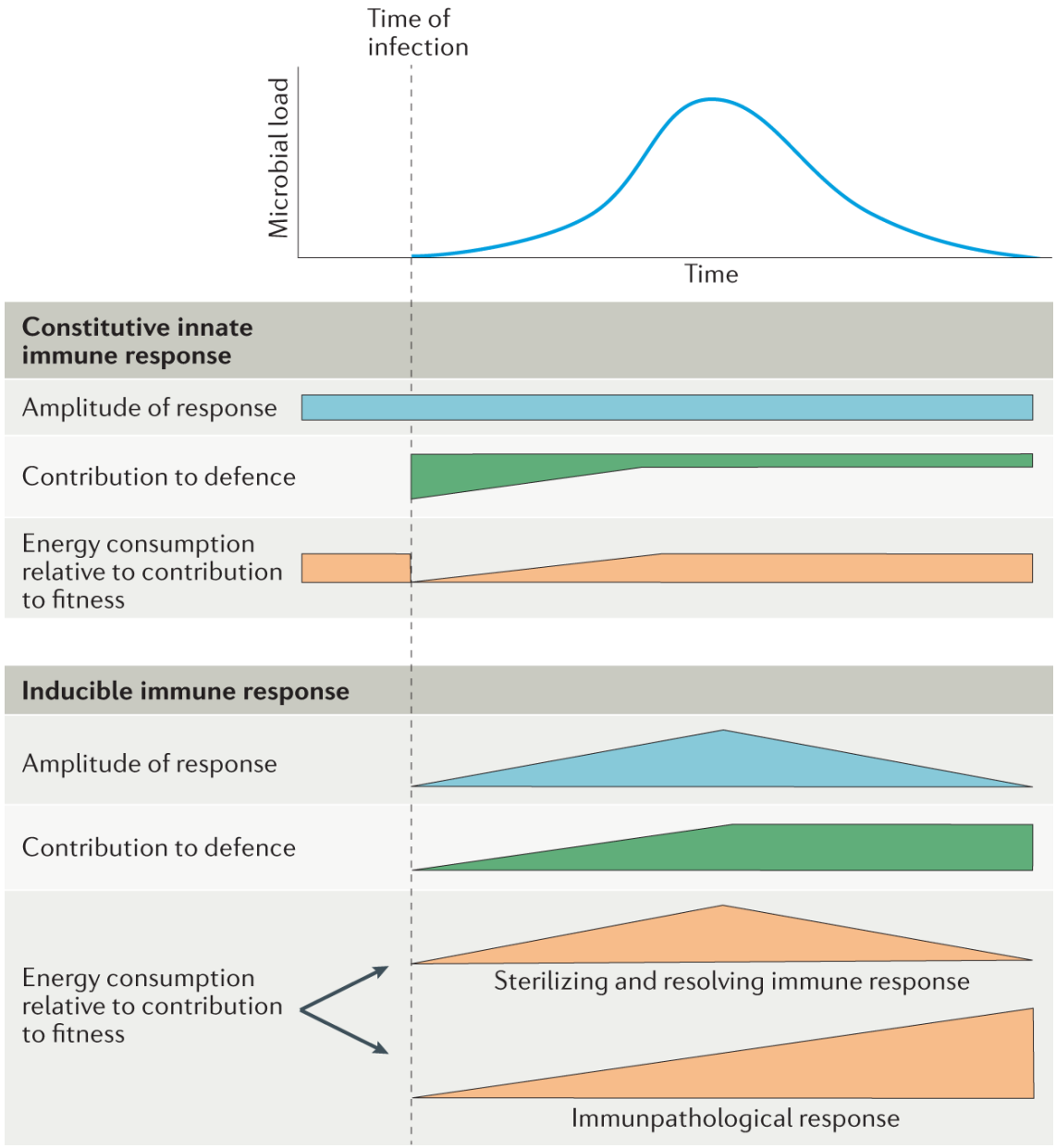

Figure 4. Illustration of how constitutive and inducible immune responses vary over time during a generalized infection, and their impact on host defence, energy consumption and host fitness. In the case of a sterilizing and resolving immune response, the additional energy consumption required by the inducible immune response is balanced by the re-establishment of homeostasis. By contrast, in the case of an immunopathological response, the energy that is consumed to mount an inducible response does not benefit the host and instead leads to tissue damage and disruption of homeostasis. Extracted from Paludan *et al*., (2021).

1.3 PLANT-HERBIVORE INTERACTION

1.3.1 PERCEPTION AND SIGNAL TRANSDUCTION PATHWAY

When herbivores begin feeding on plant tissues, it triggers the perception of the herbivore and the induction of plant defences. Initially, it occurs in the tissue where the infestation takes place (local response), and subsequently extends to undamaged tissues elsewhere in the same plant (systemic response) **(Figure 5)**. Both local and systemic responses involve structural and chemical modifications, which are specifically tailored to combat each precise feeder (Santamaria *et al.*, 2018a). The signals emitted by herbivores can be specifically recognized, enabling the plant to respond more precisely to the threat.

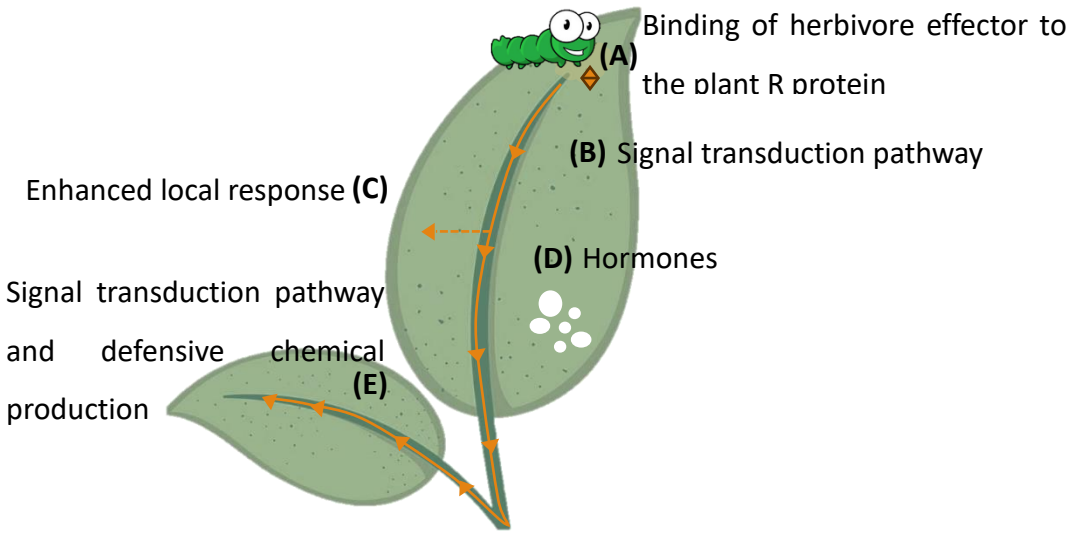

Figure 5. A general model of systemic signalling when local parts of a plant are exposed to specific herbivore. A Binding of herbivore effector to the plant R protein. **B** Signal transduction pathway, **C** Enhanced local response, **D** Hormone production, **E** Signal transduction pathway and defensive chemical production.

The perception of the feeder starts at the surface of the leaves; in the cell wall when the herbivore lands on the plant. To induce an efficient plant response requires specific recognition of the herbivore and the consequent translation into defense signalling events (Erb & Reymond, 2019). Many specific molecules from the herbivore may activate the plant defences, not only the feeding. It has been described that the chitin

from de body of the herbivore, the feces, eggs, and silk may induce plant defences and some transcriptomic changes (Reymond, 2013; Rioja *et al.*, 2017; Queiroz *et al.*, 2020; Ojeda-Martinez *et al.*, 2021; Santamaria *et al.*, 2021).Upon sensing these molecular patterns, a defense cascade is initiated, involving various defence events such as depolarization of the plasma trans-membrane potential (Vm) associated with Ca^{2+} influx (Park & Shin, 2022), phytohormones induction, reactive oxygen or nitrogen species (ROS/RNS) burst, callose deposition, and mitogen-activated protein kinase (MAPK) activation, phytohormones synthesis and finally transcriptional activation of defence genes (Santamaria *et al.*, 2018a; Li *et al.*, 2019a).

Herbivore perception in plants involves a two-tiered innate immune system known as pattern-triggered immunity (PTI) and effector-triggered immunity (ETI) (Jones & Dangl, 2006; Yuan *et al.*, 2021; Ngou *et al.*, 2022b).

1.3.1.1 PATTERN-TRIGGERED IMMUNITY (PTI)

PTI is initiated by cell surface-localized Pattern Recognition Receptors (PRRs). PRRs can detect Herbivore-Associated Elicitors (HAEs) through the recognition of Microbe-Associated Molecular Patterns (MAMPs) **(Figure 6)**. Which may come from the endosymbiosis between phytophagous and bacteria, such as *Wolbachia* sp (Bi & Wang, 2020). Similarly, chitin, a structural component of fungal cell walls, is recognized by plant cell-surface receptors (Boutrot & Zipfel, 2017; Kutschera *et al.*, 2019) and recognized as PAMP (Pathogen -associated molecular patterns).

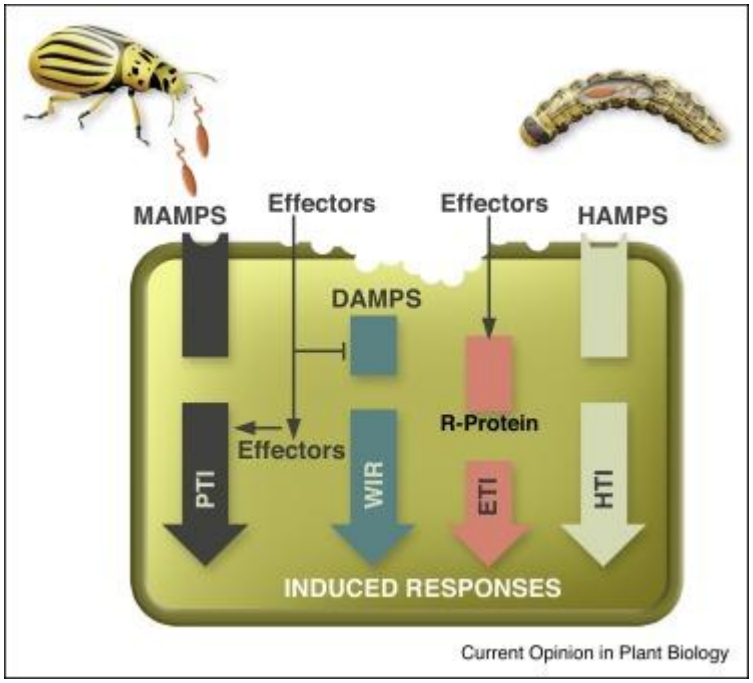

Figure 6. Model for Perception of Herbivore Feeding Cues. Microbe associated molecular patters (MAMPs); damage associated molecular patterns (DAMPs); herbivore associated molecular patterns (HAMPs); pathogen or pattern triggered immunity (PTI); wound-induced resistance (WIR); effector triggered immunity (ETI); HAMP triggered immunity (HTI). Scheme adapted from Acevedo *et al.*, 2015.

Plants can also sense Herbivore-Associated Molecular Patterns (HAMPs), with one example being the oral secretions (OS) produced by feeding insect larvae. A few chemically characterized HAMPs have been identified (Stahl *et al.*, 2018).

In addition to MAMPs from the and HAMPs, some herbivores' feeding activities may lead to the production of Damage-Associated Molecular Patterns (DAMPs). DAMPs primarily consist of cytosolic proteins, peptides, nucleotides, and amino acids released

from damaged cells or secreted by intact cells during feeding or tissue disruption caused by physical injuries, such as wounding or attacks (Hou *et al.*, 2019).

Certain herbivores have evolved the ability to evade or suppress PTI through the secretion of effector molecules, resulting in effector-triggered susceptibility (ETS). Effectors are proteins derived from herbivores that are introduced into plant cells or the apoplast, where they interfere with plant defences (Ngou *et al.*, 2022a). ETS arise from co-evolution between herbivores and plants, involving a dynamic interplay. Both plants and herbivore have developed diverse sophisticated mechanisms to adapt to each other (Wang *et al.*, 2023).

PRR) can be divided into two main groups: plasma membrane-anchored receptor-like kinases (RLKs) and receptor-like proteins (RLPs). These PRRs are primarily responsible for detecting specific molecules associated with pathogens, microbes, or damage (Boutrot & Zipfel, 2017).

In the realm of *A. thaliana*, the pioneering Plant PRR to be identified was the Receptor-Like Kinase (RLK) named FLAGELLIN SENSING 2 (FLS2). FLS2 serves as a vital detector of bacterial flagellin, specifically recognizing its distinctive 22-amino acid peptide, flg22 (Gómez-Gómez & Boller, 2000; Chinchilla *et al.*, 2007).

Subsequently, the roster of acknowledged PRRs has significantly expanded, encompassing a diverse array of RLKs and RLPs that play pivotal roles in bolstering plant immunity against herbivores. For a comprehensive overview of receptor recognition mechanisms of HAMPs derived from arthropod oral secretions or salivary glands, Eggs-Associated Molecular Patterns (EAMPs) derived from eggs, and DAMPs **(Figure 7).** Please refer to **Table 1** for further details.

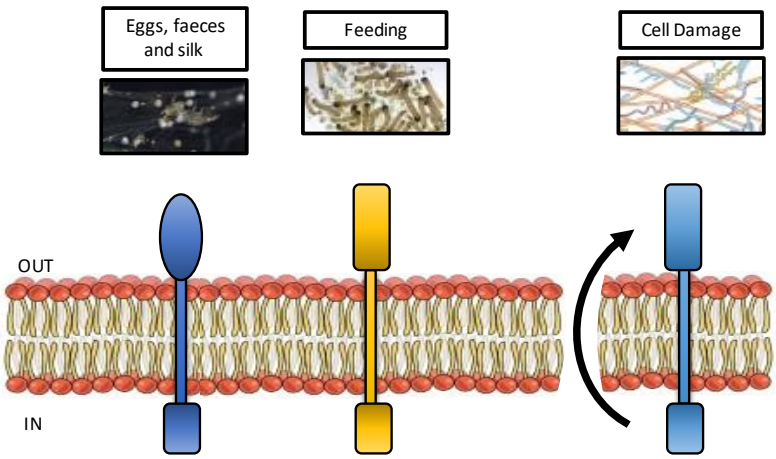

Figure 7. Pattern Recognition Receptors (PRRs) recognize specific molecular patterns associated with different herbivores. Various herbivore behaviours such as eggs, faeces, silk, feeding, or cell damage may activate PRRs.

Also, a moment of serendipity unfolded in the study of Plant PRRs with the accidental identification of the earliest DAMP as extracellular Adenosine TriPhosphate (eATP). During research into the energy utilization of stomatal movement, Fujino in 1967 chanced upon a captivating revelation. In their experimental trials, they observed that when exposed to a 10-mM eATP solution, stomata remained widely open in the light, whereas the control group showed predominantly closed stomata. This serendipitous finding provided valuable insight into the pivotal role of eATP as a DAMP and its profound impact on the regulation of stomatal behaviour.

Name	Plant	Year	References
AtPEPR1/2	Arabidopsis	2010	(Yamaguchi *et al.*, 2010)
AtWAK1	Arabidopsis	2010	(Brutus *et al.*, 2010)
LecRK1	Tobacco	2011	(Bonaventure, 2011)
SlSERK1	Tomato	2011	(Mantelin *et al.*, 2011)
NaHER1	Tobacco	2013	(Dinh *et al.*, 2013)
OsLecRK	Rice	2013	(Cheng *et al.*, 2013)
AtLecRK-I.9	Arabidopsis	2014	(Choi *et al.*, 2014)
BAK1	Arabidopsis	2014	(Prince *et al.*, 2014)
OsLecRK1/2/3	Rice	2015	(Liu *et al.*, 2015)
AtLecRK-I.8	Arabidopsis	2017	(Wang *et al.*, 2017)
SlPORK1	Tomato	2018	(Xu *et al.*, 2018)
SlSYR1	Tomato	2018	(Wang *et al.*, 2018)
OsRLK1	Rice	2018	(Hu *et al.*, 2018)
AtLecRK-VI.2	Arabidopsis	2019	(Wang *et al.*, 2019)
OsRLK2	Rice	2020	(Ye *et al.*, 2020)

GmHAK1/2	Soybean	2020	(Uemura *et al.*, 2020)
VuINR/SOBIR1	Bean	2020	(Steinbrenner *et al.*, 2020)
ZmRK	Corn	2020	(Tamiru *et al.*, 2020)
AtLecRK-I.5	Arabidopsis	2020	(Pham *et al.*, 2020)
AtHPCA1	Arabidopsis	2020	(Wu *et al.*, 2020)
AtLecRK-I.1	Arabidopsis	2021	(Groux *et al.*, 2021)
SlZRK1	Tomato	2021	(Sun *et al.*, 2021)
GLR3.3/GLR3.6	Arabidopsis	2022	(Xue *et al.*, 2022)
NaRLK1	Tobacco	2023	(Gilardoni *et al.*, 2023)

Table 1. A comprehensive overview of plant receptors and receptor recognition mechanisms of HAMPs derived from arthropod oral secretions or salivary glands, EAMPs derived from eggs, and DAMPs.

1.3.1.2 EFFECTOR-TRIGGERED IMMUNITY (ETI)

In response to recognition of effectors, plants activate the ETI response through nucleotide-binding leucine-rich repeat receptors (NLRs). NLRs are encoded by Resistance (R) genes and predominantly act as intracellular proteins sensing specific effectors.

The original model proposed by Jones & Dangl (2006) elucidated the physiological responses of the two-layered plant immune system to various pathogens through the zigzag model. The current understanding of plant immune responses suggests that PTI and ETI, once thought to be independent systems, may have interdependence, and share common signalling components. Activation of both PTI, initiated by PRRs, and ETI, initiated by NLRs, leads to similar down-stream cellular responses, such as defence-gene expression, reactive oxygen species (ROS) production, and callose deposition (Ngou *et al.*, 2022b). However, the underlying mechanisms and potential signal cooperation between cell surface and intracellular perception systems have remained elusive.

Ngou *et al.* (2021) and Yuan *et al.* (2021), investigate with pathogens the consequences of triggering ETI in the absence of PTI. In the first study, a stradiol-inducible effector protein was used to trigger ETI, while the second study employed a genetic approach to knock out cell surface receptors and co-receptors involved in PTI. Both papers reveal that neither PTI nor ETI alone confers complete immunity. Instead, the interactions between these two immune systems result in synergistic effects, leading to enhanced plant defense responses.

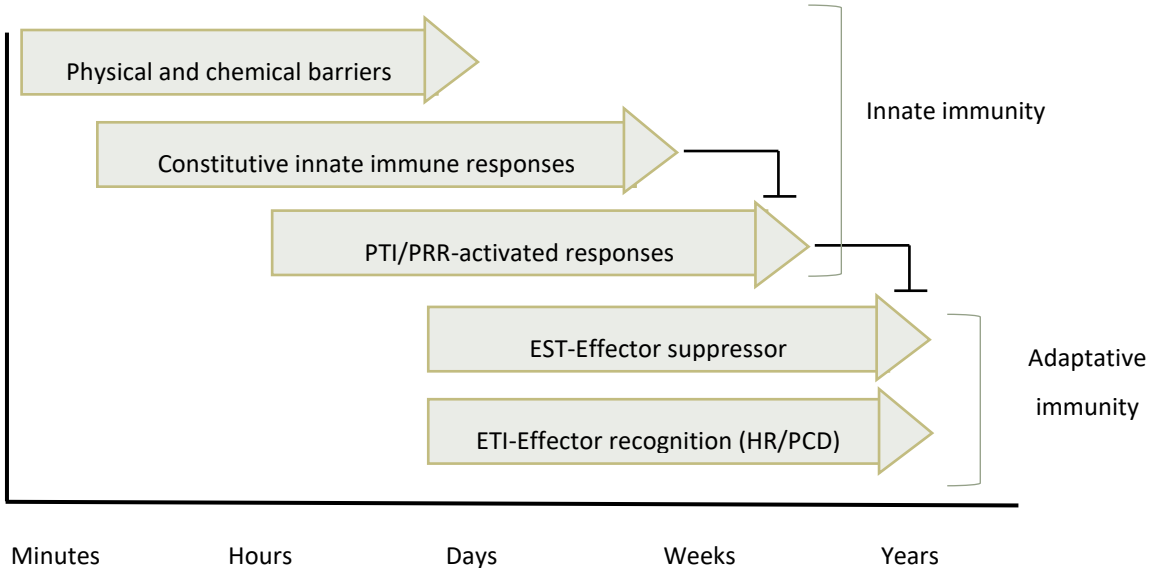

Figure 8. Scheme of plant immunity induction and evolution among the time. As first layer of immunity herbivores find the physical and chemical barriers followed by the constitutive immune responses. Within few min of activation since the herbivore arrive the PTI thorough the PRRs are induced. All together this forms the innate immunity of the plant. The adaptative immunity starts later, after the effector suppressor immunity which activates the ETI.

1.3.1.2.1 NUCLEOTIDE-BINDING LEUCINE-RICH REPEAT RECEPTORS (NLRS)

NLRs play a crucial role in recognizing non-conserved effectors derived from various biotic stresses (Dangl & Jones, 2001). Upon detecting these effectors, NLRs trigger shared responses with PTI, including the accumulation of ROS, activation of MAPK cascades, and defence gene expression. Additionally, NLR activation leads to localized programmed cell death, known as the hypersensitive response (HR).

The specific activation mechanism governing the interaction between sensor NLRs and helper NLRs remains a subject of active inquiry. However, the presence of shared domains and compelling evidence of a common evolutionary lineage give rise to the hypothesis that multimerization, facilitated by the NB-ARC domain subsequent to ADP-to-ATP exchange, and plays a central role in NLR activation. It has been observed that over-expressing the coiled-coil (CC) or Toll/Interleukin-1 receptor (TIR) domain alone is adequate to reproduce pathogen-induced immune responses similar to those observed with full-length NLRs (Baudin *et al.*, 2017).

NLRs are categorized into three classes based on their N-terminal domains: coiled-coil (CC) NLRs (CNLs), Toll/Interleukin-1 receptor/Resistance (TIR) protein NLRs (TNLs), and RPW8-like CC domain (RPW8) NLRs (RNLs), with both CNLs and RNLs possessing N-terminal CC-domains (Ngou *et al.*, 2022b). Some atypical NLRs also exist, featuring additional integrated domains (IDs) that mimic pathogen targets and are reactivated in response to modification by the effectors (Ji *et al.*, 2020; Zhang *et al.*, 2020).

The functionality of NLRs can be divided into two distinct groups depending on their interactions with effectors, either direct or indirect. NLRs that engage in direct interactions with effectors are classified as sensor NLRs (sNLRs), while those that participate in the recognition of immune signal outputs at the downstream level are referred to as helper NLRs (hNLRs) (Jubic *et al.*, 2019).

The functionality of sensor NLRs, including Toll/Interleukin-1 receptor/Resistance (TIR) NLRs (TNLs) and coiled-coil NLRs (CNLs), involves their ability to interact with effectors

either directly or indirectly. In certain instances, plant NLRs recognize effectors through protein-protein interactions. The recognition of pathogen effectors typically involves the C-terminal leucine-rich repeat (LRR) domain, leading to the oligomerization of plant NLRs and the formation of large NLR-containing complexes known as resistosomes (Ma *et al.*, 2020; Martin *et al.*, 2020; Förderer *et al.*, 2022).

In the case of CNL resistosomes, exemplified by ZAR1 in Arabidopsis, they function as Ca^{2+}-permeable influx channels (Bi *et al.*, 2021). On the other hand, TNL resistosomes possess nicotinamide adenine dinucleotide (NAD) nucleosidase (NADase) activity encoded in their N-terminal TIR domains (Ma *et al.*, 2020; Martin *et al.*, 2020).

Resistosomes, characterized by their oligomerization, play a significant role as a common signalling mechanism mediated by NLRs (Duxbury *et al.*, 2021). Additionally, recent research has proposed that NLRs may also function as a new type of Ca^{2+}-permeable cation channels associated with resistosomes. Conversely, specific Ca^{2+}-transporting membrane proteins, such as Ca^{2+}-ATPase and $Ca^{2+/H+}$ exchangers, are involved in Ca^{2+} efflux to maintain cellular Ca^{2+} homeostasis by removing excessive cytoplasmic Ca^{2+} concentrations $[Ca^{2+}]$cyt in response to external and internal stimuli (Park & Shin, 2022). These interconnected mechanisms highlight the complex regulatory network underlying NLR-mediated immune responses.

There is another class known as singleton NLRs, which possess the ability to recognize effectors and initiate downstream signalling. Notably, some well-known examples of helper NLRs (hNLRs) within this category include ACTIVATED DISEASE RESISTANCE 1 (ADR1) and N REQUIREMENT GENE 1 (NRG1) (Lapin *et al.*, 2019; Li *et al.*, 2019b).

Among singleton NLRs, representative members include the Arabidopsis coiled-coil NLRs (CNLs) RESISTANCE TO P. SYRINGAE PV MACULICOLA 1 (RPM1) (Grant *et al.*, 1995) and HOPZ-ACTIVATED RESISTANCE 1 (ZAR1) (Lewis *et al.*, 2010; Sarris *et al.*, 2015). These singleton NLRs demonstrate the ability to both recognize effectors and activate downstream immune responses.

Interestingly, certain cases of effector recognition necessitate the presence of two genetically linked NLRs, referred to as paired NLRs. An example of such paired NLRs in Arabidopsis is the TNL pair RESISTANCE TO RALSTONIA SOLANACEARUM 1 (RRS1) and RESISTANT TO P. SYRINGAE 4 (RPS4) (Le Roux *et al.*, 2015; Sarris *et al.*, 2015). The existence of these paired NLRs further adds to the complexity and diversity of NLR-mediated recognition and immune signalling in plants.

The activation mechanism governing the interplay between sensor NLRs and helper NLRs remains an active area of investigation in the field of immunology. The presence of shared domains and compelling evidence of a common evolutionary origin suggest that a crucial step in NLR activation involves the multimerization process. Notably, experiments involving over-expression CC or TIR domain alone have demonstrated the ability to replicate induced immune responses observed with full-length NLRs (Baudin *et al.*, 2017). This intriguing observation has led to the characterization of NLRs as molecular switches within the intricate immune signalling pathways (Adachi *et al.*, 2019). Moreover, proper control of NLR homeostasis is vital for their optimal function. Over-accumulation of NLRs can result in autoimmunity, whereas insufficient levels may render the host susceptible to specific pathogens. An illustrative example is the increased accumulation of the TNL protein Suppressor of *npr1*, constitutive 1 (SNC1), which triggers a constitutive defense response and causes dwarfism (Cheng *et al.*, 2011).

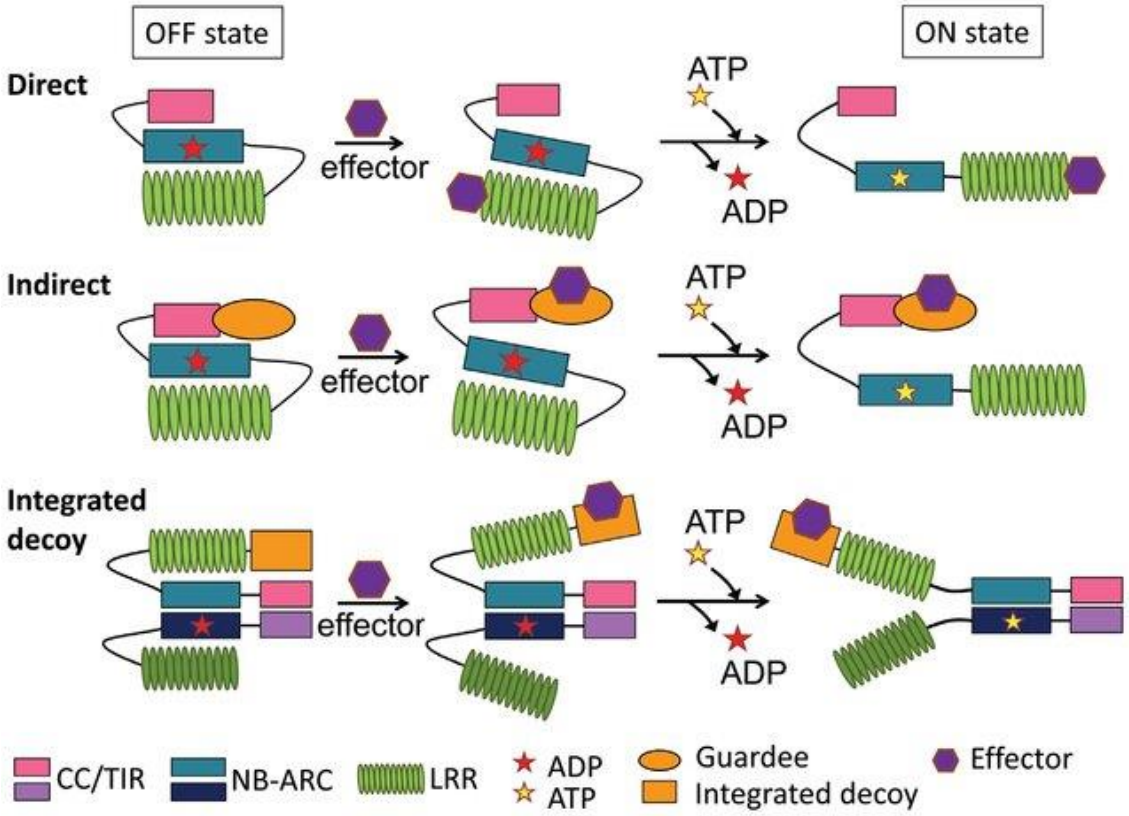

Figure 9. Models of NLR activation. Direct and indirect recognition of the effector. Integrated TNL Decoys Model extracted from Chiang and Coaker *et al*., (2015).

1.3.1.2.1.1 TIR DOMAINS IN PLANT DEFENCE

TIR domains are found across bacterial, mammalian, and plant immune systems. Most of the characterized TIR-domain proteins have functions associated with the immune system. In plants, TIR domains provide a signalling role for one of three major classes of NLRs–TIR-NLRs.

In Arabidopsis, the TIR domain is remarkably diverse, occurring in 53 distinct domain architectures as evidenced by Van de Weyer *et al.*, (2019). In Arabidopsis, these genes are rapidly induced upon encountering various PAMPs/HAMPs and upon the recognition of effectors by NLRs (López-Márquez *et al.*, 2021; Ngou *et al.*, 2021a; Yuan *et al.*, 2021).

Investigations have demonstrated that mutations affecting the catalytic glutamate residue disrupt TNL and TIR mediated immunity and cell death (Ma *et al.*, 2020; Martin *et al.*, 2020). This evidence indicates the indispensability of NADase activity in facilitating signalling processes associated with TNL and TIR domains in plants.

In this landscape the purpose of TNL domain in plant defence will remain in different aspects. First, TNL ETI provides protection and enhances immune signalling in response to PAMPs/ HAMPs. This is achieved, in part, by augmenting the triggered ROS burst, particularly observed in studies involving the TNL receptor pair RRS1-RPS4 (Ngou *et al.*, 2021a). The potentiation of ETI results in sustained accumulation of apoplastic ROS, surpassing levels induced by PTI or ETI alone upon PAMP/HAMP recognition.

Second, effectors may have the ability to target and manipulate the biosynthesis and signalling pathways of salicylic acid (SA) in the plant immune system (Tanaka *et al.*, 2015). However, the RRS1-RPS4 ETI serves as a transcriptional shield, safeguarding the SA defense from interferences (Lapin *et al.*, 2019).

Third, TNL ETI plays a role in impeding pathogen growth by inducing a state of nutrient scarcity. The RRS1-RPS4 ETI, for instance, reduces photosynthetic activity and the expression of photosynthesis-related genes (Su *et al.*, 2018; Griebel *et al.*, 2022). This physiological adjustment leads to the accumulation of ROS in chloroplasts and

subsequent cell death in Arabidopsis leaf cells (Su *et al.*, 2018), a characteristic feature of NLR ETI (Monteiro & Nishimura, 2018).

Overall, while significant strides have been made in comprehending the molecular mechanisms underpinning TNL-associated immunity, numerous gaps in the mechanistic models persist, warranting further exploration and investigation.

1.4 REGULATION OF DEFENCE SIGNALLING

1.4.1 SMALL REACTIVE MOLECULES ROS/RNS/RSS

When plants are subjected to stress, plants exhibit a common cellular reaction characterized by the rapid generation of unstable free radicals known as "reactive species" (Kaur *et al.*, 2019). Among these reactive species, ROS have been extensively studied. However, recent research has identified other types of reactive species involved in plant responses to biotic stress (Zhou *et al*., 2022). This new category includes RNS as investigated by Moreau *et al.*, (2010), reactive carbonyl species (RCS) as studied by Mano *et al.*, (2019), and reactive sulphur species (RSS) as explored by Giles *et al.*, (2017).

ROS are reactive chemicals that arise due to the incomplete reduction of molecular oxygen. These species are characterized by a short half-life and display high reactivity (Zhou *et al*., 2022).

In herbivore infestation, it has been shown that the brown marmorated stink bug, *Halyomorpha halys*, exhibits a significant increase in ROS generation within three minutes of feeding. The authors observed this response when examining the potato photosystem II (PSII) photochemistry in the feeding area (Sperdouli *et al.*, 2022).

On the other hand, NO as a gaseous molecule, NO exhibits the remarkable ability to easily diffuse across cell membranes, enabling interactions with various cellular components, as elucidated by Correa-Aragunde *et al.*, (2015).

Historically ROS and RNS were considered as toxic molecules where highest levels could provoke oxidative stress in plants leading to cellular damage and death.

However, some reports (Cejudo *et al*., 2021) show that ROS and RNS can function as signalling molecules at controlled levels, catalyzing oxidation reactions and modulating vital signalling cascades. Additionally, they play essential roles in enhancing metabolic

reactions, regulating antioxidants, crossing cellular barriers to activate signalling cascades, and providing energy to combat oxidative stress (Mittler *et al.*, 2011).

ROS and RNS also function as signalling molecules depending on the levels below a threshold by antioxidative systems, catalyzing several oxidation reactions, thereby modulating vital signalling cascades. (Mittler, 2017). In seedling leaves of pea (*Pisum sativum),* Mai *et al.*, (2014) described the convergence of NO and H_2O_2 accumulation with the induction of JA, ET, and SA, hormones that sequentially appeared within the first 24–96 h after the aphid *Acyrthosiphon pisum* feeding.

Another group of reactive species includes the reactive carbonyl and sulphur species, denoted as RCS and RSS, respectively. RSS refers to low molecular weight sulphur-containing entities, and the oxidizable sulphur present in proteins can also function as RSS. On the other hand, RCS are characterized as unsaturated aldehydes/ketones formed as a result of lipid peroxidation (Mano, 2012).

RSS induces oxidation reactions through the modification of cysteine sulphur, eliciting a response similar to that of ROS and RNS effectors. However, compared to ROS and RNS, the reactivity of RSS is more pronounced and remains stable for an extended period (Corpas *et al*., 2020). In addition, recent findings have observed the growth-stimulating impact of RSS on plant growth and development under stress conditions (Aroca *et al*., 2018). The underlying functional mechanism by which RSS exerts this stimulating effect in plants post-translational modification of cysteine residues (Cys-SSH). These modified residues, in turn, regulate the expression of stress-responsive genes and proteins (Corpas *et al.*, 2020).

Reactive species homeostasis within plant cells plays a crucial role in cellular signalling. However, excessive intra-cellular concentrations of these species can lead to cellular damage, including biomolecule degeneration, disruption of the electron transport chain, oxidative damage, cell membrane fragmentation, and cell death. The overproduction of reactive species has been established as a cause of cellular damage and programmed cell death (Mangal *et al.*, 2023). Additionally, these species are

involved in Post-Translational Modifications (PTMs), such as persulfidation, tyrosine nitration, S-nitrosylation, and carbonylation (Sánchez-Vicente *et al*., 2019; Sandalio *et al*., 2019).

Furthermore, a complex interplay exists among these reactive species during stress interactions, wherein they can act synergistically or antagonistically to regulate various physiological and metabolic processes under specific environmental conditions. These species also regulate gene expression, with NO signalling playing a significant role in controlling stomatal movement by regulating the expression of *SNF-1* and *SnRK2.6* genes (Wang *et al*., 2015; Prakash *et al.*, 2019).

Overall, maintaining reactive species homeostasis is essential for proper cellular functioning in plant cells, as these species have dual roles in cellular signalling and damage induction. Understanding their interplay and regulatory mechanisms is crucial for comprehending their impact on plant physiology and cellular responses.

1.4.2 PHYTOHORMONES

Plant hormones, also known as phytohormones, play crucial roles in various processes, such as plant growth, developmental processes, and plant responses to abiotic and biotic stresses. These hormones include Jasmonic Acid (JA), Salicylic Acid (SA), Gibberellin (GA), Auxin (indole-3-acetic acid, IAA), Cytokinin (CK), Brassinosteroids (BRs), abscisic acid (ABA), ethylene (ET), and strigolactone (SL) (Yang *et al*., 2019).

In the case of biotic stress, particularly herbivores, plants recognize specific HAMPs and DAMPs that trigger early warning cues leading to transcriptional reprogramming and the induction of signal transduction pathways, regulated by a complex hormonal crosstalk (Santamaria *et al.*, 2018a; Stahl *et al.*, 2018; Erb & Reymond, 2019). In this process, the interplay of multiple plant hormone signalling pathways regulates the delicate balance between plant growth and defence (Garcia *et al*., 2021a).

In comparison to pathogens, insects are highly complex multicellular organisms with various lifestyles and behavioural patterns (Erb *et al.*, 2012). The first contact with the herbivore often occurs at the leaf surface when the tarsi of an arriving insect touch the leaf surface. Landing and walking on a plant will exert pressure, break trichomes, and deposit chemicals from tarsal pads on the leaf (Hilker & Meiners, 2010).

Mechanostimulation by repeated touching is sufficient to induce the accumulation of JA (Tretner *et al*., 2008). Some herbivory disrupts the integrity of plant tissue, and many plant defence responses can be triggered by mechanical wounding alone (Mithöfer *et al., 2005)*. Generally, jasmonates and/or SA are the main regulators of induced defences These phytohormones together with the ethylene are considered the defensive hormonal core (Santamaria *et al.*, 2020).

1.4.2.1 JASMONIC ACID (JA)

JA and Jasmonates, are fatty acid derivatives synthesized through the octadecanoid acid pathway, originate in the plastids through the oxygenation of linolenic acid, forming allene oxide intermediates that eventually convert into 12-oxo-phytodienoic acid (OPDA). This OPDA is transported to peroxisomes, where it transforms into JA before being released into the cytosol for further modifications (Wasternack & Hause, 2013; Yang *et al.*, 2019).

Upon activation through the conjugation of the Ile amino acid residue by JASMONIC ACID RESPONSE 1 (JAR1), JA transforms into its most bioactive form, jasmonoyl-isoleucine (JA-Ile). Both JA and JA-Ile play vital roles in numerous physiological events, particularly in enhancing plant defences against chewing insects, mites, and necrotrophic pathogens (Pieterse *et al.*, 2012; Yang *et al.*, 2019).

The rapid accumulation of JA/JA-Ile in response to these pests initiates the JA signalling cascade, causing transcriptional activation of transcription factors (TF) as MYC which activate defences responses. (Erb & Reymond, 2019; Marquis *et al.*, 2022).

In tomato, the receptor-like cytoplasmic kinase, SlZRK1, acts as a negative regulator in wound-induced JA accumulation and *Helicoverpa armigera,* a lepidopteran larvae resistance. The loss of SlZRK1 significantly altered the expression of genes involved in JA and SA biosynthesis, salicylic acid biosynthesis (Sun *et al.*, 2021). Moreover, *Ectropis obliqua*, one of the most common lepidopteran pests of the tea plant in China, is capable of producing volatile compounds that induce JA accumulation and thus promote resistance of neighbouring intact plants to herbivorous (Jing *et al*., 2021).

During many years JA/JA-Ile signalling has been the focus of attention of many studies associated with plant defence to pests, but the involvement of JA-derivatives remains largely uncharacterised. JA compounds may undergo methylation, hydroxylation, carboxylation and sulfation, among other modifications, to generate active, inactive or partially active derivatives (Wang *et al*., 2021). Thus, JA can be methylated by the action

of methyl transferases to form JA methyl ester (Me-JA), a volatile organic compound with a signalling role in plant defence systems which is often used to produce a protective reaction in plants (Yu *et al.*, 2019).

1.4.2.2 SALICILIC ACID (SA)

SA is a vital plant hormone that plays a significant role in regulating plant defense mechanisms (Erb *et al.*, 2012; Erb & Reymond, 2019). Additionally, SA influences plant growth and development (Rivas-San Vicente & Plasencia, 2011).

SA can be synthesized through two pathways: isochorismate synthase (ICS) and phenylalanine ammonia-lyase (PAL), (Zhang & Li, 2019). Once SA is formed, it binds to a specific receptor known as non-expressor *of* PR gene 1 (NPR1) (Wu *et al.*, 2012). NPR1 gene activation occurs through redox pathways triggered by SA accumulation, leading to its translocation to the nucleus. However, instead of binding directly to DNA, NPR1 acts through transcription factors (Pieterse & Van Loon, 2004).

In terms of herbivores plant defense, SA is more effective against piercing and sucking insect pests than chewing ones, enhancing both local and systemic plant defense. SA induces the production of ROS. Additionally, SA triggers the release of plant volatiles, attracting natural enemies of insect pests. SA and JA have antagonistic effects, with SA inhibiting JA's activity, and vice versa. Methyl salicylate (MeSA) serves as a volatile signal, inducing plant defences and attracting predaceous arthropods (Erb *et al.*, 2012; Erb & Reymond, 2019; Zhang & Li, 2019).

1.4.2.3 ETHYLENE (ET)

ET is a vital phytohormone in plant defense against insects. It plays a key role in inducing both direct and indirect plant defense responses. Ethylene interacts with JA in regulating

defense against pathogens and herbivorous insects (van Loon *et al.*, 2006; Pattyn *et al.*, 2021). It induces the emission of various volatiles during infestation and enhances volatile release from JA-treated leaves (Ruther & Kleier, 2005).

1.4.2.4 OTHER HORMONES

In the defense process against herbivores, besides SA–JA–ET crosstalk, other hormones like ABA, IAA, GB, CK, and BR have been less explored as potential factors that may influence herbivore resistance (Erb *et al.*, 2012).

ABA is a stress hormone that accumulates in response to various abiotic and biotic stresses. It serves as a key regulator of stomatal aperture, controlling gas exchange for transpiration, photosynthesis, and responses to environmental stimuli (Kuromori *et al.*, 2018a). ABA is induced by different environmental factors, such as drought, salt, and wounding (Gilroy & Breen, 2022).

Studies with herbivores have demonstrated that both chewing and piercing-sucking arthropod pests trigger water loss, leading to ABA accumulation and subsequent stomatal closure (Lim *et al.*, 2015). In maize (*Zea mays*), ABA levels increase during attacks by the specialist root herbivore western corn rootworm, *Diabrotica virgifera virgifera*, (Erb *et al.*, 2009). Similarly, in Arabidopsis, ABA levels increase after induction with wounding and the oral secretions of the generalist herbivore desert locust, *Schistocerca gregaria* (Schäfer *et al.*, 2011). Additionally, ABA levels increase in the goldenrod species *Solidago altissima* after induction by the caterpillar of the tobacco budworm, *Heliothis virescens* (Tooker & de Moraes, 2011).

Auxin, specifically IAA, can independently regulate plant defense responses apart from SA and JA (Mapes & Davies, 2001). Machado *et al.*, (2016) demonstrated that *Manduca sexta* oral secretions strongly and specifically induce IAA. This rapid transcriptional increase of auxin biosynthetic YUCCA-like genes serves as a specific signal that regulates JA-dependent secondary metabolites in herbivore-attacked plants. Moreover, studies

indicate that IAA may also play a role in regulating gall formation associated with gall-feeding insects (Yamaguchi *et al.*, 2012; Grover, 2021).

For the gibberellins, studies on plants with altered GA signalling suggest its involvement in herbivore-induced defense responses. DELLA proteins, negative transcriptional regulators of GA-induced gene expression, play crucial roles in integrating plant responses to developmental and environmental stimuli. GAs competitively binds to JAZ proteins, affecting JA signalling, which leads to inhibition of MYC2 and reduced JA responses. Changes in DELLA levels impact JA biosynthesis and signalling (Erb *et al.*, 2012).

CKs play a role in the defense response of leaves during herbivore feeding. The CK status in a tissue may influence the intensity of the defense response upon herbivory perception, contributing to tissue-specific signalling responses (Ballaré, 2011).

BR have important roles in herbivore resistance. They counteract JA-mediated trichome density and defense metabolite accumulation in tomato (Campos *et al.*, 2009). BRs also repress JA-governed inhibition of root growth (Ren *et al.*, 2009). BR are perceived by BR insensitive 1 (BRI1), a leucine-rich repeat receptor-like kinase, BR signalling involves the essential role of BRI1-associated kinase 1 (BAK1). BAK1 not only interacts with BR but also with the flagellin receptor FLS2, playing a role in multiple MAMP-elicited responses (Vert, 2008).

1.4.3 TRANSCRIPTIONAL ACTIVATION AND GENE REGULATION UPON HERBIVORY

Once the herbivore is perceived, many transcriptional changes occur, and several genes can be up- or down-regulated (Mostafa *et al.*, 2022). Nowadays, numerous transcriptomic approaches have been used to study the transcriptional reprogramming of plants when herbivores feed or lay eggs (Garcia *et al.*, 2021b; Ojeda-Martinez *et al.*, 2022). Changes in gene expression profiles after herbivory have shown a substantial reallocation of plant resources to defense in different genotypes or species.

The transcriptomic reprogramming reflects the plant's response to the demand for activating its defense mechanisms (Garcia *et al.*, 2021b). After the perception and signalling gene system activation, the late genes involved in defense response are up-regulated (Santamaria *et al.*, 2021).

The complexity of gene regulation at different levels can be understood through the following studies conducted by Arnaiz *et al.*, (2019) research group. A bidirectional promoter induced by the mite *T. urticae*, which co-regulates two divergent genes, At5g10300 and At5g10290. These genes are also induced during pest feeding (Arnaiz *et al.*, 2023).

In herbivores, the transcriptomic reprogramming is predominantly coordinated by the differential regulation of TF and the crosstalk between the JA, ET, and SA hormones. Changes in the expression of TFs lead to shifts in the accumulation of defensive proteins and enzymes involved in secondary metabolite biosynthesis including chitinases, cysteine proteases, and lectins. This compounds may exert toxic or anti-nutritional effects acting as bioactive toxic compounds or volatiles that attract natural enemies of herbivores (Erb & Reymond, 2019).

The JA pathway responds to chewing-biting herbivores and cell-content feeders, while the SA pathway combats piercing-sucking insects. Key TF families in innate immunity are AP2/ERF, bHLH, MYB, NAC, WRKY, and bZIP (Ng *et al.*, 2018). SA signalling leads to the translocation of NPR1 to the nucleus, where it interacts with TGA bZIP family members

to activate SA-responsive genes (Fan & Dong, 2002). The ERF-branch is regulated by the ET-signalling pathway and activates genes controlled by AP2/ERF TFs ORA59 and ERF1 (Lorenzo *et al.*, 2003). Overall, this general basal induction of specific pathways suggests that there are common plant responses that are modulated during herbivore activity.

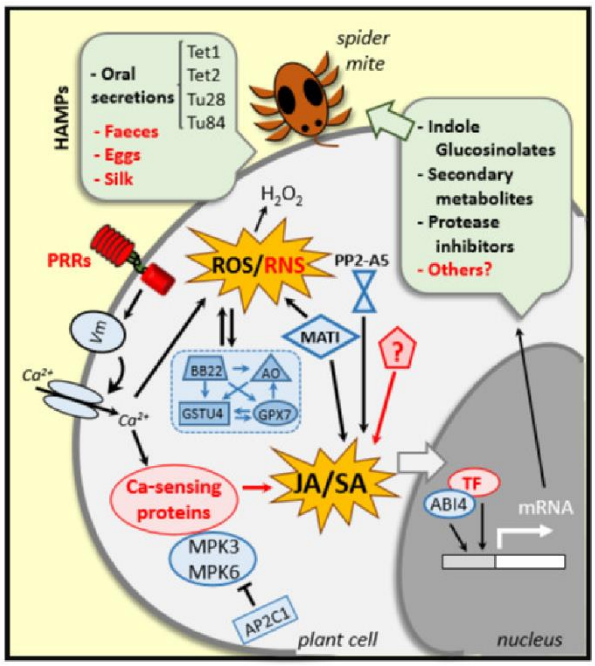

Figure 10: Plant event in responses to *T. urticae* infestation. Specific plant receptors (PRRs) recognize elicitors/effectors (HAMPs) derived from either the plant or the spider mite that induce alterations in the membrane potential (Vm), cytosolic Ca^{2+} influxes and ROS/RNS burst. Ca^{2+}-sensing proteins, MPKs and phosphatases (APC21) participate in the defense transduction pathway. H2O2 content is highly regulated by ROS-related enzymes (BB22, AO, GSTU and CPX7). Besides, *T. urticae* genes related such as MATI, PP2A5 participate in the tight regulation of the hormonal crosstalk, mainly in the Jasmonic Acid/Salicylic Acid balance. All together plus some transcription factors (ABI4 and other unknown TFs) regulate the induction of the synthesis of a battery of defense molecules. Scheme extracted from Santamaria *et al.*, 2020.

1.4.4 POST-TRANSCRIPTIONAL REGULATION: SMALL RNAS

After herbivore infestation, plants rapidly regulate gene expression to adapt to stresses. Gene expression is controlled at both transcriptional and post-transcriptional levels to fine-tune protein production. Post-transcriptional regulations involve mRNA processing (capping, splicing, and polyadenylation), mRNA stability, and translation (Floris *et al.*, 2009).

Recent studies have shown that NLRs remain inactive through intramolecular associations until effector recognition (Cesari, 2018). NLR activation requires tight control, as many NLRs are involved in trade-offs between disease resistance, growth, and response to abiotic stresses (Ariga *et al.*, 2017; Karasov *et al.*, 2017). Mis-regulated activation can lead to severe growth suppression and autoimmunity (Shirano *et al.*, 2002). NLR protein production is regulated at the transcriptional, post-transcriptional, translational, and post-translational levels (Wu *et al.*, 2017; Lai & Eulgem, 2018).

Specifically, TNL gene expression is precisely regulated by microRNAs (miRNAs) to avoid excessive activation and limit the costs of plant resistance (López-Márquez *et al.*, 2021).

miRNAs are short endogenous non-coding RNAs, approximately 21-22 nt long, originating from single-stranded MIRNA precursors (primary miRNAs) folded into hairpin stem-loop structures. These small RNAs (sRNA) can repress target gene expression by directly cleaving messenger RNAs through base pairing (Yu *et al.*, 2017). The primary miRNAs are processed by the RNAse III DICER-like1 (DCL1) into miRNA-miRNA* duplexes, which are then transported from the nucleus to the cytoplasm and loaded into ARGONAUTE (AGO) proteins, forming a functional RNA-Induced Silencing Complex (RISC). Consequently, mature miRNAs trigger transcriptional gene silencing or translational inhibition.

The expression profile of herbivore-responsive miRNAs in resistant and susceptible crop varieties after infestation has revealed a significant number of differentially expressed miRNAs in response to herbivory. Moreover, miRNA-targeted genes associated with

defense pathways have been found in resistant plants, consistent with their regulatory role in responding to plant feeders (Han *et al.*, 2022; Malhotra *et al.*, 2022). Characterizing specific miRNAs in particular plant-herbivore contexts has provided deeper insights into miRNA modulation in defences. For example, miR156, a master plant ontology regulator, was silenced in rice, conferring resistance to the brown planthopper *Nilaparvata lugens*. Molecular analysis of down-regulated miR156 rice plants showed alterations in the expression of genes involved in JA signalling, along with a reduction in JA and JA-Ile levels, indicating its negative regulatory role in *N. lugens* resistance by increasing jasmonates (Ge *et al.*, 2018). Similarly, sweet potato plants over-expressing miR408 displayed reduced resistance to *Spodoptera litura* feeding, with certain putative miR408-target genes repressed, including IbKCS, a gene involved in cuticular wax synthesis acting as a barrier against insects. *S. litura* larvae fed on IbKCS-over-expressing tobacco plants weighed less than those fed on control plants, demonstrating the coordination between miR408 modulation and IbKCS function (Kuo *et al.*, 2019). Very recently, Yan *et al.*, (2023) reported that sequestering alfalfa miR396 by over-expressing an artificial target mimicry form of miR396 improved resistance to the defoliator *S. litura* larvae, concomitantly increasing lignin, flavonoids, and glucosinolates. Additionally, Pradhan *et al*. (2017) silenced ten of the eleven AGOs in *Nicotiana attenuata* to clarify their roles in the plant-herbivory interplay, finding that AGO8-silenced plants were highly susceptible to *Manduca sexta* infestation due to compromised levels of defensive metabolites such as nicotine, phenolamides, and diterpenoid glycosides.

1.5 OBJECTIVES

Since plant defence events are orchestrated by complex and dynamic networks that respond to various input signals, it is required a fine-tune regulatory control of this multifaceted process, to be efficient and to limit costs of resistance. The main goal of this doctoral thesis is:

To identify and characterize some of the multiple regulatory elements involved in the Arabidopsis plant's defense during herbivore infestation.

This main objective has been approached through the following specific objectives:

1-. To review how NO (Nitric Oxide) involved in the redox homeostasis and molecules related to the NO metabolic pathways, contribute to modulate the plant defences against phytophagous arthropods, particularly to insects and acari.

2- To assess the role of the JA (Jasmonic Acid) catabolism to balance JA and JA-Ile accumulation, as a way of controlling the synthesis of defensive metabolites against *T. urticae*.

3- To investigate the relationship between the stomata aperture and ABA (Abscisic Acid) content within the plant-mite context since stomata are entry gates of mite stylets for getting nutrients.

4- To improve our comprehension on microRNA-mediated regulation of ETI process in the plant-herbivory interplay. For this purpose, the study is focused on the Arabidopsis miR825-5p involved in modulating NLS receptors using Pieris brassicae and Tetranychus urticae as chewing and sucking feeders, respectively.

2 MATERIALS AND METHODS

2.1 PLANT GROWTH CONDITIONS

2.1.1 ARABIDOPSIS THALIANA

A. thaliana ecotype Col-0, from Nottingham Arabidopsis Seed Collection (NASC; http://arabidopsis.info/BasicForm/), was used in all experiments as wild-type (WT). Different *A. thaliana* mutant lines have been obtained from different collections, seed banks and specific world-wide laboratories as mentioned in **Table 2.**

All Arabidopsis seeds were surface sterilized with 70% ethanol for 2 min, incubated in a solution containing 5 % SDS and 5 % NaCl for 10 min, and finally washed with sterilized deionized distilled H_2O. Seeds were planted in peat moss and vermiculite (3:2) and stratified in the dark at 4 °C for 5 d. Plants were grown in growth chambers (ARALAB mod FITOCLIMA D1.200PLH-LED and Sanyo MLR-351-H, Sanyo, Japan) under controlled conditions (23 °C ± 1 °C, > 70 % relative humidity, and a 16 h/8 h day/night photoperiod) for approximately 2 weeks. The growth chamber includes a light control program to mimic sunrise and sunset conditions. Seed used for each result chapter are shown in **Table 2**.

Seed name	Source	Purpose	Results chapter
jao2-1 (Salk_206337)	NASC	JAO2 single T-DNA mutant plants	2
jao2-2 (GABIKAT_870C04)	NASC		
jaoT	(Marquis *et al.*, 2022)	jao2-1 jao3-1 jao4-2 (jaoT) triple mutant plants	
nlsABACUS2-400n	(Rowe *et al.*, 2023)	Plants expressing nuclear localized ABA FRET biosensors (nlsABACUS2-400n)	3
aba2-1	(Gonzalez-Guzman *et al.*, 2012)	ABA biosynthesis mutant plants	
cyp707a1cyp707a3	(Okamoto *et al.*, 2009)	ABA catabolism mutant plants	
pyr1pyl1pyl2pyl4pyl5 pyl8 (hereafter *112458*)	(Gonzalez-Guzman *et al.,* 2012)	ABA insensitive plants	
ost1-3 (SALK_008068)	NASC		
epf1epf2	(Hara *et al.*, 2009)	Stomata density mutant plants	
EPF2OE	(Hunt *et al.*, 2010)		
mrt1-1 (SALK_141149)	NASC	MRT1 single mutants' plants	4

mrt1-2 (SALK_112450)			
mrt2-1 (SALK_050251)		MRT2 single mutants' plants	
mrt2-2 (SALK_040476C)			
mrt1-mrt2 #1	Crossed	MRT1 and MRT2 double mutant plants	
mrt1-mrt2 #1			
STTM825-5p#3	(López-Márquez *et al.*, 2021)	miR825-5p KD plants	
STTM825-5p#4			
amiR825-5p#3		miR825-5p OE plants	
amiR825-5p#12			

Table 2. Seed used for each result chapter.

2.1.2 NICOTIANA BENTHAMIANA

N. benthamiana plants were grown at the CBGP greenhouse facilities under controlled conditions under controlled conditions (23 °C ± 1 °C, > 70 % relative humidity, and a 16 h/8 h day/night photoperiod).

2.2 PLANTS PRETREATMENTS

Exogenous treatments were done on the aerial part of the plant by spraying with 1 mM SA, 1 mM JA, 10 µM ABA or 1 µM Fusicoccin (FC) (all from Sigma) dissolved in absolute ethanol. After 3 h treatment, mite infestation or stomata leaf impressions were performed.

2.3PEST MAINTENANCE

2.3.1 TETRANYCHUS URTICAE

T. urticae London strain (Acari: Tetranychidae) population, provided by Dr. Miodrag Grbic (UWO, Canada), was reared on *Phaseolus vulgaris* (beans) and maintained in growth chambers (Sanyo MLR-351-H, Sanyo, Japan) at 25°C±1°C, >70% relative humidity and a 16 h/8 h day/night photoperiod. Mite infestation was performed in 3-week-old Arabidopsis rosettes or leaf discs with 20 mites/plant or with 10 mites/leaf, adapting the infestation time according to the experiment. For leaf infestation assays, leaf number 5 or 6 were selected (Merchant & Pajerowska-Mukhtar, 2015), placed on a one-half-strength Murashige and Skoog (MS) (Duchefa Biochemie) medium plates, infested, and covered but ventilated with a relative humidity of 60-80%.

2.3.2 PIERIS BRASSICAE

A *P. brassicae* colony supplied by Lombrices California and maintained on growth chambers (Sanyo MLR-351-H, Sanyo, Japan) at (Sanyo MLR-351-H, Sanyo, Japan) at

25°C±1°C, >70% relative humidity and a 16 h/8 h day/night photoperiod. Freshly hatched caterpillars were placed in 3-week-old Arabidopsis rosettes with five caterpillars per plant or two caterpillars per disc adapting the infestation time according to the experiment.

2.4 PLANT DAMAGE AND PHENOTYPIC ASSAYS

2.4.1 CHLOROTIC DAMAGE

Adult *T. urticae* females fed on the Arabidopsis plants for 4 days (d). Plants were then collected, and foliar area was scanned using a conventional scanner (HP Scanjet 5590 Digital Flatbed Scanner series). Leaf area of each rosette and the damaged portion (in mm^2) was measured using Adobe Photoshop CS software and analysed using Ilastik and Fiji essentially as described by (Ojeda-Martinez *et al.*, 2020). Nine biological replicates from independent rosettes were assayed for each genotype.

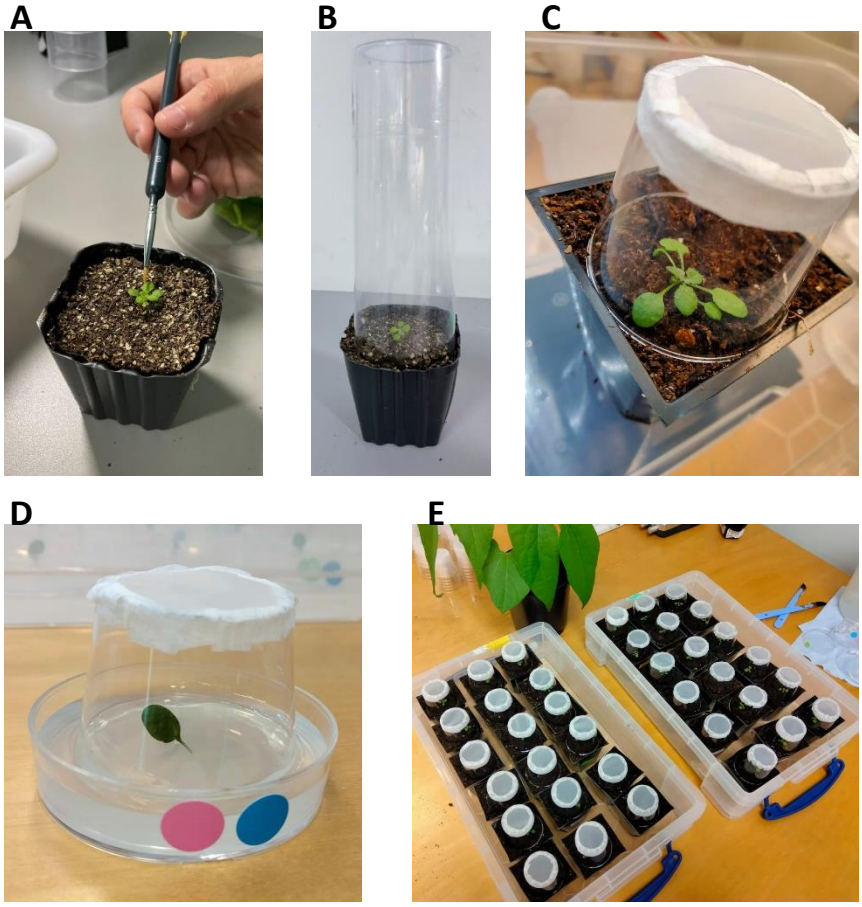

Figure 11. The experimental setup systems utilized for spider mite plant experiments. A Plants infested individually by spider mites using a brush. **B, C** final experimental set up in hole Arabidopsis rosette. **D** experimental set up for detached leaf. **E** trays with water for the plants to prevent contamination between treatments.

2.4.2 *P. BRASSICAE* DISC AREA DETERMINATION

To assess the feeding activity of *P. brassicae* larvae, the extent of unconsumed leaf area on the disc was measured following an 8-hour feeding period. Each disc's area was captured through scanning using a conventional scanner (HP Scanjet 5590 Digital Flatbed Scanner series). The leaf area of individual rosettes was also quantified. For each genotype, nine biological replicates derived from independent rosettes were included in the assay.

2.4.3 H_2O_2 DETERMINATION

H_2O_2 accumulation and callose deposition were determined in 9 mm discs of Arabidopsis plants, after 24 h of being infested with 10 mites per disc. Reactive oxygen species production was quantified using 3,3-diaminobenzidine tetrachloride hydrate (DAB) as a substrate (Sigma-Aldrich) as described Martinez de Ilarduya *et al.*, (2003)

2.4.4 CALLOSE QUANTIFICATION

To observe callose deposition, leaves were incubated in 95 % (V/V) ethanol and stained with aniline blue according to Sánchez-Vallet *et al.*, (2012). Ten biological replicates (discs) from independent rosettes were assayed for each genotype. Discs were mounted on slides with glycerol and observed with a Leica MZ10F epifluorescence stereoscope using UV filters (Leica MZ10F). Pixel quantification of callose was performed using Adobe Photoshop.

2.4.5 CELL DEATH QUANTIFICATION

Cell death quantification was performed by trypan blue staining (Sigma) after 16 or 24 h of infestation in light and dark conditions. Leaf discs (0.8 cm diameter each) were

boiled in trypan blue solution followed by a clarification process with 2.5 g/ml of chloral hydrate (Sigma) solution Sanchez-Vallet *et al.*, (2010). Discs were placed onto glass slides in 50% (V/V) glycerol and observed under an epifluorescence stereoscope using UV filters. Quantification was performed with Pixel quantification was performed using Adobe Photoshop (Luna *et al.*, 2012).

2.4.6 ELECTROLYTE LEAKAGE

We determined electrolyte leakage in 0.8 cm diameter leaf discs after 24 h of mite infestation. Mites and eggs were removed, discs washed with 10 mL ultrapure water, and dried. Next, the samples were shaken in 10 ml ultrapure water for 3 h at 25°C. Conductivity (L1) was measured with an MPC227 meter (Mettler Toledo, Switzerland). After heating at 95°C for 20 min, the final conductivity (L2) was measured. Electrolyte leakage (EL) was calculated as EL (%) = (L1/L2) * 100.

2.4.7 STOMATA LEAF IMPRESSION AND APERTURE QUANTIFICATION

Stomata leaf impressions were done using detached leaves, either treated and/or mite infested (after a previous mite removing). Leaves were pressed on fast-setting dental resin AquasilUltra+ (Dentsply Sirona) which was allowed to set, then leaf material was removed. Transparent nail polish was spread onto the resin pieces (Wang *et al.*, 2006) . After they had thoroughly dried, nail varnish impressions were peeled using Sellotape and affixed to a glass microscope slide. These slides were then imaged on a Leica DM1000 LED with an ICC50 W camera. Stomatal density and aperture were quantified with Fiji ImageJ software (Schindelin *et al.*, 2012).

2.4.8 THERMAL IMAGING DETERMINATION

Thermal images were obtained using a FLIR® infrared camera (FLIR-T600) equipped with a 16° lens, 24 h after infestation. To avoid changes in leaf temperature due to environmental conditions, experiments were conducted inside a walk-in growth chamber set at 25°C, 60 ± 10% relative humidity, and light intensity of 105 µmol.m−2.s−1. The camera was vertically mounted at approximately 20 cm above the set up. Images were saved as 8-bit TIFF files and pictures were analysed using ImageJ (Fiji), in which all pictures were set at constant range of temperature based on pictures of Col-0 WT control conditions, emissivity of the samples was 0.925.

2.4.9 YFP SIGNAL TRACK

Fluorescence emission of *N. benthamiana* discs after transient transformations were measured using a SpectraMax i3x (Molecular Devices) and a Perkin EnVision 2104-0010 TRF Multilabel microplate reader among time.

2.5 PEST PERFORMANCE

2.5.1 *T. URTICAE* EXPERIMENTS PERFORMANCE

Spider mite development was studied on detached leaves from 3-week-old plants. Small dishes (35 mm diameter) filled with some water and covered with Parafilm were used for these assays. The newest emerged leaf (about 1 cm long) from each plant was fit in the plate by introducing its petiole across the Parafilm to keep contact with water.

2.5.1.1 *T. URTICAE* FECUNDITY

Twelve synchronised females were used to infest each leaf, and the number of eggs laid was counted under stereoscope after 36 h of infestation according to (Arnaiz *et al.*, 2022). Six biological replicates from independent rosettes were used for each genotype.

2.5.1.2 *T. URTICAE* MORTALITY

Leaves were infested with 25 neonate larvae mites (24 h). After infestation, the plates were covered with a lid with ventilation and Parafilm to avoid possible escapes. Every day, the number of larvae becoming protonymph that died were counted to calculate developmental stages and mortality rates. Every 2 d, a new leaf from a new plant was added. Results were represented as percentages of mortality and the number of d that larva needed to become protonymph. Eight replicates from eight independent plants were used for each plant genotype.

2.5.2 *P. BRASSICAE* EXPERIMENTS PERFORMANCE

2.5.2.1 *P. BRASSICAE* LARVAE WEIGHT

Five freshly hatched neonate *P. brassicae* were placed on 3-week-old plants, allowing a continuous feeding for 24 h, in growth chambers (Sanyo MLR-351-H, Sanyo, Japan) at 25°C±1°C, >70% relative humidity and a 16 h/8 h day/night photoperiod. Afterall, larvae were removed, and each larvae weigh was measured by an analytical balance Radwag AS220 R2 PLUS.

2.6 CONFOCAL IMAGE

2.6.1 CONFOCAL MICROSCOPY AND IMAGES PROCESSING

An inverted SP8 confocal microscope (Leica) was used for biosensor imaging assays. All images were acquired as Z-stacks in 16-bit mode, with a 10X dry objective. Samples were mounted in ¼ MS, pH 5.7. Typical settings were as follows: sequential scanning was performed with excitation lasers and HYD detectors. 442 nm excitation 3-10% was used with– HYD1: 460-500 nm, 100 gain for a first acquisition to detect the donor T7edCerulean fluorescence (donor excitation, acceptor emission or DxAm). Second, 442 nm excitation 3-10% was used with HYD2 525-560 nm, 100 gain to acquire energy transfer fluorescence (donor excitation, donor emission or DxDm). Next, 514 nm excitation 5-10% was used with HYD2 525-560nm, 100 gain for a third acquisition to detect the edCitrineT7 acceptor protein fluorescence (acceptor excitation, acceptor emission or AxAm). Scan speed was set at 400, Line averaging: 2-4, Bidirectional X: on.

2.6.2 FRET CELL AND TISSUE CLASSIFICATION

The image processing for fluorescence emission ratio (DxAm/DxDm) quantification was carried out using the "FRETNATOR" tool reported by Rowe *et al.*, (2022, 2023). The AxAm images were used for segmentation of nuclei. The specific cell-type emission ratio classification was done by the FRETcelltype extension plugin. The extension was developed by using Apache Groovy and reads each series of acquisitions (Leica file format (.lif). FRETcell type uses the "FRETENATOR_Segment_and_ratio'' output, specifically the "threshold image output" and "The label map" to classify the nuclei based on the ROI shape. Cell types were defined as Vascular Bundle, Bundle Sheath, Spongy Mesophyll, Pavement and Stomata cells. The plugin provides two tables (.csv) for each image. The "Result Table" and the "Summary Table". The "Result Table" displays the number of pixels, the coordinates, and the emission ratio value for each

nucleus **(Annexed Figure 1B)**. provides information about the nuclei classification shape validation.

2.6.3 DAPI NUCLEI/DAMAGE PER CELL

To assess chlorotic damage caused by *T. urticae* in PDC from HR, we performed DAPI staining on 3-week-old leaf discs (0.8 mm diameter each) after 24 h of feeding. This method involved counting total cells using ImageJ (Fiji).

Leaf discs were stained with a DAPI solution (0.2 mg/l) and incubated for 10 min under vacuum. Afterward, the leaf discs were washed three times with distilled water. An inverted SP8 confocal microscope (Leica) was employed to count the total cells, chlorotic cells, and cells with DAPI-stained nuclei. The resulting overlapping images, saved as 8-bit TIFF files, were analyzed using ImageJ (Fiji) to calculate the ratios between DAPI nuclei and chlorotic cells.

2.7 HORMONE ANALYSIS

Plant hormones (JA, JA-Ile, 12-OPDA, SA and ABA) were determined by De Ollas *et al*., (2021). Briefly, frozen powdered plant samples (c.a. 50 mg, actual amount was recorded) were extracted in ultrapure water after spiking with 25 ng of appropriate internal standards (dihydrojasmonic acid and 13C6-SA, purchased from OlchemIm s.r.o, Olomouc, Czech Republic) with a bead beater. After centrifugation at 4 ºC and 10,000 rpm for 10 min, supernatants (1 ml) were recovered, and pH adjusted to 3.0 with a 30 % (V/V) aqueous solution of acetic acid. Acidified extracts were partitioned against an equal volume of diethyl ether and the organic layer evaporated under vacuum. The dry residue was resuspended in a 10% (V/V) aqueous methanol solution and filtered through 0.2 µm PTFE syringe filters before LC analysis (Acquity SDS, Waters Corp., USA). Sample separation was carried out in reversed phase using acetonitrile and water, both supplemented with formic acid to a concentration of 0.1% (V/V), as solvents at a flow rate of 0.3 ml/min. The column was a C18 (Luna C18 Omega Polar, 1.6 µm, 2.1 × 50 mm, Phenomenex, Torrance, USA). Analysis of eluates was carried out by tandem mass spectrometry (TQS, Micromass Ltd., UK) after electrospray ionisation (ESI). Identification of analytes was carried out in negative ESI according to their specific precursor-to-production transition (209 >59, JA; 322 >130, JA-Ile; 291 >165; 12-OPDA and 137 >93, SA). Quantitation of analytes in samples was achieved after external calibration with standard samples with known amounts of each plant hormone. Inactive forms of jasmonates and indole glucosinolates were analyzed in a non-targeted fashion using a LC/ESI-QqTOF-MS instrument (Synapt XS, Micromass Ltd., UK). Plant samples (c.a. 50 mg, actual amount was recorded) were extracted in 80% (V/V) aqueous methanol supplemented with biochanin A (1 mg/L) as internal standard by ultrasonication (10 min). After centrifugation at 4 ºC and 10,000 rpm for 10 min, supernatants were filtered through 0.2 µm PTFE syringe filters directly into amber glass vials prior to LC/MS analysis. Separation of samples was carried out as for plant hormones using the same column, solvents, and conditions. Mass chromatographic profiles were acquired in negative ESI in centroid mode using Leucine enkephalin as lockmass reference. After acquisition, all chromatograms were converted to mzXML with msconvert

(http://proteowizard.sourceforge.net/tools.shtml) and subsequently processed with xcms running under R environment 4.2.0 (https://cran.r-project.org/). Identification of metabolites was achieved by comparison of mass spectra with those available in databases (HMDB, metlin, Massbank) and literature (Bruckhoff *et al.*, 2016). Levels of metabolites were expressed as normalised values respect to internal standard area and sample weight (g) and to peak area values.

2.8 NUCLEIC ACIDS ANALYSIS

2.8.1 PLANT GENOTYPING

Genomic DNA was isolated from Arabidopsis T-DNA insertion lines and Col-0 plants. T-DNA homozygous status was validated by conventional PCR using ExTaq DNA Polymerase (Takara) and the following conditions: 3 min at 98 °C, followed by 30 cycles of 30 s at 94 °C, 40 s at 55 °C, 20 s at 72 °C, and finally 7 min at 72 °C. Primer sequences are stated in **Annexed table S1**.

2.8.2 GENE EXPRESSION ANALYSIS

Total RNA was extracted from Arabidopsis rosettes by the phenol/chloroform method, and precipitated with 8 M LiCl as described Oñate-Sánchez & Vicente-Carbajosa, (2008). Complementary DNAs (cDNAs) were synthesized from 2 µg of RNA using the Revert AidTM H Minus First Strand cDNA Synthesis Kit (Fermentas). RTqPCR was performed using LightCycler® 480 SYBR® Green I Master (Roche), a SYBR Green Detection System (Roche) and the LightCycler®480 Software release 1.5.0 SP4 (Roche). mRNA quantification was expressed as relative expression levels (2-dCt) or as fold change (2-ddCt) (Livak & Schmittgen, 2001). Arabidopsis ubiquitin 21 was used as a housekeeping control.

For miRNA expression analysis, we employed a stem-loop primer to quantify miRNAs (Varkonyi-Gasic, 2017). A pulsed reverse transcription reaction was conducted, involving steps at 16°C for 30 min, followed by 60 cycles at 30°C for 30 s, 42°C for 30 s, and 50°C for 1 min, and a final step at 85°C for 5 min (Varkonyi-Gasic, 2017). This procedure utilized the Revert Aid First Strand cDNA Synthesis Kit (Thermo Fisher Scientific, USA) along with specific miRNA primers and oligo(dT). Primer sequences can be found in **Annexed table 1**.

2.8.3 CLONING

MRT1 and MRT2 CDS fragments were amplified using conventional PCR with Phusion Hot Start II High-Fidelity PCR Master Mix (Thermo Scientific™). The PCR conditions for cDNA amplification were as follows: an initial denaturation at 98 °C for 30 s, followed by 30 reaction cycles consisting of denaturation at 98 °C for 10 s, primer annealing for 20 s, elongation at 72 °C, and a final extension at 72°C for 5 min.

Site-directed mutations of the *MRT1* and *MRT2* TIR domains were carried out using the QuikChange II XL (Agilent) site-directed mutagenesis kit, following the manufacturer's instructions. Once the desired sequences were obtained, they were cloned using NEBridge® Golden Gate Assembly in the pICH86966 backbone.

To clone artificial microRNAs, the designer WMD provides four oligonucleotide sequences (I to IV). These sequences are employed to engineer your artificial microRNA into the endogenous miR319a precursor using site-directed mutagenesis. The plasmid pRS300 and specific primer pairs for each phased secondary siRNA (phasiRNA) were used as templates for the PCRs. After obtaining the phasiRNA sequence within the pRS300 vector, it is transferred to the PBSK vector through PCR cloning with the assistance of restriction enzymes. Primers used for cloning also in **Annexed table 1**.

2.9 IN SILICO ANALYSIS

2.9.1 DEGS GENES FROM TRANSCRIPTOMIC ANALYSIS CLASSIFIED IN GENE ONTOLOGY CATEGORY

NO-related genes from an RNAseq data of *A. thaliana* in response to the spider mite *T. urticae* at different time points (0.5, 1, 3 and 24 h) of feeding (Santamaria *et al.*, 2021). Differentially expressed genes involved in NO pathway were identified and those showing a p-adjusted value < 0.05 and a log2Ratio (fold change) higher than 1 were selected. These genes were differentially expressed at least in one of the infestation times.

Gene Ontology analysis (GO) using Gene Ontology Consortium tools (http://www.geneontology.org) was performed to find related genes with NO pathway. GO selected categories passes. Then, a manually selection based on the literature, was applied. NO-associated genes are represented as a heat map, showing de row Z-score. Z-score allows the categorization of each gene by its expression level. Analysis of chosen data was conducted by Python 3.9, NumPy and Seaborn libraries. Additionally, to determine protein locations, the SUBcellular location database for Arabidopsis proteins (SUBA4: http://suba.live) were used (Hooper *et al.*, 2017). All the represented localizations have a SUBAcon score $\geq$0.5

2.9.2 CHARACTERIZATION TIR DOMAINS OF *MRT1* AND *MRT2* GENES

To assess the functional relevance of these MRT1 and MRT2 proteins, we conducted a comparative analysis of their features and sequences with Multiple sequence alignment (Muscle). The Protein domain analysis was done by PFAM and Prosite databases. Gene Ontology analysis (GO) using Gene Ontology Consortium tools (http://www.geneontology.org).

2.10 STATISTICAL ANALYSIS

Statistical analysis of the results was conducted using GraphPad Prism v9.5.0. Prior to performing the statistical analysis, we assessed the normality and homoscedasticity of the data. When the data met both assumptions, we employed a One-way ANOVA followed by Tukey's multiple comparisons test. In experiments where both Row (R) and Column (C) were simultaneously analysed, a Two-way ANOVA was performed, and Tukey's multiple comparisons test was utilized when the interaction (R × C) was significant. The T-Student test was applied to compare two data sets. For JAOs RT-qPCRs, we employed the Wald X2 test followed by the LSD test.

To assess the relationship between RNAseq and RTqPCR, we performed a Pearson Product Moment correlation test, drawing a linear trend and calculating the R2 value to evaluate the goodness of fit. Additionally, we conducted Fisher's exact test to summarize the significance levels (P values), with values indicated as follows: $P < 0.001$ (*), and $P < 0.0001$ (**) for the Gene Ontology (GO) biological function analysis, all of which were related to RNS metabolic processes. All statistical analyses are included in **Annexed table 2.**

3 RESULTS

3.1 CHAPTER 1: PERSPECTIVE NITRIC OXIDE, AN ESSENTIAL INTERMEDIATE IN THE PLANT–HERBIVORE INTERACTION

3.1.1 FRAMEWORK

Despite all the information available about the plant defense against arthropods, the knowledge on oxidative and particularly on nitrosative signalling, as sensors of defences to herbivory is still poorly understood. Levels of ROS and RNS, mainly H_2O_2 and NO, increase during insect and acari infestation. The redox status balance in the cell determines their function since moderate ROS/RNS concentrations differentially sense defense signalling, but an excess of oxidative stress produces chemical oxidation and induces programmed cell death (Foyer & Noctor, 2005; Santamaria *et al.*, 2017a)

3.1.2 RESULTS

3.1.2.1 NO METABOLISM

NO is clearly recognized as an intra- and intercellular signalling molecule involved in the regulation of a huge range of plant processes ranging from development to resistance and defense responses to biotic and abiotic stresses (Sánchez-Vicente *et al.*, 2019). Two pathways co-exist in plants to produce NO, reductive and oxidative ones, involving nitrite and arginine as substrates, respectively (León & Costa-Broseta, 2020) **(Figure 12)**. Within reductive pathways, NO production arises by both enzymatic and non-enzymatic reactions and is usually dependent on oxygen and NO_2^- concentrations. Nitrate reductase (NR), a multifunctional cytoplasmic enzyme, whose main function is nitrate assimilation to produce NO_2^- in a NADPH-dependent way (Campbell, 2001), also shows nitrite reductase activity, although this represents only 1% of its reductase ability under normal conditions (Yamasaki & Sakihama, 2000; Rockel *et al.*, 2002; Astier *et al.*, 2019). NO production through the action of NR has been demonstrated using different approaches. The mitochondrial electron transport chain under anaerobic/hypoxic conditions and the xanthine dehydrogenase–oxidase under anaerobic conditions or phosphate deficiency may also produce NO (Wang *et al.*, 2010; Gupta *et al.*, 2011; Cantu-Medellin & Kelley, 2013). On the other hand, under specific environmental conditions, such as low pH and high concentrations of NO_3^-, non-enzymatic reduction into NO takes place (Wendehenne *et al.*, 2001; Bethke *et al.*, 2004; Stöhr & Stremlau, 2006; Fancy *et al.*, 2017).

The oxidative pathway involves the activity of specialized enzymes as the nitric oxide synthases (NOSs), which oxidize L-arginine to form L-citrulline and NO, and they are well characterized in mammals (Alderton *et al.*, 2001). However, controversial results about this activity have been shown in plants. Bioinformatics approaches have shown no NOS gene/protein in higher plants (Jeandroz *et al.*, 2016; Hancock, 2019), excluding some algae (Foresi *et al.*, 2015), and the typical mammalian NO–cGMP signalling pathway has been also questioned (widely reviewed in Astier *et al.*, 2018). Nevertheless, NOS-like activity has been extensively described in plants by the use of NOs inhibitors and even

by heterologous expression of mammalian NOS (Zeidler *et al.*, 2004; Ali *et al.*, 2007; Astier *et al.*, 2019), and the denomination "NOS-like" is adopted for this activity.

Once synthesized, NO is highly reactive, and there are three main types of molecules that react with NO: ROS, glutathione (GSH), and metals (Romero-Puertas & Sandalio, 2016). NO rapidly reacts when present, with the radical superoxide (O2–) generating peroxynitrite (ONOO–), which is one of the most potent oxidant molecules in the cell leading to lipid peroxidation, protein nitration (Ischiropoulos & Al-Mehdi, 1995; Radi, 2004), oxygenated forms of cysteine (Cys) residues (sulfenic, sulfinic, and sulfonic acids), and S-glutathionylation (Martínez-Ruiz *et al.*, 2013). ONOO– has been shown to be produced under different stress conditions in plants (Romero-Puertas & Sandalio, 2016; Arasimowicz-Jelonek & Floryszak-Wieczorek, 2019). NO can also react with lipid peroxyl radical (LOO·) to produce nitro-fatty acids that are related to plant development and plant response to abiotic stress (Rubbo, 2013; Mata-Pérez *et al.*, 2017). Besides, the reaction of NO with GSH produces nitrosoglutathione (GSNO), which is considered an endogenous NO reservoir (Noctor *et al.*, 2012) and acts as an S-nitrosylating agent. GSNO is metabolized by GSNO reductase (GSNOR) to transform GSNO into glutathione disulfide (GSSG) and ammonia. Thus, GSNOR controls intracellular levels of GSNO and NO and, therefore, plant responses under different conditions (Liu *et al.*, 2001; Yun *et al.*, 2016). On the other hand, globins are proteins able to metabolize NO producing NO3– (Perazzolli *et al.*, 2004; Becana *et al.*, 2020), and consequently, these proteins can control NO levels by detoxification or through post-translational modification (PTM) reactions (Perazzolli *et al.*, 2006) **(Figure 12).**

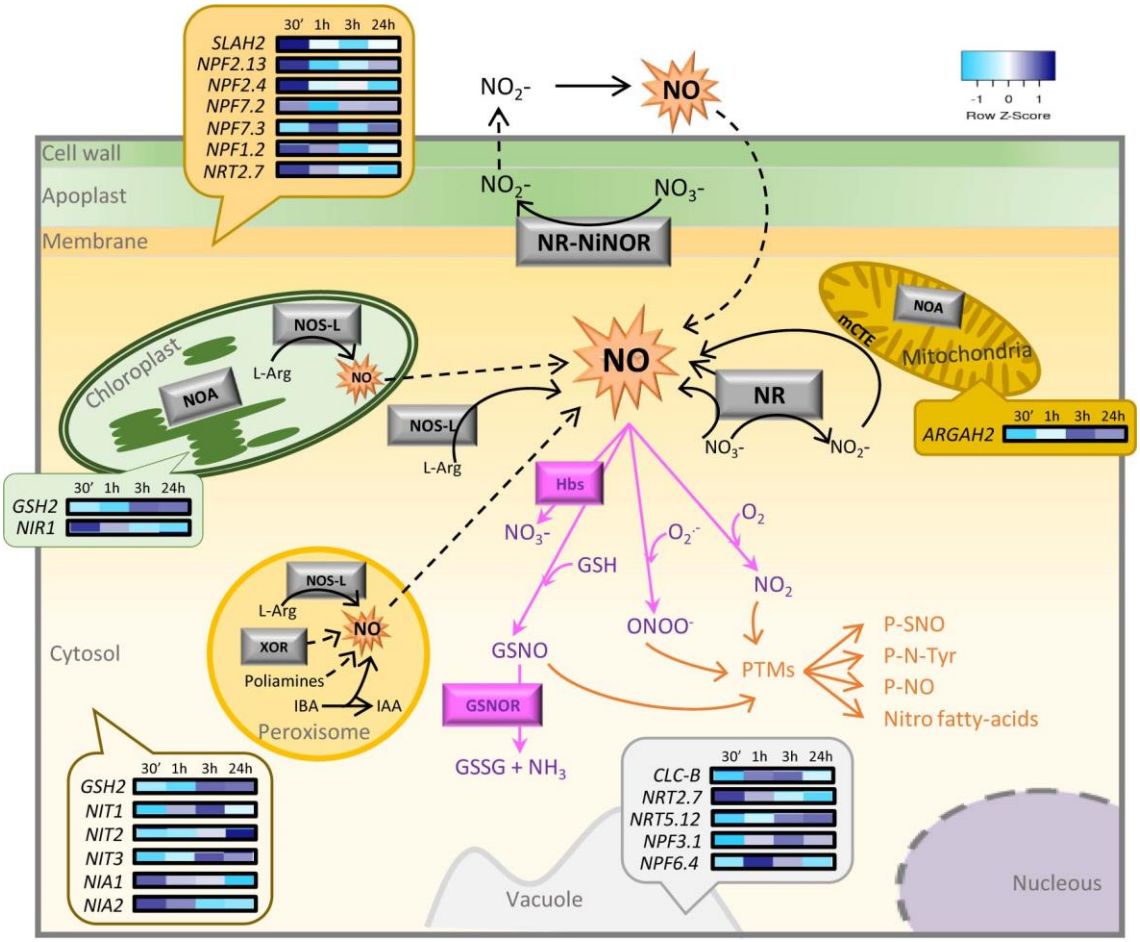

Figure 12. Schematic overview of NO sources and pathways in a plant cell and a heatmap of NO-associated genes expressed in the subcellular locations of *A. thaliana* after spider mite feeding. The diagram shows the main sources and pathways of NO (black arrows) including both oxidative and reductive pathways, the main scavengers (pink arrows) including superoxide ion, GSH, and hemoglobins, and the main NO mechanisms of action (orange arrows). Discontinued lines represent the mechanisms not experimentally demonstrated. A heatmap showing transcriptomic data of NO-associated genes from *A. thaliana* at different infestation times (0.5, 1, 3, and 24 h) with *T. urticae* is comprised within bubbles, positioned over the subcellular compartment where genes are expressed according to SUBA predictions, with a score ≥0.5. IAA, indole-3-acetic acid; IBA, indole-3-butyric acid; GSH, glutathione; GSNO, S-nitrosoglutathione; GSNOR, S-nitrosoglutathione reductase; Hbs, hemoglobins; L-Arg, L-arginine; mETC, mitochondrial electron transport chain; NR, nitrate reductase; NO, nitric oxide; NOS-L, nitric oxide synthase-like; NOA, NO-associated protein; P-NO, nitrosylated protein; P-N-Tyr, nitrated protein; P-SNO, S-nitrosylated protein; PTMs, post-translational modifications; XOR, xanthine oxidoreductase.

Based on the complexity of NO sources and pathways in a plant, we did a search of NO-associated genes expressed in the subcellular locations in *A. thaliana* RNAseq after spider mite feeding (Santamaria *et al.*, 2021), to determine what genes involved in NO pathways responded to mites. A heatmap comprise bubbles within the whole scheme

of pathways **(Figure 12)** summarizing the transcriptomic data of NO-associated genes at different mite infestation times (0.5, 1, 3, and 24 h) shown in **Figure 12**.

3.1.2.2 NO MECHANISM OF ACTION: CROSSTALK WITH ROS AND H_2S

NO reactivity leads to its main mechanism of action being PTM of proteins, which are carried out by a series of RNS produced by the reaction of NO with other free radicals as described before. PTMs best studied in plants are: (i) S-nitrosylation/S-nitrosation, referred to the formation of a nitrosothiol group in cysteines, with more than thousand targets described in plants, although a small number have been characterized (Sánchez-Vicente *et al.*, 2019; Sandalio *et al.*, 2019); (ii) nitration, being mainly studied the addition of a nitro group to Tyr side chain, with more than hundred targets described and only a dozen characterized (Rubbo & Radi, 2008; Sánchez-Vicente *et al.*, 2019); and (iii) nitrosylation of transition metals, with the formation of complex bonds to heme groups (Martínez-Ruiz *et al.*, 2013), scarcely studied in plants. NO-dependent PTMs result in the induction of different physiological responses and/or signalling processes as alteration of gene expression, metabolic changes, and phytohormone signalling. Furthermore, NO may regulate other signalling pathways, such as phosphorylation, oxidation, and ubiquitinylation (Cui *et al.*, 2018; León & Costa-Broseta, 2020; Lindermayr *et al.*, 2020). Therefore, the ability to regulate virtually all processes in the plant makes NO a do it all molecule (Delledonne, 2005).

Post-translational modification regulation of proteins is quite complex, however, due to the synergistic and antagonistic interplays between the different PTMs (Sandalio *et al.*, 2019). Overlapping of different PTMs on the same protein is very often and follows common pattern in different species, which demonstrate the importance of multilevel PTM regulation in cell metabolism (Duan & Walther, 2015). NO crosstalk with other signalling molecules, such as the well-known ROS and the lesser-known sulfide (H_2S), leads to an interplay between redox-dependent PTMs being targets the sulfur-containing amino acids, such as cysteine. Thus, the first step in Cys oxidation is S-

nitrosylation while the main ROS involved in signalling, H_2O_2, leads Cys to the following steps, its reversible oxidation to sulfenic acid (–SOH; sulfenylation) and sulfinic acid (–SO_2H; sulfinylation). Excessive ROS accumulation gives rise to the irreversible sulfonic acid (–SO3H; sulfonylation) derivative (Young *et al.*, 2018). S-nitrosylation, sulfenylation, sulfinylation, and intra- and intermolecular disulfide bond formations are rapid and reversible mechanisms to regulate protein function, stability, and location of proteins (Young *et al.*, 2018; Sandalio *et al.*, 2019). Due to their transient nature, these sulfur modifications, which can be reversibly reduced by thioredoxin and glutaredoxin pathways, are regarded as redox switches, giving rise to rapid finely tuned regulation of metabolic pathways and signalling processes (Sandalio *et al*., 2019; Young *et al.,* 2019). H_2S, involved in regulating various processes essential for plant survival, has been demonstrated recently to be a signalling molecule in the same degree of NO and H_2O_2 in plant systems (Hancock, 2019; Sandalio *et al.*, 2019). The mechanism of action of H_2S is related with its high affinity for metals from metalloproteins, but it also can oxidize Cys thiol groups to persulfide groups (R-S-SH) promoting covalent PTMs termed persulfidation, which could play a protective role for thiols against oxidative damage (Gotor *et al.,* 2019). Interestingly, RNS and ROS levels are regulated by the interplay between ROS-, H_2 S-, and NO-dependent PTMs. Curiously, S-nitrosylation prevents ROS-dependent oxidative damage to several proteins involved in the Calvin–Benson cycle, probably by inducing conformational changes in specific proteins (Tanou *et al.*, 2012). Crosstalk between NO and H_2S has been reported in acclimation processes in citrus plants (Molassiotis *et al.*, 2016). On the other hand, antagonistic interplay between protein Tyr nitration and phosphorylation competing for the same Tyr sites has been reported, interfering with different cellular processes, such as cell signalling via MAP kinase cascades (Arasimowicz-Jelonek and Floryszak-Wieczorek, 2019). Although several proteins have been shown as targets of NO-dependent PTMs under different stress conditions, in particular, plant–herbivore interaction is a field that needs to be better explored.

3.1.2.3 NO IN PLANT–HERBIVORE INTERACTIONS

Some publications have described the rapid accumulation and participation of NO as a common feature to insect-infested plants **(Table 3)**. Different arthropods including hemipteran (Burch-Smith & Dinesh-Kumar, 2007; Liu *et al.*, 2011; Mai *et al.*, 2014; Li *et al.*, 2019b; Xu *et al.*, 2020) and lepidopteran species (Arimura *et al.*, 2008; Bricchi *et al.*, 2010) cause a rapid and transient increase of NO levels in insect-damaged tissues. However, its physiological significance remains to be established. NO has not been linked to Vm depolarization as H_2O_2 has, but it has been related to Ca^{2+} homeostasis and cGMP signalling (Wu & Baldwin, 2009; Misra *et al.*, 2011). Thus, it could exert its biological function through the mobilization of secondary messengers or by the modulation of protein kinase activity. NO interacts with ROS and phytohormones (Mur *et al.*, 2013) and, in consequence, may indirectly act as regulator of the gene expression. In addition, the PTM of proteins mediated by NO, described above, may have potential regulatory effects in plant defense against herbivores as it does toward plant pathogens (Mur *et al.*, 2006; Martínez-Medina *et al.*, 2019).

Species				
Plant	**Herbivore**	**Description**	**Effects**	**Reference**
Several species	*Several aphids*	Infestation	-Accumulation of NO	(Smith & Boyko, 2007)
Phaseolus lunatus	*Spodopetra littoralis*	Infestation	-Accumulation of NO	(Arimura *et al.*, 2008)
Triticum aestivum	*Diuraphis noxia*	Infestation	-Accumulation of NO	(Moloi & Van der Westhuizen, 2009)
Phaseolus lunatus	*Spodoptera littoralis*	Infesttaion	-Accumulation of NO	(Bricchi *et al.*, 2010)
Oryza sativa	*Nilaparvata lugens*	Infestation	-Accumulation of NO -Induction of NOS activity	(Liu *et al.*, 2011)
Nicotiana attenuata	*Manduca sexta*	Infestation of *GSNOR* knock-down	-Reduction of JA and ethylene -Reduction of trypsin proteinase inhibitor activity	(Wünsche *et al.*, 2011a)

			and diterpene glycosides	
Nicotiana attenuata	*Manduca sexta*	Infestation of *NOA1* Knock-out	-Reduction of carbon-based defensive molecules	(Wünsche *et al.*, 2011b)
Pisum sativum	*Acyrthosiphon pisum*	Infestation	-Accumulation of NO, H_20_2, JA, SA and ethylene	(Mai *et al.*, 2014)
Pisum sativum	*Acyrthosiphon pisum*	Infestation and application of NO donors	-Accumulation of NO -Induction of defensive molecules (phenylalanine-ammonia-lyase and pisatin)	(Woźniak *et al.*, 2017)
Nicotiana tabacum	*Manduca sexta*	Infestation	-Induction of nitrogen-derived defensive metabolites (alkaloids) -Decrease in foliar N-uptake	(Campbell & Vallano, 2018)
Oryza sativa	*Nilaparvata lugens Sogatella furcifera*	Infestation of *MAPK20-5* Knock-out	-Accumulation of NO and ethylene	(Li *et al.*, 2019b)

Table 3. Participation of NO and NO-related enzymes in the plant defences against phytophagous insects.

In seedling leaves of pea (*Pisum sativum*), Mai *et al*. (2014) described the convergence of NO and H_2O_2 accumulation with the induction of JA, ET, and SA, hormones that sequentially appeared within the first 24–96 h after the aphid *Acyrthosiphon pisum* feeding. The simultaneous generation of hormones and free radicals at the same time points suggested a synergistic defense action in pea plants to aphid infestation. Moreover, the application of exogenous NO donors (NO, GSNO, and SNP, sodium nitroprusside) to pea plants infested with *A. pisum* revealed the induction of defense reactions leading to a deterrent result on the pea aphid feeding and the reduction in its population growth (Wozniak *et al.,* 2017). A side effect of SNP treatment is the release of cyanide, a potent respiratory poison with a deterrent effect on phytophagous arthropods who try to elude it or detoxify (Pentzold *et al.*, 2014; Keisham *et al.*, 2019). Campbell and Vallano (2018) analysed the effects of atmospheric NO_2 leaf uptake on tobacco (*Nicotiana tabacum*) metabolism and its impact in the tobacco responses to the lepidopteran *Manduca sexta*. Results showed that the foliar assimilation of NO_2 increased the nitrogen-derived defensive metabolites, particularly of some alkaloids, and diminished insect feeding and growth. To avoid this defense mechanism, herbivore modified somehow the plant capacity to absorb the reactive nitrogen, prompting a decrease in foliar nitrogen uptake and limiting the concentration of metabolites in leaves. Moreover, accumulating evidences indicate that an interactive fashion of phytohormones and NO regulates guard cell ABA-signalling and stomatal closure, which restricts the foliar uptake of NO_2 (Sun *et al.*, 2019). In turn, only few available reports have demonstrated the function of enzymes and other molecules associated with NO metabolic pathway in the generation of plant defences to pests. Li *et al.* (2019) showed that the NO production in rice (*Oryza sativa*) plants was associated with their responses to *N. lugens* infestation, in both susceptible and resistant cultivars. The rice planthopper feeding induced the activity of the NOS-like enzyme only in the susceptible cultivar, whereas no significant alterations of the NR enzymatic activity were observed, in none of the two rice-infested cultivars. These results suggested the active role of NOS in rice

defense mediated by NO. Likewise, Wünsche *et al*. (2011a) examined the function of the GSNOR enzyme in the plant–herbivore interaction by knocking-down GSNOR in *Nicotiana attenuata* plants. A decrease in JA and ET levels in the silenced plants was observed concomitant to an elevated susceptibility to *M. sexta* attack. Accordingly, the GSNOR-silenced tobacco plants showed a significant reduction of the trypsin proteinase inhibitor activity and in the diterpene glycosides content, both considered secondary defensive metabolites dependent on the JA derivatives. Wünsche *et al*. (2011b) also proved that the *N. attenuata* NO-associated protein 1 (NOA1) was required for the accumulation of JA and JA-Ile and the generation of defences against *M. sexta*. NOA1-silenced tobacco plants compromised the production of most of the carbon-based defensive compounds while the synthesis of nitrogen-rich defense metabolites was not altered. These results were probably due to the role of NOA1 in plant chloroplast functions and in the allocation of carbon resources within phenylpropanoid pathway (Wünsche *et al*., 2011b). Very recently, Xu *et al.* (2020) have demonstrated that the hemipteran *B. tabaci* infestation activated NO signalling in tobacco, leading to suppression of JA-dependent defences and improving nymph performance. Additionally, they have confirmed the NOA1 involvement in the JA-mediated responses to *B. tabaci*.

The mechanism by which NO mediates the enhancement of plant defences against pests is still poorly studied, but a recent publication by Li *et al*. (2019b) has linked a mitogen-activated protein kinase, OsMAPK20-5, to NO production in *N. lugens*-infested rice plants. The OsMAPK20-5 gene expression was up-regulated by female adult feeding, which presumably could be a response to oviposition. Surprisingly, the levels of NO and ET increased after insect feeding in the OsMAPK20-5-silenced plants and consequently improved rice resistance to brown planthopper and oviposited eggs. According to the authors, OsMAPK20-5 could enable rice plants to control excessive hyperaccumulation of NO and ET and thereby to prevent autotoxicity. Importantly, in field trials, MAPK20-5-silenced rice lines displayed a wide protection not only to the *N. lugens* but also to the white-backed planthopper *Sogatella furcifera*. Therefore, NO could mediate defense

responses in plants against pests acting as a signal molecule, a metabolic intermediate, or a toxic oxidative product.

Since no information on the NO's role in the interplay between plant and phytophagous acari was available, we did a search of NO-related genes in the RNA sequencing of *A. thaliana* in response to the spider mite *T. urticae* after 0.5, 1, 3, and 24 h of feeding (Supplementary Material; Santamaria *et al.,* 2020). Nineteen NO-associated genes, mainly encoding nitrate transporters, NRs, and nitrilases, were differentially expressed at different time points of infestation. Nitrate transporters showed different expression patterns based on their subcellular *in silico* location. Generally, those transporters located at the cytoplasmic membrane were rapidly induced by mite infestation, followed by the ones located at the vacuole. *NIA1* and *NIA2* genes that encode RNS were highly up-regulated at 0.5 h after mite feeding but were repressed at 24 h. Glutathione synthetase 2 (GSH2) gene putatively located at the chloroplast and cytosol and arginine amidohydrolase 2 (ARGAH2) gene product located at the mitochondria presented the opposite expression pattern being induced at longer infestation time **(Figure 12)**. These differential expression profiles are according to the consecutive steps of plant defense to mite attack since after mite perception, signalling is first activated at the cell membrane level and then transmitted through the cytosol to the rest of the organelles to finally induce the expression of defensive genes. In addition, the identified genes were classified into five different over-expressed categories based on their GO biological function, all of them related to RNS metabolic processes **(Table 4)**. These data suggested their functional significance during *T. urticae* infestation. Further studies are needed to clarify the NO and NO metabolic pathways in the plant defences against acari feeders.

Go ID	Term	User data	Genome data	Fisher test significance
GO:0010243	Response to organonitrogen compound	97	166	****
GO:2001057	Reactive nitrogen species metabolic process	15	46	****
GO:1901698	Response to nitrogen compound	108	264	****
GO:1901565	Organonitrogen compound catabolic process	41	164	****
GO:0071941	Nitrogen cycle metabolic process	15	46	****

Table 4: NO related genes classified by GO terms. Fisher's exact test (*, P, 0.05; **, P, 0.01; ***, P, 0.001; and ****, P, 0.0001) performed using DEGs from Santamaria *et al* 2020 and Arabidopsis genome genes that belong to each category.

In conclusion, the current information on how plant responses are regulated by NO and NO-related molecules constitutes still a set of unknown events to be explored, particularly, in the plant-acari interplay. An advanced understanding of the NO function in plant-herbivore interactions will be a strong tool to enhance crop performance and potentially lead to biotechnological approaches for pest control in agricultural systems.

3.2 CHAPTER 2: JASMONIC ACID CATABOLISM IN ARABIDOPSIS DEFENCE AGAINST MITES

3.2.1 FRAMEWORK

The JA/JA-Ile signalling has been the focus of attention of many studies associated with plant defence to pests, but the involvement of JA-derivatives remains largely uncharacterised. JA compounds can undergo various modifications, such as methylation, hydroxylation, carboxylation, and sulfation, resulting in active, inactive, or partially active derivatives (Wang *et al.*, 2021). JA can be hydroxylated to form 12-OH-JA, which can be further sulfated (12-HSO_4-JA) or glycosylated (12-OH-Glc-JA). Four jasmonic acid oxidases (*JAO1* to *JAO4*) are responsible for the hydroxylation of JA, with *JAO2* being the most relevant regulator in response to biotic stresses (Smirnova *et al.*, 2017). However, it remains to be clarified whether JA-derivatives participate in the signalling cascade to modulate plant resistance to mites.

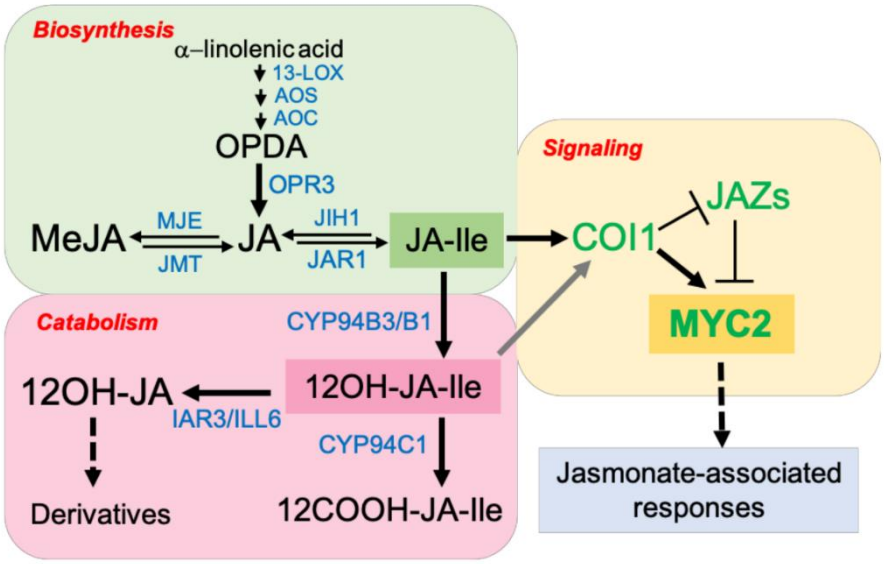

Figure 13. Overview of the jasmonate pathway including the major molecular players involved in biosynthesis, signalling, and catabolism. Black font means the chemical compound, blue font means the enzymes involved, and green fonts shows the main metabolites, enzymes, and proteins, respectively, for each section of the pathway. Scheme extracted from (Delgado *et al.*, 2021).

3.2.2 RESULTS

3.2.2.1 SEARCH OF GENES LINKED TO JA METABOLISM IN MITE-INFESTED ARABIDOPSIS PLANTS

Jasmonates are crucial regulators of plant defences to phytophagous mites but the participation of JA-derivatives in the plant-herbivory context remains largely uncharacterised. In order to gain knowledge on the compounds derived from the JA catabolism in the plant-mite interplay, we reanalysed previous RNAseq data regarding transcriptomic analyses of Arabidopsis plants after 0.5, 1.0, 3.0 and 24 h of being infested with *T. urticae* (Santamaria *et al.*, 2021). A search of genes associated with JA metabolism in this RNAseq allowed the identification of differentially expressed genes (DEGs) linked to JA biosynthesis, signalling and catabolism, for each time point **(Figure 14)**. Among them, there were some genes involved in the transformation of α-linolenic acid into 12-OPDA with different temporal expression patterns in response to mites. Genes responsible of the conversion of OPDA into JA and the inter-conversion between JA and JA-Ile were also altered by mite attack.

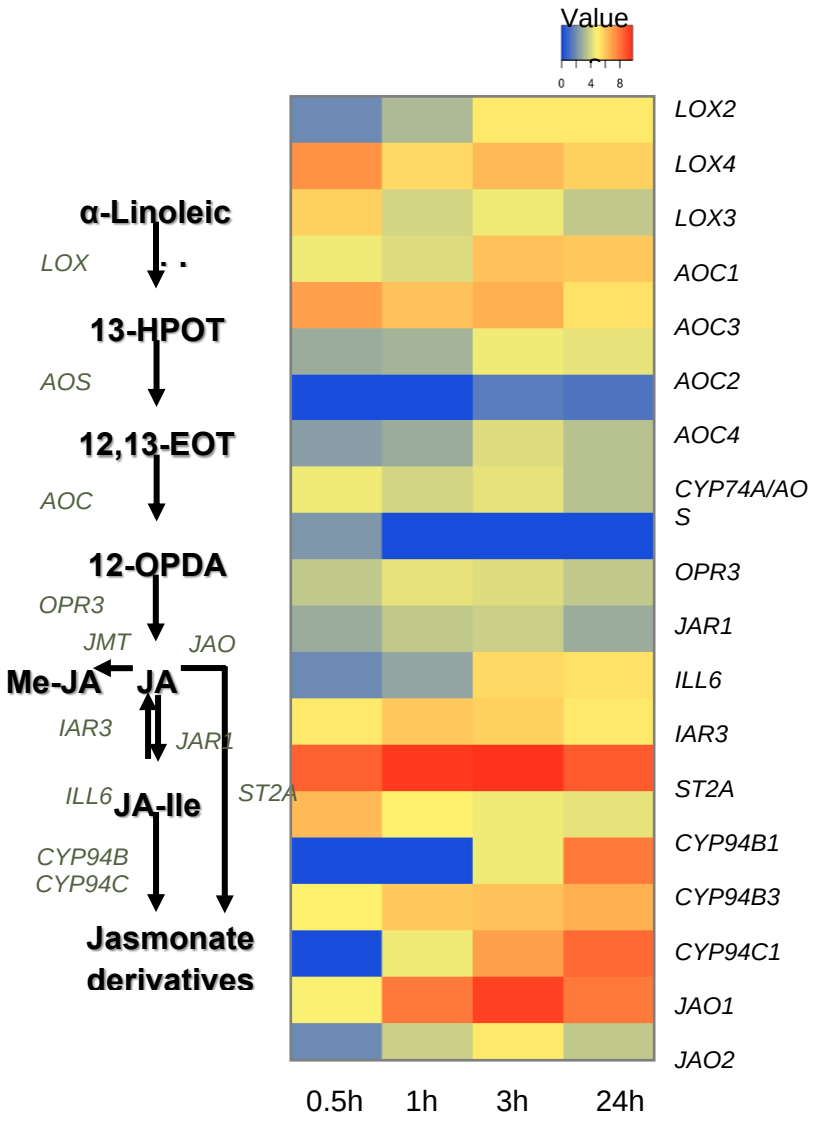

Figure 14. Scheme of *JA* metabolism and expression of genes involved in the pathway, in Arabidopsis Col-0 at different *T. urticae* infestation times. Scheme of the JA metabolic pathway indicating genes encoding enzymes involved in each reaction. Differential expression of JA metabolism genes at 0.5, 1, 3 and 24 h after *T. urticae* infestation. 13-HOPT: 13-hydroperoxyliolenic acid; 12,13-EOT: 12,13-Epoxy-9-octadecenoic acid; 12-OPDA:12-oxo-phytodienoic acid; JA: Jasmonic acid; JA-Ile: JA-Isoleucine; Me-JA: methyl-JA; LOX: Lipoxygenase; AOS: Allene oxide synthase; AOC: Allene oxidase cyclase; OPR3: Cis-12-oxo-ohytodienoic acid reductase 3; JMT: JA methyl transferase; IAR3 and ILL6: amydohydrolases; JAR1: jasmonate resistant 1; CYP94B and CYP94C: JA-Ile oxidases; JAO: Jasmonic acid oxidase; ST2A: sulfotransferase 2A.

Respect to JA catabolic pathway, probably the most relevant DEGs were *JAO* genes since they participate in the first step of the route catalysing the hydroxylation of JA into 12-OH-JA, and consequently, determine the formation of other JA-derivatives. Particularly, *JAO2* and *JAO4* genes resulted of high interest because were up-regulated since the earliest time point tested after infestation, and their expression increased during the

first 24 h of mite feeding. In addition, the expression of other genes with a role downstream of the pathway was also altered by mites. The gene responsible of the 12-HSO_4-JA production, *ST2A*, was slightly induced but at later infestation times. Likewise, the CYP94B3 gene of the clade CYP94 encoding JA oxidases involved in the hydroxylation and further carboxylation of JA-Ile was highly expressed along the 24 h of mite infestation.

Based on this set of transcriptomic results, we selected *JAO2* as a candidate gene for performing further experiments because, besides the features mentioned above, presented high basal expression levels in leaves which are the main target of mite feeding, and is considered the most relevant regulator of jasmonates linked to responses to biotic stresses (Smirnova *et al.*, 2017; Marquis *et al.*, 2022).

3.2.2.2 JAO2 PARTICIPATION IN ARABIDOPSIS DEFENCE TO T. URTICAE

In the dataset coming from the Arabidopsis-mite RNAseq, *JAO2* gene appeared up-regulated along the different time points of *T. urticae* infestation. RTqPCR assays confirmed the induction of JAO2 gene after 0.5 h of mite infestation which increased at longer infestation times **(Figure 15A)**. RTqPCR studies were also carried out in the major Arabidopsis tissues and results demonstrated that *JAO2* mRNA accumulated in rosettes at different developmental stages reaching the maximum expression levels in cauline leaves, flowers and roots, while was undetectable in siliques and seeds **(Figure 15B)**. Thus, *JAO2* is highly expressed in the rosettes and leaves, the main target tissues of mites.

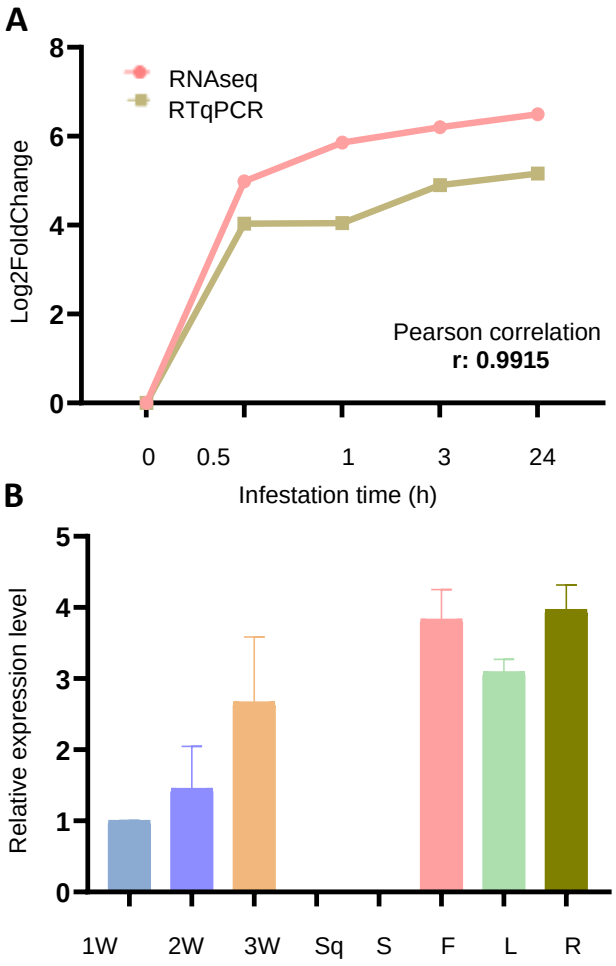

Figure 15. JAO2 gene expression in Arabidopsis Col-0. A Correlation between RNAseq data and RTqPCR validation for *JAO2* gene in Arabidopsis Col-0 at 0.5, 1, 3 and 24 h post-infestation, expressed as Log2fold change, are mean of three biological replicates. r value indicates Pearson correlation between RNAseq and RTqPCR data**. B** Relative expression level of *JAO2* gene in different tissues (1W-3W: 1-3 week rosettes, Sq: siliques, S: seeds, F: flowers, L: leaves stem and R: roots). Data, **B** are mean ± SE of three replicates.

To elucidate the potential function of JAO2 in plant defence to mites, Arabidopsis Col-0 plants and two *JAO2* T-DNA-insertion lines, *jao2-1* and *jao2-2* **(Annexed Figure 2A)**, (Smirnova *et al.*, 2017) were selected for further experiments. As expected, the expression patterns of the two mutant lines analysed by RTqPCR assays, showed that the JAO2 transcript content was significantly reduced in both mutant lines in comparison to the Col-0 plants **(Annexed Figure 2B)**. No differences in terms of growth or development were found between jao2 mutant lines and Col-0 plants at the time of experiments performance **(Annexed Figure 2C, D)**.

Mite feeding assays were performed with the two genotypes and total rosette damage was quantified 4 d after infestation. Mutant lines resulted in approximately four times less damage than Col-0 infested plants **(Figure 16A)**. These differences in damage correlated with the callose deposition levels **(Figure 16B)**. The injury produced by mites is associated with alterations in the plant redox homoeostasis (Santamaria *et al.*, 2017b). Thus, the H_2O_2 concentration was also measured in the two infested genotypes. The accumulation of H_2O_2, expressed as DAB units, significantly decreased in the mutant *jao2-2* line in comparison to DAB values found in Col-0 or *jao2-1* plants **(Figure 16C)**. Additionally, the effect of the presence/absence of *JAO* gene in the plant was also studied on the mite side by analysing mite fecundity after feeding on jao2 lines and Col-0 plants. In this case, the cumulative number of eggs was significantly greater when mites fed on Col-0 plants and *jao2-1* line than when they fed on *jao2-2* line **(Figure 16D)**.

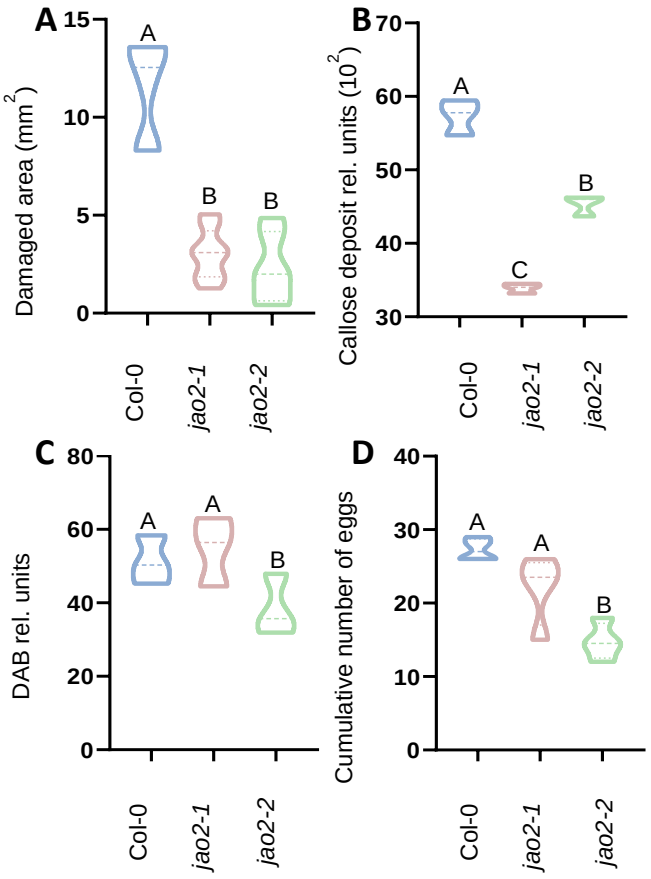

Figure 16. Plant damage, hydrogen peroxide and callose determination in jao2 and Col-0 Arabidopsis genotypes after *T. urticae* infestation and mite performance after feeding in these plants. A Foliar damaged area was quantified in Col-0 and *jao2* mutants after 4 d of mite infestation. **B** Callose deposition in leaves after 24 h of mite infestation. **C** Hydrogen peroxide expressed as DAB units, after 24 h of mite infestation. **D** Effects of Arabidopsis genotypes on *T. urticae* fecundity measured 36 h after infestation with synchronized mite females. Data are mean ± SE of nine **A, B, C** and six **D** replicates. Different letter indicates significant differences (P<0.5, One way ANOVA followed by Tukey's multiple comparison test).

3.2.2.3 EXPRESSION OF JAO GENES AFTER MITE INFESTATION

Since four JAO proteins (JAO1 to 4) are involved in the JA oxidation to produce 12-OH-JA in Arabidopsis (Smirnova *et al*., 2017), the expression of the other three *JAO* genes (*JAO1*, *JAO3* and *JAO4*) was assessed in the RNAseq data at different time points after mite infestation, and then was validated by RTqPCR assays. The three *JAO* genes were up-regulated by *T. urticae* infestation although presented different expression patterns upon infestation time **(Figure 17A-C).** Concomitantly, we analyzed the expression of *JAO1*, *JAO3* and *JAO4* genes in infested and non-infested jao2 lines and in Col-0 plants. All *JAO* genes were induced by mite feeding in the two genotypes, suggesting a functional redundancy of JAO proteins (**Figure 17D-F**). *JAO1* mRNA content was higher in infested *jao2* mutant lines than in infested Col-0 plants while *JAO4* presented the opposite expression pattern. The accumulation of *JAO3* messengers didn't show significant differences between genotypes. Thus, the participation of the four *JAO* genes in response to mite attack was clear and redundant but the expression levels of *JAO3*, *JAO4*, and specially *JAO1*, were lower than the levels detected for *JAO2* gene either in non-infested or infested plants, particularly at the earliest infestation times. Thus, we selected the triple mutant termed *jaoT* (*jao2-1, jao3-1, jao4-2)* to perform mite infestation and to analyze their functional relevance in plant defence to mites. Damaged leaf area, callose deposition and cumulative number of eggs were significantly reduced in *jaoT* triple mutant compared to Col-0 plants **(Figure 18A, B, D).** Only the accumulation of H_2O_2 did not show differences between *jaoT* and Col-0 plants **(Figure 18C)**, as occurred in *jao2-1* infested plants. These data mimic the role of *JAO2* gene and confirmed its function as the main JAO regulator in the plant defence to mites.

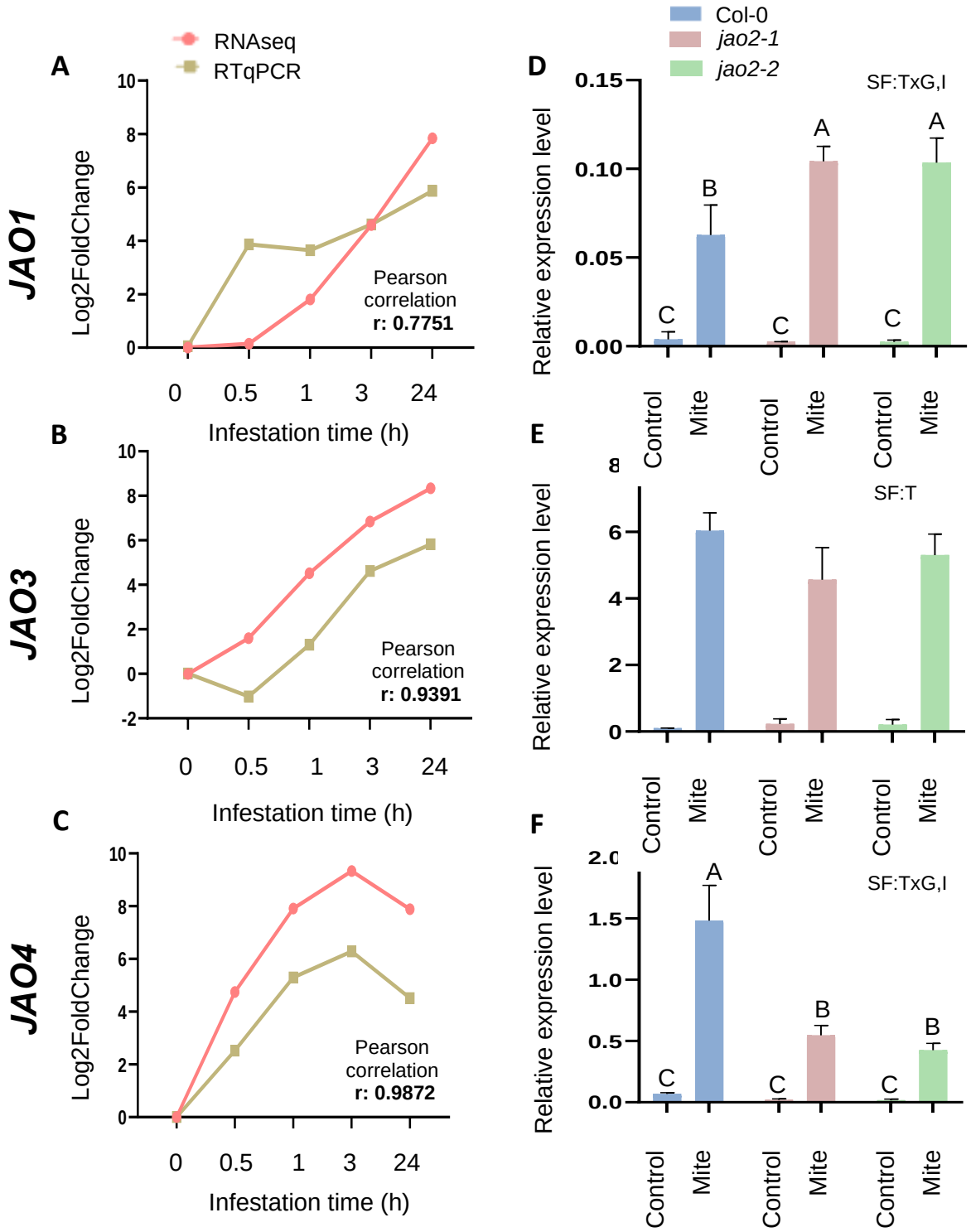
A
RNAseq
RTqPCR
JAO1
Log2FoldChange
Pearson correlation
r: 0.7751
Infestation time (h)
B
JAO3
Log2FoldChange
Pearson correlation
r: 0.9391
Infestation time (h)
C
JAO4
Log2FoldChange
Pearson correlation
r: 0.9872
Infestation time (h)
D
Col-0
jao2-1
jao2-2
SF:TxG,I
Relative expression level
Control
Mite
E
SF:T
Relative expression level
F
SF:TxG,I
Relative expression level

Figure 17. Expression of *JAO* genes in Arabidopsis Col-0 in response to *T. urticae* infestation and in *jao2*-2 mutant line. Correlation between RNAseq and RTqPCR data for *JAO1*; **A**, *JAO3*; **B** and *JAO4*; **C** genes in Arabidopsis Col-0 at 0.5, 1, 3 and 24 h after *T. urticae* infestation. Expression of *JAO1*; **D**, *JAO3*; **E** and *JAO4*; **F** genes in *jao2* mutant lines and Col-0 plants after 24h of mite infestation, by RTqPCR assays. Data, expressed as Log2 fold change. r value indicates Pearson correlation between RNAseq and RTqPCR data. Data are mean of three biological replicates. Significant factors (SF) indicate whether the two independent factors, G (genotype) and T (mite treatment), and/or their interaction (TxG,I), were statistically significant. Different letter indicates significant differences (P<0.5, Two-way ANOVA followed by Tukey's multiple comparison test).

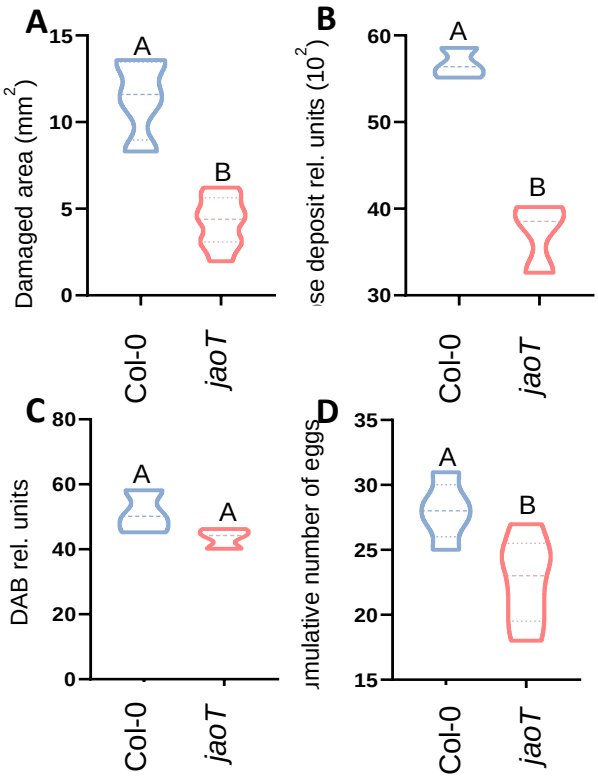

Figure 18. Plant damage, hydrogen peroxide and callose determination in *jaoT* and Col-0 Arabidopsis genotypes after *T. urticae* infestation and mite performance after feeding in these plants. A Foliar damaged area was quantified in Col-0 and *jaoT* (jao2-1, jao3-1, jao4-2) mutant after 4 d of mite infestation. **B,** Callose deposition in leaves after 24 h of mite infestation. **C,** Hydrogen peroxide expressed as DAB units, after 24 h of mite infestation. **D,** Effects of Arabidopsis genotypes on *T. urticae* fecundity measured 36 h after infestation with synchronized mite females, Data are mean ± SE of nine A, B, C and six **D** replicates. Different letter indicates significant differences (P<0.5, Two-way ANOVA followed by Tukey's multiple comparison test).

3.2.2.4 JAO2 GENE AND HORMONAL CROSSTALK IN ARABIDOPSIS RESPONSES TO MITES

To further analyse the molecular basis of JAO2 function, the expression of some marker genes for the JA pathway, *AOS*, *JAR1* and *MYC2*, was determined in non-infested and 24 h post-infestation in Col-0 and *jao2-2* mutant plants. In infested plants, the three marker genes were induced but *AOS* and *MYC2* genes displayed a significant greater mRNA accumulation in *jao2-2* mutant than in Col-0 plants. Statistical analysis demonstrated that the expression pattern of *AOS* was dependent on the genotype and the mite treatment **(Figure 19A)**, and *MYC2* gene expression was also dependent on the interaction between both **(Figure 19C)** and on the interaction between both in the case of *MYC2* gene **(Figure 19C).** In contrast, the up-regulation of *JAR1* gene was mainly dependent on the mite infestation **(Figure 19D).** Additionally, the quantification of JA, JA-Ile and SA, the main hormones linked to plant defence against mites, showed that all these hormones were accumulated in response to mite infestation in the *jao2* and Col-0 Arabidopsis genotypes, although the induction of SA was notably lower than JA and JA-Ile induction **(Figure 20A-C).** JA and JA-Ile were also increased in response to mites in the *jaoT* mutant lines but the concentration of SA was not altered **(Figure 20D-F).**

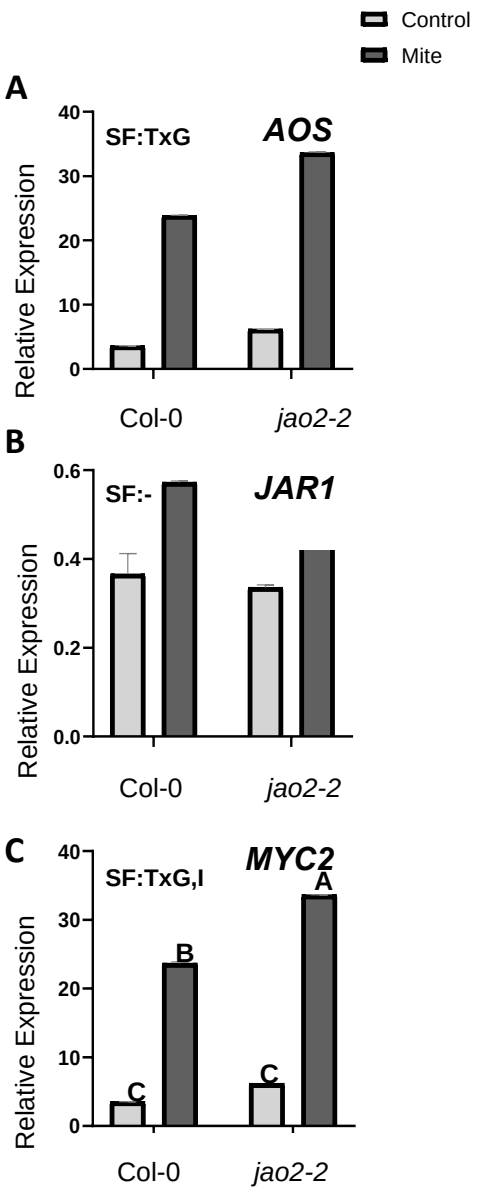

Figure 19. Expression of genes involved in JA/JA-Ile biosynthetic pathway in Arabidopsis *jao2* mutant line and Col-0 plants 24 h after mite infestation. Relative expression of genes involved in the JA biosynthetic pathway. *AOS*: Allene Oxide Synthase; **A**, *JAR1*: Jasmonic acid response 1; **B**, *MYC2*: MYC transcription factor; **C**, Data are mean of three biological replicates. Significant factors (SF) indicate whether the two independent factors, G (genotype) and T (mite treatment), and/or their interaction (TxG,I), were statistically significant. Different letter indicates significant differences (P<0.5, Two-way ANOVA followed by Tukey's multiple comparison test).

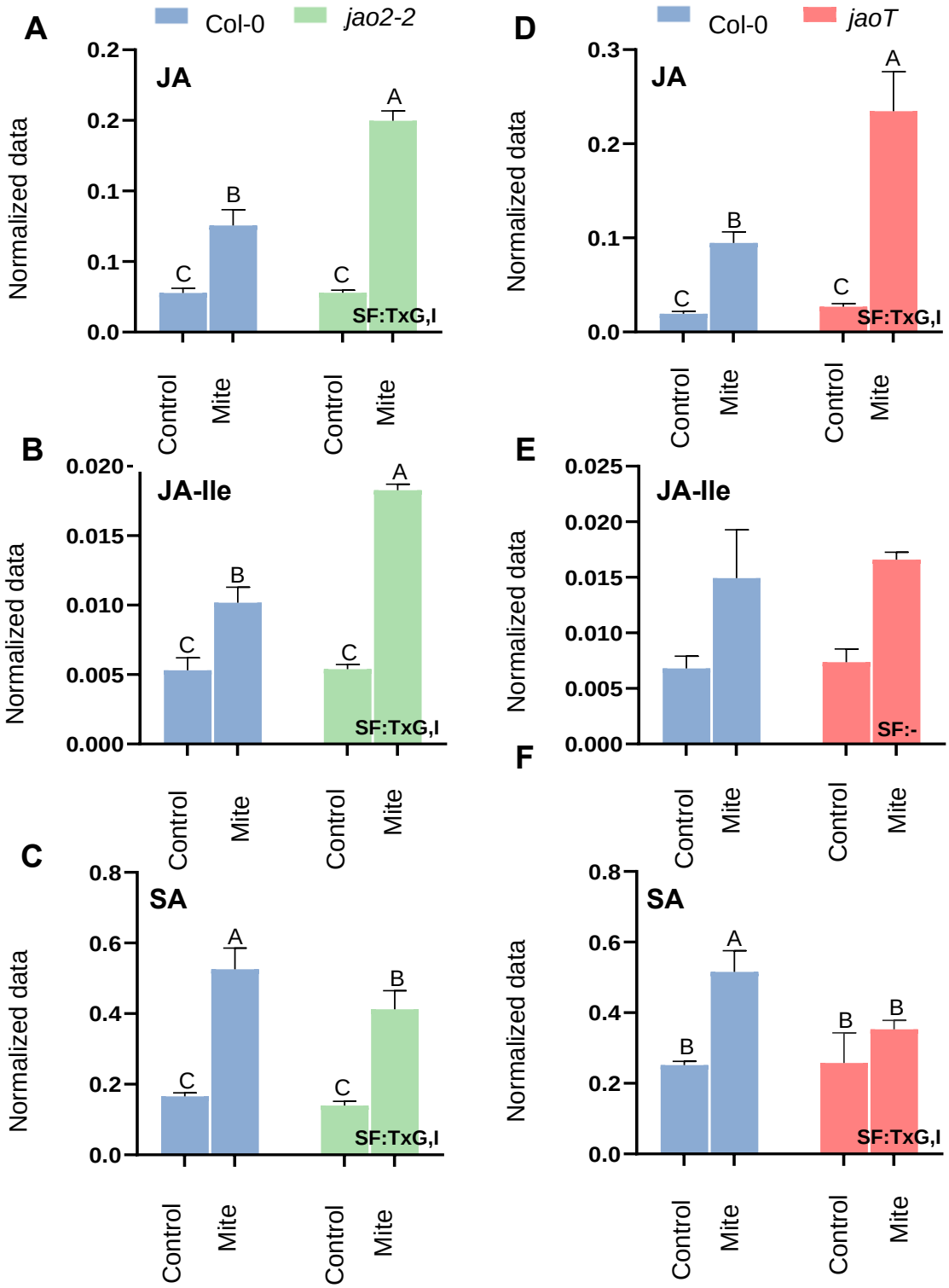
A
Col-0
jao2-2
JA
Normalized data
0.2
0.2
0.1
0.1
0.0
C
B
C
A
SF:TxG,I
Control
Mite
Control
Mite
D
Col-0
jaoT
JA
Normalized data
0.3
0.2
0.1
0.0
C
B
C
A
SF:TxG,I
Control
Mite
Control
Mite
B
JA-Ile
Normalized data
0.020
0.015
0.010
0.005
0.000
C
B
C
A
SF:TxG,I
Control
Mite
Control
Mite
E
JA-Ile
Normalized data
0.025
0.020
0.015
0.010
0.005
0.000
SF:-
Control
Mite
Control
Mite
C
SA
Normalized data
0.8
0.6
0.4
0.2
0.0
C
A
C
B
SF:TxG,I
Control
Mite
Control
Mite
F
SA
Normalized data
0.8
0.6
0.4
0.2
0.0
B
A
B
B
SF:TxG,I
Control
Mite
Control
Mite

Figure 20. Quantification of hormones in Arabidopsis *jao2, jaoT* mutant lines and Col-0 after 24 h of *T. urticae* infestation. JA: Jasmonic Acid **A, B**, JA-Ile: Jasmonic-isoleucine acid **C, D**, SA: Salicylic Acid **E, F**. Values are normalized respect to internal standard area and sample fresh weight. Data are mean of three biological replicates. Significant factors (SF) indicate whether the two independent factors, G (genotype) and T (mite treatment), and/or their interaction (TxG,I), were statistically significant. Different letter indicates significant differences (P<0.5, Two-way ANOVA followed by Tukey's multiple comparison test).

Taking into consideration the essential role of JAO2 as an enzyme involved in the first step of the JA-catabolism, JA-derivatives were also quantified in the three Arabidopsis genotypes **(Figure 21 and Annexed tables 3 and 4).** Results showed that the amount of the five tested JA-derivatives increased after mite infestation in *jao2-2, jaoT* and Col-0 plants. Notably, the hydroxylated and sulfated jasmonates, 12-OH-JA and 12-HSO_4-JA, although increased in infested *jao2-2* and *jaoT* plants, presented lower concentrations than in infested Col-0 plants. These findings indicate that the JA catabolism is altered when *JAO2* gene is not expressed and expressed, and consequently, JA and JA-Ile forms accumulated triggering the synthesis of defensive compounds.

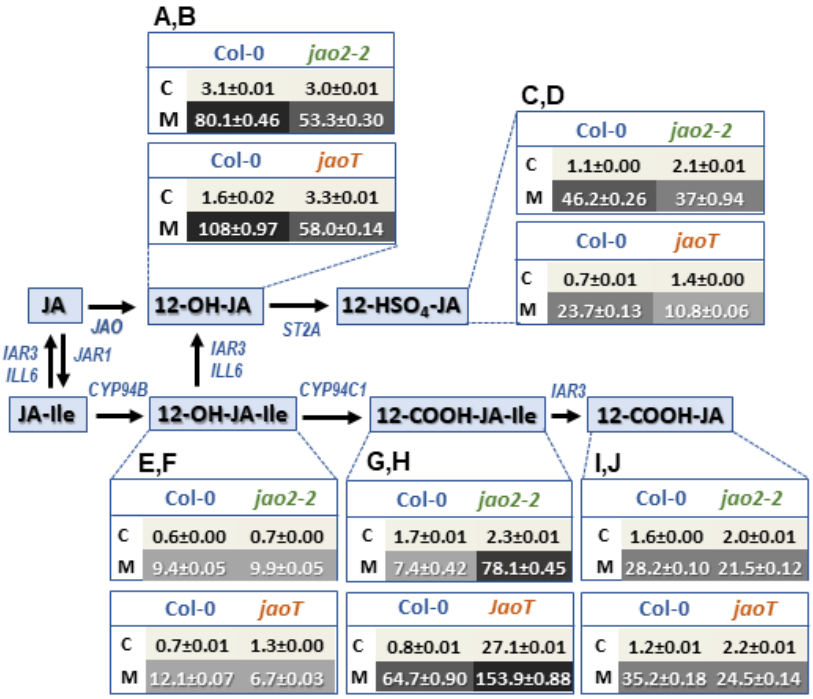

Figure 21. Scheme of the JA catabolic pathway and quantification of JA/JA-Ile-derivatives in Arabidopsis *jao2-2, jaoT* mutant lines and Col-0 after 24 h of *T. urticae* infestation. Scheme of the JA catabolism indicating the genes encoding enzymes involved in each reaction. Quantification of JA-derivatives (12-OH-JA, 12-HSO_4-JA, 12-COOH-JA, 12-OH-JA-Ile and 12-COOH-JA-Ile) expressed as normalized values (x10) respect to internal standard area and sample fresh weight, normalized peak area values. Values are mean ± SE of three biological replicates. C: control plants, M: mite infested plants. Compounds with differential significant levels respect to the control are highlighted in darker o weaker grey colour.

3.2.2.5 ACCUMULATION OF INDOLE GLUCOSINOLATES AND CAMALEXIN IN JAO2 MUTANT LINE IN RESPONSE TO *T. URTICAE*

Tryptophan-derived metabolites such as glucosinolates and camalexin have a demonstrated protective function in plant defence against mites. In particular, indole glucosinolates and camalexin accumulated in response to herbivory to protect plants against *T. urticae* (Zhurov *et al.*, 2014; Santamaria *et al.*, 2019). To know whether the effect of JAO2 was linked to these compounds, we measured the content of I3M and its derivatives, and camalexin, in *jao2* and *jaoT* mutant lines and Col-0 plants. Results demonstrated that three glucosinolates I3M,1-MeO-I3M and 4-MeO-I3M and camalexin accumulated in leaves in response to mite infestation independently on the genotype **(Figure 22)**. Furthermore, the content of I3M and 4-MeO-I3M was higher in *jao2-2* line than in Col-0 plants after mite infestation **(Figure 22A, B).** In contrast, the amount of 1-MeO-I3M and camalexin did not change in infested *jao2* mutant line compared to infested Col-0 plants **(Figure 22C, D).** Thus, the absence of JAO2 protein causes differential defence response in mite-infested plants and alter the content of defensive metabolites to fight against these phytophagous.

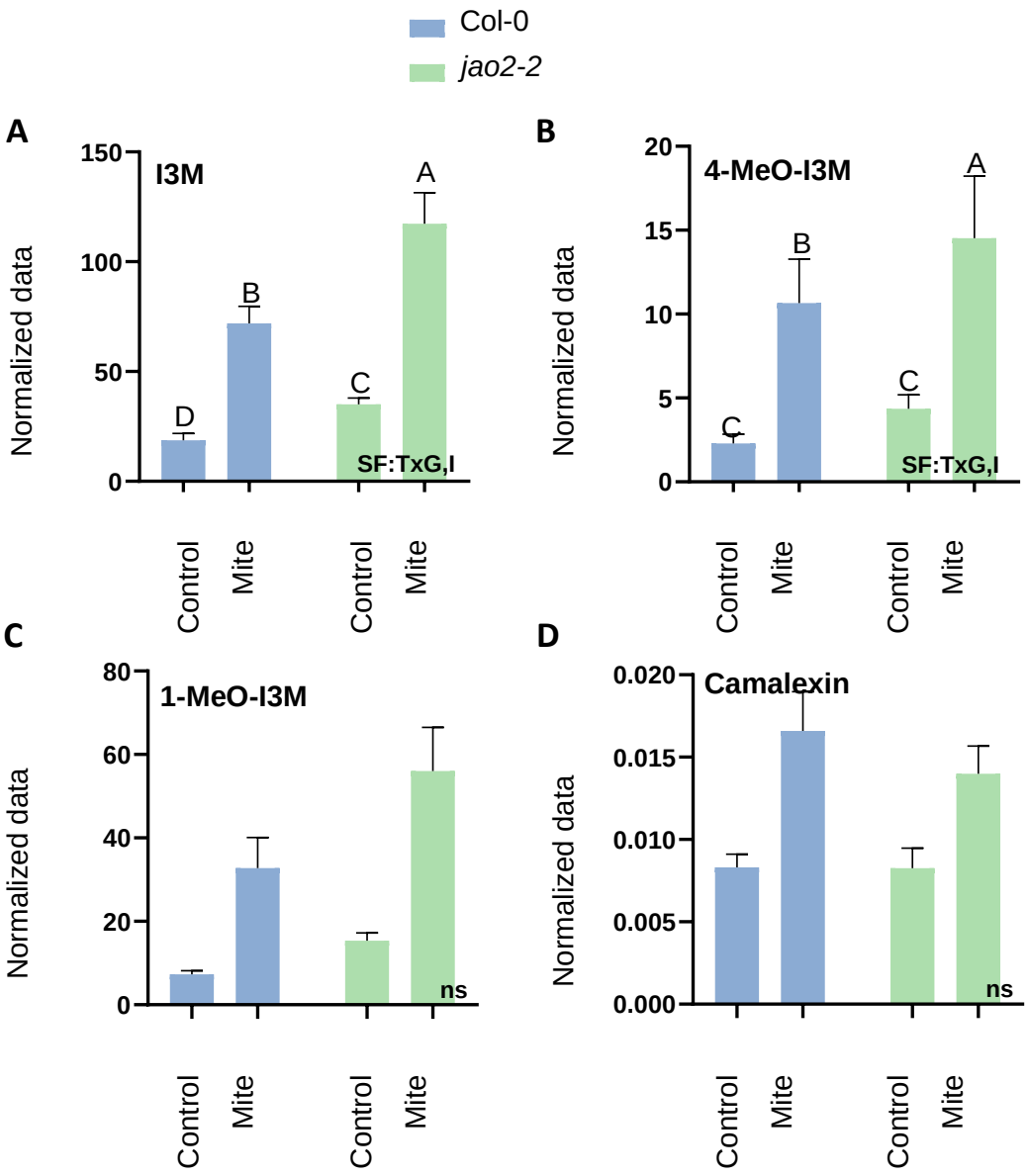

Figure 22. Quantification of indole glucosinolates and camalexin in Arabidopsis *jao2* mutant lines and Col-0 after *T. urticae* infestation. A I3M, **B** 4-MeO-I3M, **C** 1-OH-I3M and **D** camalexin quantified in *jao2-2* mutant lines and Col-0 plants 24 h after mite infestation. Data are expressed as normalized values respect to internal standard area and fresh sample weight (g), normalized peak area values. Values are normalized respect to internal standard area and sample fresh weight. Data are mean of three replicates. Significant factors (SF) indicate whether the two independent factors, G (genotype) and T (mite treatment), and/or their interaction (TxG,I), were statistically significant. ns: no statistically significant. Different letter indicates significant differences (P<0.5, Two-way ANOVA followed by Tukey's multiple comparison test).

3.3 CHAPTER 3: STOMATA, A VULNERABILITY IN THE PLANT DEFENCE AGAINST PHYTOPHAGOUS MITES THAT ABA CAN OVERCOME

3.3.1 FRAMEWORK

Stomatal closure has been observed in response to phytophagous arthropods (Sances *et al.*, 1979; Pincebourde & Casas, 2006; Schmidt *et al.*, 2009), though whether closure constituted a defence mechanism or contributed to the infestation remained unclear. ABA is the key hormone regulating stomatal aperture, which gates gas exchange for transpiration, photosynthesis and responses to abiotic stimuli (Kuromori *et al.*, 2018a).

Open stomata are natural apertures where piercing-sucking herbivores like mites insert their stylets, specialized feeding structures, to access nutrient rich sub-epidermal cells.

Feeding via opening stomata is potentially faster and avoids the damage of cell walls, which can trigger rapid plant defences (Mathen *et al.*, 1988; Bensoussan *et al.*, 2016). Stomatal aperture is also influenced SA and methyl-JA can promote stomatal closure while other jasmonates, particularly the bioactive JA-Ile, can induce stomatal opening (Munemasa *et al.*, 2011), though their contribution might be secondary to ABA signalling (Zamora *et al.*, 2021).

3.3.2 RESULTS

3.3.2.1 STOMATA RESPONSES TO *T. URTICAE* INFESTATION ARE DRIVEN BY HORMONE CONTENT

To study time-resolved dynamics of defence and stomatal regulation upon mite infestation, stomatal aperture on the abaxial leaf surface was analysed in epidermal samples at four infestation time points **(Figure 23A)**. Leaf epidermal impressions showed open stomata during the day with subtle reductions in aperture in wild-type Col-0 non-infested plants towards the end of the light period **(Figure 23A)**. Mite infestation induced a striking stomatal closure reaching the maximum closure at 24-30 h post-infestation **(Figure 23A, B)**. To also explore if natural stomatal closure in darkness could alter mite feeding habits and resultant leaf cell death, plants were grown in regular conditions, infested, incubated under constant dark or light environment for 16 h, and then cell damage was assayed. Results demonstrated that mites fed better under light conditions, when stomata were open, as plant cell death was increased **(Figure 23C)**.

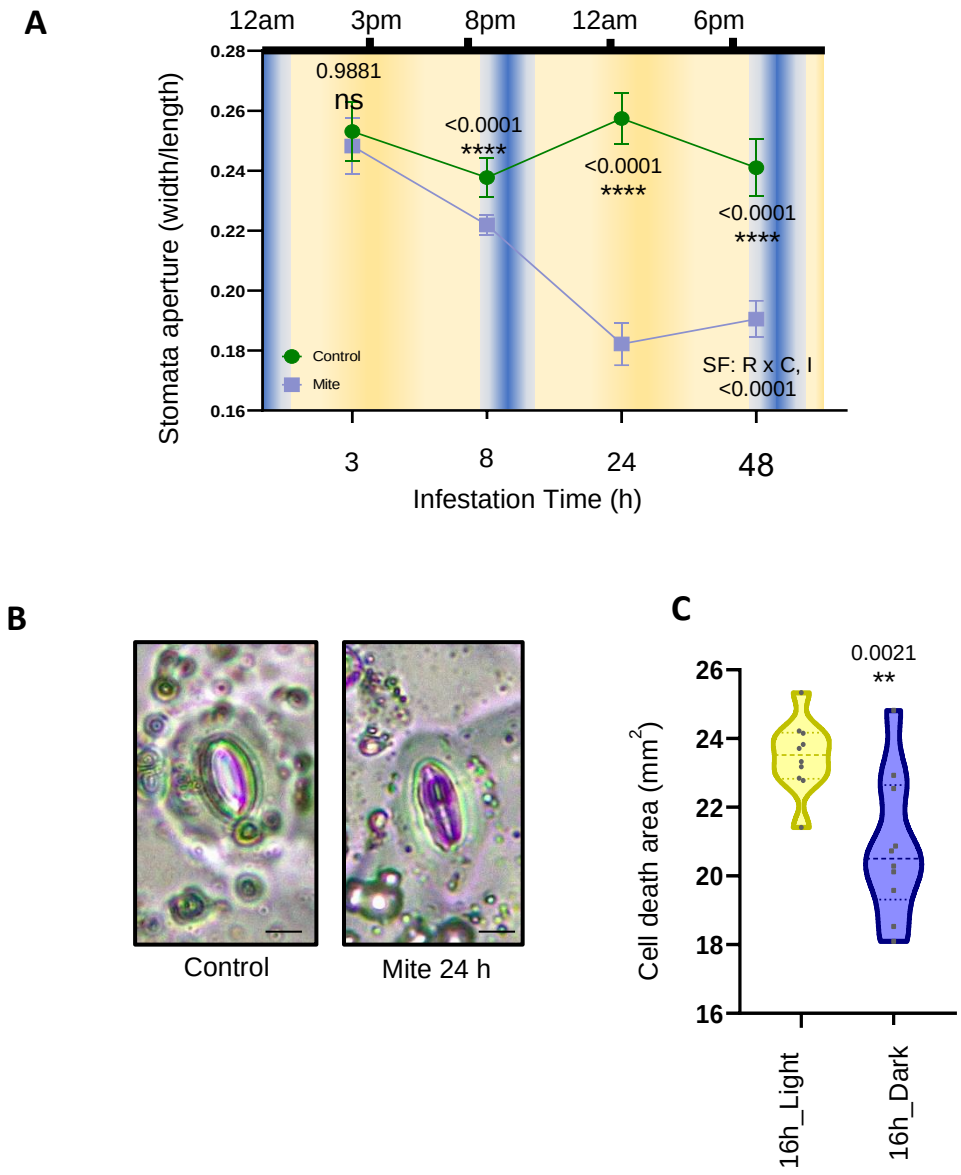

Figure 23. Effects of mite infestation on stomata aperture, and on the leaf cell death when plants are incubated under light or dark conditions. A, Stomata aperture measured in Arabidopsis Col-0 detached leaves after 3, 8, 24 and 30 h of mite infestation. Results referred as width/length ratio. Significant factors (SF) indicate whether the two independent factors, R (infestation time) and C (mite treatment), and/or their interaction I (RxC) were statistically significant (Two-way ANOVA followed by Sidak's multiple comparison test, P<0.05). Numbers indicate significant differences between control and mite treatment at each point of infestation. Data are means ± SE of 10 biological replicates. **B**, Image of stomata closure 24 h after mite infestation. Bars = 8µm **C,** Cell death, measured in leaf discs by trypan blue staining after 16 h of mite infestation under dark and light conditions, is expressed in mm^2. t-Student test was accomplished to assess differences due to light treatments (P<0.05). Data are means ± SE of 15 biological replicates.

Since hormone accumulation in response to mites might be responsible for phenotypic changes in stomatal behaviour, SA, JA, JA-Ile and ABA were quantified in mite infested Arabidopsis Col-0 leaves at four post-infestation time points. The accumulation of all four compounds was induced by mites, but with distinct temporal profiles. SA content was significantly increased from the earliest infestation time while JA, JA-Ile and ABA required longer times to be differentially accumulated in comparison to non-infested plants **(Figure 24A-D).** The highest hormone levels were detected at 24 h of infestation, except for the JA-Ile, which reached the highest content at 30 h of infestation, in accordance with a reduction in its JA precursor at this time point. Interestingly, ABA levels were maintained at 30 h, while SA was reduced.

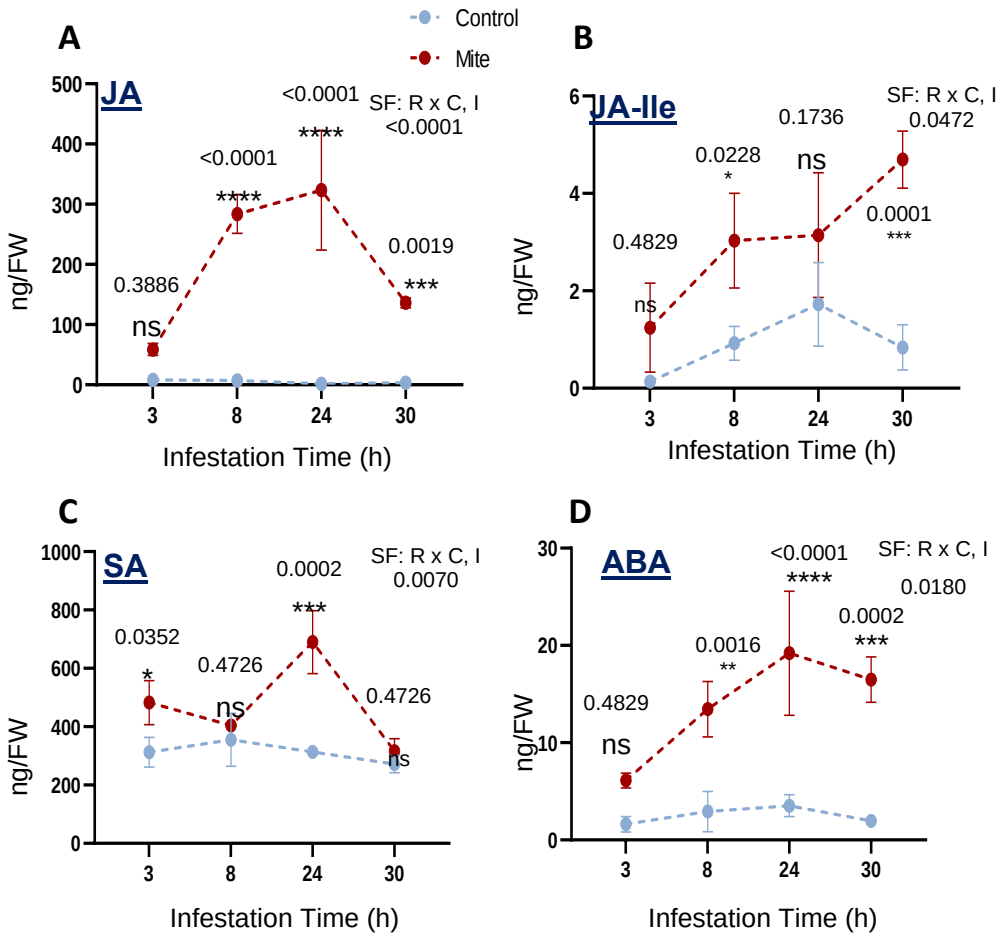

Figure 24. Quantification of hormone content in Arabidopsis Col-0 upon mite infestation. JA; **A**, JA-Ile; **B**, SA; **C** and ABA; **D** accumulation was quantified at 3, 8, 24 and 30 h after mite infestation. Values are expressed as ng of hormone per g of fresh weight (FW). Significant factors (SF) indicate whether the two independent factors, R (Infestation time) and C (mite treatment), and/or their interaction I (RxC) were statistically significant (Two-way ANOVA followed by Tukey's test, P<0.05). Asterisks and numbers indicate significant differences compare to control conditions. Data are means ± SE.

To determine the impact of SA, JA and ABA on leaf stomatal aperture, these hormones were exogenously applied to Arabidopsis Col-0 plants. SA and ABA treatment triggered stomatal closure in treated leaves, as expected (effect size in **Annexe table 5**), though the effect of JA was negligible **(Figure 25A-C).**

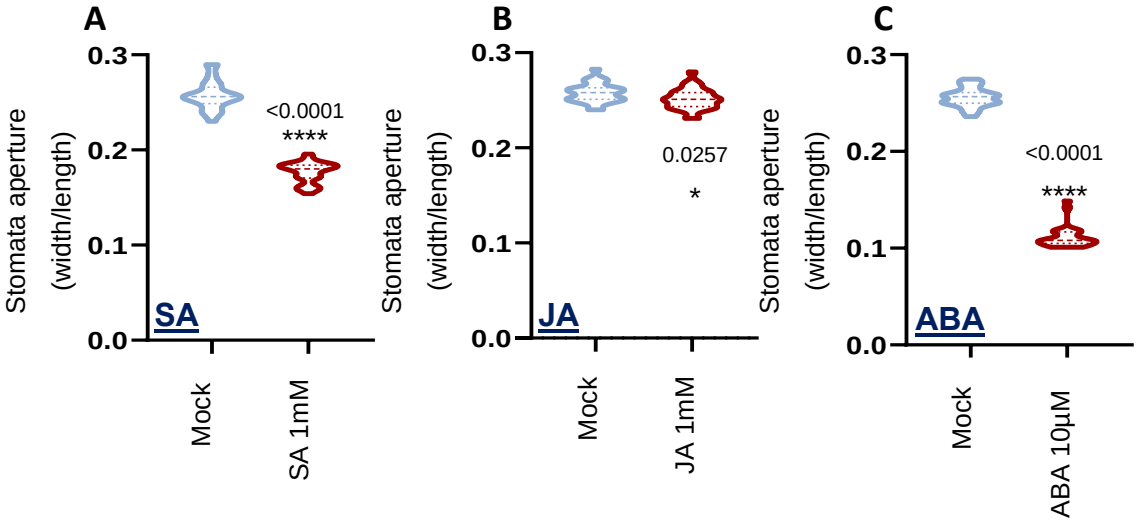

Figure 25. Stomata aperture after exogenous hormonal treatments. Stomata aperture measured at 3 h after spraying on the aerial part of the plant with 1 mM SA; **A**, 1 mM JA; **B** and 10 µM ABA; **C**. Results referred as width/length ratio. t-Student test was accomplished to assess differences due to hormone treatments (P<0.05) marked with one, two or three asterisks depending on significance. Data are means ± SE.

3.3.2.2 ABA ACCUMULATION DETECTED UPON MITE INFESTATION

Since ABA accumulates in leaves during mite infestation concomitantly with stomatal closure, we sought to identify in which cells ABA could be functionally relevant for Arabidopsis defence using the high-resolution nlsABACUS2-400n FRET-based biosensor for ABA (Rowe *et al.*, 2023). In leaves of Arabidopsis plants expressing the biosensor, nuclei of epidermal and internal cell types showed sufficient biosensor expression for segmentation **(Figure 26A**, upper images**)**. In all detected cell types, nuclear ABACUS2-400n fluorescence emission ratios were higher in infested plants than in **(Figure 26B**, bottom images**)**, indicating higher ABA concentrations. Mean emission ratio for all cells was significantly higher for mite infested leaf images **(Figure 26B)**. To better understand the cellular distribution of ABA accumulation, we used a nuclear morphology classifier based on the "FRETENATOR" tool to analyse cell type emission ratios. Nuclei were classified into five cell type groups: stomata, pavement, spongy mesophyll, bundle sheath, and vascular bundle cells. With infestation, the signal increased in all cell type groups, but stomatal and vascular bundle cell groups showed the highest emission ratios **(Figure 26C, D)**.

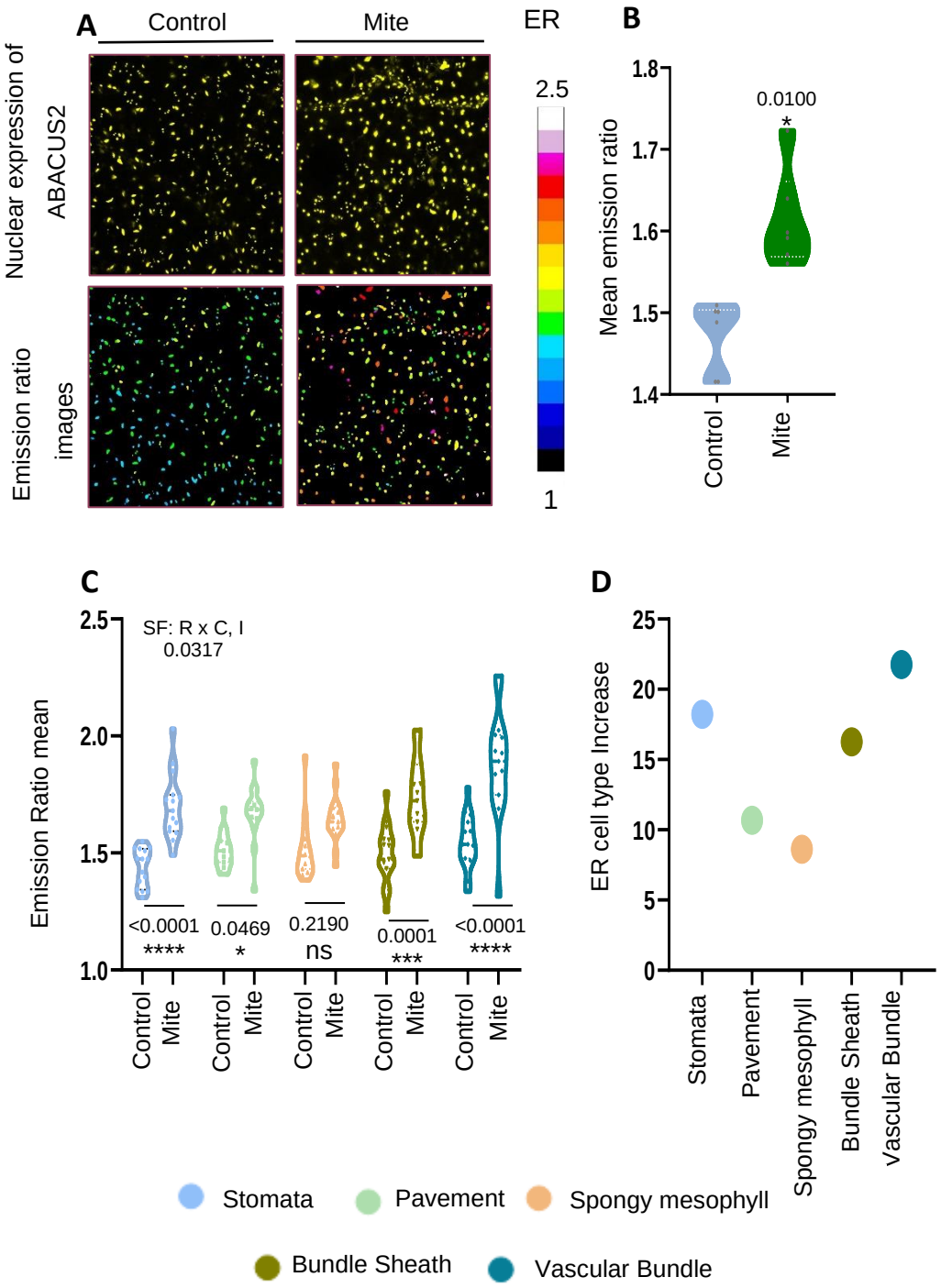
A
Control
Mite
ER
2.5
1
Nuclear expression of ABACUS2
Emission ratio images
B
Mean emission ratio
0.0100
*
Control
Mite
C
Emission Ratio mean
SF: R x C, I
0.0317
<0.0001
****
0.0469
*
0.2190
ns
0.0001
***
<0.0001
****
Control
Mite
D
ER cell type Increase
Stomata
Pavement
Spongy mesophyll
Bundle Sheath
Vascular Bundle

Figure 26. ABA accumulation at subcellular resolution level in leaf tissues of nuclear ABA-biosensor plants nls-ABACUS2-400n, after mite infestation. A, Projections of analysed images. Upper images correspond to nuclei expressing the biosensor and bottom images to FRET-processed results in detached leaves. **B**, Maximum Z- projections of the data quantified in A. Upper images correspond to nuclei expressing the biosensor and bottom images to Emission ratios. t-Student test was accomplished to assess differences due to control and mite conditions ($P<0.05$). Data are means ± SE of 8 biological replicates. **C,** Emission ratios of nlsABACUS2-400n biosensor in cells of Vascular Bundle, Bundle Sheath, Spongy Mesophyll, Pavement and Stomata type cells, after 24 h of mite infestation in detached leaves. Significant factors (SF) indicate whether the two independent factors, R (mite treatment) and C (nucleus type), and/or their interaction I (RxC) were statistically significant (Two-way ANOVA followed by Tukey's test, $P<0.05$). Data are means ± SE of 8 biological replicates. **D**, Increased levels of emission ratio in the different five cell types after infestation respect to non-infested ones.

Because *T. urticae* cause cell death by inserting their stylets either in between epidermal pavement cells or through stomatal pores to suck mesophyll cell contents **(Figure 27A**; Bensoussan *et al.,* 2016**)**, it was important to get information about the viability status of leaf cells after the infestation. The ABA biosensor allowed us to detect cell viability since nuclei detected by biosensor fluorescence reflect viable cells. The comparison between infested and non-infested plants showed no significant changes in the total number of quantified nuclei **(Figure 27B, Annexed Figure 1A, B).** However, when this comparison was independently done in each of the five cell type groups, the mesophyll cell type presented lower number of nuclei in the infested plants than in non-infested **(Figure 27C-G).** Taken together, these results corroborated that spongy mesophyll cells were the target tissue where mites suck nutrients upon their feeding and indicated that nlsABACUS2-400n biosensor was able to detect local ABA increases in response to mites in leaf cell types directly involved in feeding as well as in distal cells and cell types not directly involved in feeding, i.e. bundle sheath and vascular cells. Interestingly, vascular cells have been proposed to be the major sites of foliar ABA biosynthesis (Endo *et al.*, 2008), and thus our data provide support for a model in which mite feeding triggers ABA synthesis in the vasculature and this results in the translocation of ABA across the leaf cell types.

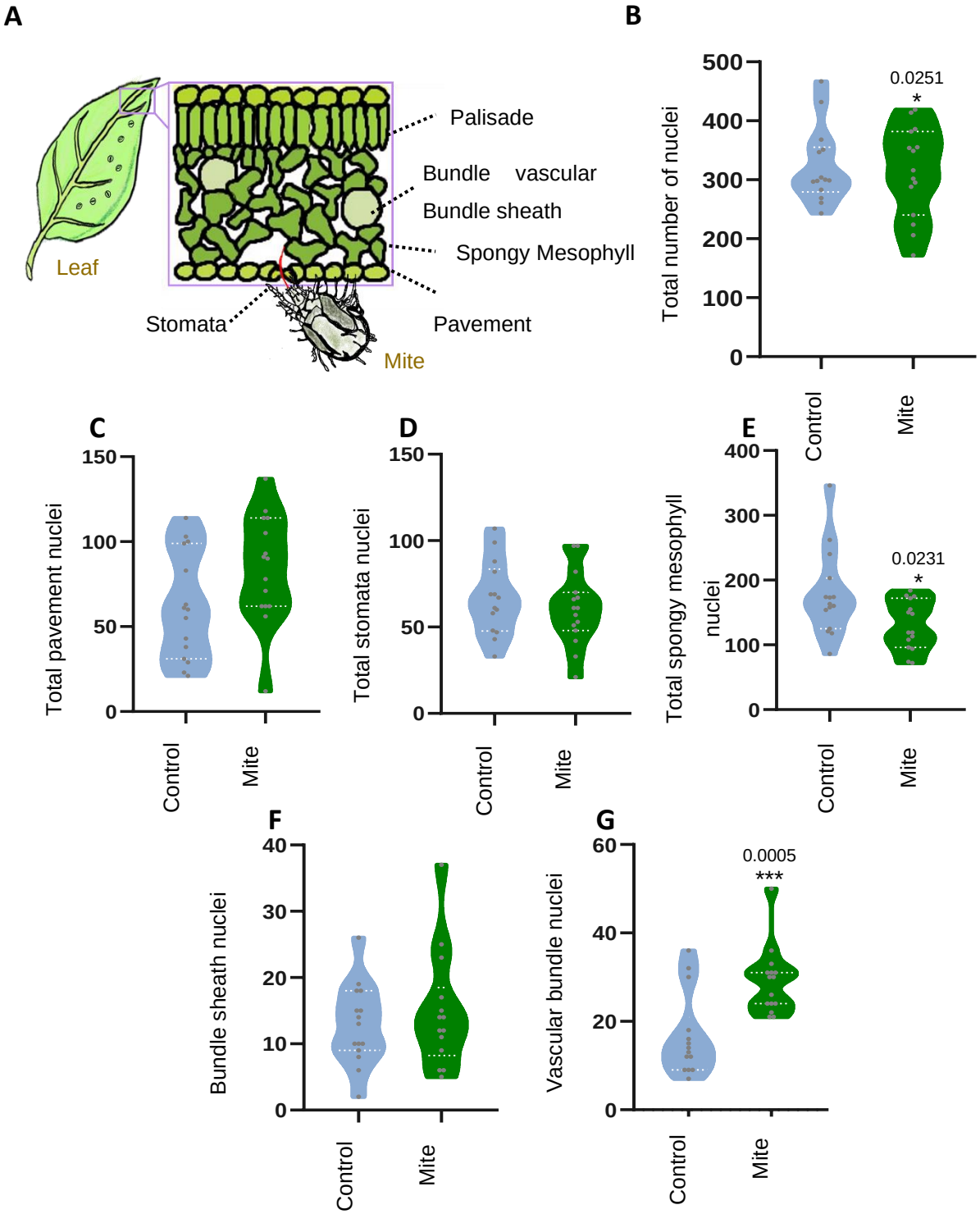

Figure 27. Quantification of nuclei number in different cell type groups of nls-ABACUS2-400n plants after mite infestation. A, Scheme of the leaf tissues and a mite feeding through stomata. **B,** Total number detected nuclei in infested and control leaves. Total number of nuclei in different cell types: **C,** Pavement, **D,** Stomata, **E,** Spongy mesophyll, **F,** Bundle sheath and **G,** Vascular bundle, after 24 h of mite infestation. Asterisks and numbers indicate significant differences between control and mite treatment (P<0.5, t-student test). Data are means ± SE of 8 biological replicates.

3.3.2.3 ABA IS INVOLVED IN PLANT DEFENCE AGAINST MITES

To study how changes in endogenous ABA levels affect mite infestation, Arabidopsis mutants in ABA biosynthesis and catabolism, *aba2-1* and *cyp707a1cyp707a3*, respectively, which result in lower and higher ABA concentrations (González-Guzmán *et al.*, 2002; Okamoto *et al.*, 2009) were selected to perform mite infestation. *aba2-1* lines showed significantly greater damage than control plants upon mite feeding for 4 days while the damaged area in *cyp707a1cyp707a3* line was lower than in Col-0 plants **(Figure 28A)**. Likewise, fecundity rates, measured as cumulative number of eggs after 36 h, were higher when mites fed on the mutant *aba2-1* mutant line than when they fed on Col-0 plants, and were significantly reduced in the *cyp707a1cyp707a3* line **(Figure 28B)**. These data indicated that ABA promotes plant defences against mite damage and antagonises mite oviposition. Additionally, two Arabidopsis ABA insensitive mutants, the *112458* ABA receptor sextuple mutant and *ost1-3* SnRK2 kinase mutant, were also examined to determine if the canonical ABA signalling pathway participated in ABA-dependent mite responses. The *OST1* gene is preferentially expressed in guard cells and the vasculature (Mustilli *et al.*, 2002), cell types that exhibited the most pronounced increase in ABA levels **(Figure 28)**. While mite females laid a similar number of eggs in mutants as in control plants, both mutant lines showed more damage than Col-0 plants after infestation **(Figure 28C, D)**. Overall, these results revealed that ABA signalling, including in the vasculature or stomata, is important for mite defence.

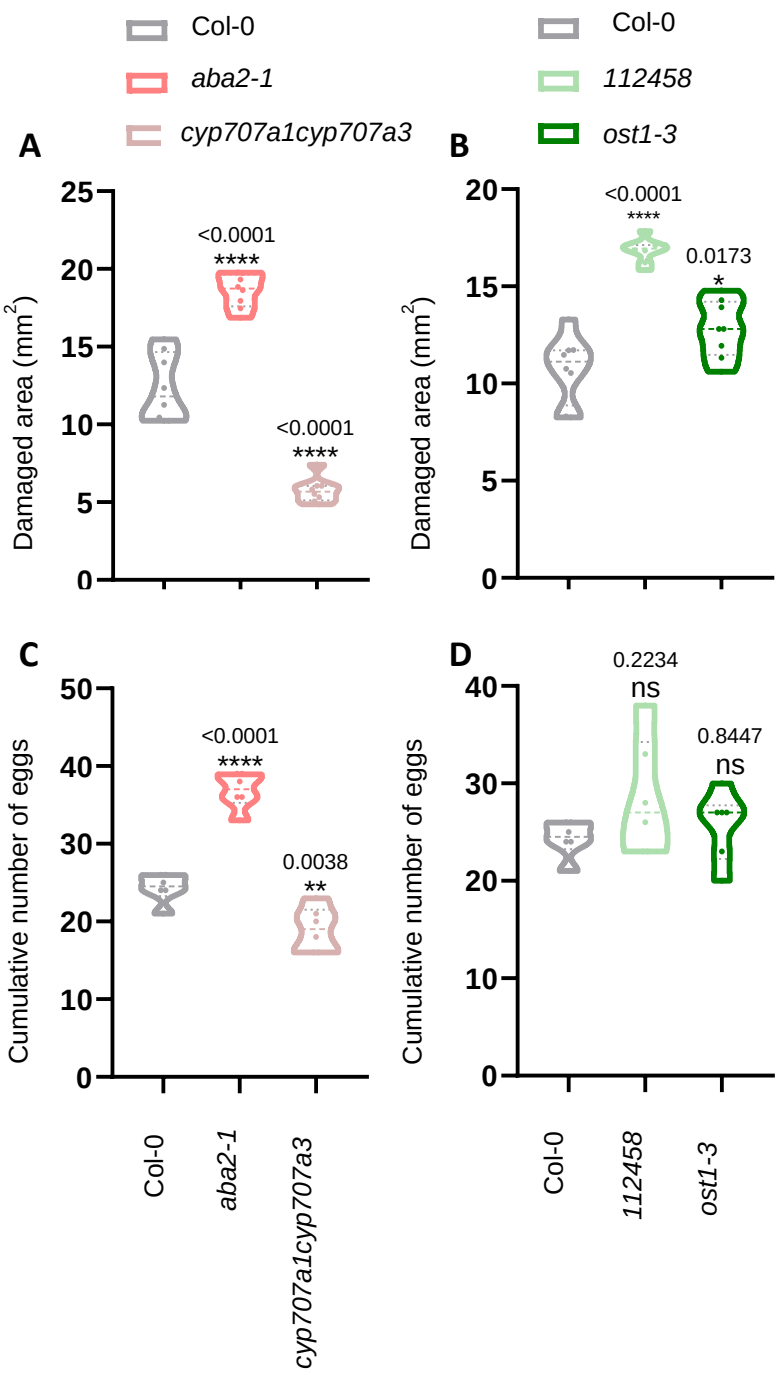

Figure 28. Plant damage and mite fecundity after mite infestation of *aba2-1* and *cyp707a1cyp701a3* and *pyr1pyl-112458, ost1-3* Arabidopsis mutants and Col-0 plants. A, Foliar damage quantified 4 d after mite infestation in whole plants in *aba2-1*, *cyp707a1cyp707a3* and Col-0 plants, and in **B,** *112458, ost1-3* and Col-0 plants. Data, expressed in mm^2. Effects on *T. urticae* fecundity measured 36 h after the infestation with synchronized mite females in detached leaves on **C**, *aba2-1 cyp707a1cyp707a3* and Col-0 plants, and in **D**, *112458, ost1-3* and Col-0 plants. Numbers indicate significant differences compare to Col-0 genotype. Data are means ± SE 10 biological replicates for Damage and 6 biological replicates for eggs. One-way ANOVA followed by Tukey's multiple comparisons test, P<0.05.

Because all cells respond with increased ABA, we sought to determine whether ABA accumulation had further impact on SA and JA, considered as the core hormones involved in plant defences. We examined the expression of *PR1* and *MYC2*, marker genes of SA and JA signalling, respectively, in the five Arabidopsis genotypes, at two infestation times. The expression of the *PR1* gene was induced at 8 h post-infestation and decreased 24 h after mite feeding in all studied genotypes. However, *PR1* levels were lower *in aba2-1* line and higher in *cyp707a1cyp707a3* line than in Col-0 plants at 8 h time point and displayed the opposite expression pattern at 24 h **(Annexed Figure 3A).** No differences in PR1 behaviour were found between *112458*, *ost1-3* mutants and WT plants **(Annexed Figure 3B).** Together these results indicate that ABA could crosstalk with SA signalling positively early in mite infection and negatively later in infection. In contrast to *PR1*, which peaked at 8 h, *MYC2* presented the maximum induction at 24 h after infestation **(Annexed Figure 3C, D).** In the five tested genotypes, only the *aba2-1* mutant line showed altered *MYC2* expression, i.e. elevated at 24 h **(Annexed Figure 3C, D).** The observation that the reduced ABA levels in the *aba2-1* mutant increased expression of both *PR1* and *MYC* genes at 24 h could be an indication of hormone crosstalk but could also be an indirect result of increased mite infestation in *aba2-1*. Certainly, the over accumulation of *MYC2* transcript suggests that a positive crosstalk of ABA with JA signalling is unlikely to explain the role of ABA in mite resistance.

One physiological response associated with ABA is the production of ROS, in particular H_2O_2, a signalling molecule that regulates plant stress response genes (Li *et al.*, 2022). To further confirm such an association, the H_2O_2 content was determined in detached leaves of the four Arabidopsis mutants and Col-0 plants after 24 h of mite infestation **(Figure 29A, B)**. The measurement of H_2O_2 concentration is represented as relative DAB staining units **(Figure 29A)**. and demonstrated that *aba2-1* and *cyp707a1cyp707a3* infested lines accumulated higher and lower levels of H_2O_2, respectively, than Col-0 plants. In contrast, number of DAB deposits in the *ost1-3* mutant was only slightly reduced and was not altered in *112458* after mite feeding **(Figure 29)**. As with JA signalling, a negative association between ABA levels and ROS production suggests ROS accumulation is unlikely to explain the role of ABA in resistance to mite infestation.

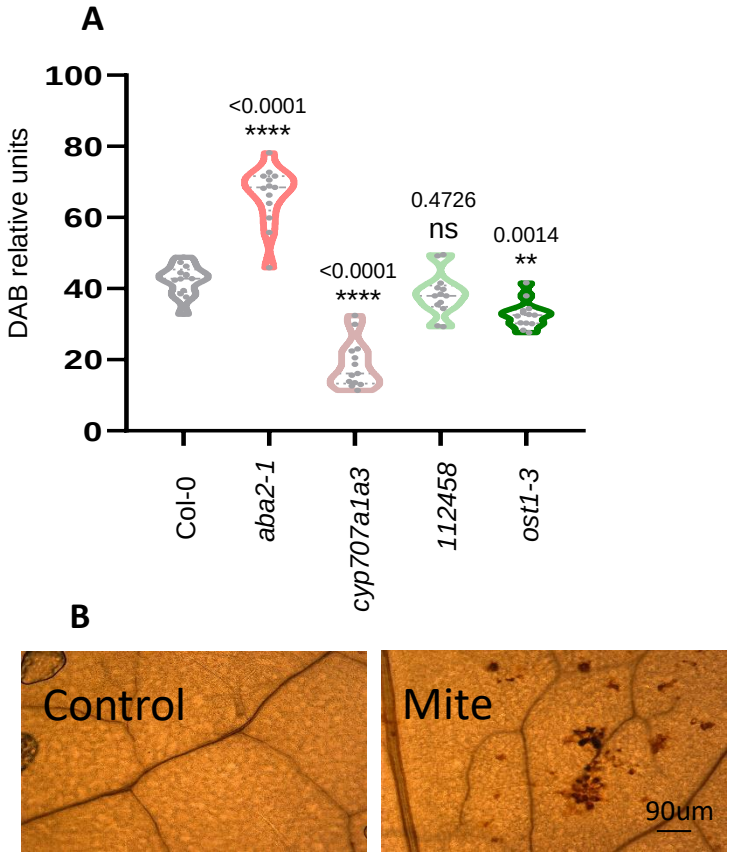

Figure 29. Redox status in the five Arabidopsis genotypes. A, Accumulation of H_2O_2 in detached leaves after 24 h of mite infestation, expressed as DAB units. Asterisks and numbers indicate significant differences compared to Col-0 genotype. Different letter indicates significant differences (P<0.5, One way ANOVA followed by Tukey's multiple comparison test). **B,** Pictures showing the H_2O_2 deposits during *T. urticae* feeding.

3.3.2.4 THE EFFECTS OF EXOGENOUS ABA APPLICATION ON MITE INFESTATION

As demonstrated above, exogenous ABA application induces stomata closure **(Figure 25C)**. To elucidate if ABA treatment affected plant defences, we pre-treated nlsABACUS2-400n plants by spraying ABA on the leaves 3 h before mite infestation and analysed cellular ABA levels and leaf responses to mites. As expected, ABA pre-treated and mite-infested plants displayed higher nlsABACUS2-400n biosensor emission ratios, indicating higher ABA levels, and the highest emission ratios were observed in those plants that were first pre-treated and then infested **(Figure 30A)**. Both ABA pre-treatment and mite infestation triggered stomata closure, with no synergistic or additive effects observed when the treatments were combined **(Figure 30B)**. The exogenous application of ABA before mite infestation helped plant defences since they showed less damage than non-pre-treated plants, and provided positive effects on plant growth, as shown in measurements of the rosette area **(Figure 30C, D, E)**. Thus, ABA pre-treatment enhanced mite defences and favoured plant growth during infestation.

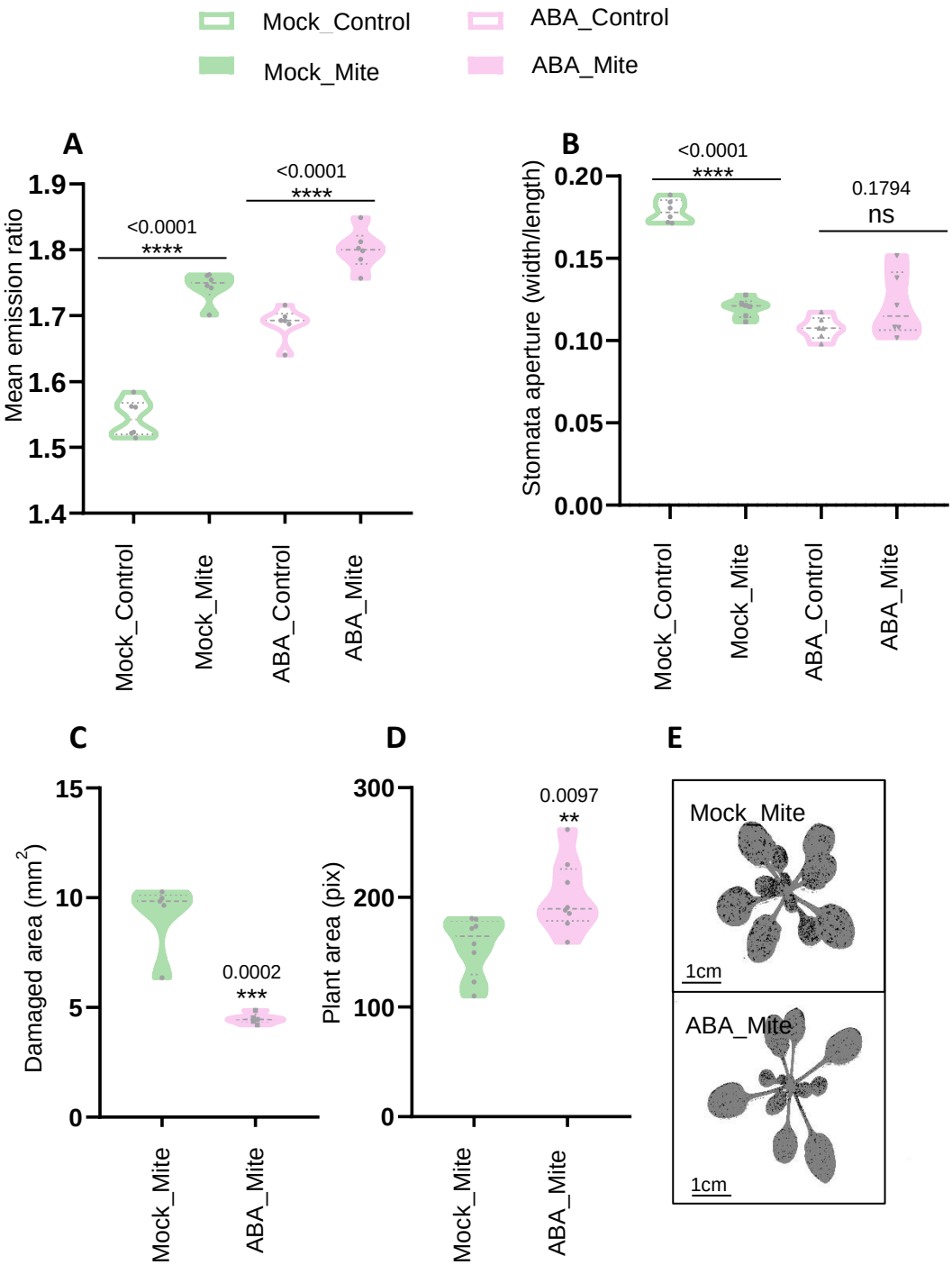
Mock_Control
Mock_Mite
ABA_Control
ABA_Mite
A
Mean emission ratio
1.9
1.8
1.7
1.6
1.5
1.4
<0.0001
****
<0.0001
****
Mock_Control
Mock_Mite
ABA_Control
ABA_Mite
B
Stomata aperture (width/length)
0.20
0.15
0.10
0.05
0.00
<0.0001
****
0.1794
ns
Mock_Control
Mock_Mite
ABA_Control
ABA_Mite
C
Damaged area (mm2)
15
10
5
0
0.0002
***
Mock_Mite
ABA_Mite
D
Plant area (pix)
300
200
100
0
0.0097
**
Mock_Mite
ABA_Mite
E
Mock_Mite
1cm
ABA_Mite
1cm

Figure 30. Effect of ABA pre-treatment of nls-ABACUS2-400n plants before mite infestation. Total emission ratio of biosensor signal **A**, stomata aperture is referred to width/length the width/length ratio **B**, damaged area expressed in mm_2 **C**, plant growth quantified in pixels **D** and infested Arabidopsis plant images ABA pre-treated and non-pre-treated **E**, of nls-ABACUS2-400n leaves either ABA-pre-treated for 3 h or non-pretreated, and then mite infested for 24h or in non-infested. A $P<0.05$ t-Student test was accomplished in all the panel. marked with one, two or three asterisks depending on significance. Data are means ± SE.

3.3.2.5 STOMATAL APERTURE DETERMINES MITE INFESTATION OUTCOME

As ABA accumulation and stomata closure are induced in response to mites, we questioned whether increased stomata aperture could provide any advantage for mite infestation. To clarify this point, Col-0 plants were pre-treated with FC, a compound that promotes stomata opening (Hunt *et al.*, 2010), with ABA to close stomata, or with both. After treatments, stomatal aperture and plant damage were measured, and results were compared with mock-treated and non-infested plants. Plants pre-treated either with ABA or FC presented closed and opened stomata, respectively, and the combination of both produced a stomatal aperture comparable to mock plants **(Figure 31A, B).** An experiment using different FC+ABA ratios demonstrated that low concentrations of FC (5 µM) were sufficient to keep stomata open (**Annexed Figure 4).** Upon mite infestation, stomata remained closed in ABA treated plants, remained open in FC treated plants, and were actively closed similarly to mock when ABA and FC were previously combined **(Figure 31B).** Plant damage results showed that more open stomata in the FC treatment correlated with higher leaf damaged area, indicating that open stomata facilitated mite **(Figure 31C).** As leaf damage increased in plants subjected to combined ABA and FC treatments compared with the ABA treatment alone, the control over stomatal aperture function of ABA is likely key for resistance to mite infestation.

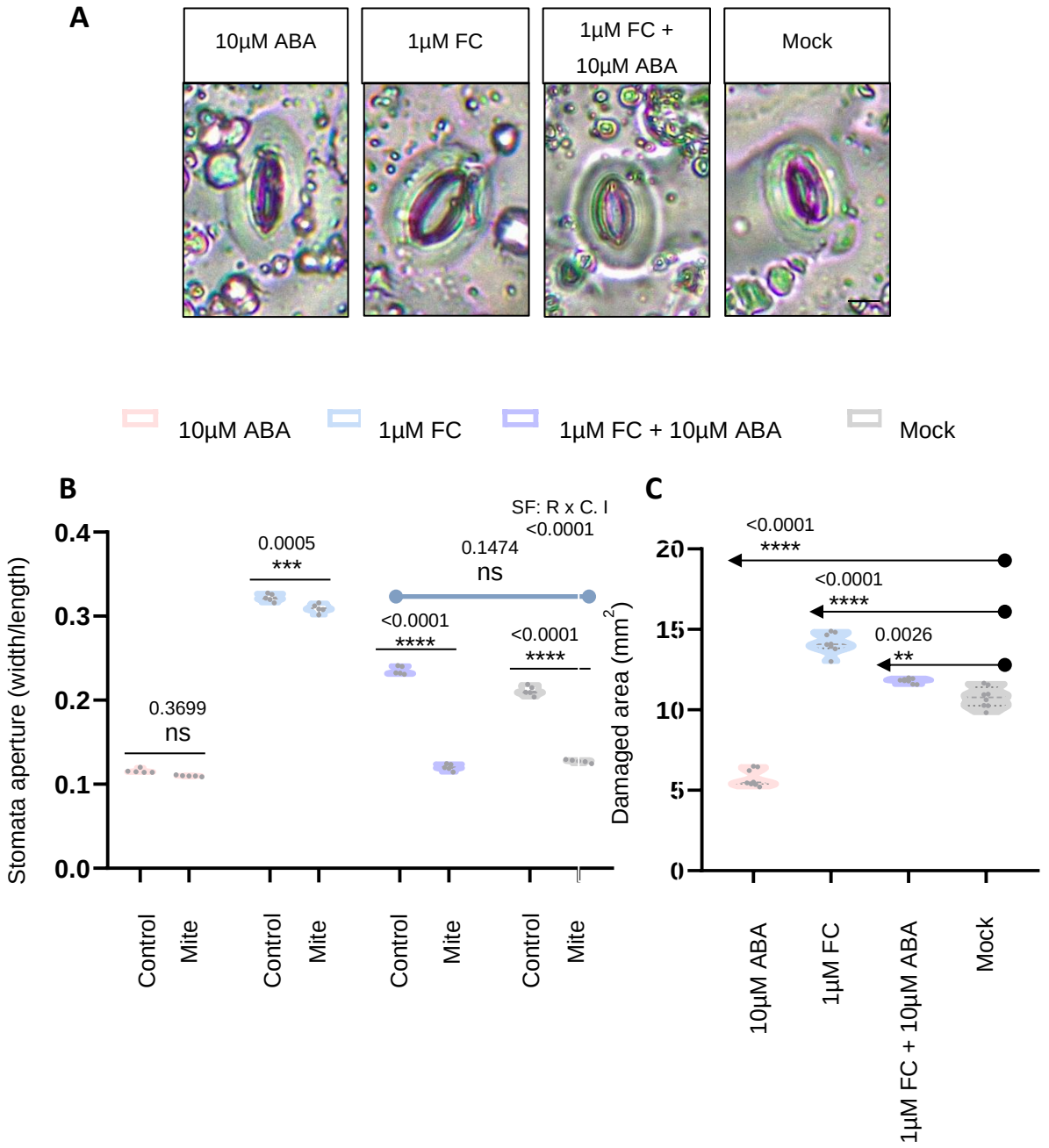

Figure 31. Effects of ABA (10 µM) and/or fussicoccin (1 µM) pre-treatments on stomata aperture and on Arabidopsis plant responses to mite infestation. A, Images of stomata behaviour in ABA and/or fusicoccin (FC) pre-treated plants. Bars = 8µm **B**, Stomata aperture in ABA and/or fusicoccin (FC) pre-treated plants after 24 h of mite infestation in detached leaves. Significant factors (SF) indicate whether the two independent factors, R (mite treatment) and C (Pre-treatment), and/or their interaction I (RxC) were statistically significant (Two-way ANOVA followed by Tukey's multiple comparison test, P<0.05). **C,** Plant damage in whole plant of ABA and/or fusicoccin (FC) pre-treated plants after 4 d of mite infestation. Numbers indicate significant differences compare to Mock treatment. One-way ANOVA followed by Tukey's multiple comparison test, P<0.05. Data are means ± SE of 8 biological replicates for the aperture and 9 biological replicates for damage.

3.3.2.6 EFFECT OF STOMATAL DENSITY ON MITE INFESTATION

Given the significance of stomatal closure as a defence mechanism against mite infestation, we investigated the potential involvement of stomatal density in the leaf as a contributing factor using Arabidopsis lines with higher and lower number of stomata than Col-0 plants. The selected plants were mutants in epidermal patterning factors (EPF), a family of secreted peptides that inhibit stomatal development (Hepworth *et al.*, 2015). We selected the *epf1epf2* mutant line and *EPF2OE*, an EPF2 over-expressing line. First, stomatal density was measured prior to mite infestation **(Figure 32A)**, and as expected, the *epf1epf2* mutant exhibited an elevated stomatal count, while the EFF2OE line displayed a reduced number of stomata. Then, we evaluated stomatal aperture in the three Arabidopsis genotypes with and without mite infestation and found that stomatal aperture in *EPF2OE* plants was higher than in *epf1epf2* or Col-0 plants **(Figure 32B).** Interestingly, infested *epf1epf2* mutant exhibited somewhat lessened stomatal closure than Col-0, though infestation closed stomata in all genotypes **(Figure 32B).** As stomata allow gas exchange between leaf mesophyll cells and atmosphere, contributing to leaf cooling (Chowdhury *et al.*, 2021), we also analysed whether the leaf temperature was dependent on the stomata number and if temperature variations were produced during mite infestation. Uninfested temperature of *epf1epf2* leaves was 2.2 ºC less than Col-0 and 3.1 ºC less than *EPF2OE* leaves (**Annexed table 6**, **Figure 32C).** consistent with stomatal density measurements. After mite infestation, an expected increase in leaf temperature was detected in Col-0 (+2.2 ºC) and to a lesser extent in *EPF2OE* (+1 ºC) plants that have fewer stomata. Mite infestation augmented leaf temperature in *epf1epf2* (+3.0 ºC), the mutant line with more stomata, although infested leaves remained cooler than in infested Col-0 and *EPF2OE* (**Annexed table 6**, **Figure 32C).** These temperature data corroborated the interrelationship between stomatal aperture and density in the plant response to mite infestation.

Finally, the damage produced by mites **(Figure 32D)** was quantified in these Arabidopsis plants. The *epf1epf2* line displayed more damage than Col-0 plants, while in the *EPF2OE*

line the mite damage was significantly reduced. The close correlation between stomatal density and damage (R squared = 0.9920; **Figure 32E)** indicate that the density of stomata in leaves is an essential feature that determines the success of mite infestation.

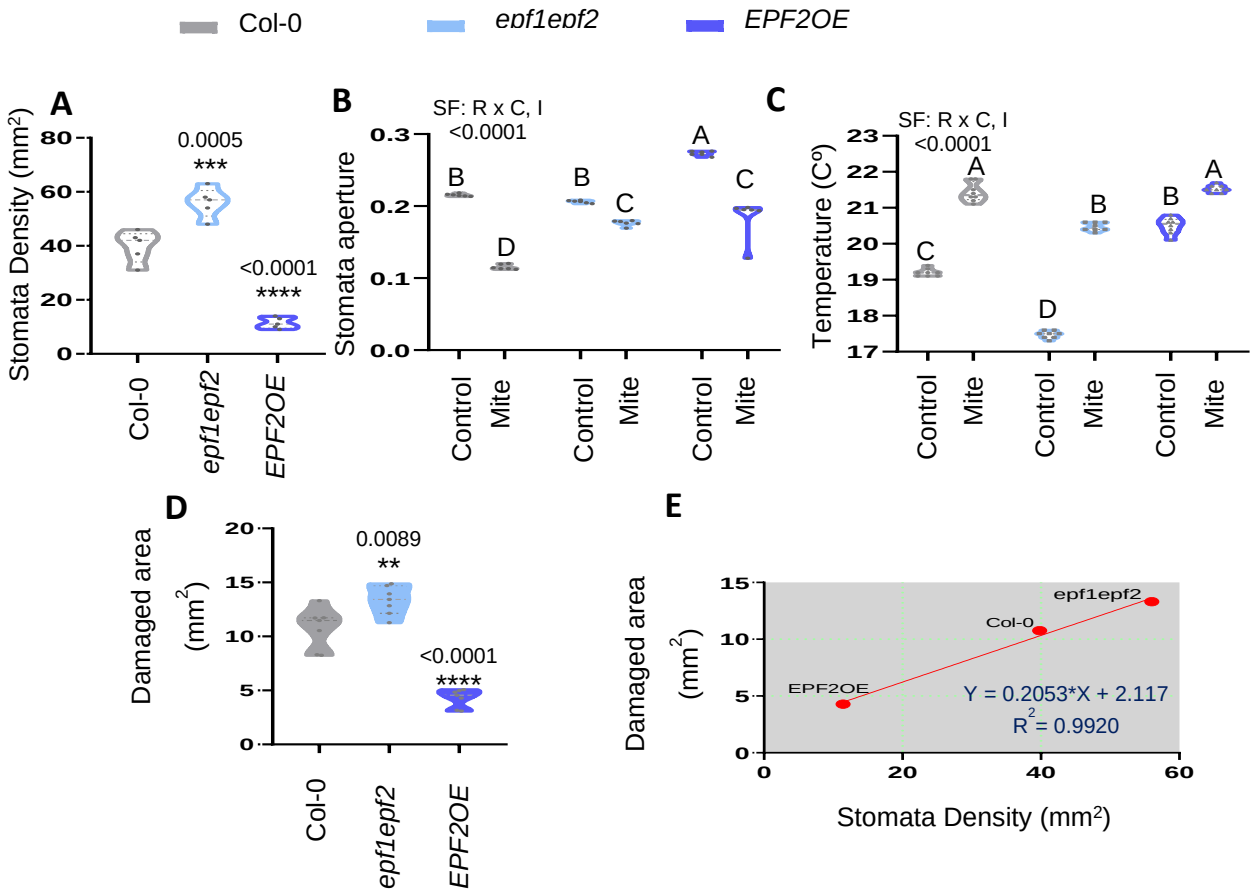

Figure 32. Stomata density in *epf1epf2* mutant, *EPF2OE* over-expressing line and Col-0 plants, and determination of damage, stomata aperture and temperature in the three genotypes after mite infestation. A, Stomata density is expressed as mm^2 per detached leaves. (P<0.05). Numbers indicate significant differences compare to Col-0 genotype. Data are means ± SE 9 biological replicates. One-way ANOVA followed by Tukey's multiple comparisons test, P<0.05. **B,** Stomata pore aperture is referred to the width/length ratio in detached leaves. **C,** Temperature in ºC measured in whole plants. Significant factors (SF) indicate whether the two independent factors, R (mite treatment) and C (genotype), and/or their interaction I (RxC) were statistically significant (Two-way ANOVA followed by Tukey's multiple comparison test, P<0.05). Data are means ± SE of 8 biological replicates. **D,** Foliar damage in whole plant, expressed in mm^2, was quantified 4 d after mite infestation. t-Student test was accomplished. Data are means ± SE for 8 biological replicates **E,** Correlation between stomata density and damaged area for the three Arabidopsis genotypes.

3.4 CHAPTER 4: TINY BUT MIGHTY: HOW A MIRNA MODULATES TARGET-NLRS UP TO THWART PLANT FEEDERS

3.4.1 FRAMEWORK

To optimize defense mechanisms, the expression of TNL genes is strictly regulated, maintaining a delicate balance between defense and growth. miRNAs play a crucial role in these precise regulatory mechanisms, modulating TNL production at the post-transcriptional level. This modulation prevents excessive activation while also minimizing the costs associated with plant resistance (López-Márquez *et al.*, 2023).

sRNAs exert post-transcriptional control over NLR production and bind to their target mRNAs through base pairing, thereby reducing protein expression by influencing mRNA stability or inhibiting translation. Besides the direct targeting to specific genes, miRNAs may also indirectly regulate gene expression by promoting the production of a phased array of secondary interfering RNAs, phasiRNAs, which act in a homology-dependent manner to amplify the silencing effects (Liu *et al.*, 2020; Kumar *et al.*, 2022).

Collectively, these findings underscore the intricate nature of miRNA-mediated defense regulation against herbivores. Furthermore, it would be intriguing to investigate whether distinct types of herbivores feeding elicit varying forms of post-transcriptional regulation.

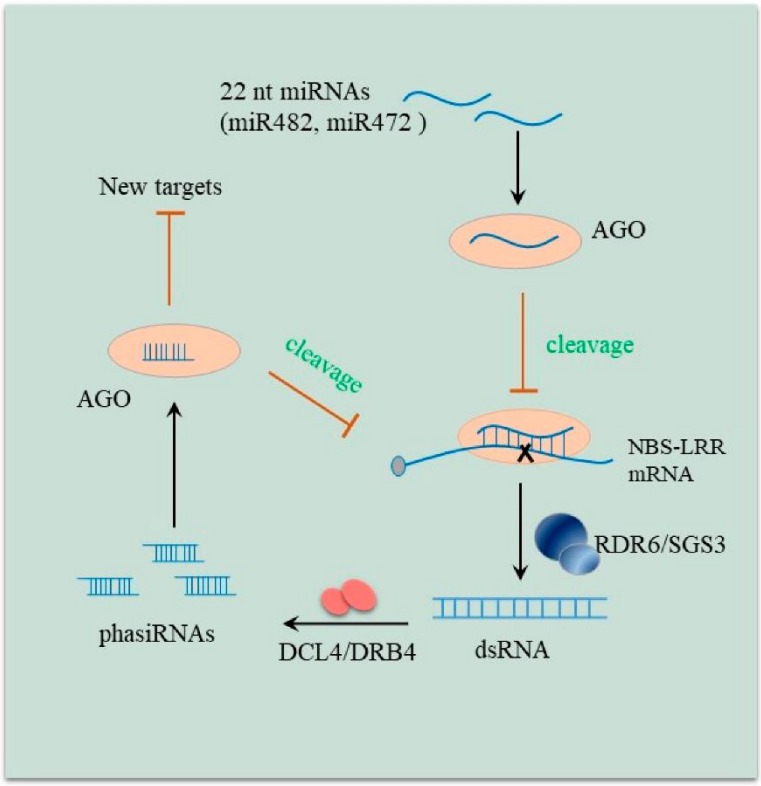

Figure 33. The regulatory network of 22 nucleotides (nt)-long miRNAs and NBS-LRR mRNAs involved in production of phasiRNAs. The 22-nt miRNA guides AGO protein to cleave the target site on the NBS-LRR transcript, triggering dsRNA synthesis mediated by RDR6 (RNA-DEPENDENT RNA POLYMERASES 6) and SGS3 (SUPPRESSOR OF GENE SILENCING 3). dsRNA is subsequently processed by DCL4 (DICER-LIKE 4) and DRB4 (DOUBLE-STRANDED-RNA-BINDING PROTEIN 4) to generate a cluster of 21-nt phased siRNAs (phasiRNAs). These 21-nt phasiRNAs are loaded into AGO proteins, which in turn can lead to NBS-LRR mRNAs cleavage. On the other hand, these siRNAs will depress newer targets. Scheme from (Yang *et al.*, 2021).

3.4.2 RESULTS

PLANT RECEPTORS ENCODING-GENES ARE UP-REGULATED BY MITES AND INSECT INFESTATION

Since receptors, either PRRs or NLRs have a crucial role at the starting step of PTI and ETI immune responses, respectively, we decided to identify and functional characterize receptor genes involved in triggering defence responses to *T. urticae*, a mite focus of our research in last years. We reanalysed previous RNAseq data derived from mite infested Arabidopsis plants after 0.5, 1, 3 and 24 h post-infestation (Santamaria *et al.*, 2021), and found a substantial set of up-regulated genes encoding receptors for each time point. The highest number of induced genes for all receptor types was detected at 0.5 h of infestation. Of particular interest were the 21 TNLs containing a TIR domain at the N-terminal of the protein, which were highly induced by mites at the earliest pot-infestation time to be then reduced to 7, 6 and 8 *TNL* mite-induced genes at 1, 3 and 24 h post-infestation **(Figure 34A)**. Among them, we selected AT4G14370.1 and AT5G41550.1 genes, referred from now on as *MRT1* and *MRT2* (Mite Related *TNL1* and *TNL2*), respectively, to further assays. This selection was based on: i) their up-regulation levels in response to mites; ii) their proteins contained a highly conserved TIR motif, adjacent to the catalytic residue for NAD^+-cleaving enzymatic activity, described as essential for TNL immune function (Wan *et al.*, 2019); iii) this TIR motif possessed a target sequence of the miR825-5p for TNL regulation (López-Márquez *et al.*, 2021).

The expression patterns of *MRT1* and *MRT2* genes found in the dataset coming from the Arabidopsis-mite transcriptomic analysis were confirmed by qRTPCR assays **(Figure 34B, C)**. The expression levels of the miR825-5p and its primary miRNA (PrimiR825-5p) were also analysed by qRTPCR at different mite post-infestation times. Results demonstrated that both, primary and mature forms, were induced by mites and showed a negative correlation with mRNA profiles of *MRT1* and *MRT2* genes along the infestation times. miR825-5p and PrimiR825-5p presented the lowest expression levels at 0.5 h post-infestation and increased at longer infestation times, which was the opposite to expression pattern observed for *MRT1* and *MRT2* genes **(Figure 34D)**.

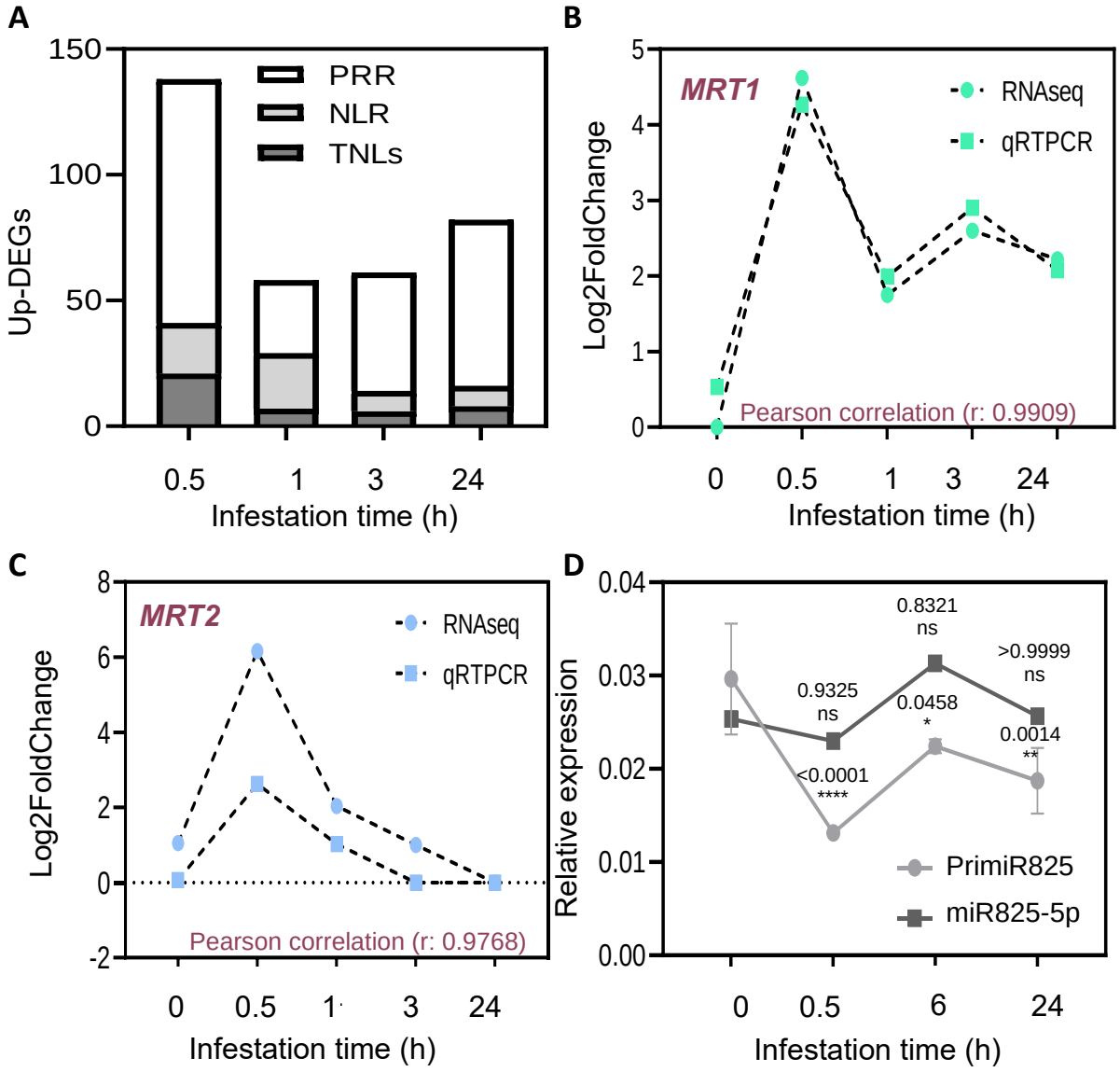

Figure 34. Expression of receptor genes in Arabidopsis Col-0 plants in response to *T. urticae* infestation at 0.5, 1, 3 and 24 h post-infestation. A PRR, NLR and TNL up-regulated genes at different mite infestation times detected in RNAseq data from Santamaria *et al*., 2021. Relative expression of *MRT1*; **B**, *MRT2*; **C** and miR825-5p and its primary form (PrimiR825); **D** at different infestation times. r value indicates Pearson correlation between RNAseq and qRTPCR data **B, C**. **D** Asterisks indicates significant differences for PrimiR825-5p or miR825-5p respect time 0 h (P<0.5, Two-way ANOVA followed by Tukey's multiple comparison test).

Using WM3 and default parameters on Araport11 tools, Lopez-Marquez *et al*. (2021) predicted a group of *TNLs* as putative targets of miR825-5p. Six of these *TNLs*, including *MRT1* and *MRT2*, were highlighted because displayed lower hybridization energies and better paring than the rest (**Figure 35**; Lopez-Marquez *et al.,* 2021).

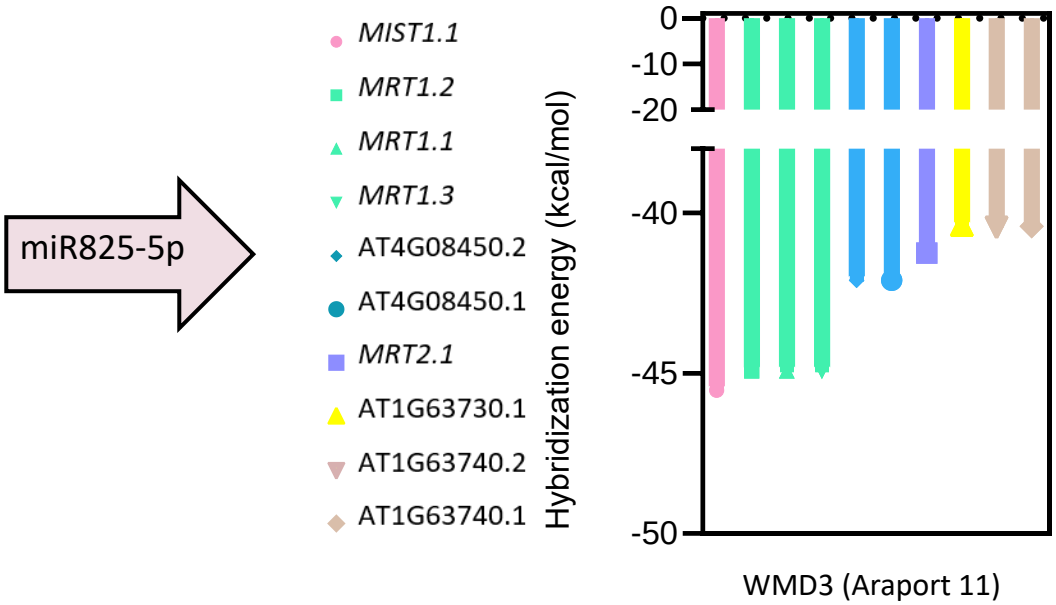

Figure 35. Hybridization energies of TNL genes putative targets of the miR825-5p. Hybridization energies of 6 TNL gene isoforms potential targets of miR825-5p using WM3 and default parameters on Araport11 tools. Extracted from López-Márquez *et al*., 2021.

We also analysed the expression profiles of the six genes at 0.5 h of mite infestation by qRTPCR assays. Results demonstrated that only *MRT1* and *MRT2* genes were significantly induced by mites, while neither AT5G38850 gene, previously termed *MIST1* (Lopez-Marquez *et al.,* 2021) or AT4G8450, AT1G63730 and AT1G63740 genes altered their expression patterns **(Figure 36).** Additionally, we checked whether these six *TNL* genes responded to an infestation mediated by the chewing larvae of *P. brassicae*. RTqPCR assays and revealed that not only *MRT1* and *MRT2* were significantly up-regulated at 0.5 h post-infestation but also the levels of *MIST1* and AT1G63740 genes were induced by this feeder **(Figure 37).** Moreover, the expression of miR825-5p and PrimiR825-5p were tested at 0.5, 1, 3 and 24 h of *Pieris* post-infestation, and qRTPCR

experiments showed that the expression profiles of both miR825-5p forms perfectly mimicked the profiles obtained in response to mite feeding along the infestation times **(Figure 38).**

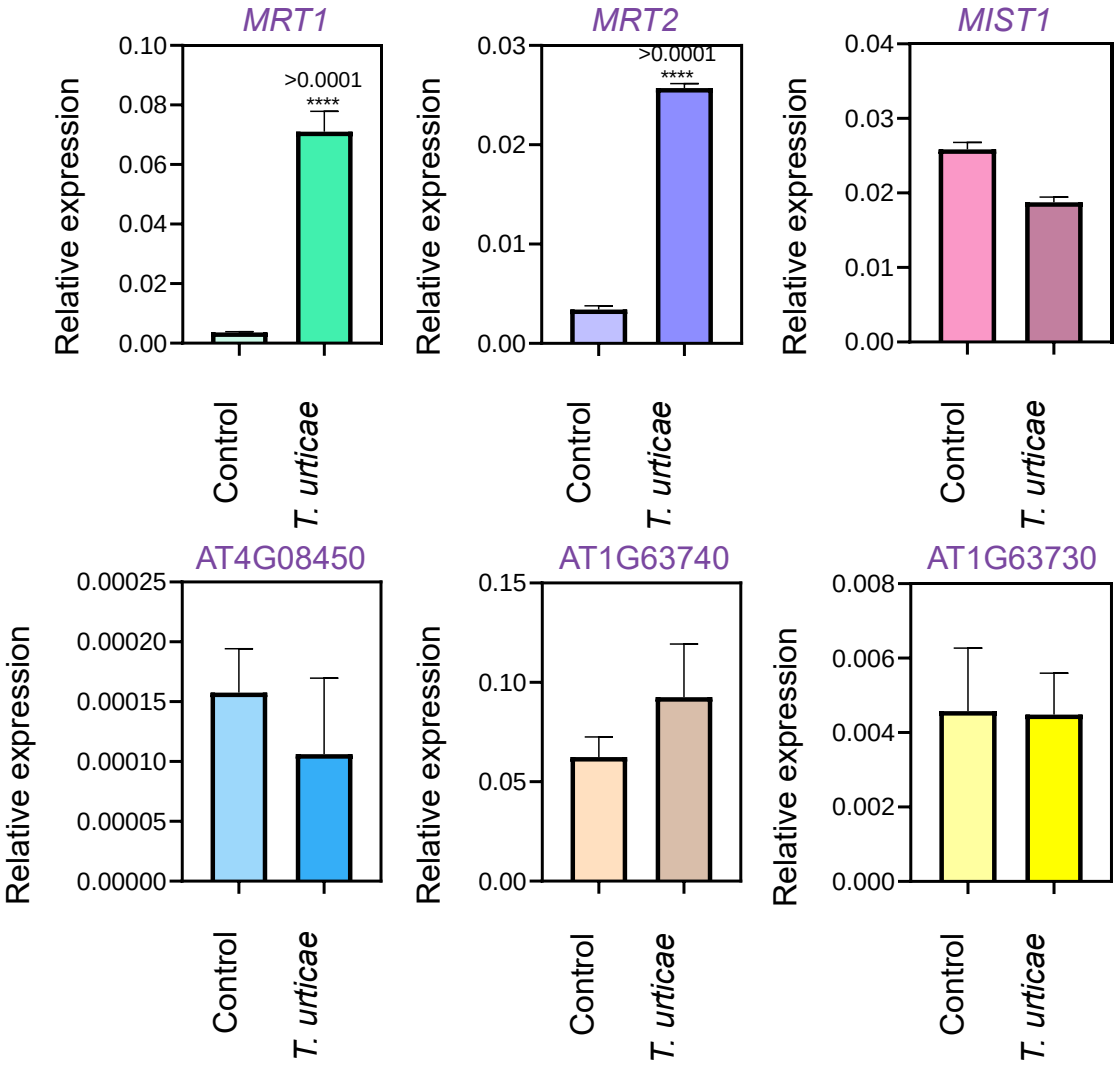

Figure 36. Gene expression profiles TNL genes putative targets of the miR825-5p at 0.5 h after *T. urticae* infestation. Relative expression levels of TNL genes in Col-0 Arabidopsis plants after 0.5 h of mite infestation. TNL genes: *MRT1* isoforms, AT4G14370.1, AT4G14370.2 and AT4G14370.3; *MRT2*: AT5G41550; *MIST1*, AT5G38850.1, and AT4G08450.1; AT4G08450.2; AT1G63730.1; AT1G63740.1 and AT1G63740.1. Data are mean ± SE of three replicates. Asterisks indicates significant differences respect control plants (P<0.5, t- student test).

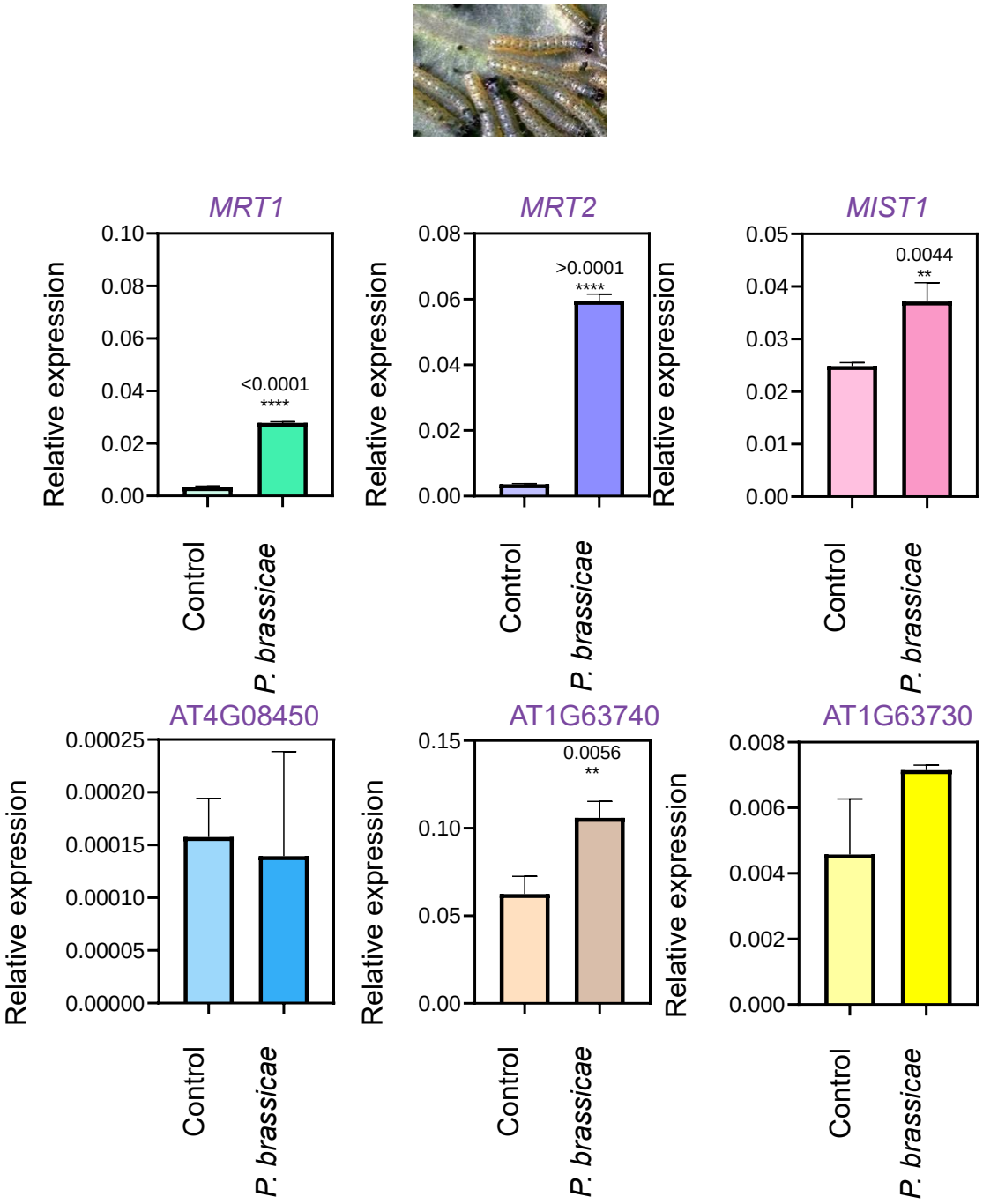

Figure 37. Expression profiles of TNL genes 0.5 h after *P. brassicae* infestation. Relative expression levels of TNL genes in Col-0 Arabidopsis plants after 0.5 h of *Pieris* larvae infestation. TNL genes: *MRT1* isoforms, AT4G14370.1, AT4G14370.2 and AT4G14370.3; *MRT2*: AT5G41550; *MIST1*, AT5G38850.1, and AT4G08450.1; AT4G08450.2; AT1G63730.1; AT1G63740.1 and AT1G63740.1. Data are mean ± SE of three replicates. Asterisks indicates significant differences respect control plants (P<0.5, t-student test).

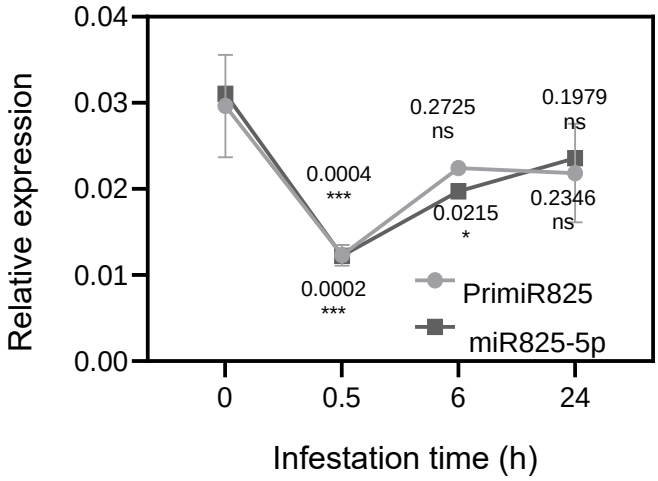

Figure 38. Expression of and miR825-5p and its primary form (PrimiR825-2p) in Arabidopsis Col-0 plants in response to *P. brassicae* infestation at 0.5, 1, 3 and 24 h post-infestation. Data are mean ± SE of three replicates. Asterisks indicates significant differences for PrimiR825-5p or miR825-5p respect time 0 h (P<0.5, Two-way ANOVA followed by Tukey's multiple comparison test).

MRT1 AND *MRT2* SHARE A HIGHLY SIMILAR TIR DOMAIN BUT DIFFER IN OTHER PROTEIN DOMAINS

To assess the functional relevance of these proteins, we conducted a comparative analysis of their features and sequences. Both proteins were found to belong to the Disease R genes family, with three primary domains: a Toll/interleukin-1 receptor homology domain, an NB-ARC domain, and a Leucine-rich repeat domain superfamily domain (TIR-BNS-LRR) **(Annexed Figure 5A).**

A closer look at the Leucine-rich repeat domain superfamily revealed differences between MRT1 and MRT2. MRT1 has three LRR_8 subdomains and two LRR_4 subdomains, while MRT2 has the same three LRR_8 subdomains and an additional subdomain labelled LRR_5. Comparing the entire proteins, MRT1 and MRT2 share 50% identity, but when aligning both TIR domains, they exhibit over 80% identity **(Annexed Figure 5B).** GO analysis also suggests that both genes have common biological functions related to signal transduction. Notably, the putative binding site for miR825-5p is located within this shared TIR domain at the transcription level **(Annexed Figure 5C).**

MRT1 AND MRT2 ARE INVOLVED IN ARABIDOPSIS DEFENCE AGAINST *T. URTICAE* AND *P. BRASSICAE* INFESTATION

To investigate the potential role of the two *MRT* genes in defence against the two pest species, Arabidopsis Col-0 and two T-DNA insertion lines for *MRT1* and two for *MRT2* genes, *mrt1-1, mrt1-2,* and *mrt2-1, mrt2-2*, respectively **(Annexed Figure 6A, B)**, were selected for further studies. All mutants were analysed and results from qRTPCR assays showed a significant reduction of the transcript content of *MRT1* and *MRT2* in the corresponding mutant lines indicating that the four mutants were knock-down lines **(Annexed Figure 6C, D)**. We also studied the gene expression patterns of *MRT1* in *mrt2* lines and *MRT2* in *mrt1* lines after mite infestation. Notably, mRNA levels of both genes were much higher in the infested complementary mutant lines than in infested Col-0 plants **(Annexed Figure 7A, B)**. These data indicated the functional redundancy of both genes and how each *MRT* highly compensated the lack of the other gene. Likewise, the expression levels of miR825-5p were also determined in infested *mrt1*, *mrt2* and Col-0 plants, but no significant alterations in none of the genotypes was observed **(Annexed Figure 7C, D)**.

Arabidopsis mutant lines for *MRT1* and *MRT2* genes and Col-0 plants were used to perform infestation bioassays. After 4 d of mite feeding, the rosette damage was significantly lower in all mutant lines than in Col-0 plants **(Figure 39A, B).** These differences in leaf damage correlated with a higher number of nuclei detected by DAPI staining, which indicated cell viability, and higher levels of callose deposition detected in the mutant lines in comparison to Col-0 plants **(Annexed Figure 8A, B, D, E).** Besides, the cell death area and the electric leakage determined after 24 h of mite infestation resulted much greater in *mrt1* and *mrt2* lines than in Col-0 plants **(Figure 39C, D**; **Annexed Figure 8C, F**). The effect of the five Arabidopsis genotypes on *T. urticae* was evaluated by measuring mite mortality and fecundity after feeding on mutants and Col-0 plants. The percentage of mite mortality increased when they fed on mutant lines,

except for the *mrt1-1* line, and the cumulative number of eggs was also higher in the four knock-down lines than in Col-0 plants **(Figure 40 A, B, C, D).**

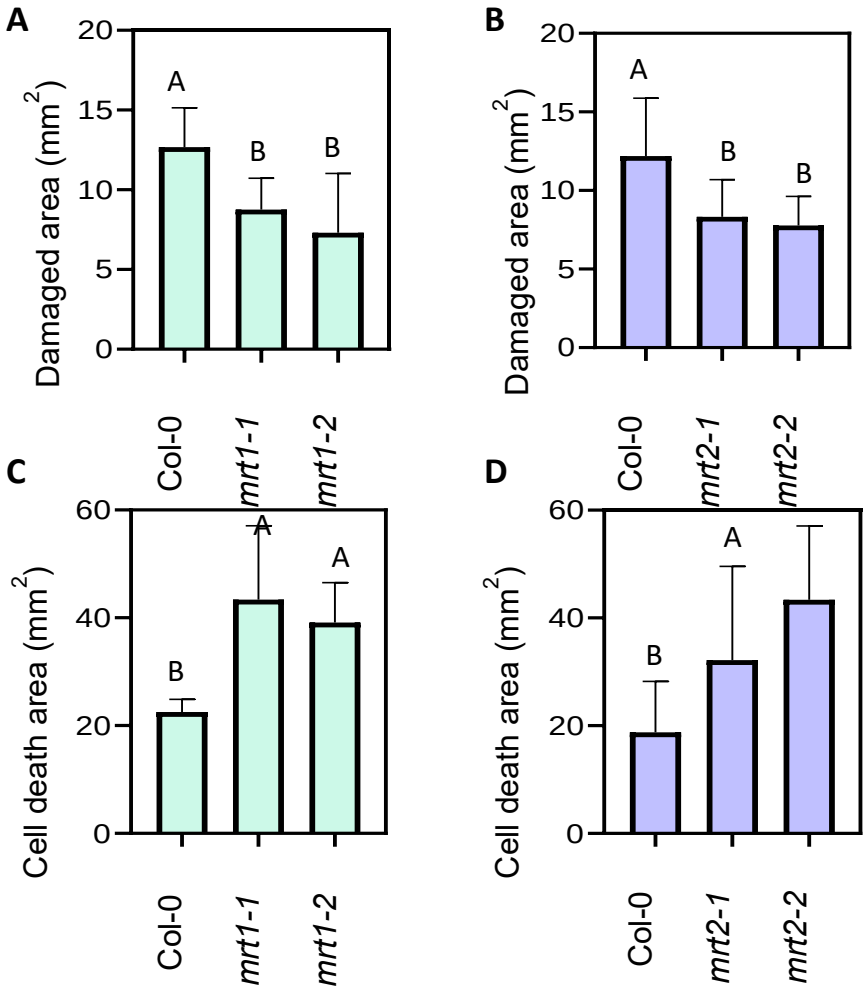

Figure 39. Plant damage, cell death after feeding on Col-0 and *mrt1* and *mrt2* mutant lines. A, B, Foliar damage quantified in Col-0 and *mrt* mutant lines after 4 d of mite infestation. **C, D,** Cell death quantified in Col-0 and *mrt* mutant lines after 24 h of mite infestation. Data are mean ± SE of nine **(A, B)** and ten **(C, D)** replicates. Different letter indicates significant differences (P<0.5, One way ANOVA followed by Tukey's multiple comparison test).

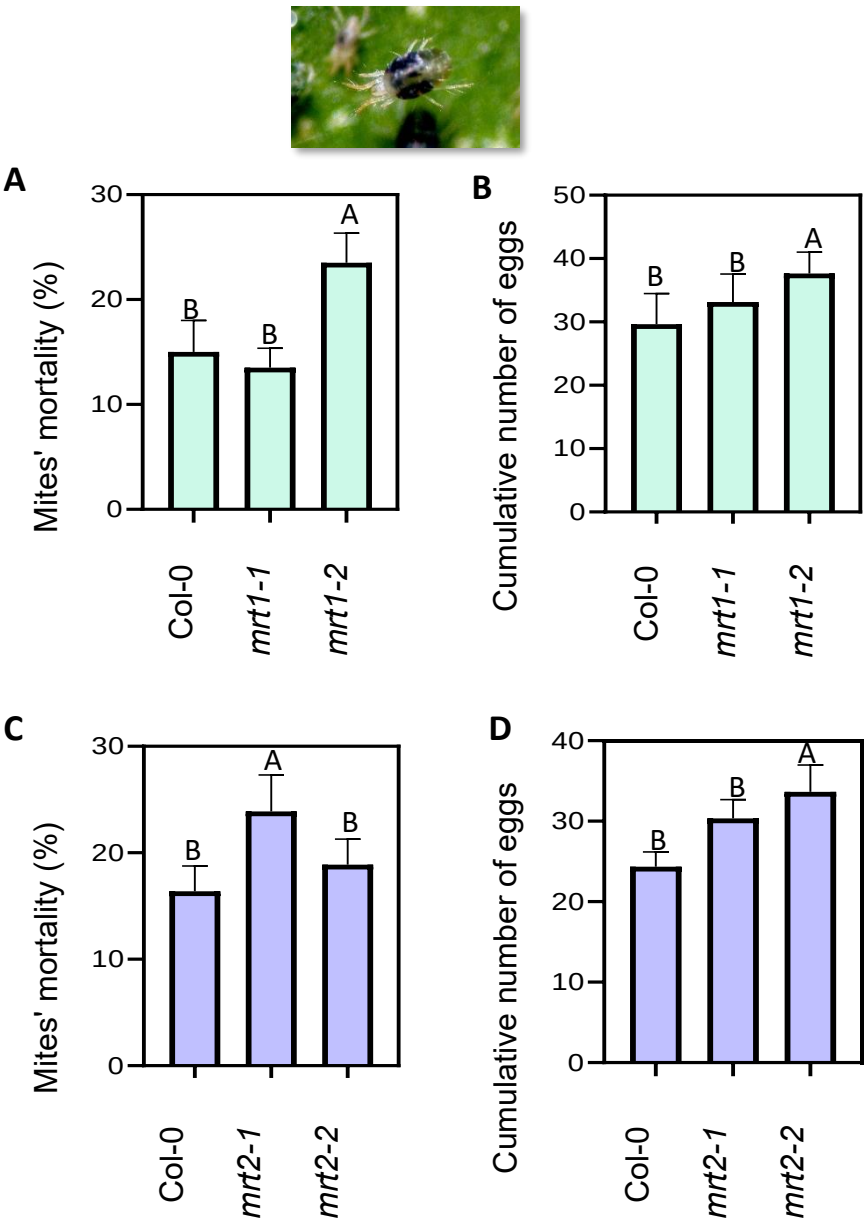

Figure 40. *T. urticae* mortality and fecundity after feeding on Col-0 and *mrt1* and *mrt2* mutant lines. A, B, Mite mortality quantified in Col-0 and *mrt* mutant lines 24 h of mite infestation. **C, D,** Cumulative number of mite eggs measured 36 h of infestation with synchronized mite females. Data are mean ± SE of six replicates. Different letter indicates significant differences (P<0.5, One way ANOVA followed by Tukey's multiple comparison test).

On the other hand, feeding experiments with *P. brassicae* on Arabidopsis mutant lines for the *MRT1* and *MRT2* genes resulted in a smaller remaining area of leaf discs after feeding compared to Col-0 plants **(Figure 41A)**. Additionally, a significant increase in larval weights was observed in the *mrt1-1* and *mrt2-2 mutant lines* **(Figure 41B)**. This results, together with *T. urticae* data pushed us to generate double *mrt1-mrt2* mutant lines by crossing single *mrt1-2* and *mrt2-1* lines to confirm the defence role of both *MRT* genes to both herbivores.

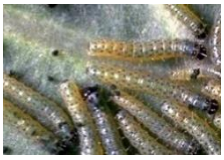

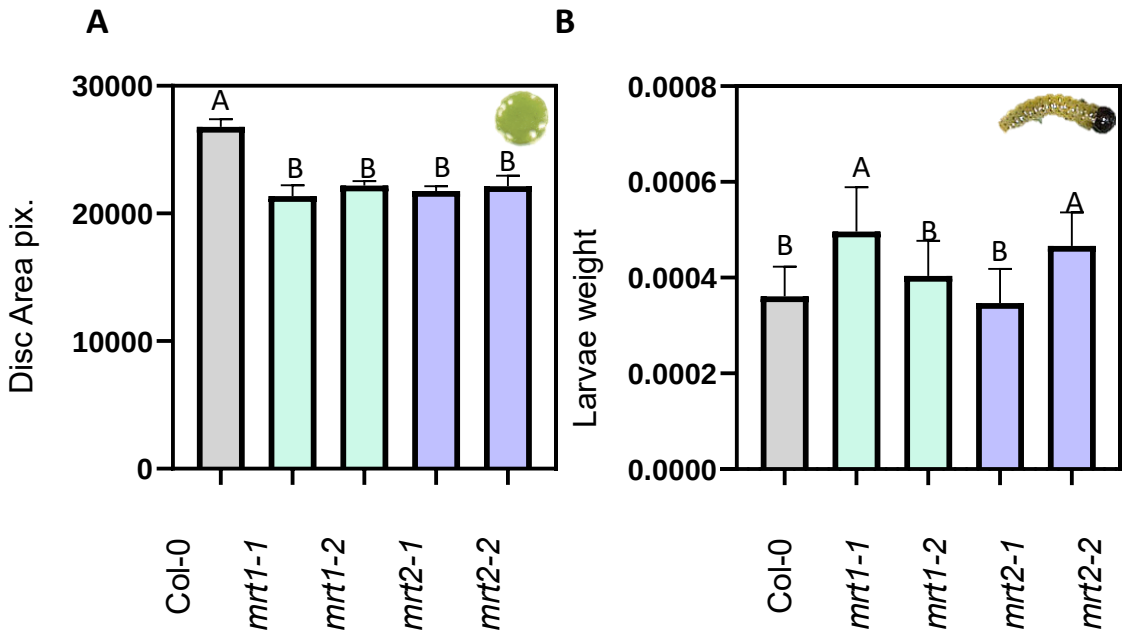

Figure 41. Plant damage, larvae weight after *P. brassicae* feeding on Col-0 and *mrt1* and *mrt2* single mutant lines. A, Remaining leaf tissue area after 8 h of Pieris larvae feeding on Col-0 and *mrt1-mrt2* mutant lines. **B,** Pieris larvae weight after 24 h of feeding on Col-0 and *mrt1-mrt2* mutant lines. Data are mean ± SE of twelve **(A)** and twenty-four **(B)** replicates. Different letter indicates significant differences (P<0.5, One way ANOVA followed by Tukey's multiple comparison test).

To assess the lack of expression of both genes in double mutants, RTqPCR assays were conducted, confirming the knock-down character of double *mrt1-mrt2* mutant plants **(Annexed Figure9A, B).** Notably, no discernible differences in terms of growth or

development were observed when comparing double *mrt1-mrt2* mutant lines with Col-0 plants **(Annexed Figure 9C).**

Considering the compensatory effect observed between the *MRT1* and *MRT2* genes in single mrt1 and mrt2 mutants, it became crucial to analyze the basal expression levels of other R genes, *MIST1,* AT4G08450*,* AT1G63740 and AT1G63730, two of them also induced by *Pieris* infestation. RTqPCR assays were employed to assess this **(Annexed Figure 10).**

To conclusively demonstrate the functional relevance of *MRT1* and *MRT2* in defense mechanisms, feeding bioassays with *T. urticae* and *P. brassicae* were performed using double *mrt1-mrt2* double mutant lines and Col-0 plants.

The lack of expression of MRT1 and MRT2 in *mrt1-mrt2* double mutant displayed significantly more damage than the Col-0 plants **(Figure 42A)**. Concomitantly, fecundity of mites fed on *mrt1-mrt2* double mutant showed greater rates than the ones fed on Col-0 **(Figure 42B).**

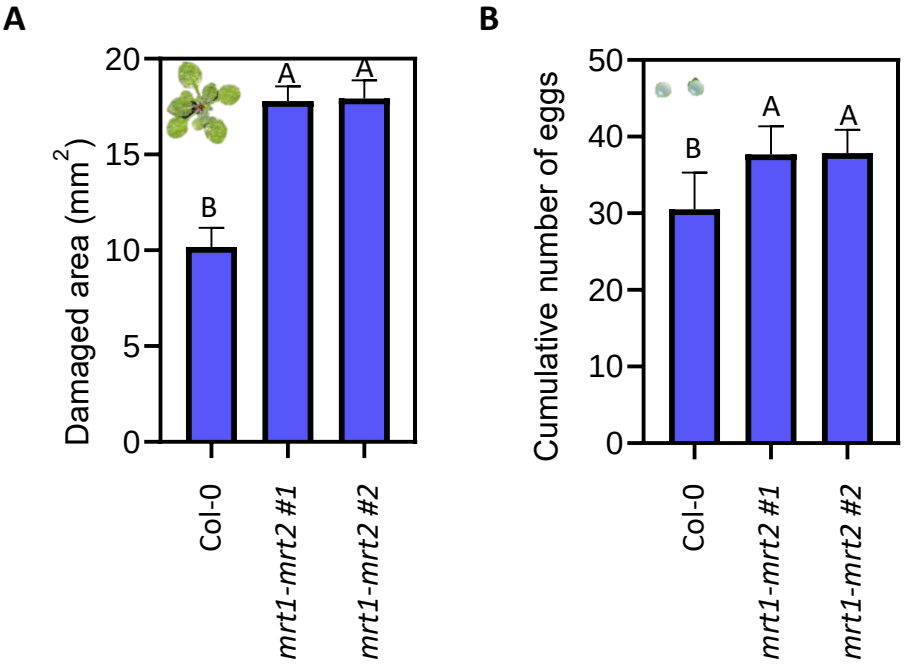

Figure 42. Plant damage and mite performance in *mrt1-mrt2*- double mutant and Col-0 Arabidopsis genotypes. A, Foliar damaged area was quantified in Col-0 and *mrt1-mrt2* double mutant after 4 d of mite infestation. **B,** Effects of Arabidopsis genotypes on *T. urticae* fecundity measured 36 h after infestation with synchronised mite females. Data are mean ± SE of nine **(A)** and six **(B)** replicates. Different letter indicates significant differences (P<0.5, One way ANOVA followed by Tukey's multiple comparison test).

Furthermore, feeding experiments conducted with *Pieris* larvae revealed that *mrt1-mrt2* double mutant plants decreased resistance to *Pieris* infestation, as evidenced by a significantly larger remaining area of leaf discs after feeding compared to both Col-0 plants and silencing lines. Additionally, a substantial increase in larval weights was observed **(Figure 43A, B**).

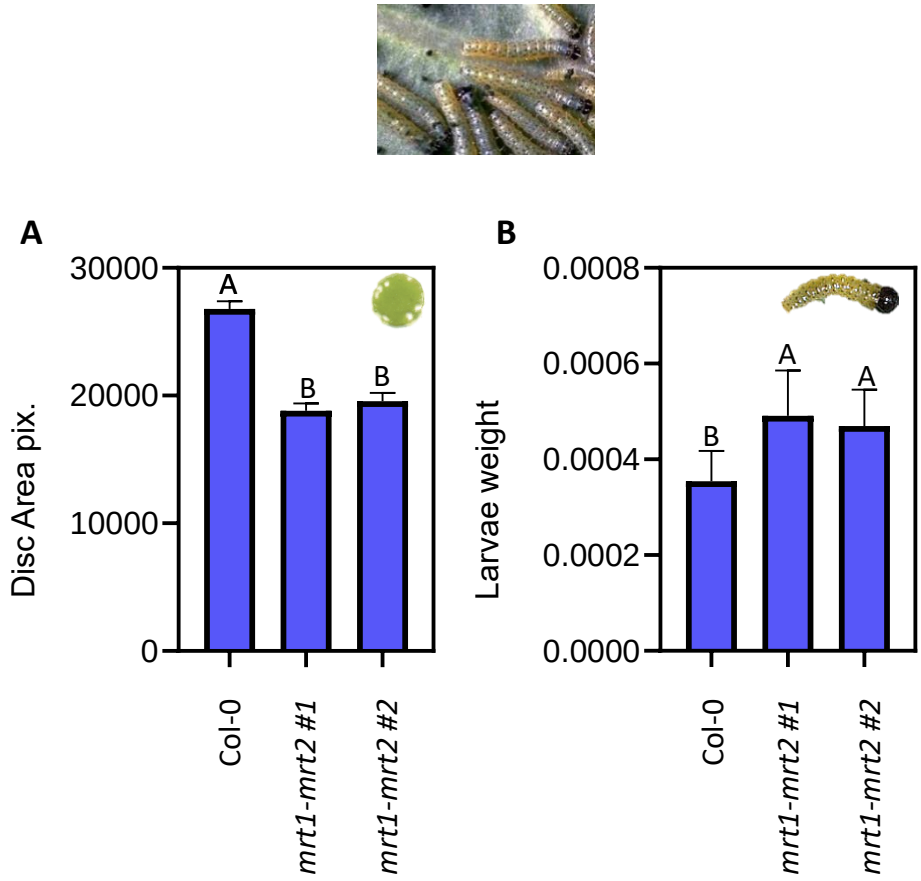

Figure 43. Plant damage, larvae weight after *P. brassicae* feeding on Col-0 and *mrt1-mrt2* double mutant lines. A, Remaining leaf tissue area after 8 h of Pieris larvae feeding on Col-0 and *mrt1-mrt2 double mutant*. **B,** *Pieris* larvae weight after 24 h of feeding on Col-0 and *mrt1-mrt2 double mutant* lines. Data are mean ± SE of twelve **A** and twenty-four **B** replicates. Different letter indicates significant differences (P<0.5, One way ANOVA followed by Tukey's multiple comparison test).

The examination of plant phenotypic responses and herbivore performance necessitates the assessment of key defensive markers, including plant hormones associated with defense against herbivores.

The expression of *VSP2* marker gene for the JA and *PR1* for SA pathway were determined in non-infested and 24 h mite post-infestation in Col-0 and *mrt1-mrt2* double mutant plants. In infested plants, both marker genes were induced but *mrt1-mrt2* double mutant displayed less mRNA levels than Col-0 **(Figure 44)**.

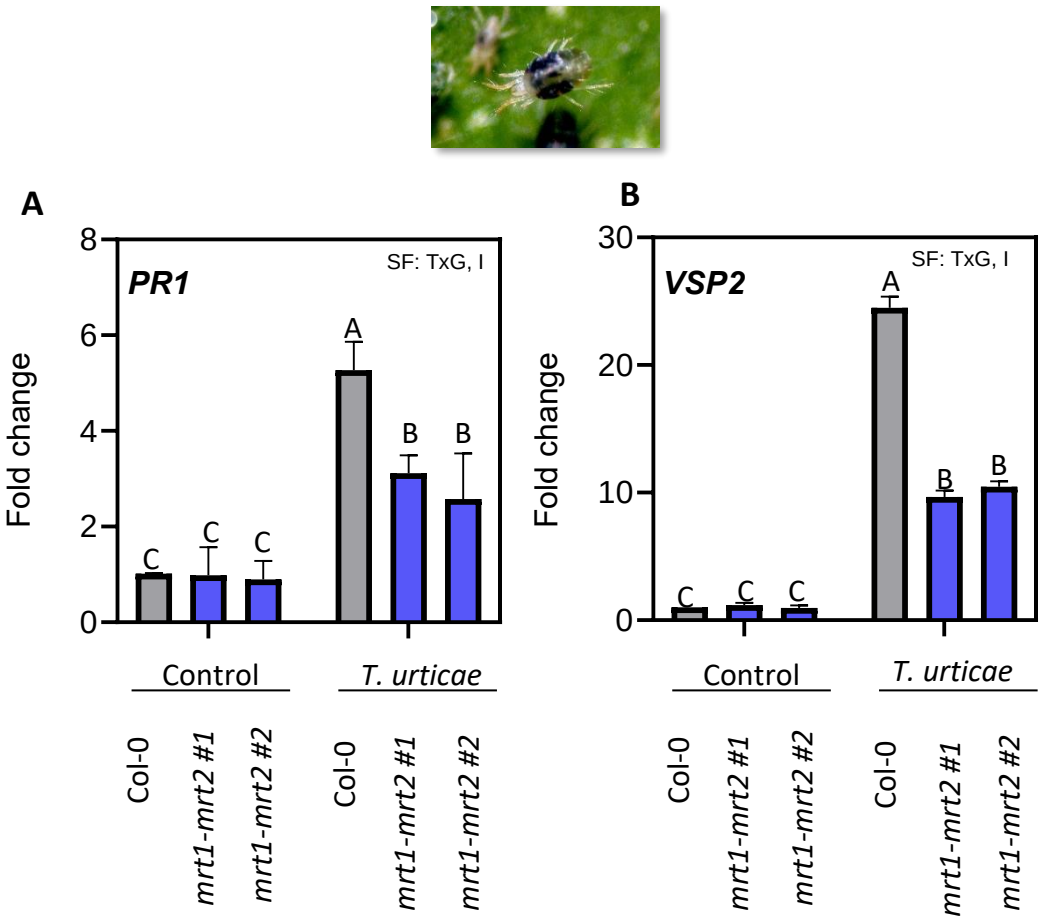

Figure 44. Gene expression analysis of *PR1*, *VSP2* in *mtr1-mrt2* double mutant after 24 h of *T. urticae* infestation. A, *PR1* and **B,** *VSP2* relative expression in *mtr1-mrt2* double. Data are means ± SE of three replicates. Significant factors (SF) indicate whether the two independent factors, G (genotype) and T (mite treatment), and/or their interaction (TxG,I) were statistically significant. Different letter indicates significant differences (P<0.5, Two-way ANOVA followed by Tukey's multiple comparison test).

Same situation occurs when the chewer *P. brassicae* feed from *mrt1-mrt2* double mutant plants. mRNA of *PR1* and *VSP2* hormone gene markers were also induced during the feeding. In addition, differences between the genotype's Col-0 and *mrt1-mrt2* double mutant plants were also found **(Figure 45)**. Specifically for *P. brassicae,* we also measured the expression of *MIST1* during the chewing feeding. *MIST1* was induced

during the infestation, and *mrt1-mrt2* double mutant displayed more mRNA levels than Col-0 **(Figure 46)**.

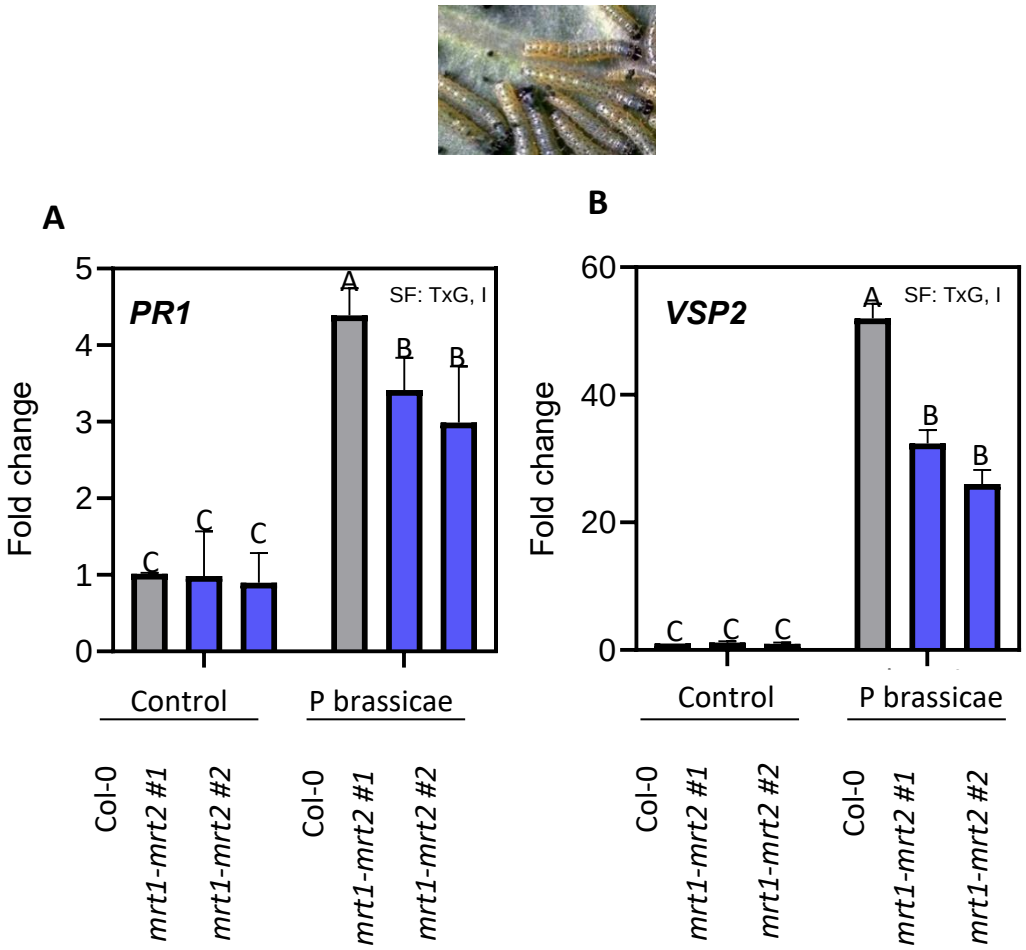

Figure 45. Gene expression analysis of *PR1*, *VSP2* in *mtr1-mrt2* double mutant after 24 h of *P. brassicae* infestation. A, *PR1* and **B,** *VSP2* relative expression in *mtr1-mrt2* double. Data are means ± SE of three replicates. Significant factors (SF) indicate whether the two independent factors, G (genotype) and T (mite treatment), and/or their interaction (TxG,I) were statistically significant. Different letter indicates significant differences (P<0.5, Two-way ANOVA followed by Tukey's multiple comparison test).

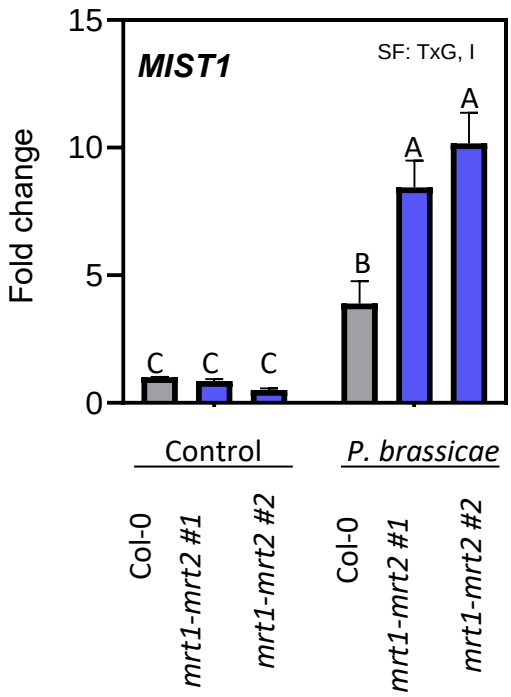

Figure 46. Gene expression analysis of *MIST1* in *mtr1-mrt2* double mutant after 24 h of *P. brassicae* infestation. Data are means ± SE of three replicates. Significant factors (SF) indicate whether the two independent factors, G (genotype) and T (mite treatment), and/or their interaction (TxG,I) were statistically significant.

In both herbivore situations, statistical analysis demonstrated that the expression pattern of hormone marker genes was dependent on the genotype and the mite treatment and the interaction between both **(Figures 44** and **45)**. These events suggested that the lack of *MRT1* and *MRT2* genes has a repercussion in the activation of plant hormone defences.

MIR825-5P DIFFERENTIALLY REGULATE DEFENCES AGAINST *T. URTICAE* AND *P. BRASSICAE*

To determine the participation of the miR825-5p in plant defence to herbivory, Arabidopsis transgenic plants silencing or over-expressing this microRNA, (*STTM825-5p* line #3 and #4 lines and amiR825-5p lines #3 and #12 lines, respectively), previously generated by Lopez-Marquez *et al.* (2021) were used. The miR825-5p expression levels in these Arabidopsis genotypes after 24 h of mite infestation demonstrated a high basal accumulation of miR825-5p in the over-expressing lines which was significantly reduced after mite feeding, but no alterations in the low basal miR825-5p levels were detected in infested knock-down lines **(Figure 47A)**. Moreover, cell death was triggered in the mir825-5p knock-down lines but was not modified in the over-expressing lines **(Figure 47B)**. When the accumulation of endogenous *MRT1* and *MRT2* transcripts were measured in these lines, only the amount of *MRT1* transcripts negatively correlated with miR825-5p content. **(Figure 48A, B)**. Similar correlation was previously reported for the expression levels of *MIST1* in over-expressing miR825-5p lines (Lopez-Marquez *et al*., 2021). These results suggested that miR825-5p might regulate *MRT1* and *MIST1* protein production.

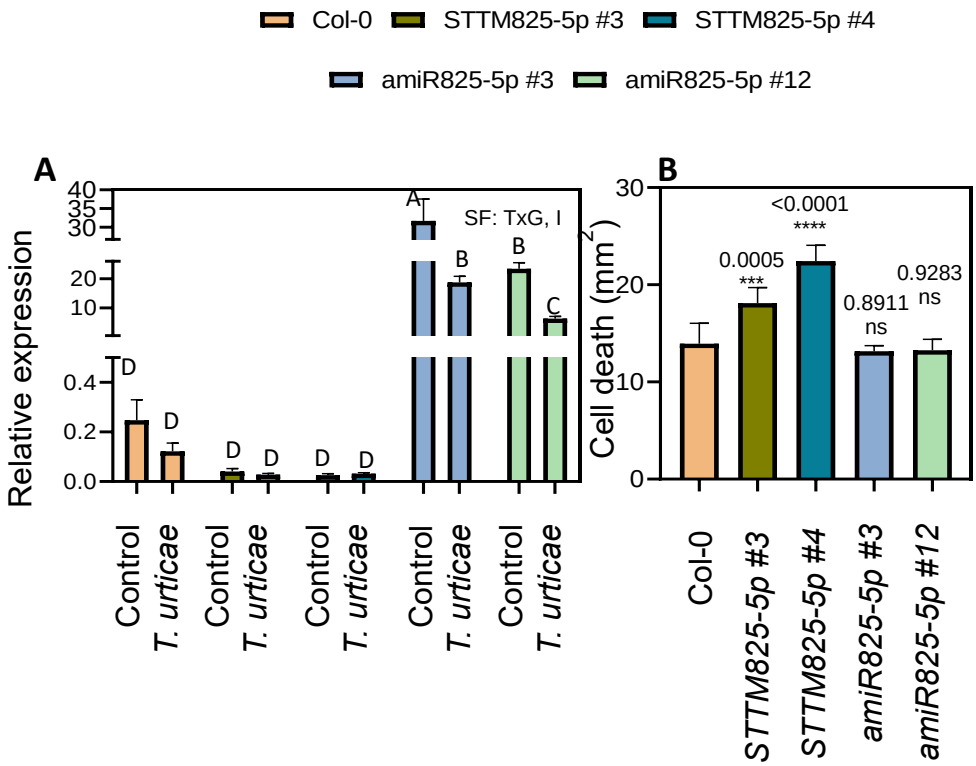

Figure 47. Molecular characterization of miR825-5p lines from López-Márquez *et al., (*2021) after *T. urticae* infestation. A, Relative expression of miR825-5p after 0.5 h of infestation**. B,** Cell death measured by Trypan blue after 24 h post infestation. Data are mean ± SE of three **A** and ten **B** replicates. **A** Asterisks indicates significant differences respect control plants differences (P<0.5, Two-way ANOVA followed by Tukey's multiple comparison test). **B** Asterisks indicates significant differences respect Col-0 plants (P<0.5, One way ANOVA followed by Tukey's multiple comparison test).

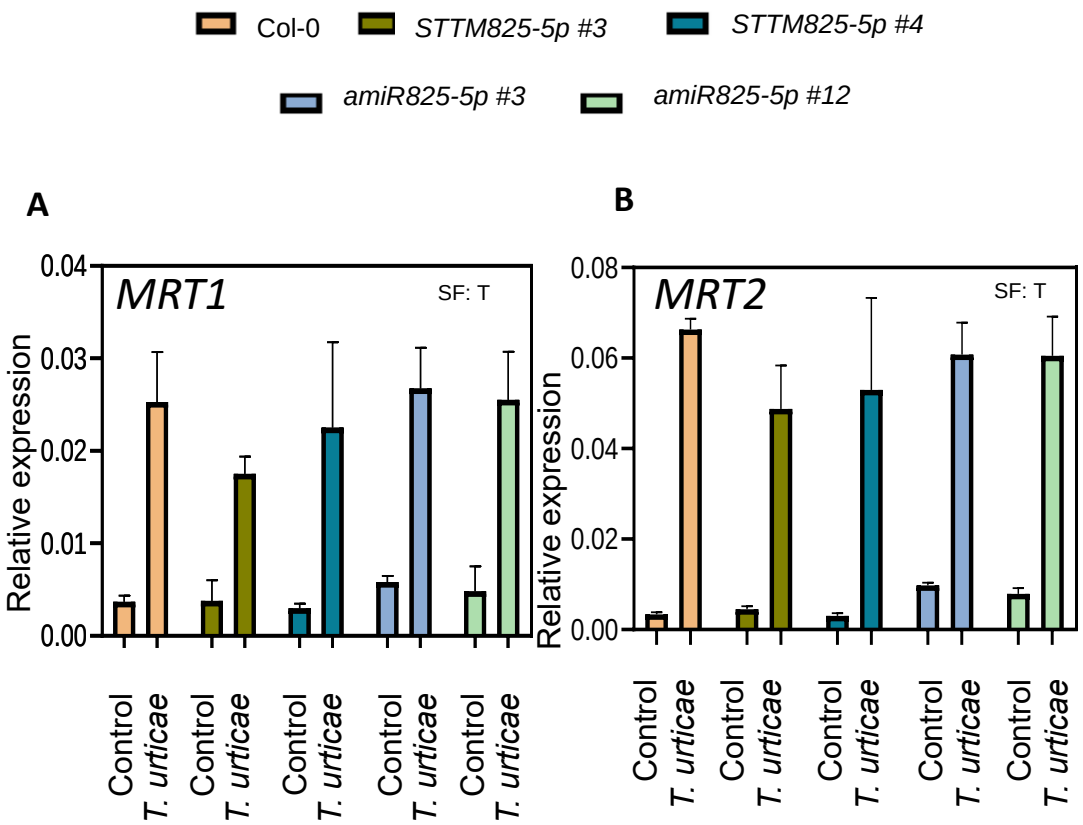

Figure 48. Molecular characterization of miR825-5p lines from López-Márquez *et al.,* (2021) after *T. urticae* infestation. Relative expression of *MRT1*, **A** and *MRT2*, **B** after 0.5 h of mite feeding. Data are mean ± SE of three replicates.

Additionally, mite feeding bioassays demonstrated that silenced miR825-5p plants were more resistant to mite infestation as shown the reduction of damaged area and the decrease in cumulative number of eggs **(Figure 49A, B)**. Nonetheless, no differences on leaf damage were observed in infested over-expressing lines although the oviposition rates were also reduced in these transgenic lines **(Figure 49B)**. Surprisingly, feeding experiments done with Pieris larvae, showed that miR825-5p over-expressing plants resulted more resistant to Pieris infestation since the remaining area of leaf discs after

feeding was significantly higher than in Col-0 plants or in silencing lines. Concomitantly, it was detected a significant decreased in the larvae weights **(Figure 50A, B)**.

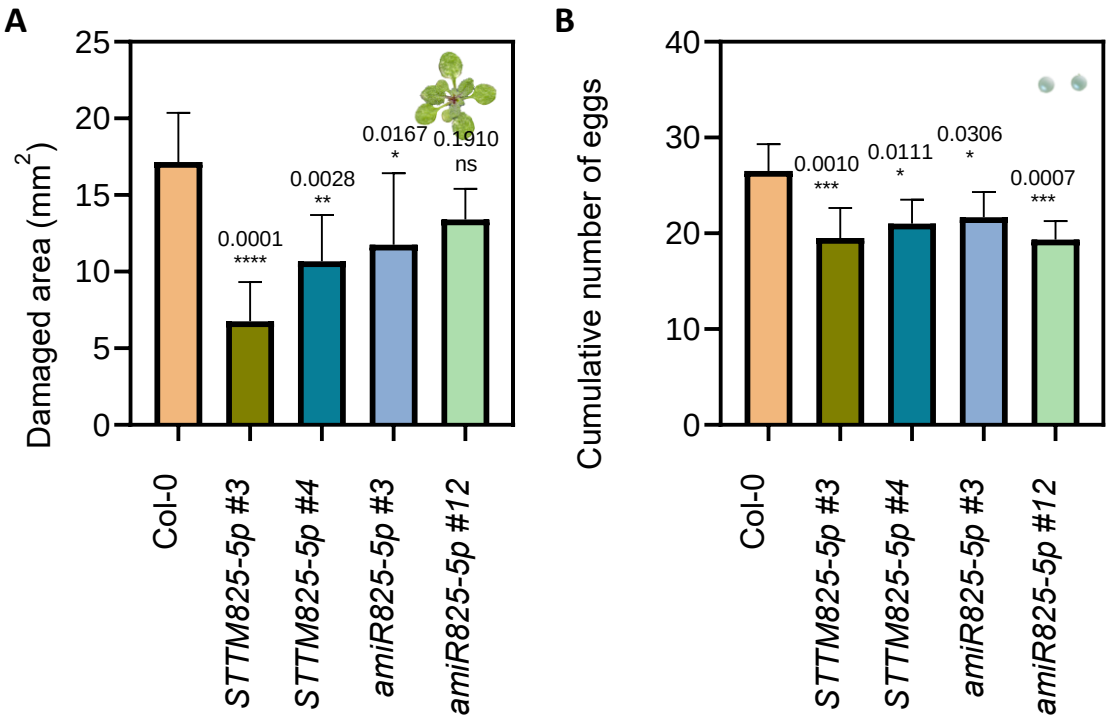

Figure 49. Plant damage, *T. urticae* fecundity after feeding on Col-0 and miR825-5p silencing and over-expressing lines. A, Foliar damage quantified in Col-0 and miR825-5p silencing and over-expressing lines**.** after 4 d of mite infestation. **B,** Cumulative number of mite eggs measured 36 h of infestation with synchronized mite females on Col-0 and miR825-5p silencing and over-expressing lines**.** Data are mean ± SE of nine **(A)** and six **(B)** replicates.

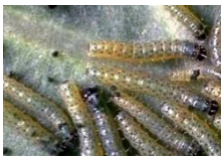

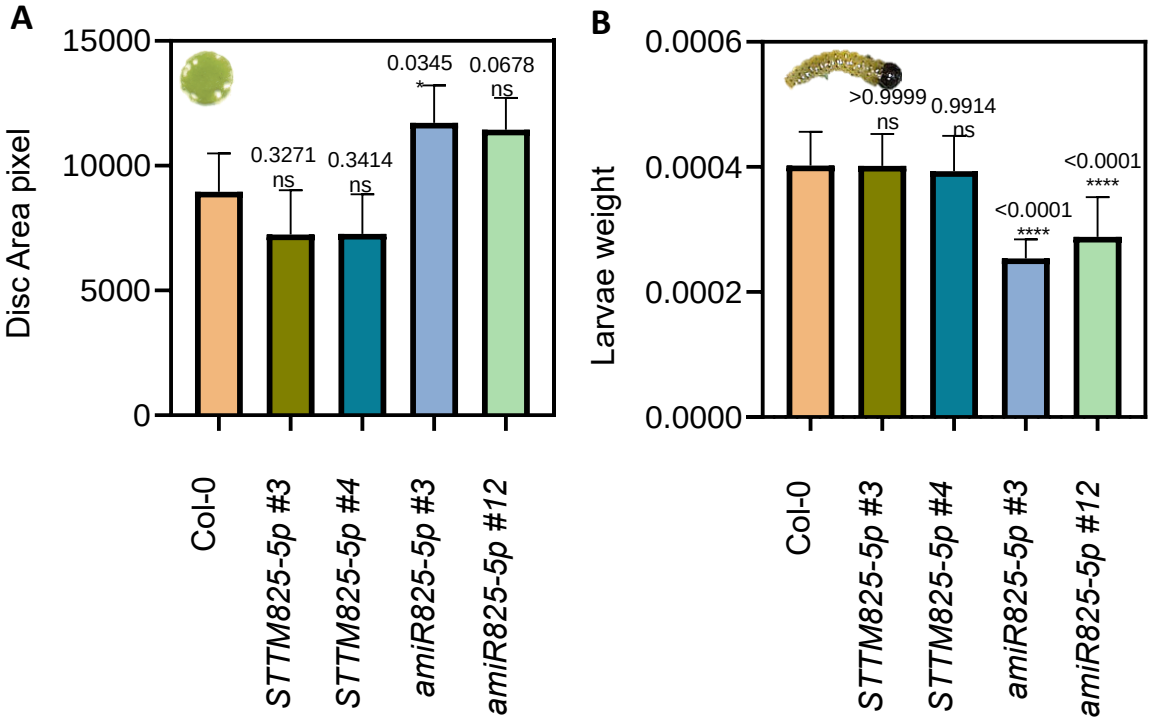

Figure 50. Plant damage, larvae weight after *P. brassicae* feeding on Col-0 and miR825-5p silencing and over-expressing lines. A, Remaining leaf tissue area after 8 h of *Pieris* larvae feeding on Col-0 and miR825-5p silencing and over-expressing lines. **B,** Pieris larvae weight after 24 h of feeding on Col-0 and miR825-5p silencing and over-expressing lines. Data are mean ± SE of twelve **(A)** and twenty-four **(B)** replicates.

To clarify whether miR825-5p regulates *MRT1* and *MRT2* by targeting the sequence located at the end of the TIR domain of these TNL transcripts, we generated translational fusions of the two *MRT* genes to the reporter YFP-encoding gene controlled by the 35S CaMV promoter. Besides, mutated versions lacking the miRNA cleavage site without altering amino acid sequences were also created (**Figure 51A**).

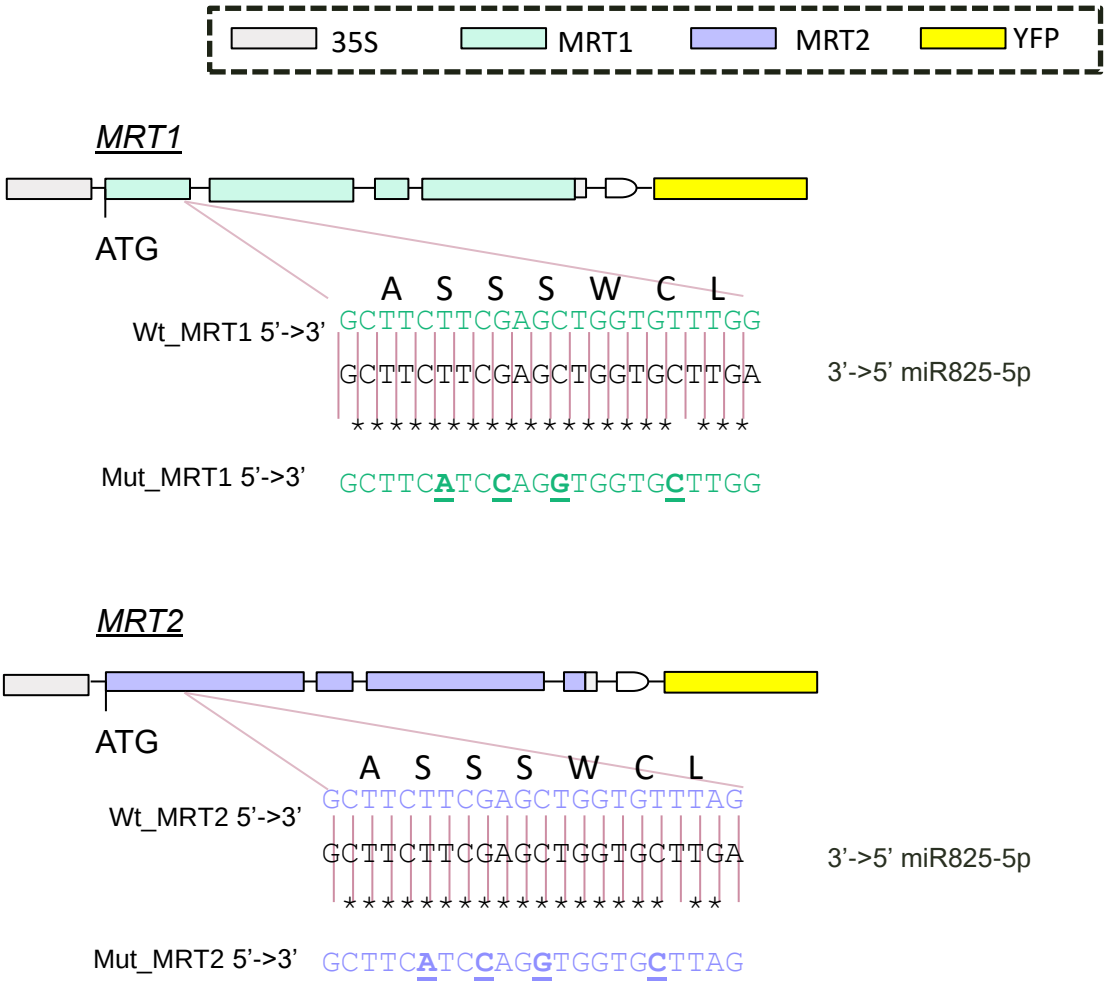

Figure 51. Scheme of MRT1 and MRT2 gene fusions to the yellow fluorescent protein gene (YFP) and their mutated versions. Punctual mutations are indicted in Mut_MRT1 or Mut_MRT2 constructions.

Transient co-expression assays were performed by agroinfiltration of in *N. benthamiana* leaves either expressing these constructs alone or in combination with the miR825-5p or with the unrelated miR319. As shown in **Figure 52A, B**, YFP fluorescence quantified

every 12 h during the first 48 h post-infiltration displayed a constant emission of fluorescence along the time when *MRT1-YFP* and *MRT2-YFP* were expressed alone, either in their non-mutated or mutated versions. *N. benthamiana* leaves co-expressing *MRT1-YFP* or *MRT2-YFP* together with miR825-5p presented a clear decrease of the YFP fluorescence since the earliest tested time (12 h), which was drastically reduced at longer incubation times **(Figure 52).** This reduction in the YFP levels was not observed in leaves co-expressing the mutated MRT1 and MRT2 constructs and the miR825-5p or co-expressing the gene fusion and the unrelated miR319 **(Figure 52)**. These results demonstrated that miR825-5p recognizes the complementary sequence in *MRT1* and *MRT2* transcripts modulating the TNL protein accumulation. In addition, transcript levels of the fluorescent protein YFP decreased when miR825-5p was co-infiltrated with MRT1 and MRT2 constructions. **(Annexed Figure 11A, B).**

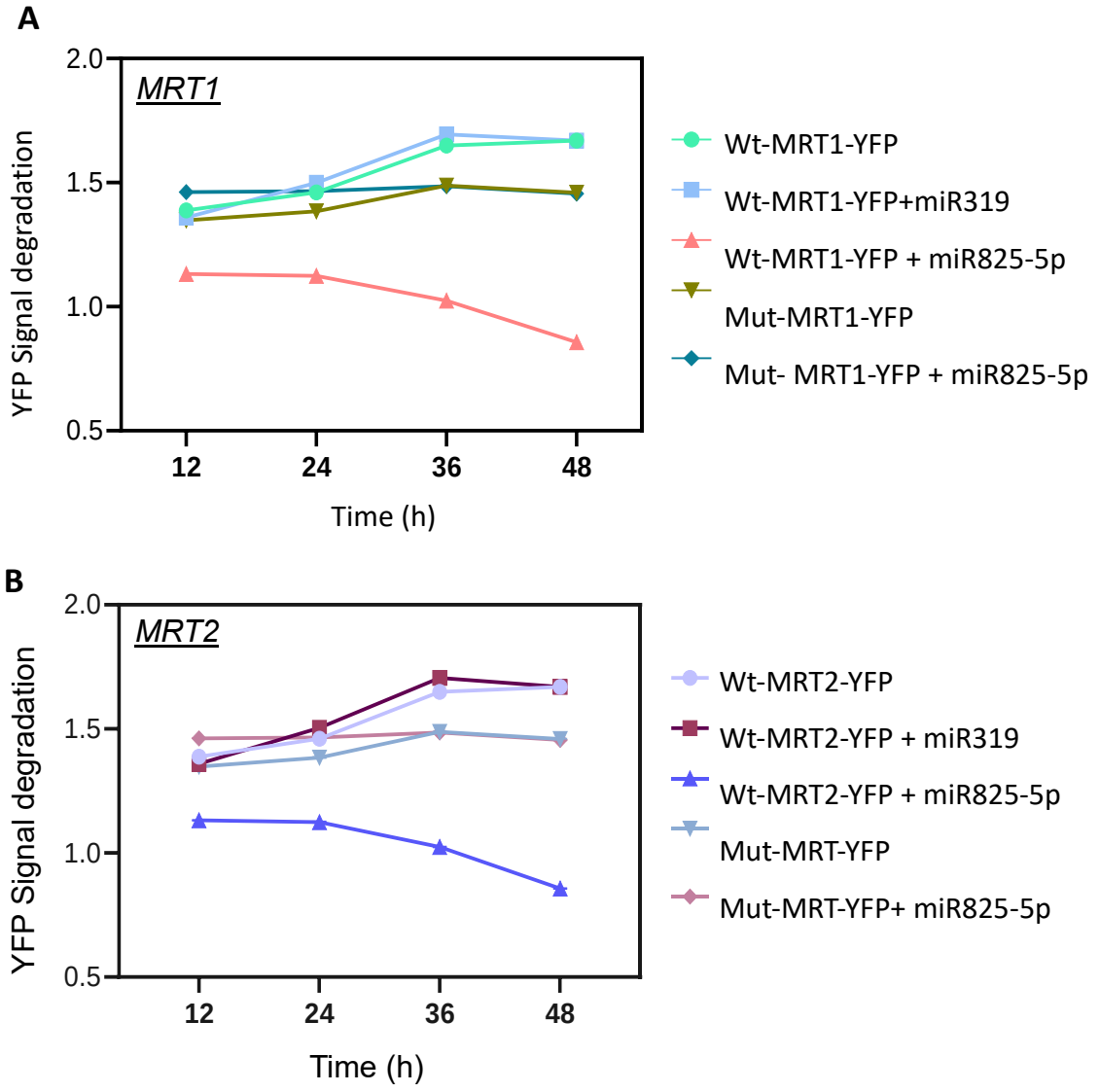

Figure 52. Quantification of MRT1-YFP and MRT2-YFP fluorescence constructs in *N. benthamiana* plants expressing them alone or co-expressing with miRNAs. A, Quantification of fluorescence emitted by *N. benthamiana* agroinfiltrated with Wt_MRT1-YFP or its mutated version Mut_MRT1-YFP, alone or combined with miR825-5p or miR319 at different expression times. **B,** Quantification of fluorescence emitted by *N. benthamiana* agroinfiltrated with Wt_MRT2-YFP or its mutated version Mut_MRT2-YFP or alone or combined with miR825-5p or miR319, at different expression times. Data are means ± SE of 24 biological replicates. Statistics indicated in **Annexed tables 7** and **8** (P<0.5, Two-way ANOVA followed by Tukey's multiple comparison test).

In accordance with previous research demonstrating the ability of miRNAs to initiate the production of phasiRNAs from the same gene family as the initial miRNA, López-Márquez *et al.* (2021) reported that miR825-5p can trigger phasiRNA production from its target genes. Among the targets of miR825-5p, MIST1 was identified as a potential candidate for a negative feedback loop, with predictions suggesting the production of phasiRNAs for *MRT1* and *MRT2* transcripts.

Moreover, having confirmed through previous experiments that with the chewer *P. brassicae* the double mutant plants displayed the same phenotype as the single mutants and that the *MIST1* gene exhibited significant up-regulation in the double mutant plants, it strongly suggested the presence of a negative feedback mechanism. In light of this discovery, we proceeded to clone the phasiRNA-specific sequences associated with *MRT1* and *MRT2*, both of which are implicated in the post-transcriptional silencing of MIST1 through miR825-5p.

We conducted transient co-expression assays by agroinfiltration *N. benthamiana* leaves with constructs fused to a fluorescent reporter gene. To monitor the expression dynamics, we quantified YFP fluorescence at 12 h intervals during the first 48 h post-infiltration. When MRT1-YFP and MRT2-YFP were expressed individually, either in their non-mutated or mutated forms, we observed a sustained level of fluorescence over time.

In leaves co-expressing MRT1-YFP or MRT2-YFP with the phasiRNAs derived from *MIST1*, namely phasiR263-1 and phasiR263-2 targeting *MRT1* **(Figure 53A)**, and phasiR263-9 targeting *MRT2* **(Figure 53B)**, we noticed a notable reduction in YFP fluorescence as early as 36-48 h post-infiltration. This reduction became even more pronounced with longer incubation times. This decrease in YFP levels was not observed in leaves co-expressing the mutated *MRT1* and *MRT2* constructs with the phasiRNAs **(Figure 53).**

In addition, we also decided to confirm that the binding sequence region of the phasis was distinct from that of miR825-5p. Therefore, we co-infiltrated the mutated versions

of *MRT1-YFP* or *MRT2-YFP* along with miR825-5p. In both cases, we observed a decrease in the YFP signal **(Figure 53).**

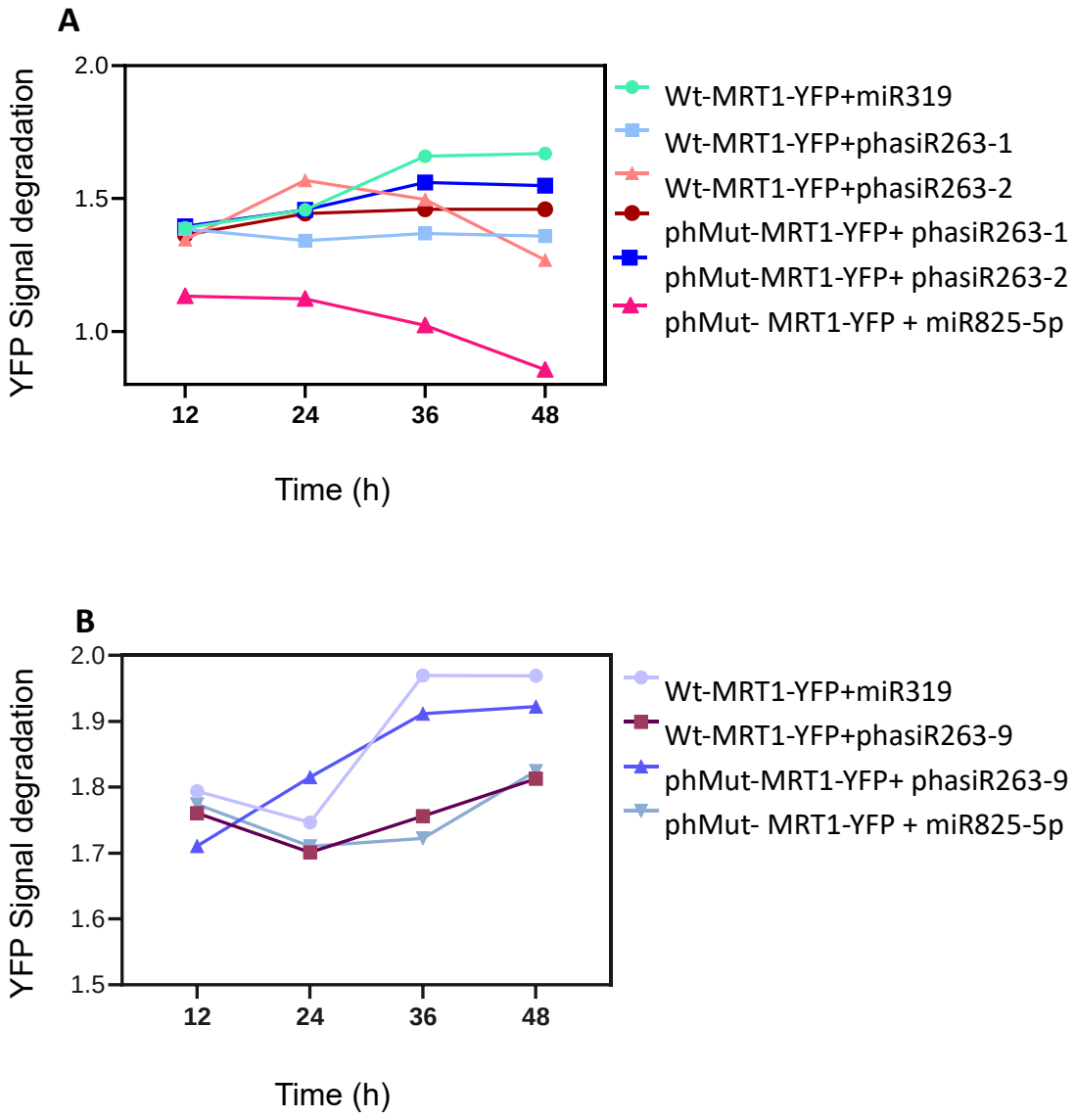

Figure 53. Quantification of MRT1-YFP and MRT2-YFP fluorescence constructs in *N. benthamiana* plants co-expressing them alone or with phasiRNAs. A, Quantification of fluorescence emitted by *N. benthamiana* agroinfiltrated with Wt_MRT1-YFP or its mutated version Mut_MRT1-YFP, alone or combined with miR319 or specific phasiRNAs at different expression times. **B,** Quantification of fluorescence emitted by *N. benthamiana* agroinfiltrated with Wt_MRT2-YFP or its mutated version Mut_MRT2-YFP or alone or combined with miR319 or specific phasiRNAs, at different expression times. Data are means ± SE of 24 biological replicates. Statistics indicated in **Annexed tables 9** and **10** (P<0.5, Two-way ANOVA followed by Tukey's multiple comparison test).

NO PLAYS A VERSATILE ROLE IN PLANT DEFENCE AGAINST HERBIVORES

NO as the main representative molecule of the RNSs involved in redox homeostasis, plays a versatile role in plant defense against biotic stresses, notably to herbivorous mites like *T. urticae* (Santamaria *et al.*, 2018). In addition, NO also participates in response to abiotic stresses and in response to moderate changes in environmental conditions like light, temperature, and humidity, which may have an important impact on the effectiveness in defending against herbivores (Nabi *et al.*, 2019).

NO exhibits different functions dealing with mite infestation and effectively activating specific responses, although the information on early mite-induced NO-related genes is very limited. When plants face herbivore attacks, including those by *T. urticae*, they trigger defence mechanisms which can be divided into early and late plant signalling events. Early actions start with the feeder perception, essential for initiating the activation of short-term responses, that end with the defensive compound production (late-term responses). Among the early features, the redox status of the cell is modified and moderate changes in the ROS/NRS concentration are enough to sense defence signalling (Foyer & Noctor, 2005; Santamaria *et al.*, 2017a, 2018b). Since an excess of oxidative stress may result in programmed cell death, the maintenance of an appropriated redox homeostasis is crucial in the plant-herbivore context.

During mite infestation, ROS and RNS increase, particularly, H_2O_2 and NO levels, but the physiological significance of having higher NO concentrations is still not clear. It has been demonstrated that is not associated with changes in the Vm depolarization as is the case of H_2O_2. It seems to be linked to Ca^{2+} homeostasis and cGMP signalling, and consequently, it could be involved in the mobilization of secondary messengers or alternatively, in the activity of protein kinases, being both players of the early defense responses (Misra *et al.*, 2011; Santamaria *et al.*, 2018a). Additionally, NO has been shown to act as an inducer or suppressor of signalling along defence hormone pathways. Specifically, NO initiates SA biosynthesis and nitrosylates key cysteines on TGA-class

transcription factors to aid in the initiation of SA-dependent gene expression (Mur *et al.*, 2013). This nitrosylation of NPR1 promotes the NPR1 oligomerization within the cytoplasm to reduce TGA activation. Similarly, NO also triggers the expression of JA biosynthetic enzymes, presumably to over-come the potential antagonistic effect of SA. The SA and JA/ET cross-talk allows the plant to select to the most appropriate defense mechanisms (Pieterse *et al.*, 2012).

Other evidences indicate that phytohormones and NO regulate guard cell ABA-signalling, and in consequence, the stomata closure (Sun *et al.*, 2019), a physiological event crucial for mite feeding as has been demonstrated in this thesis. Thus, NO may function as a signal molecule, a metabolic intermediate, or even a toxic oxidative product, but mostly, NO acts as a secondary messenger in various signalling cascades initiated by herbivore attacks. These roles influence, and probably modulate the activation of defence genes, production of secondary metabolites, and post-translational modifications (Misra *et al.*, 2011).

So, as it has been mentioned, NO does not operate in isolation but interacts with other signalling molecules, varying the balance between them based on the specific plant-mite interaction, resulting in diverse defense responses. Collectively, these events enhance plant resistance against herbivores, including mites, by activating defense mechanisms, such as defensive protein production and cell wall reinforcement, making it challenging for herbivores to feed and reproduce on the plant. Our genetic and molecular studies have contributed to a deeper understanding of NO's role in plant defense against herbivorous mites, aiding in the identification of specific genes and enzymes involved in NO production and its downstream effects.

JA CATABOLISM BALANCE THE SYNTHESIS OF DEFENSIVE METABOLITES AGAINST *T. URTICAE*

One of the major challenges in plant responses to herbivores is to understand the molecular mechanisms that plants use to cope with them. This requires the integration of multiple approaches to get results and delve into the functional complexity of plant defences associated with the plant-herbivore interaction (Barah and Bones, 2015). Many genes, regulators and molecules participating in plant defences have been independently characterised, but the functional relationship between players within the whole defence puzzle is still partially known. Some master pieces of this puzzle are related to appropriated regulatory events mainly mediated by a complex hormonal crosstalk, to synthesise specific defences against specific feeders. In the case of the plant-*T. urticae* interplay, there is a good set of information which is wider when the plant host is Arabidopsis. In particular, the modulation of defences to mites by JA and JA-Ile in this model species has been intensively investigated at transcriptional and genetic levels (Zhurov *et al.*, 2014; Santamaria *et al.*, 2020) Thus, Arabidopsis mutants with disrupted JA biosynthesis (*aos*) or signalling (*myc2, myc3, myc4*) resulted more severely damaged by mites than Col-0. Concomitantly, a dramatic reduction in mite mortality was observed when mites fed on these mutant lines (Zhurov *et al.,* 2014). However, studies on JA metabolism in the plant-mite context are incomplete since both JA and JA-Ile may be catabolized generating inactive or partially active forms which alter JA homoeostasis, and consequently readjust the modulation of defences.

We selected the *JAO2* gene which encodes one of the four JA oxidases responsible for the hydroxylation of JA into 12-OH-JA to deepen into the JA catabolism effects on plant defences against mites. *JAO2* participates in the first step of JA catabolism contributing to attenuate JA and JA-Ile formation and signalling. The inactivation of this gene has profound effects on JA and JA-Ile content, causing a reduction in the synthesis of defensive compounds. Our findings corroborate these data because mite feeding in *jao2* mutant lines produced less leaf damage, minor accumulation of callose and lower mite fecundity rates than in Col-0 plants. Other JAO isoforms may exert similar attenuation

functions either in the same or in different plant tissues and/or under different traits to ensure a JA response compatible with a growth-defence trade-off. Some results have evidenced that the timing and amplitude of the expression induced by Me-JA*, B. cinerea*, and *M. brassicae* were different between the four *JAO* genes (Caarls *et al.*, 2017). Moreover, the quadruple *jao* Arabidopsis mutant caused the over-accumulation of JA and increased resistance to the caterpillar *M. brassicae*. Likewise, the transcriptional pattern for *JAO* genes differed in *N. attenuata* responses to *S. litura* feeding, and the silencing of the four *JAO* homologues in this tobacco species enhanced defences to the tobacco cutworm *S. litura* linked to increased JA-Ile levels (Tang *et al.*, 2020). Our findings revealed that the triple mutant *jaoT* mimic the responses to mite infestation found on plants mutated only in the *jao2* gene. So, our data confirmed the induction of all *JAO* genes by mites but they present different temporal expression profiles and at distinct expression levels, in Col-0 and particularly in *jao2* mutant lines. These observations indicate a functional redundancy of *JAO* genes to defend plants to biotic stresses.

Besides the induction of JA and JA-Ile to enhance Arabidopsis defences to *T. urticae*, a certain increase in SA content at the initial infestation time, has also been described not only in Arabidopsis but also in crop species (Zhurov *et al.*, 2014; Agut *et al.*, 2014; Martel *et al.*, 2015; Santamaria *et al.*, 2017b, 2019). In our experiments, the accumulation of JA and JA-Ile was higher in the *jao2* and *jaoT* mutant lines than in Col-0 when plants were infested with *T. urticae*. SA levels, although also induced by mite feeding, presented lower concentrations in *jao2* and *jaoT* lines than in Col-0 infested plants. These data are in line with the mentioned crosstalk established between hormones to modulate defence responses and support the antagonistic role of JA and SA in protective function to biotic stresses (Yang *et al.*, 2019).

Therefore, JAO2 acts as a negative player in Arabidopsis defences against mites having an important function in the turnover of JA and JA-Ile into inactive derivatives. The impairment of JA oxidation in *jao2* mutant lines diminishes the 12-OH-JA content and turns off a further sulfation step as is demonstrated by the significant reduction of 12-

OH-JA and 12-HSO_4-JA forms in *jao2-2*. Contrary, 12-COOH-JA-Ile increased in *jao2* mutant line more than in Col-0 plants as consequence of mite feeding. The same behaviour observed in infested *jaoT* mutant lines highlighted the relevance of *JAO2* within the four *JAO* genes as the main modulator of the JA catabolism. Moreover, the conversion of JA into 12-OH-JA also limits the JA-Ile production, and in consequence, the accumulation of its catabolic products as the 12-COOH-JA-Ile. Then, the manipulation, upstream JA-Ile homoeostatic steps, indicates that in the defence signalling participate distinct JA metabolites and suggests that may exit different regulatory nodes. In an alternative pathway, the oxidation and further carboxylation of JA-Ile by *CYP94B1/B3* and *CYP94C1* genes, generate 12-OH-JA-Ile and 12-COOH-JA-Ile, respectively, reducing JA-Ile content and the impact on defences (Heitz *et al.*, 2012; Wang *et al.*, 2021). CYP94B3 over-expressing Arabidopsis plants exhibited phenotypes with severe depletion of JA-Ile content and high susceptibility to the lepidopteran *S. exigua*, while *cyp94b3* mutant lines produced the opposite effect (Koo *et al.*, 2011). Double and triple *cyp94b1, cyp94b3* and *cyp84c1* knockout mutants blocked the oxidation steps and increased JA-Ile content and enhanced the resistance to the chewing lepidopterans. Moreover, larvae fed on these mutant plants weighed almost twice as those fed on WT plants (Poudel *et al.*, 2016).

In our experiments, the *jao2* defence phenotype to *T. urticae* infestation was supported by an increase in the levels of the indole Trp-derived glucosinolates. These metabolites together with camalexin increased in all infested plants, but only I3M and 4-MeO-I3M presented higher accumulation in *jao2* lines after mite infestation than in Col-0. These results agree with previous reports indicating that indole glucosinolates were more relevant as defensive metabolites than camalexin in the Arabidopsis defence against mites. Accumulation of camalexin did not correlate with defence since mutants in camalexin production were not more sensitive to mite infestation than WT plants (Widermann *et al*., 2021, Zhurov *et al.,* 2014). Besides, it was demonstrated that I3M, 1-MeO-I3M and 4-MeO-I3M indole glucosinolate metabolites were necessary and sufficient to protect Arabidopsis plants against *T. urticae* (Widemann *et al.*, 2021).

In conclusion, our findings demonstrate that JAO2 is induced by spider mite infestation and acts as a negative modulator of Arabidopsis defences altering the content of active/inactive jasmonates, which modulate the synthesis of camalexin and glucosinolates. Although there are some studies analysing the regulatory role of JA catabolism in defence to pests, as far as we know, all are done using insects, and the majority with chewing lepidopteran species. For the first time it is shown how changes in JA-derivatives mediated by impairing the JAO2 gene affect defensive responses against an acari, a relevant pest species with a sucking feeding mode.

ABA-MEDIATED STOMATAL CLOSURE IN ARABIDOPSIS DEFENSE AGAINST *T. URTICAE*

Stomata are specialized microscopic gates at the epidermal plant surface with the ability to be opened or closed in response to environmental and endogenous signals.

Stomatal movement depends largely on the content of ABA, considered as the key hormone that closes stomata, although other hormones also participate in governing stomata responses (Wei *et al.*, 2021). Under a subset of biotic stresses, ABA levels and stomata behaviour play an essential plant defence role by hindering adversary access to the leaf interior (Lim *et al.*, 2015; Melotto *et al.*, 2017). In the plant-mite context, stomata are target sites where mites insert their stylets to gain access to nutrient rich mesophyll cells. Once the plant perceives the mites, a signal transduction cascade is triggered that activates the synthesis of JA and SA, besides other chemical responses, to generate defences (Zhurov *et al.,* 2014; Santamaria *et al*., 2019). Our results confirmed that mite infestation induced JA and SA, demonstrated the timeline of this response, and also revealed a mite induced increase of ABA. Other studies have linked stomata movement with response to light and circadian-clock pathways (Tallman, 2004) and we observed that *T. urticae* caused less cell damage by feeding under dark conditions when stomata are closed. We also observed stomatal closure concomitant with ABA accumulation in response to herbivory during the day. Additionally, the temporal pattern of the phenotypic changes in stomatal behaviour in response to mite infestation during the day matched with the ABA accumulation more than the JA or SA content. Together, these data pointed to ABA accumulation and stomatal closure as a plant response to herbivory acting to limit leaf cell damage associated with mite infestation.

Stomatal closure has been previously described as a plant response to other phytophagous species (Sances *et al.*, 1979; Pincebourde & Casas, 2006; Schmidt *et al.*, 2009), though whether closure constituted a defence mechanism or contributed to the infestation remained unclear. DNA microarray experiments of Arabidopsis infiltrated with *Myzus persicae* saliva allowed the identification of a number of aphid saliva up-regulated genes that also responded to ABA treatment (Hillwig *et al.*, 2016). Aphid

infestation induced ABA production in Arabidopsis, but aphids showed preference for and performed better on wild-type plants than on ABA deficient mutants, suggesting that ABA might not be a plant defence response. These authors also demonstrated that ABA increased the synthesis of some glucosinolates with defensive properties. We demonstrated a positive role for ABA in the plant defence to the mite *T. urticae* since mutant lines in ABA biosynthesis and catabolism showed higher and lower leaf damage, respectively, than Col-0 infested plants. These data directly corresponded to the higher and lower number of eggs accumulated in these mutants. Thus, mite infestation results in ABA accumulation as a plant defence response that closes stomata, reduces mite feeding ability, lessens leaf damage and lowers mite fecundity rates.

Vos *et al.*, (2013) also reported that ABA is a crucial regulator of induced resistance against *Pieris rapae* by activating primed JA-regulated defence responses in Arabidopsis. Additionally, ABA has also been associated with redox homeostasis (Li *et al.*, 2022), in particular with ROS accumulation, which is also essential in the plant defence against mites (Santamaria *et al.*, 2017b; Arnaiz *et al.*, 2021). Our results showed increased levels of JA signalling and H_2O_2 production in ABA deficient mutants after mite infestation where leaf damage was increased. Based on the current observations, it can be concluded that ABA signalling, independent of positive crosstalk with ROS and JA signalling, plays a critical role as a defence determinant against mite infestation.

In order to probe the regulation and function of ABA accumulation, we used nlsABACUS2, a FRET-based biosensor for ABA, as a tool to quantify in vivo ABA at high spatio-temporal resolution in response to mite infestation. Elevated levels of ABA were broadly detected in the nuclei of a range of leaf cell types, with slightly stronger responses in stomata and vascular tissues. These ABA dynamics are consistent with an ABA regulation model in which the leaf vasculature is the key site of biosynthesis triggered by mite infestation, with ABA subsequently transported to guard cells for stomatal closure, similar to that proposed for ABA during water stress by Kuromori *et al.*, (2018b). However, we also show induction of ABA in all leaf cells involved in feeding by mites, including pavement cells and the mesophyll cells on which they feed.

Given the pronounced stomatal closure observed during infestation, an additional significant aspect of this study focused on clarifying the impact of stomatal status versus ABA signalling more generally. This was achieved by administering exogenous ABA or FC, to induce or repress stomatal closure. When pre-treated with ABA and subsequently infested with mites, plants were protected without sacrificing their growth. Pre-treatment with FC increased leaf damage, consistent with a protective role for stomatal closure. In an ABA + FC treatment, mite damage correlated with stomatal aperture rather than ABA levels, providing further support for the role of stomata in ABA mediated mite defence. The closure of stomata likely hindered mite feeding through the natural openings on the leaf, compelling them to utilize their stylets for penetrating closed stomata or between the epidermal pavement cells. This mode of stylet penetration could trigger earlier damage and possibly defence signalling and likely reduces feeding success since mites try to avoid epidermal cell damage (Bensoussan *et al.,* 2016) and we observed ABA to reduce overall leaf damage and defence signalling at 24 h infestation.

We also investigated the importance of leaf stomatal density upon infestation based on the hypothesis that higher number of stomata could facilitate mite feeding. In mutants with more and less stomata, we observed lower and higher leaf temperature that increased with mite feeding, indicating that mite induced stomatal closure remained functional in leaves with altered stomatal density. Indeed, stomatal density was tightly correlated with mite induced leaf damage, suggesting that the number of stomata, in conjunction to their aperture, is a highly relevant trait for plant resistance to mite infestation.

This study provides valuable insights into the important role of stomata and its regulation mediated by ABA in the Arabidopsis defence against *T. urticae*. We demonstrate that ABA, possibly of vascular origin, accumulates in the guard cells of the stomata as a result of mite feeding and triggers stomatal closure as a structural defence response. We also show stomatal aperture and abundance play a crucial role in determining the success of infestation. As both traits are regulated by ABA, the levels of

this phytohormone, which also integrate myriad other biotic and abiotic stress cues, is an important determinant of mite infestation that could be considered in breeding programs for pest control.

MIR825-5P ROLE IN POST-TRANSCRIPTIONAL REGULATION AGAINST *T. URTICAE*

ETI is considered an accelerated and amplified PTI response in which some R genes involved in the plant immunity are used to recognize specific effectors triggering defense signalling which results in disease resistance (Dangl & Jones, 2001; Martin *et al.*, 2003). In this study, we aimed to identify and characterize R genes involved in the defense response against *T. urticae* mites, mainly those induced at early time of infestation (0.5 h), in Arabidopsis plants. Of particular interest were 21 TNLs (TIR-NLRs) with a TIR domain, which were induced early but reduced in numbers over time. Two of these genes, AT4G14370 and AT5G41550, referred to as *MRT1* and *MRT2*, were selected to deepen in their function within the plant-spider mite context. They were chosen due to their up-regulation in response to mites, the presence of a conserved TIR motif essential for immune function, and the potential regulation by miR825-5p. It is known that the regulation of plant immunity via small RNA-mediated control of NLR expression, and consequently, R-genes regulation during plant immunity (Zhai *et al.*, 2011; López-Márquez *et al.*, 2023)

MRT1 and *MRT2*, identified as potential miR825-5p targets, were significantly induced during infestations by both *T. urticae* (a sucking feeder) and *P. brassicae* (a chewer feeder). When examining their expression at 0.5 h post-mite infestation, only *MRT1* and *MRT2* showed significant induction when the mites feed, while other genes remained unchanged. In response to *P. brassicae* infestation, besides *MRT1* and *MRT2*, other genes such as *MIST1*, and *AT1G63740* were also up-regulated at 0.5 h. Several NLRs have been shown to play a role in diverse plant-herbivore systems, but often without knowledge of the involvement of herbivore effectors. The activation or the requirement of each specific NLR may depend on various factors such as feeding mode, OS composition, and the primary PTI induced (Douglas, 2018). The same R-genes may act differently in various herbivore systems and/or in cooperation with other genes, depending on the stress. For instance, the tomato R-gene *Mi1-2* not only acts against

root-knot nematodes but also against arthropods such as aphids, reducing the number of whitefly adults and pupae (Kant & Schuurink, 2021).

It is established that sRNAs, and particularly miRNAs, can modulate the expression of R-genes by targeting co-expressed genes, thus contributing to negative feedback mechanisms (López-Márquez *et al.*, 2023). Both *MRT1* and *MRT2* are co-expressed in defense systems and belong to the Disease R-genes family, sharing common structural domains. Notably, their TIR domains exhibit a significant degree of similarity, surpassing 80%. It is of particular importance to highlight that the binding site of miR825-5p resides within their shared TIR domain at the transcriptional level. These structural resemblances and distinctions in domain composition may bear significance in their regulatory functions. This observation could be linked to the well-established phenomenon that R-genes, as a group, exhibit a high susceptibility to recombination, potentially facilitating the generation of new resistance variants aimed at combating diverse stresses.

We also investigate the roles of *MRT1* and *MRT2* genes in defense against the two pests, acari and insects. The singles *mrt1*- and *mrt2*- mutant plants displayed high expression levels of both genes and less damage and death areas, indicating functional redundancy. Moreover, mite mortality increased when feeding on mutant lines, except for *mrt1-1*, and the cumulative number of mite eggs was higher on the mutant lines. Probably, their functional redundancy underscores their significance in mediating the defense response. On the other hand, feeding experiments with *P. brassicae* on Arabidopsis mutants lacking *MRT1* and *MRT2* genes resulted in increased resistance, with smaller leaf damage and reduced larval weights. Probably because there are still other TNLs (MRT1, MRT2 or MIST1, and AT1G63740) that are also induced and can transmit the signalling burst when the chewer feds.

To confirm compensating roles of *MRT1* and *MRT2* in defense against both herbivores, double mutant lines in feeding bioassays, exhibited greater susceptibility to *T. urticae*, with more damage and higher mite fecundity compared to Col-0 plants. Feeding experiments with Pieris larvae revealed that *mrt1-mrt2* double mutant plants exhibited

the same increased resistance as the single mutant plants. Given the compensatory effect observed between MRT1 and MRT2 in single mutants, we analysed the expression *MIST1* which was also more induced in the double mutant plants than in Col-0 during the feeding.

Collectively, these results underscore the essential roles of *MRT1* and *MRT2* in plant defense against herbivores. Their absence disrupts the expression of defense hormone marker pathways, specifically SA and JA, compromising the plant's ability to effectively defend against herbivores. In many cases, induced defences against phytophagous species like the *T. urticae* mite are primarily regulated by jasmonates and/or SA. However, in the case of specialist herbivores like *P. brassicae*, defense mechanisms are predominantly driven by JA (Stahl *et al.*, 2022).

Recognizing the significance of R-genes in herbivore defences, the precise induction and regulation of these genes in the absence of stress is crucial. Unregulated expression of R-genes can potentially lead to autoimmunity, further impeding plant growth (Brant & Budak, 2018). HR, a well-studied trait associated with plant defense against pests, is often governed by individual R genes (Wagner *et al*., 2022). In our study, we demonstrated an increase in HR, linked to cell death, in single *mrt* mutant plants. This phenomenon appears to be regulated constantly even in non-stress conditions. Interestingly, HR is not only induced when adult herbivores feed; Pieris eggs also trigger HR-like cell death in their host plants (Caarls *et al.*, 2023).

Moreover, in our study the plants with altered miR825-5p levels exhibited increased cell death in knock-down lines but not in over-expressing lines. This highlights the importance of finely regulating R-genes when defense mechanisms are not needed.

In addition, feeding assays revealed that miR825-5p knock-down plants were more resistant to mite infestation, with reduced damage and fewer mite eggs. Interestingly, miR825-5p over-expressing plants were more resistant to *Pieris* larvae, displaying larger remaining leaf areas and reduced larval weights. miR825-5p appears to influence plant

defense against herbivores, with its over-expression enhancing resistance against both mites and Pieris larvae, while silencing increases resistance to mites specifically.

Given the critical role of *MRT1* and *MRT2* in defense against herbivores and the importance of precise regulation of R-genes through miR825-5p, our study aimed to ascertain whether miR825-5p recognizes the complementary sequences in *MRT1* and *MRT2* transcripts, thereby influencing the accumulation of TNL proteins. This investigation helps to elucidate our feeding phenotype assay results, particularly concerning *T. urticae.*

To go further in this fine-tune regulation, we also demonstrate that miR825-5p, which induces the production of secondary phased RNAs (phasiRNAs) from *MIST1* are able to bind to *MRT1* and *MRT2* in a different sequence from miR825-5p. This phenomenon likely contributes to the post-transcriptional silencing through a negative feedback loop. Which can explain the phenotypes of *P. brassicae* feeding experiments.

MOLECULAR REGULATORY CROSSTALK IN ARABIDOPSIS DEFENSE AGAINST HERBIVORES

In response to biotic threats, plants employ rapid and precise defense mechanisms to ward off herbivores. This immune response is triggered when plants detect specific signals such as HAMPs, PAMPs, and DAMPs (Macho & Zipfel, 2014; Erb & Reymond, 2019; Groux *et al.*, 2021; Ngou *et al.*, 2021b), which activate the PTI pathway. Additionally, plants can sense physical damage caused by herbivores during feeding. This perception initiates a series of down-stream signalling events, including membrane depolarization, rapid influx of calcium ions (Ca^{2+}), phosphorylation of mitogen-activated protein kinases (MAPKs), production of ROS and RNS, and alterations in the expression of genes encoding defensive compounds (Fürstenberg-Hägg *et al.*, 2013; Bigeard *et al.*, 2015; Bjornson *et al.*, 2021; Santamaria *et al.*, 2021). While the early signalling events are common responses to various pests, the subsequent hormonal and metabolic reactions tend to be more specific and tailored to the type of invading herbivore. In this second line of defense, known as ETI, is specifically crucial and depends on the herbivore's identity.

The nature of signalling and regulatory molecules in plant-herbivore interactions remains poorly understood. Therefore, this thesis aims to explore some of the molecules and pathways involved in regulating plant defense at various stages. This research primarily focuses on the specific interactions between two model species, *A. thaliana* and *T. urticae*, as well as the specialist herbivore *P. brassicae*.

Plants have the ability to recognize the nature of the pest and develop an appropriate response in terms of quantity and timing. To achieve this, plants need to finely control the induction, activation, or repression of certain defensive pathways. Many regulatory molecules play roles at different stages of defense, resulting in diverse natures of these molecules. Some molecules are present in small amounts in plants and need rapid induction, as in the case of NO. Others are present under basal conditions and are repressed by the pest, as seen in the case of miR825-5p. Additionally, some regulators are part of more complex, time-dependent pathways, such as hormonal pathways.

In the context of our most studied pest, *T. urticae*, the current understanding reveals the general defensive profile activated during feeding (Santamaria *et al.,* 2020) or oviposition (Ojeda-Martinez *et al.*, 2022).

In the context of the spider mite feeding process, several specific pathways have been extensively examined. One of the most activated signalling pathways in defense is the rapid and specific activation of Mitogen-Activated Protein Kinases (MAPKs). Notably, a study conducted by Romero-Hernandez & Martinez, (2022) highlighted the opposing roles of two MEKK-like kinases, with *MAPKKK17* acting as a positive regulator of defense and *MAPKKK21* as a negative regulator in the plant's response to *T. urticae*. The authors concluded that the induction of both MAPKKKs during infestation represents a strategic approach to regulate and control the multitude of signalling pathways activated, ultimately balancing the plant's response to biotic stress.

One of the extensively studied regulator-signalling molecules in plant defense are the ROS species. It is well-documented that during mite infestation, specifically the over-accumulation of H_2O_2, is induced. Furthermore, the induction of certain ROS-related enzymes has been explored in various Arabidopsis accessions, demonstrating their role in protecting against mite feeding (Santamaria *et al.,* 2018b). Very recently, integrated with the rapid redox homeostasis in perception and signalling, a study revealed that the thiorredoxin *TRXh5* has multiple roles in defense (Arnaiz *et al.*, 2023). TRXh5 was found to be involved in ROS induction, alterations in NO accumulation, regulation of certain JA/SA levels, and post-translational modifications, mainly changes in nitrosylation patterns of proteins, and particularly in the denitrosylation of the specific defense protein, THIOREDOXIN INTERACTING RECEPTOR KINASE (TIRK). This study provides significant evidence highlighting the importance of rapid pest perception by plants and the subsequent induction of defense mechanisms.

The swift perception of pests is fundamental for activating plant defense mechanisms. Several works perfectly illustrate how the transcriptomic response changes over time. At very early infestation points, many protein receptors are induced, in particular transmembrane receptor potentially involved in the feeder perception Additionally,

intracellular receptors such as MRT1 and MRT2 are also induced at early time points, both playing roles in specific perception and signalling bursts against the mite, contributing to the plant's defense. This thesis emphasizes the crucial role of their regulation through miRNA during interactions with different herbivores. Once again, these findings highlight how plants can modulate their responses based on specific stresses. Moreover, and following the perception of the specific stress, in 2019 Santamaria *et al*. (2019), also described a PP2-A5, a Toll/Interleukin-1 receptor (PP2-A5) which conferred tolerance to *T. urticae* by unbalancing the hormone defensive activation profile of the plant.

As discussed earlier and demonstrated in this thesis, numerous genes and signalling pathways play a significant role in influencing hormonal balance during mite infestation. The timing of pathway inductions is just as crucial as the induction of defense hormones. For instance, transcriptomic analysis revealed that regulatory genes involved in the JA pathway, such as jasmonic transcription factors (JA-TF) reach maximum expression at 3 h post-infestation, which decreases by 24 h (Santamaria *et al*., 2021). These observations, coupled with our final hormone measurement in JAO2, explains the peak accumulation of JA and JA-Ile around 24 h post-infestation. Consequently, various late defensive pathways, such as glucosinolates (Widemann *et al.,* 2021), are activated, necessitating fine-tuned regulation by the *JAOs*.

Hormonal responses often culminate in the production of defensive compounds, serving as toxins, repellents, and/or antifeedants (Santamaria *et al*., 2020). Notably, cyanide-derived products are toxic molecules directly targeting pest physiology. For instance, Arnaiz *et al.* (2022) found a gene encoding hydroxynitrile lyase (*AtHNL*) that catalyzes the reversible interconversion between cyanohydrins and derived carbonyl compounds with free cyanide, proving lethal to mites. Conversely, Dixit *et al.*, (2022) and Arnaiz *et al.* (2022) demonstrated that a b-cyanoalanine synthase of *T. urticae* (*TuCAS*) assists mites in detoxifying HCN. These studies underscore the mite's remarkable adaptability as an extreme polyphagous herbivore, allowing them to exploit cyanogenic host plants effectively.

The accumulation of specific hormones, such as ABA, can induce notable phenotypic changes, including the closure of stomata. Our research has uncovered that infestation by *T.urticae* results in elevated ABA levels, particularly in specific cell types, leading to stomatal closure. This discovery gains significance when considering the findings from Benssousan et al. (2016) study, which highlighted the mite's remarkable ability to exploit stomata as natural entry points into leaves. This underscores the pivotal role of maintaining a well-balanced ABA level. Stomatal closure becomes essential for the plant as it serves as a deterrent against mite feeding while ensuring the continuation of vital photosynthetic processes.

Based on previous data already published, and data obtained in this thesis, a model deciphering the crosstalk between players and molecules in the *T. urticae-A. thaliana* interplay is proposed **(Figure 54)**, trying to summarize the molecular events behind this interaction.

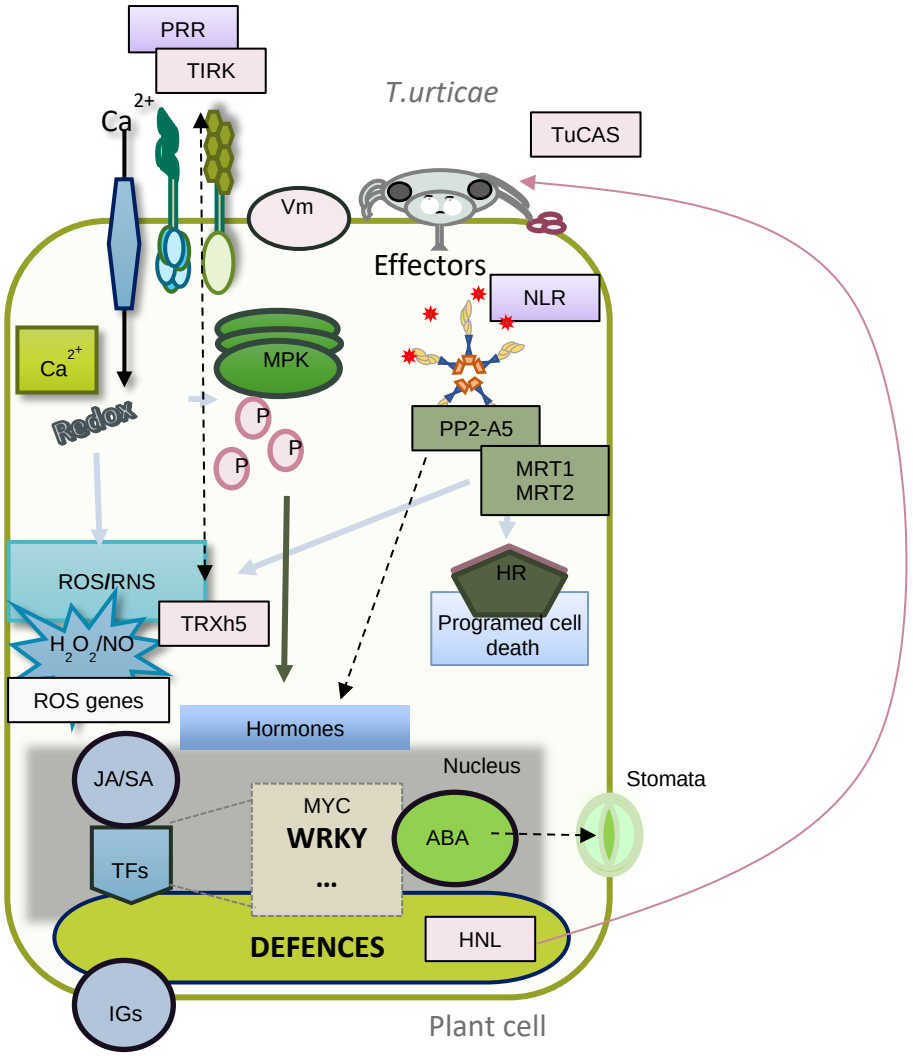

Figure 54. A model depicting the crosstalk between various players and molecules identified thus far in the *T. urticae-A. thaliana* interaction. Specific mite elicitors/effectors are recognized by receptors (PRR or NLR; TIRK, MRT1, MRT2, PP2-A5) that induce alterations in the membrane potential (Vm) and Ca2+ influx. Subsequently, reactive oxygen species (ROS) and nitrogen species (RNS) are triggered. Some ROS genes (and *TRXh5*) associated to ROS/RNS balance participate in the defense process, modulating somehow the hormonal signalling pathways, mainly through the JA/ABA ratios to finally induced appropriated plant defences and phenotypical changes in stomata. Among them, HCN and quinones mediated by the hydroxynitrile lyase enzyme (HNL) and cyanoalanine synthase of *T. urticae* (TuCAS), respectively. Finally, the glucosinolates (IGs) and other defensive metabolites are produced.

Overall, this thesis delves into the crucial realm of regulating plant defences against pests. It emphasizes the nuanced intricacies involved in this process:

Firstly, the thesis underscores the significance of accurate perception and activation of defense mechanisms. Plants must possess diverse mechanisms to discern the identity of herbivores feeding on them and to determine the most effective defensive strategies against each pest.

Secondly, precise activation of defences is paramount. The timing of induction and repression of specific processes and pathways during infestation is essential. Failure to maintain this delicate balance could lead to plant intoxication from endogenous molecules, jeopardizing the plant's overall viability.

Furthermore, the modulation of defense cascades emerges as a vital factor. Different defense events occur, some swift and robust, necessitating the plant's ability to finely regulate these responses based on the type of pest and the extent of infestation.

In parallel, the diversity of defense regulatory elements is explored. From highly reactive small molecules like NO to enzymes in metabolic pathways (*JAO2*), and complex molecules in hormonal pathways such as ABA, to small RNA molecules with potent transcriptional regulatory abilities. These elements constitute the complex arsenal plants employ to defend against pests.

This in-depth investigation sheds light on the complexity of plant defense, revealing it as a multifaceted and adaptable interplay shaped by diverse external factors. These factors encompass additional stressors like simultaneous pathogen infestations (Contreras & Martinez, 2022) and unfavourable environmental conditions such as drought (Santamaria *et al.*, 2018c; Gomez-Sanchez *et al.*, 2019). The primary goal of the thesis is to enhance our comprehension of plant-pest interactions, laying the groundwork for innovative pest control approaches. The urgency of this research is underscored by the critical situation posed by *T. urticae*, a pest whose far-reaching impact on global crops is exacerbated by the escalating challenges of rising

temperatures and drought. Addressing this issue becomes paramount to ensure the sustainable supply of both animal and human food sources.

CONCLUSSIONS

1. Nitric oxide plays a vital role in plant defense against herbivorous mites, regulating early signalling events, defense hormones, and stomatal closure. Its interaction with other molecules enhances plant resistance, making it challenging for mites to feed and reproduce.
2. *JAO2*, a gene regulating the first step of JA catabolism, significantly impacts Arabidopsis defense against spider mite infestation. By altering active and inactive jasmonates, *JAO2* influences camalexin and glucosinolates synthesis, emphasizing the gene's pivotal role in plant resistance to sucking pests.
3. ABA accumulation in stomata, induced by mite feeding, triggers stomatal closure, hindering mite access to leaf interiors. Pre-treatment with ABA protects plants without growth compromise, emphasizing stomatal closure as a crucial defense mechanism.
4. Stomatal density, coupled with aperture regulation mediated by ABA, significantly impacts plant resistance to mite infestation. A higher number of stomata, in conjunction with their closure, plays a pivotal role in reducing leaf damage, highlighting their importance in defense strategies.
5. Functional redundancy of *MRT1* and *MRT2* TNL intracellular receptors play vital roles in plant defense against herbivores. Their absence leads to increased damage and disrupts defense hormone pathways, highlighting their importance in mediating the plant's response to pests.
6. miR825-5p fine-tunes herbivore defense by regulating R-genes like *MRT1* and *MRT2*. Altered miR825-5p levels influence plant resistance, and its interaction with the TNL *MIST1* receptor generates phasiRNAs, forming a negative feedback loop essential for defense against specific herbivores.
7. In summary, in our study, we've revealed the complexity of plant defense, emphasizing the crucial role of every element in maintaining a delicate balance. The precise regulation of various molecules, pathways, and regulators at specific times is essential for the plant's survival in challenging environments.

ANNEXED FIGURES

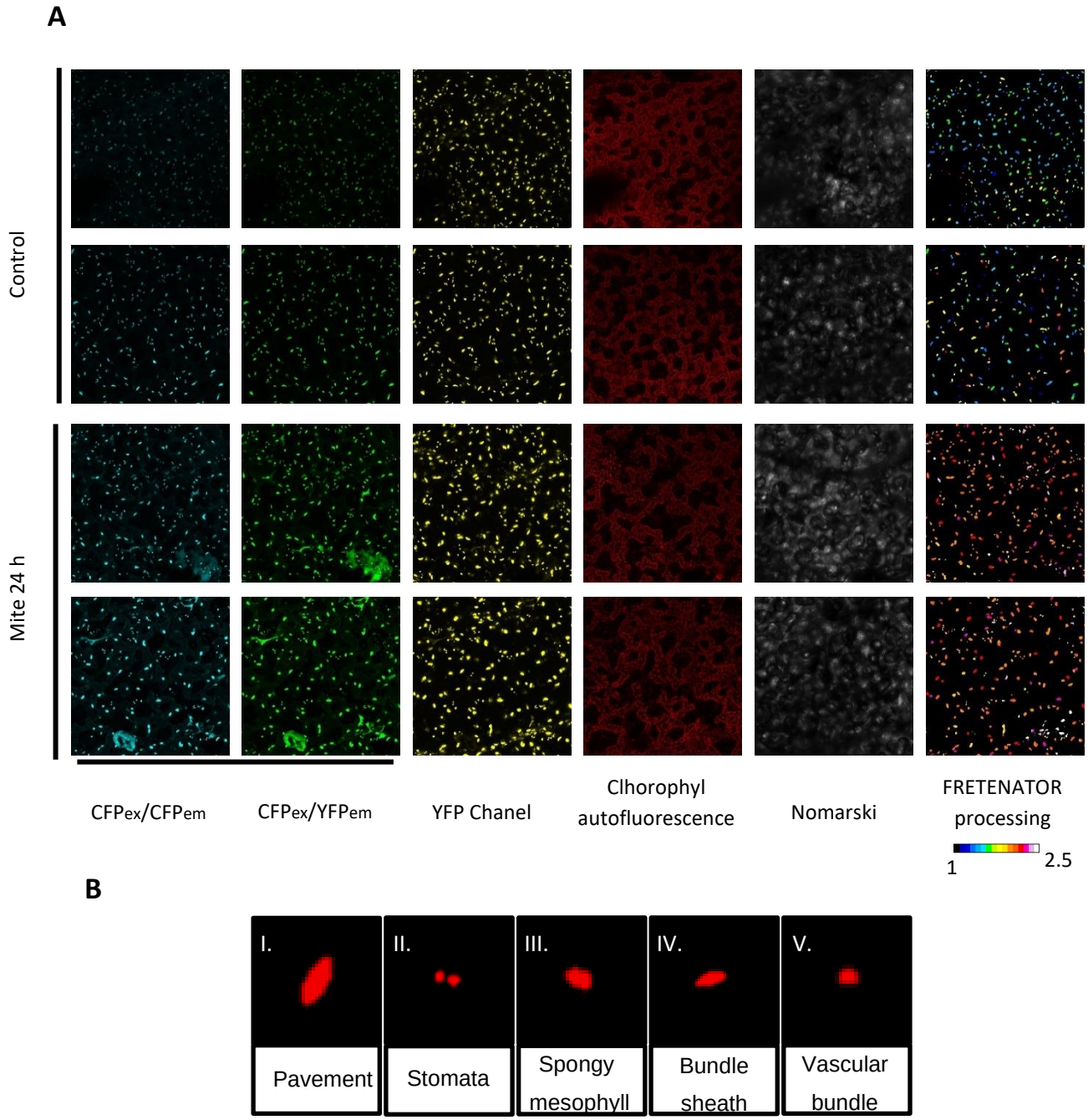

Annexed Figure 1. FRET-images processing. A Raw Confocal image after 24 h of mite infestation **B** FretCellType nucleus determination based on their shape. I. Pavement nuclei. II. Stomata nuclei III. Spongy mesophyll nuclei, IV. Bundle sheath nuclei, V. Vascular bundle nuclei.

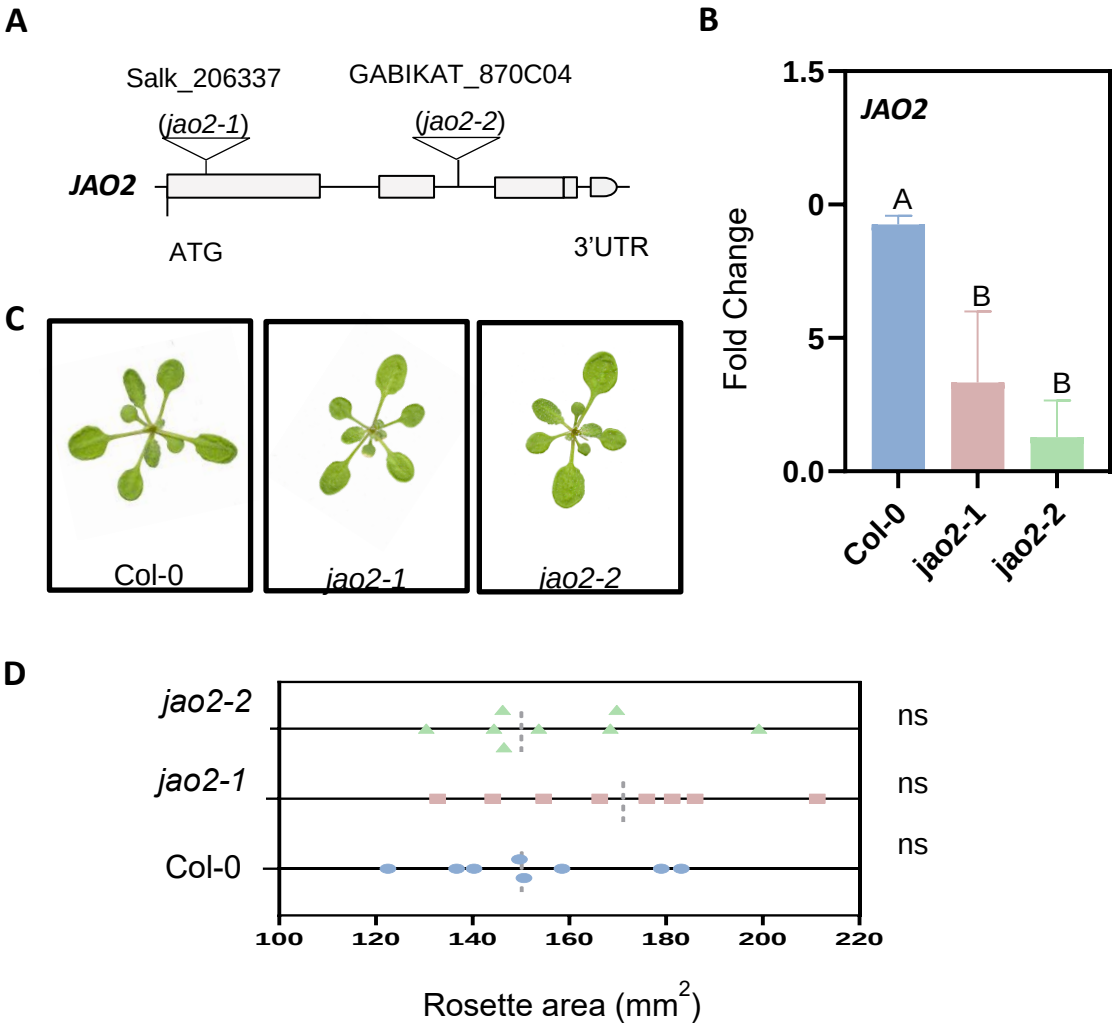

Annexed Figure 2. Molecular characterization of Arabidopsis jao2 mutant lines. **A** Scheme of the position of the T-DNA insertion (arrowhead) in the JAO2 gene. **B** Expression levels of JAO2 gene in leaves of *jao2-1* and *jao2-2* mutant lines and Col-0 plants. Data are means ± SE of three replicates. **C** Plant phenotypes of j*ao2* and Col-0 rosettes 2 weeks after germination. **D** Determination of rosette area of jao2 lines. Different letter indicates significant differences **(B, D)** P<0.5, One way ANOVA followed by Tukey's multiple comparison test.

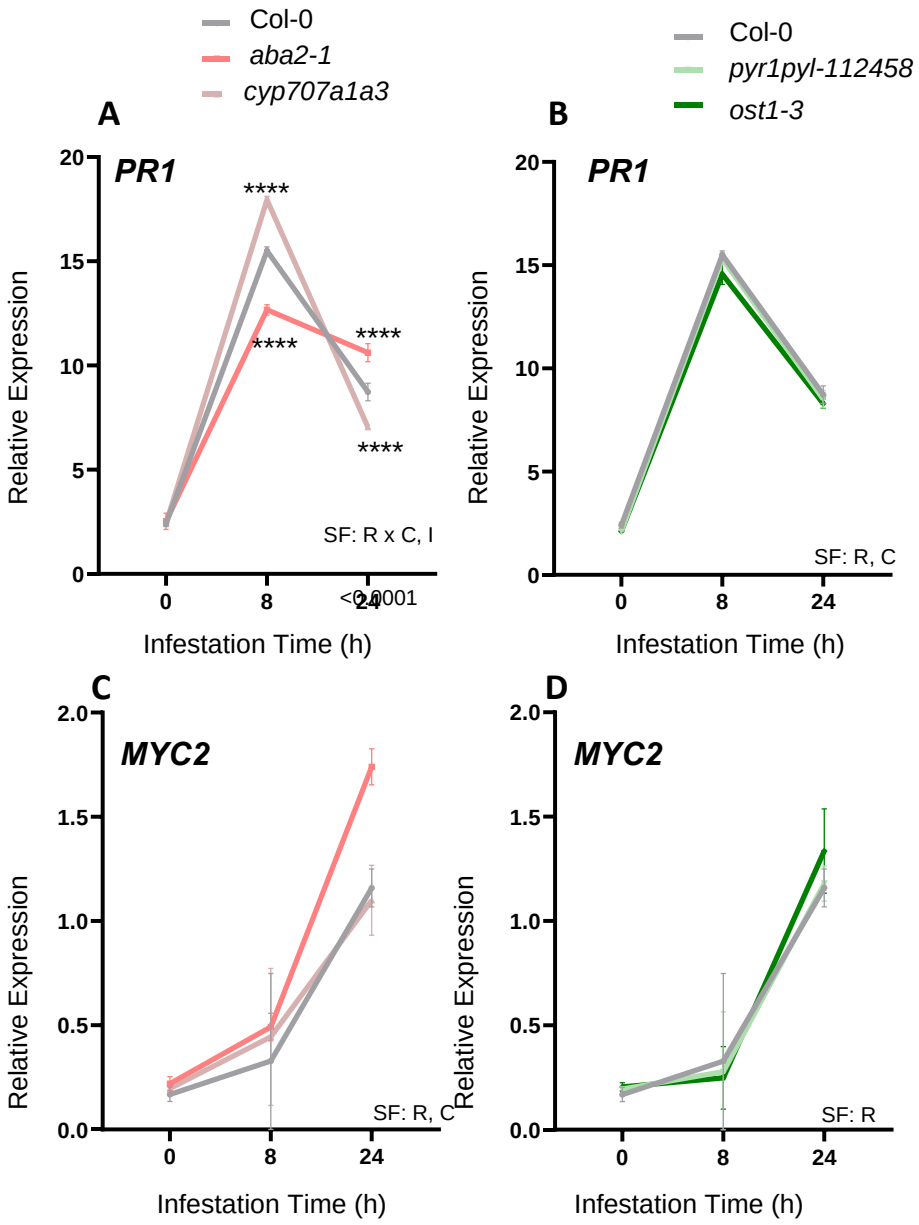

Annexed Figure 3. Expression levels of PR1 and MYC2 genes in the five Arabidopsis genotypes. PR1 gene **A, B** and MYC2 gene **C, D.** Gene expression levels were determined in aba2-1, cyp707a1cyp707a3, and in pyr1pyl-112458, ost1-3 and Col-0 whole plants. Values indicated as relative expression. Significant factors (SF) indicate whether the two independent factors, R (infestation time) and C (genotype), and/or their interaction I (RxC) were statistically significant (Two-way ANOVA followed by Tukey's multiple comparison test, P<0.05). Data are means ± SE of 3 pools of 6 biological replicates.

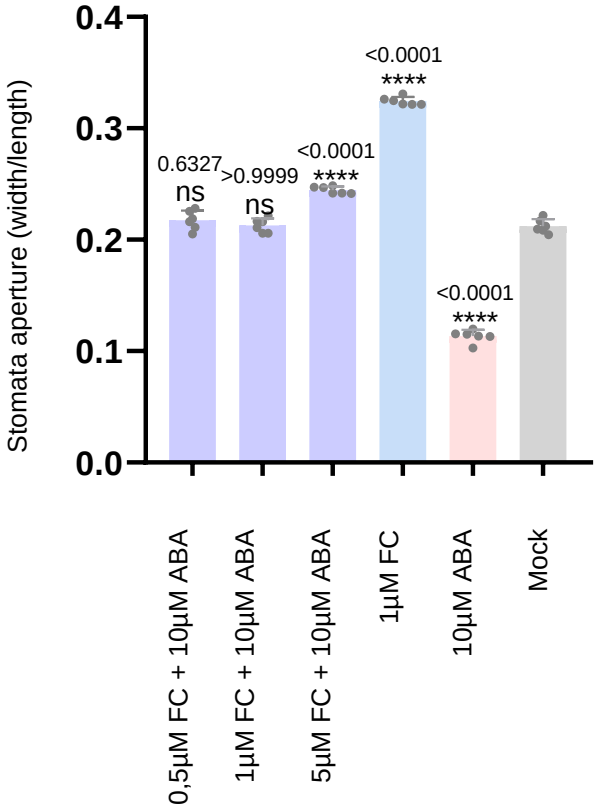

Annexed Figure 4. Effects of different ratios Fussicoccin/ABA on stomata aperture in Arabidopsis Col-0 plants. Stomata aperture of Arabidopsis detached leaves pre-treated with 10 µM ABA, 1 µM of fusicoccin (FC), or a combination of 10 µM ABA plus different concentrations (0.5, 1.0, and 5.0 µM) of FC. Numbers indicate significant differences compare to mock treatment. Data are means ± SE of 8 biological replicates.

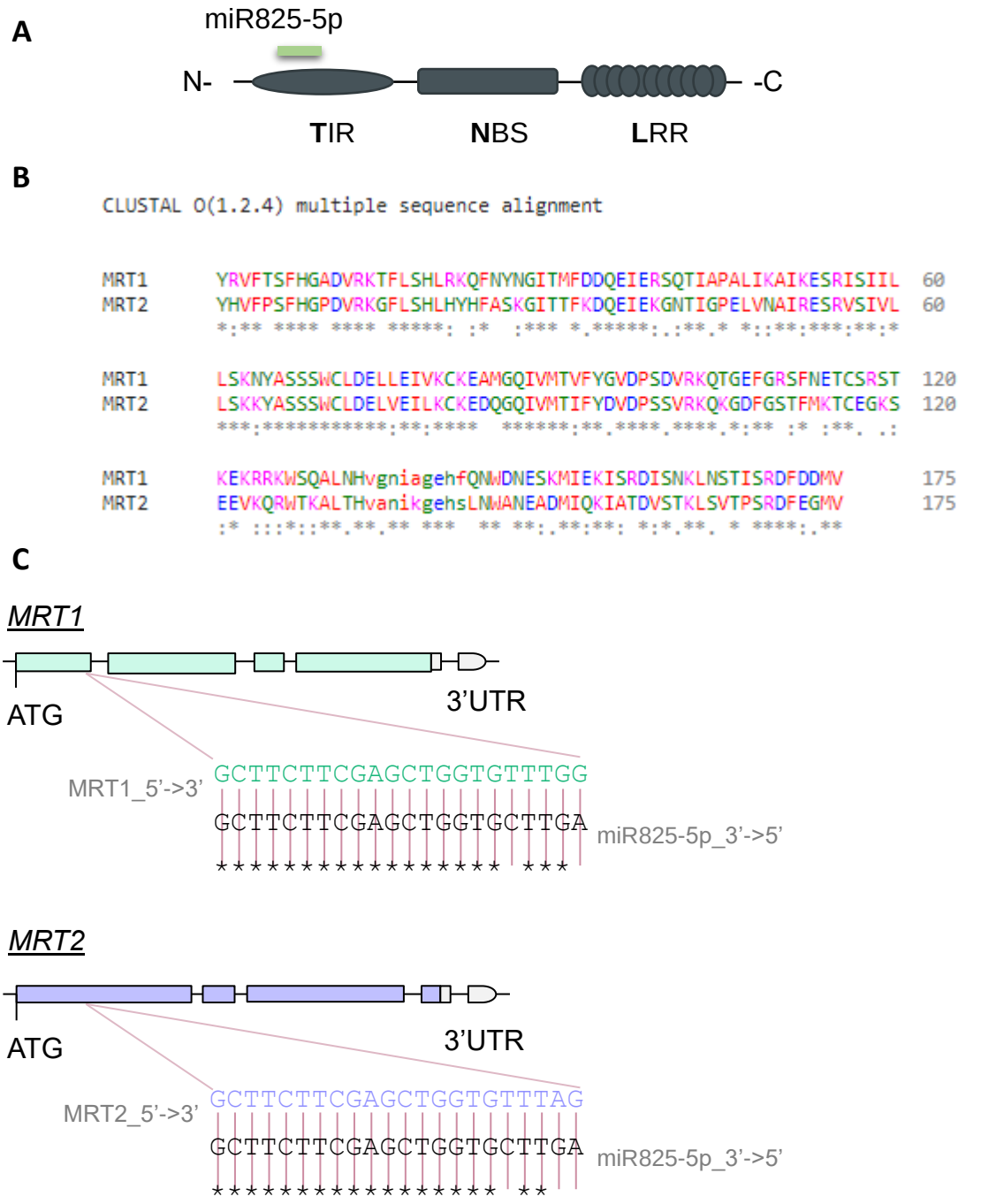

Annexed Figure 5. miR825-5p binding side and the sequence characteristics. A miR825-5p binds Toll Interleukin domain in TNL proteins. **B** Alignment of the nucleotide sequences of TIR domain of MRT1 an MRT2**. C** Specific binding nucleotide sequences of miR825-5p for *MRT1* and *MRT2* genes.

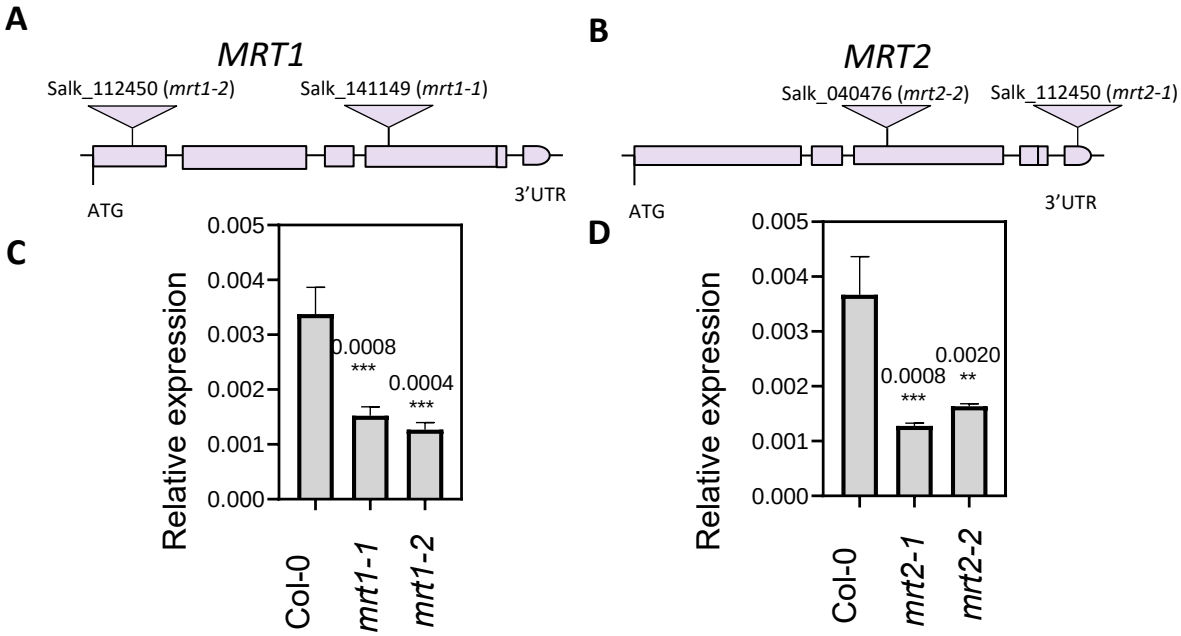

Annexed Figure 6. Molecular characterization of Arabidopsis *mrt*- mutant lines. Scheme of the position of the T-DNA insertion (arrowhead) in **A**, *MRT1* and **B**, *MRT2* gene. Expression levels of **C**, *MRT1* and **D**, *MRT2* genes in leaves of *mrt* mutant lines and Col-0 plants. Data are means ± SE of three replicates. Asterisks and numbers indicate significant differences compare to Col-0 genotype.

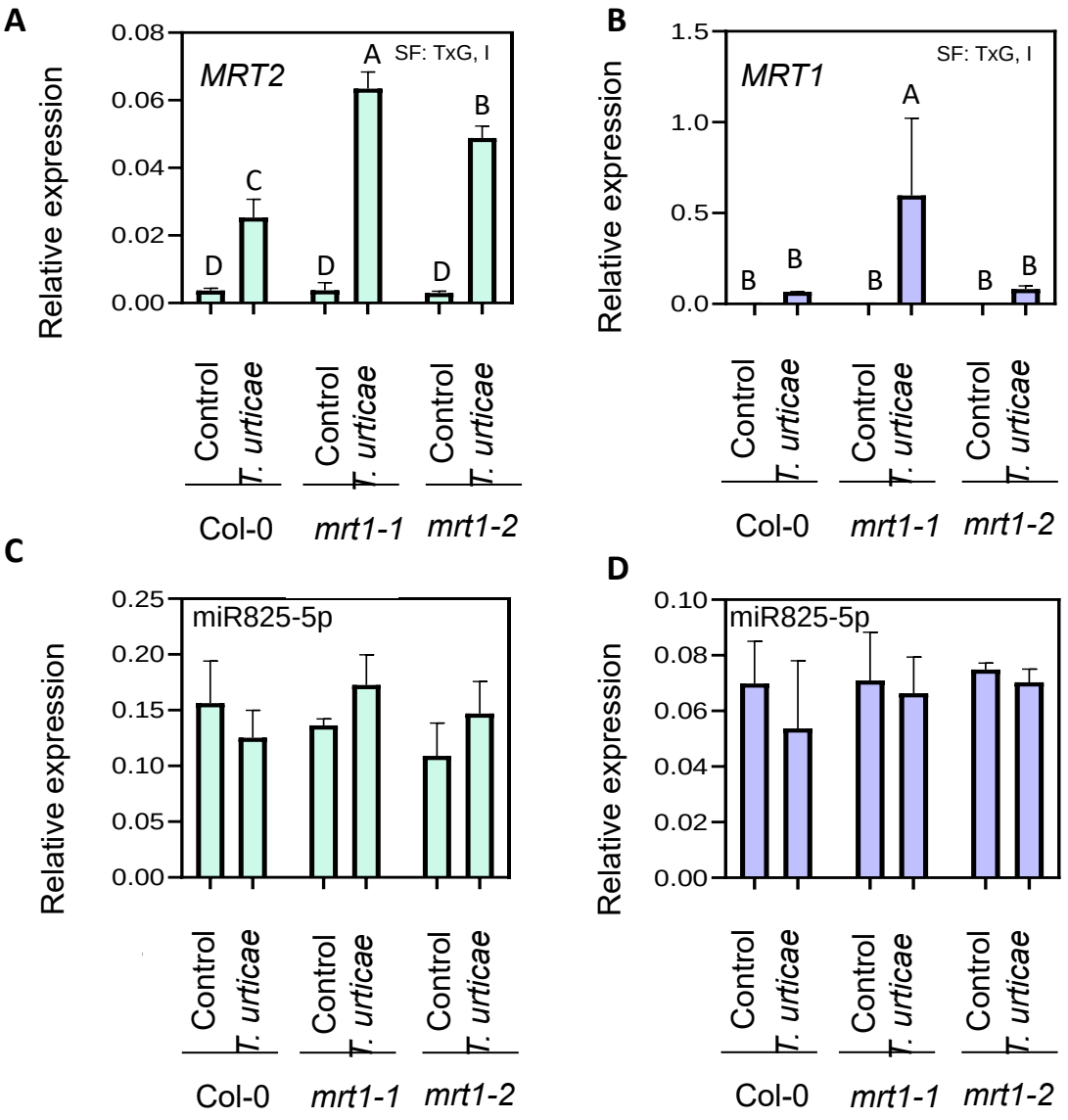

Annexed Figure 7. Gene expression analysis of MRT1, MRt2 and miR825-5p in mrt mutant lines after 0.5 h of *T. urticae* infestation. A MRT2 relative expression in mtr1-1 and mtr1-2 mutant lines. **B** MRT1 relative expression in mtr2-1 and mtr2-2 mutant lines. **C, D** relative expression of miR825-5p in mrt lines. Data are means ± SE of three replicates. Significant factors (SF) indicate whether the two independent factors, G (genotype) and T (mite treatment), and/or their interaction (TxG,I) were statistically significant. ns: no statistically significant.

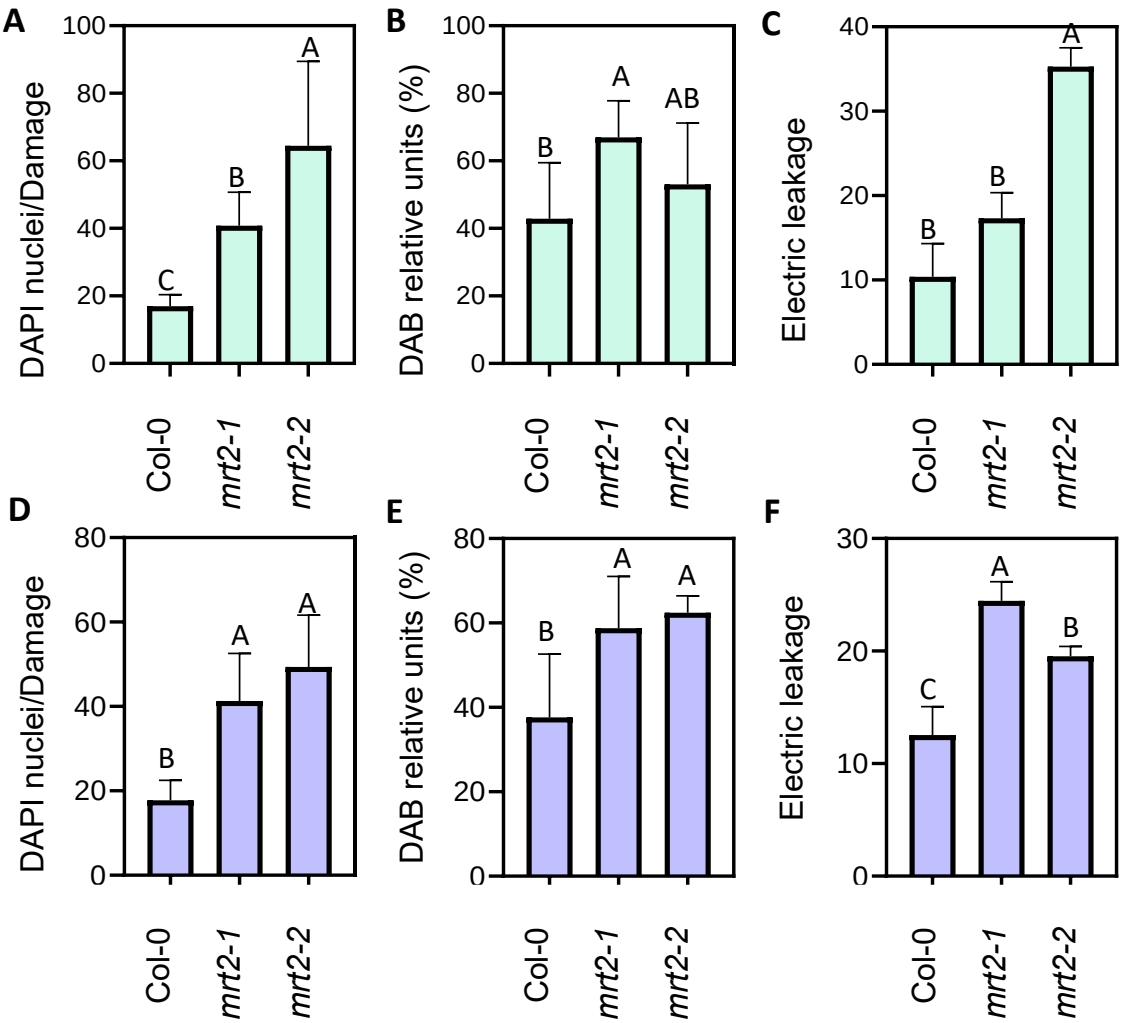

Annexed Figure 8. DAPI/nuclei damage relation, H_2O_2 and membrane depolarization after *T. urticae* feeding 24 h in mrt1- and mrt2- single mutant plants. A, D DAPI staining overlapped in damaged zones after 24 h of mite infestation. **B, E** ROS production measured by DAB staining after 24h of mite infestation. **C, F** Membrane depolarization measured by electric leakage after 24 h of mite infestation. Letters indicate significant differences compare to Col-0 genotype. (P<0.5, One way ANOVA followed by Tukey's multiple comparison test).

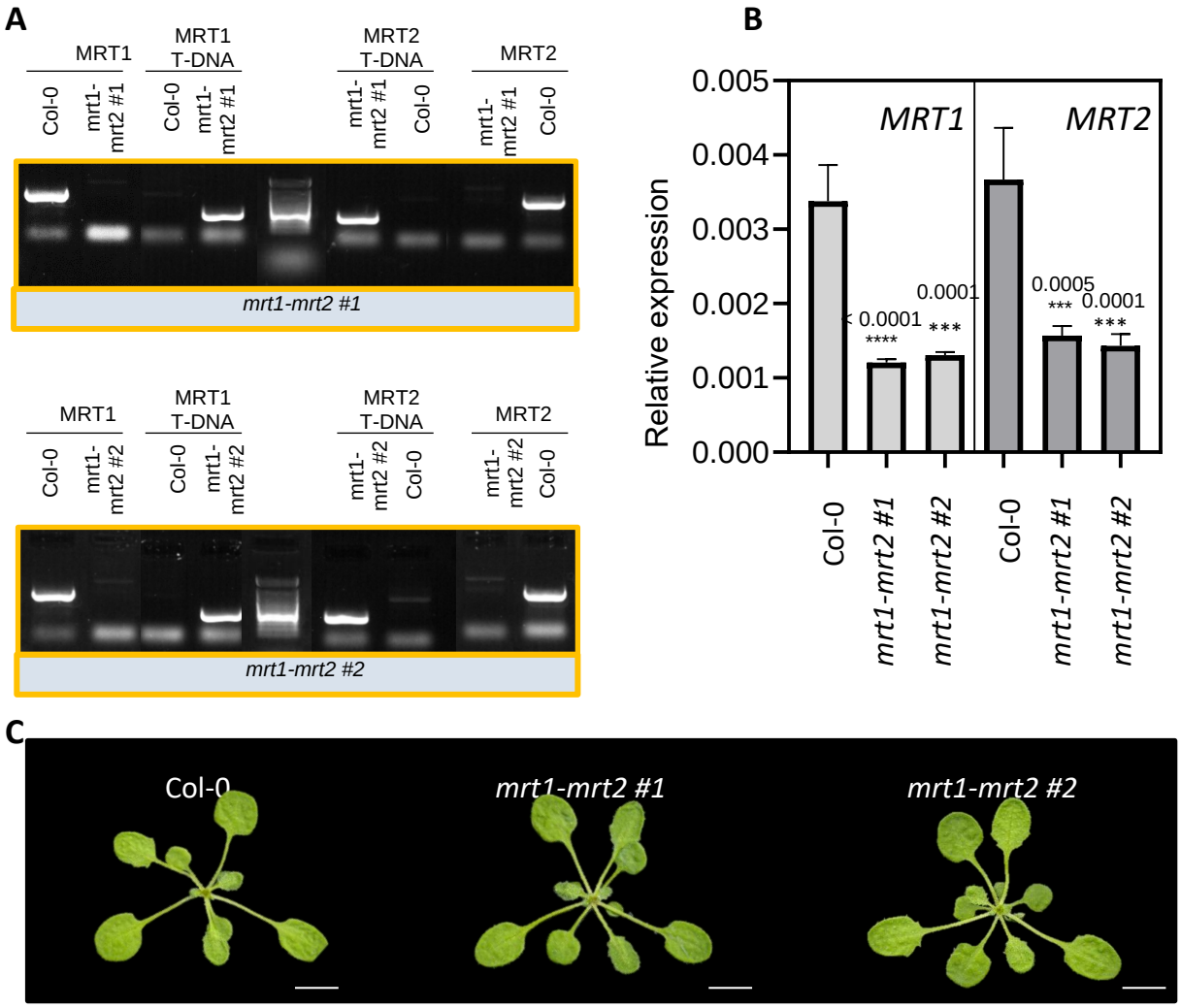

Annexed Figure 9. Molecular characterization of Arabidopsis *mrt1*-mrt2 mutant lines. **A** PCR assays of MRT1 and MRT2 genes in WT and mrt1-mrt2 double mutants' lines to show homozygous status. **B** Gene. expression levels of *MRT1* and *MRT2* in leaves of *mrt1-mrt2 double* mutant plants and Col-0 plants. Data are means ± SE of three replicates. Asterisks and numbers indicate significant differences compare to Col-0 genotype. **C** Phenotypes of 3 weeks-old wild-type and mrt1-mrt2 double mutant plants grown in soil. Bars = 0.5 cm.

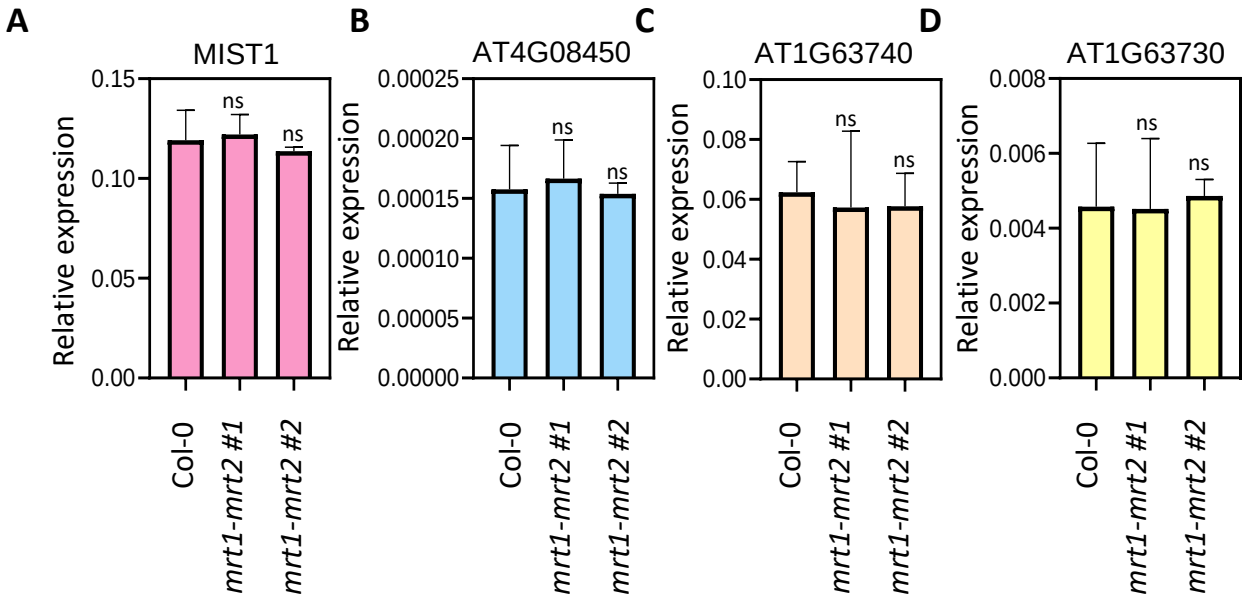

Annexed Figure 10. Gene expression analysis R genes in *mrt1-mrt2* mutant lines. Relative expression of **A**; MIST1, **B**; AT4G08450, **C**; AT1G63740, **D**; AT1G63730 in *mrt1-mrt2* double mutant lines. Data are means ± SE of three replicates. Asterisks and numbers indicate significant differences compare to Col-0 genotype.

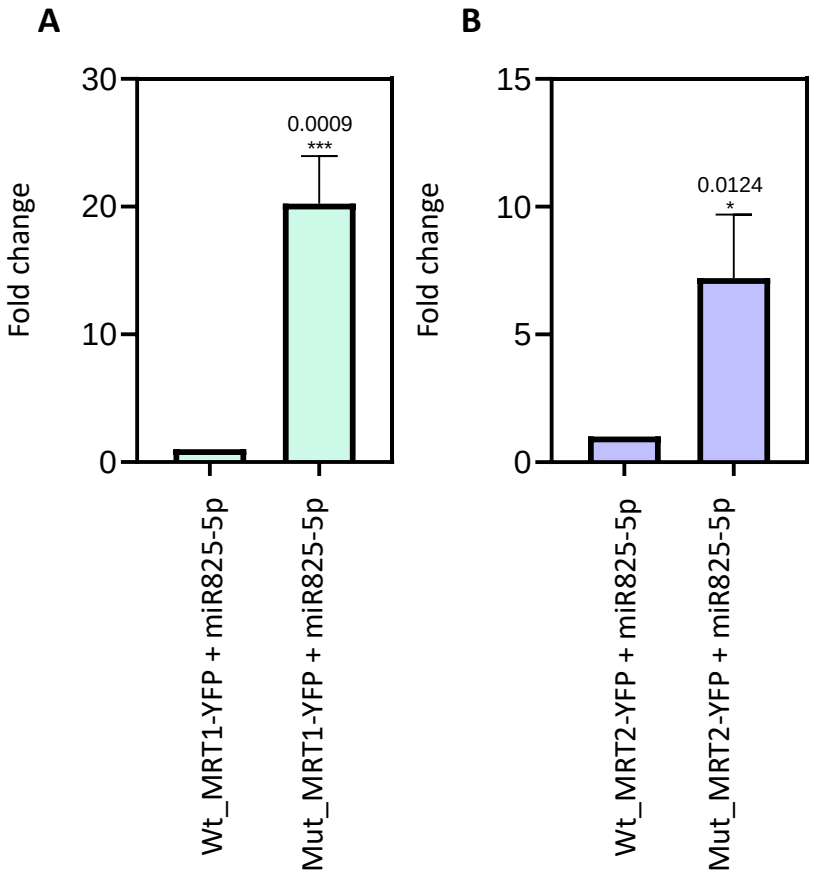

Annexed Figure 11: Expression levels of YFP in MRT1-YFP and MRT2-YFP in *N. benthamiana* plants. A Expression of fluorescence YFP protein emitted by *N. benthamiana* agroinfiltrated with Wt_MRT1-YFP or its mutated version Mut_MRT1-YFP, combined with miR825-5p at 36 h post agroinfiltration. **B** Expression of fluorescence YFP protein emitted by *N. benthamiana* agroinfiltrated with Wt_MRT2-YFP or its mutated version Mut_MRT2-YFP, combined with miR825-5p at 36 h post agroinfiltration. Asterisks and numbers indicate significant differences compare to Wt_MRT1 or Wt_MRT2 construction.

ANNEXED TABLES

Primers sequence used for T-DNA insertion validation

Gene	Primer name	Sequence (5'->3')
	LB-8409 GABI	ATATTGACCATCATACTCATTGC
	LB-BP643 SALK	GCAATCAGCTGTTGCCCGTCTCACTGGTG
At5g05600	SALK_206337-LP	CGTTGTGTGTCATCTATTGTGC
	SALK_206337-RP	AATCAGCCTTCTCACATTCCC
	GABI_870C04-LP	CTCATCCCCATGCTTTCATC
	GABI_870C04-RP	CCACGTTTTTCAAACATGACG
AT4G14370	SALK_112450-LP	ATGGTTGGACTTGAAGCACAC
	SALK_112450-RP	CAAGCGATATGCCTAAAGCAG
	SALK_149141.16-LP	TGTGTCGTTATTGTCGTCAGC
	SALK_149141.16-RP	AAAGTCCCTGGGTATTTGGTG
AT5G41550	SALK_050251-LP	GTTAAGACCAAAGAGACCGGC
	SALK_050251-RP	CACCAGCTCGAAGAAGCATAC
	SALK_040476 -LP	TGGCATATGGAGTTCCAAGAG
	SALK_040476-RP	TTCATGGTTTGGTTCTGGAAG

Primers sequence used for RTqPCR assays

Gene	Primer name	Sequence (5'->3')
At5g25760	AtUBQ F	GCTCTTATCAAAGGACCTTCGG
	AtUBQ R	CGAACTTGAGGAGGTTGCAAAG
AY179605	NbACT F	GATGGACAAGTCATCACCATTG
	NbACT R	CTGAGACAATGTTTCCGTACA
YFP	YFP-F	GAACGGCATCAAGGTGAACT
	YFP-R	CACCATGTGGTCCCTCTTCT
At5g05600	JAO2 F	CTCATCCCCATGCTTTCATC
	JAO2 R	TCCGAGTTCACTATCACTCTATGC
At3g11180	JAO1 F	CGTGGATCACTGTCAATCCT
	JAO1 R	CGATGTTCCACGCTCTTGTA
At5g55970	JAO3 F	GAACCAGCTCCTCATG CTTT
	JAO3 R	GGGTTCACGATCACTCTGTG
At2g38240	JAO4 F	ATGGCTGGGTCACCATTAAA
	JAO4 R	GTTCCACGCTTTTGTAAATTCC
At5g42650	AOS F	CGTTAGGAAGCTCCGTTAATTTCTC
	AOS R	TTCACGAAACTGGAACAAGAAAACA
At2g46370	JAR1 F	ACGTGTACCGCAACCCTAAC

	JAR1 R	CGTGAACTAGACCGTGAGCA
At1g32640	MYC2 F	TCCGAGTCCGGTTCATTCT
	MYC2 R	TCTCGGGAGAAAGTGTTATTGAA
At2g14610	PR1 F	TCAGTGAGACTCGGATGTGC
	PR1 R	CGTTCACATAATTCCCACGA
AT4G14370	MRT1 F	TCTCATGATAAGCGGCAGTG
	MRT1 R	TTGAAACGCAAGCAACACTC
AT5G41550	MRT2 F	CCCAGCAGAGTTCAGTCACA
	MRT2 R	CCCAGGAGACCAATCTGAAA
AT5G38850	MIST1 F	GAGAGGAGCCAAACCATAGC
	MIST1 R	TCGGCATCACTACGTCTTTGC
AT4G08450	AT4G08450 F	GAGCAAGCTCGAGAAGCTGT
	AT4G08450 R	GTGGAAGGAACCTCAACCAA
AT1G63740	AT1G63740 F	AAGGGAAATACCTGCGGAGT
	AT1G63740 R	GCTTGGAGTTTACGGAGCTG
AT1G63730	AT1G63730 F	CCATTGCAAGGGCTTTACAT
	AT1G63730 R	AACATTTTGGTCGCATAGCC
Pri-miR825	Pri-miR825 F	ACTCGTTCAAGCACCAGCTC
	Pri-miR825 R	CATCAACTTGTTCATGCACCTT
miR825-5p	miR825-5p SL F	TGGCTCAAGCACCAGCTCGA
	Universal SL R	GTGCAGGGTCCGAGGT

Primers sequence used for RTqPCR assays

Gene	Primer name	Sequence (5'->3')
phasiR263-1	phasiR263-1 I	GAAGAAGATCGGCATCACTACGTTCTCTCTTTTGTATTCC
	phasiR263-1 II	GAACGTAGTGATGCCGATCTTCTTCAAAGAGAATCAATGA
	phasiR263-1 III	GAACATAGTGATGCCCATCTTCTTCACAGGTCGTGATATG
	phasiR263-1 IV	GAAGAAGATGGGCATCACTATGTTCTACATATATATTCCT
phasiR263-2	phasiR263-2 I	GATAGAAGATCGGCATCACTACGTCTCTCTTTTGTATTCC
	phasiR263-2 II	GACGTAGTGATGCCGATCTTCTATCAAAGAGAATCAATGA
	phasiR263-2 III	GACGCAGTGATGCCGTTCTTCTTTCACAGGTCGTGATATG
	phasiR263-2 IV	GAAAGAAGAACGGCATCACTGCGTCTACATATATATTCCT

phasiR263-9	phasiR263-9 I	GAACGGAAACAGAAGGGAGATTTTCTCTCTTTTGTATTCC
	phasiR263-9 II	GAAAATCTCCCTTCTGTTTCCGTTCAAAGAGAATCAATGA
	phasiR263-9 III	GAAACTCTCCCTTCTCTTTCCGTTCACAGGTCGTGATATG
	phasiR263-9 IV	GAACGGAAAGAGAAGGGAGAGTTTCTACATATATATTCCT
Universal vector	pRS300 A	CTGCAAGGCGATTAAGTTGGGTAAC
	pRS300 B	GCGGATAACAATTTCACACAGGAAACAG

Annexed table 1. Oligonucleotide sequences used.

Annotation	*mz*	Rt [min]	MS/MS
4-OH-I3M	463.0479	3.15	300, 271, 255, 96
I3M	447.0532	4.05	447, 96
SA-Glc	299.0764	4.14	137, 93
12-HSO_4-JA	305.0693	4.62	97
4-MeO-I3M	477.0641	4.86	434,96
1-MeO-I3M	477.0640	5.16	477, 44, 96
12-OH-JA	225.1126	5.29	225, 59
12-COOH-JA	239.0918	5.31	195, 141, 59
12-COOH-JAIle	352.1745	6.70	308, 130
12-OH-JAIle	338.1874	6.78	338, 130
JA	209.1079	8.09	209, 165, 59
Camalexin	199.0238	8.10	199, 158, 141, 130
JA-Ile	322.1987	9.12	322, 130
12-OPDA	291.1936	11.12	165, 59

Annexed Table 2. Identification of metabolites by reversed phase LC/ESI-QqTOF-MS.

JA-derivative	Panel	Test	Combination	95,00 % CI of diff	Significant?	Summary		Adjusted P Value
12-OH-JA	A	Tukey's	Col-0: Control vs. Col-0: Mite	-64,49	-71,40 to -57,57	Yes	****	<0,0001
			Col-0: Control vs. *jao2-2*: Control	0,01905	-6,892 to 6,931	No	ns	>0,9999
			Col-0: Control vs. *jao2-2*: Mite	-33,78	-40,69 to -26,87	Yes	****	<0,0001
			Col-0: Mite vs. *jao2-2*: Control	64,51	57,59 to 71,42	Yes	****	<0,0001
			Col-0: Mite vs. *jao2-2*: Mite	30,71	23,79 to 37,62	Yes	****	<0,0001
			jao2-2: Control vs. *jao2-2*: Mite	-33,8	-40,71 to -26,89	Yes	****	<0,0001
12-HSO4-JA	C	Tukey's	Col-0: Control vs. Col-0: Mite	-38,39	-42,74 to -34,04	Yes	****	<0,0001
			Col-0: Control vs. *jao2-2*:Control	-0,8976	-5,249 to 3,454	No	ns	0,9089
			Col-0: Control vs. *jao2-2*:Mite	-24,42	-28,77 to -20,07	Yes	****	<0,0001
			Col-0: Mite vs. *jao2-2*:Control	37,49	33,14 to 41,84	Yes	****	<0,0001
			Col-0: Mite vs. *jao2-2*:Mite	13,97	9,618 to 18,32	Yes	****	<0,0001
			jao2-2: Control vs. *jao2-2*: Mite	-23,52	-27,87 to -19,17	Yes	****	<0,0001
12-OH-JAIle	E	Tukey's	Col-0: Control vs. Col-0: Mite	-13,98	-101009 to 100981	No	ns	>0,9999
			Col-0: Control vs. *jao2-2*: Control	-0,4053	-100996 to 100995	No	ns	>0,9999
			Col-0: Control vs. *jao2-2*: Mite	-44615	-145610 to 56380	No	ns	0,525
			Col-0: Mite vs. *jao2-2*:Control	13,58	-100982 to 101009	No	ns	>0,9999
			Col-0: Mite vs. *jao2-2*: Mite	-44601	-145596 to 56394	No	ns	0,5252
			jao2-2: Control vs. *jao2-2*: Mite	-44615	-145610 to 56380	No	ns	0,525
12-COOH-JAIle	G	Tukey's	Col-0: Control vs. Col-0 :Mite	-61,58	-71,24 to -51,92	Yes	****	<0,0001
			Col-0: Control vs. *jao2-2*:Control	-0,5362	-10,20 to 9,129	No	ns	0,9978
			Col-0: Control vs. *jao2-2*: Mite	-52,05	-61,71 to -42,39	Yes	****	<0,0001
			Col-0: Mite vs. *jao2-2*: Control	61,04	51,38 to 70,71	Yes	****	<0,0001
			Col-0: Mite vs. *jao2-2*: Mite	9,53	-0,1349 to 19,19	No	ns	0,0532
			jao2-2: Control vs. *jao2-2*: Mite	-51,51	-61,18 to -41,85	Yes	****	<0,0001
12-COOH-JA	I	Tukey's	Col-0: Control vs. Col-0:Mite	-7,375	-8,973 to -5,777	Yes	****	<0,0001
			Col-0:Control vs. *jao2-2*:Control	-0,1102	-1,708 to 1,488	No	ns	0,9959
			Col-0:Control vs. *jao2-2*:Mite	-6,248	-7,846 to -4,650	Yes	****	<0,0001

			Col-0: Mite vs. *jao2-2*: Control	7,265	5,667 to 8,863	Yes	****	<0,0001
			Col-0: Mite vs. *jao2-2*: Mite	1,127	-0,4709 to 2,725	No	ns	0,1873
			jao2-2: Control vs. *jao2-2*: Mite	-6,138	-7,736 to -4,540	Yes	****	<0,0001

Annexed table 3. Values and statistics applied to the quantification of JA-derivatives determined in *jao2-2, jaoT* mutant lines and Col-0 under control or mite infested conditions.

JA-derivative	Panel	Test	Combination	95,00% CI of diff	Significant?	Summary		Adjusted P Value
12-OH-JA	B	Tukey's	Control: Col-0 vs. Control: *jaoT*	-0,01234	-0,1788 to 0,1541	No	ns	0,996
			Control: Col-0 vs. Mite: Col-0	-0,9002	-1,067 to -0,7337	Yes	****	<0,0001
			Control: Col-0 vs. Mite: *jaoT*	-0,1505	-0,3170 to 0,01589	No	ns	0,0811
			Control: *jaoT* vs. Mite: Col-0	-0,8878	-1,054 to -0,7214	Yes	****	<0,0001
			Control: *jaoT* vs. Mite: *jaoT*	-0,1382	-0,3046 to 0,02823	No	ns	0,1169
			Mite: Col-0 vs. Mite: *jaoT*	0,7496	0,5832 to 0,9161	Yes	****	<0,0001
12-HSO4-JA	D	Tukey's	Control: Col-0 vs. Control: *jaoT*	-0,001907	-0,02619 to 0,02237	No	ns	0,9953
			Control: Col-0 vs. Mite: Col-0	-0,1204	-0,1447 to -0,09615	Yes	****	<0,0001
			Control: Col-0 vs. Mite: *jaoT*	-0,05292	-0,07720 to -0,02864	Yes	***	0,0002
			Control: *jaoT* vs. Mite: Col-0	-0,1185	-0,1428 to -0,09425	Yes	****	<0,0001
			Control: *jaoT* vs. Mite: *jaoT*	-0,05101	-0,07529 to -0,02673	Yes	***	0,0002
			Mite: Col-0 vs. Mite: *jaoT*	0,06751	0,04323 to 0,09179	Yes	****	<0,0001
12-OH-JAIle	F	Tukey's	Control: Col-0 vs. Control: *jaoT*	-0,01234	-0,1788 to 0,1541	No	ns	0,996
			Control: Col-0 vs. Mite: Col-0	-0,9002	-1,067 to -0,7337	Yes	****	<0,0001
			Control: Col-0 vs. Mite: *jaoT*	-0,1505	-0,3170 to 0,01589	No	ns	0,0811
			Control: *jaoT* vs. Mite: Col-0	-0,8878	-1,054 to -0,7214	Yes	****	<0,0001
			Control: *jaoT* vs. Mite: *jaoT*	-0,1382	-0,3046 to 0,02823	No	ns	0,1169
			Mite: Col-0 vs. Mite: *jaoT*	0,7496	0,5832 to 0,9161	Yes	****	<0,0001
12-COOH-JAIle	H	Tukey's	Control: Col-0 vs. Control: *jaoT*	-0,008501	-0,1404 to 0,1234	No	ns	0,9974
			Control: Col-0 vs. Mite: Col-0	-0,9059	-1,038 to -0,7740	Yes	****	<0,0001
			Control: Col-0 vs. Mite: *jaoT*	-0,8588	-0,9907 to -0,7269	Yes	****	<0,0001
			Control: *jaoT* vs. Mite: Col-0	-0,8974	-1,029 to -0,7655	Yes	****	<0,0001
			Control: *jaoT* vs. Mite: *jaoT*	-0,8503	-0,9822 to -0,7184	Yes	****	<0,0001
			Mite: Col-0 vs. Mite: *jaoT*	0,04715	-0,08476 to 0,1791	No	ns	0,7182
12-COOH-JA	J	Tukey's	Control: Col-0 vs. Control: *jaoT*	-0,003096	-0,03925 to 0,03305	No	ns	0,9939

			Control: Col-0 vs. Mite: Col-0	-0,1636	-0,1998 to -0,1275	Yes	****	<0,0001
			Control: Col-0 vs. Mite: *jaoT*	-0,1273	-0,1634 to -0,09114	Yes	****	<0,0001
			Control: *jaoT* vs. Mite: Col-0	-0,1605	-0,1967 to -0,1244	Yes	****	<0,0001
			Control: *jaoT* vs. Mite: *jaoT*	-0,1242	-0,1603 to -0,08804	Yes	****	<0,0001
			Mite: Col-0 vs. Mite: *jaoT*	0,03632	0,0001662 to 0,07246	Yes	*	0,0488

Annexed table 4. Values and statistics applied to the quantification of JA derivatives determined in *jaoT* mutant lines and Col-0 under control or mite infested conditions.

	SA	JA	ABA
Mean of Mock	0.2574	0.2577	0.2557
Mean of Hormone	0.1766	0.2513	0.1114
Difference between means (Hormone - Mock) ± SEM	-0.08073 ± 0.003475	-0.006482 ± 0.002826	-0.1444 ± 0.002810
95% confidence interval	-0.08769 to -0.07376	-0.01215 to -0.0008169	-0.1500 to -0.1387
R squared (eta squared)	0.909	0.0888	0.98

Annexed table 5. Effect size between SA. JA and ABA treatments in Arabidopsis plants while measuring stomata aperture.

Treatment	Mean (ºC)		
	Col-0	***epf1epf2***	***EPF2OE***
Control	19.2 ± 0.038	17.4 ± 0.037	20.5 ± 0.080
Mite	21.4 ± 0.092	20.4 ± 0.041	21.5 ± 0.037

Annexed table 6. Leaf temperatures in Arabidopsis mutants con different stomata density after mite infestation. Data are mean ± SE.

Tukey's multiple comparisons test	Mean Diff,	95,00% CI of diff,	Significant?	Summary	Adjusted P Value
12:Wt-MRT1-YFP vs. 12:Wt-MRT1-YFP+miR319	0.028	0,01272 to 0,04328	Yes	****	<0,0001
12:Wt-MRT1-YFP vs. 12:Wt-MRT1-YFP +miR825-5p	0.256	0,2407 to 0,2713	Yes	****	<0,0001
12:Wt-MRT1-YFP vs. 12:Mut-MRT1-YFP	0.0395	0,02422 to 0,05478	Yes	****	<0,0001
12:Wt-MRT1-YFP vs. 12:Mut-MRT1-YFP + miR825-5p	-0.0745	-0,08978 to -0,05922	Yes	****	<0,0001
12:Wt-MRT1-YFP vs. 24:Wt-MRT1-YFP	-0.072	-0,08728 to -0,05672	Yes	****	<0,0001
12:Wt-MRT1-YFP vs. 24:Wt-MRT1-YFP+miR319	-0.111	-0,1263 to -0,09572	Yes	****	<0,0001
12:Wt-MRT1-YFP vs. 24:Wt-MRT1-YFP +miR825-5p	0.2635	0,2482 to 0,2788	Yes	****	<0,0001
12:Wt-MRT1-YFP vs. 24:Mut-MRT1-YFP	0.003	-0,01228 to 0,01828	No	ns	>0,9999
12:Wt-MRT1-YFP vs. 24:Mut-MRT1-YFP + miR825-5p	-0.077	-0,09228 to -0,06172	Yes	****	<0,0001
12:Wt-MRT1-YFP vs. 36:Wt-MRT1-YFP	-0.262	-0,2773 to -0,2467	Yes	****	<0,0001
12:Wt-MRT1-YFP vs. 36:Wt-MRT1-YFP+miR319	-0.307	-0,3223 to -0,2917	Yes	****	<0,0001
12:Wt-MRT1-YFP vs. 36:Wt-MRT1-YFP +miR825-5p	0.364	0,3487 to 0,3793	Yes	****	<0,0001
12:Wt-MRT1-YFP vs. 36:Mut-MRT1-YFP	-0.1	-0,1153 to -0,08472	Yes	****	<0,0001
12:Wt-MRT1-YFP vs. 36:Mut-MRT1-YFP + miR825-5p	-0.098	-0,1133 to -0,08272	Yes	****	<0,0001
12:Wt-MRT1-YFP vs. 48:Wt-MRT1-YFP	-0.282	-0,2973 to -0,2667	Yes	****	<0,0001
12:Wt-MRT1-YFP vs. 48:Wt-MRT1-YFP+miR319	-0.281	-0,2963 to -0,2657	Yes	****	<0,0001
12:Wt-MRT1-YFP vs. 48:Wt-MRT1-YFP +miR825-5p	0.531	0,5157 to 0,5463	Yes	****	<0,0001
12:Wt-MRT1-YFP vs. 48:Mut-MRT1-YFP	-0.0715	-0,08678 to -0,05622	Yes	****	<0,0001
12:Wt-MRT1-YFP vs. 48:Mut-MRT1-YFP + miR825-5p	-0.068	-0,08328 to -0,05272	Yes	****	<0,0001
12:Wt-MRT1-YFP+miR319 vs. 12:Wt-MRT1-YFP +miR825-5p	0.228	0,2127 to 0,2433	Yes	****	<0,0001
12:Wt-MRT1-YFP+miR319 vs. 12:Mut-MRT1-YFP	0.0115	-0,003778 to 0,02678	No	ns	0.2973
12:Wt-MRT1-YFP+miR319 vs. 12:Mut-MRT1-YFP + miR825-5p	-0.1025	-0,1178 to -0,08722	Yes	****	<0,0001
12:Wt-MRT1-YFP+miR319 vs. 24:Wt-MRT1-YFP	-0.1	-0,1153 to -0,08472	Yes	****	<0,0001
12:Wt-MRT1-YFP+miR319 vs. 24:Wt-MRT1-YFP+miR319	-0.139	-0,1543 to -0,1237	Yes	****	<0,0001
12:Wt-MRT1-YFP+miR319 vs. 24:Wt-MRT1-YFP +miR825-5p	0.2355	0,2202 to 0,2508	Yes	****	<0,0001

12:Wt-MRT1-YFP+miR319 vs. 24:Mut-MRT1-YFP	-0.025	-0,04028 to -0,009722	Yes	***	0.0002
12:Wt-MRT1-YFP+miR319 vs. 24:Mut-MRT1-YFP + miR825-5p	-0.105	-0,1203 to -0,08972	Yes	****	<0,0001
12:Wt-MRT1-YFP+miR319 vs. 36:Wt-MRT1-YFP	-0.29	-0,3053 to -0,2747	Yes	****	<0,0001
12:Wt-MRT1-YFP+miR319 vs. 36:Wt-MRT1-YFP+miR319	-0.335	-0,3503 to -0,3197	Yes	****	<0,0001
12:Wt-MRT1-YFP+miR319 vs. 36:Wt-MRT1-YFP +miR825-5p	0.336	0,3207 to 0,3513	Yes	****	<0,0001
12:Wt-MRT1-YFP+miR319 vs. 36:Mut-MRT1-YFP	-0.128	-0,1433 to -0,1127	Yes	****	<0,0001
12:Wt-MRT1-YFP+miR319 vs. 36:Mut-MRT1-YFP + miR825-5p	-0.126	-0,1413 to -0,1107	Yes	****	<0,0001
12:Wt-MRT1-YFP+miR319 vs. 48:Wt-MRT1-YFP	-0.31	-0,3253 to -0,2947	Yes	****	<0,0001
12:Wt-MRT1-YFP+miR319 vs. 48:Wt-MRT1-YFP+miR319	-0.309	-0,3243 to -0,2937	Yes	****	<0,0001
12:Wt-MRT1-YFP+miR319 vs. 48:Wt-MRT1-YFP +miR825-5p	0.503	0,4877 to 0,5183	Yes	****	<0,0001
12:Wt-MRT1-YFP+miR319 vs. 48:Mut-MRT1-YFP	-0.0995	-0,1148 to -0,08422	Yes	****	<0,0001
12:Wt-MRT1-YFP+miR319 vs. 48:Mut-MRT1-YFP + miR825-5p	-0.096	-0,1113 to -0,08072	Yes	****	<0,0001
12:Wt-MRT1-YFP +miR825-5p vs. 12:Mut-MRT1-YFP	-0.2165	-0,2318 to -0,2012	Yes	****	<0,0001
12:Wt-MRT1-YFP +miR825-5p vs. 12:Mut-MRT1-YFP + miR825-5p	-0.3305	-0,3458 to -0,3152	Yes	****	<0,0001
12:Wt-MRT1-YFP +miR825-5p vs. 24:Wt-MRT1-YFP	-0.328	-0,3433 to -0,3127	Yes	****	<0,0001
12:Wt-MRT1-YFP +miR825-5p vs. 24:Wt-MRT1-YFP+miR319	-0.367	-0,3823 to -0,3517	Yes	****	<0,0001
12:Wt-MRT1-YFP +miR825-5p vs. 24:Wt-MRT1-YFP +miR825-5p	0.0075	-0,007778 to 0,02278	No	ns	0.8756
12:Wt-MRT1-YFP +miR825-5p vs. 24:Mut-MRT1-YFP	-0.253	-0,2683 to -0,2377	Yes	****	<0,0001
12:Wt-MRT1-YFP +miR825-5p vs. 24:Mut-MRT1-YFP + miR825-5p	-0.333	-0,3483 to -0,3177	Yes	****	<0,0001
12:Wt-MRT1-YFP +miR825-5p vs. 36:Wt-MRT1-YFP	-0.518	-0,5333 to -0,5027	Yes	****	<0,0001
12:Wt-MRT1-YFP +miR825-5p vs. 36:Wt-MRT1-YFP+miR319	-0.563	-0,5783 to -0,5477	Yes	****	<0,0001
12:Wt-MRT1-YFP +miR825-5p vs. 36:Wt-MRT1-YFP +miR825-5p	0.108	0,09272 to 0,1233	Yes	****	<0,0001
12:Wt-MRT1-YFP +miR825-5p vs. 36:Mut-MRT1-YFP	-0.356	-0,3713 to -0,3407	Yes	****	<0,0001
12:Wt-MRT1-YFP +miR825-5p vs. 36:Mut-MRT1-YFP + miR825-5p	-0.354	-0,3693 to -0,3387	Yes	****	<0,0001
12:Wt-MRT1-YFP +miR825-5p vs. 48:Wt-MRT1-YFP	-0.538	-0,5533 to -0,5227	Yes	****	<0,0001
12:Wt-MRT1-YFP +miR825-5p vs. 48:Wt-MRT1-YFP+miR319	-0.537	-0,5523 to -0,5217	Yes	****	<0,0001

12:Wt-MRT1-YFP +miR825-5p vs. 48:Wt-MRT1-YFP +miR825-5p	0.275	0,2597 to 0,2903	Yes	****	<0,0001
12:Wt-MRT1-YFP +miR825-5p vs. 48:Mut-MRT1-YFP	-0.3275	-0,3428 to -0,3122	Yes	****	<0,0001
12:Wt-MRT1-YFP +miR825-5p vs. 48:Mut-MRT1-YFP + miR825-5p	-0.324	-0,3393 to -0,3087	Yes	****	<0,0001
12:Mut-MRT1-YFP vs. 12:Mut-MRT1-YFP + miR825-5p	-0.114	-0,1293 to -0,09872	Yes	****	<0,0001
12:Mut-MRT1-YFP vs. 24:Wt-MRT1-YFP	-0.1115	-0,1268 to -0,09622	Yes	****	<0,0001
12:Mut-MRT1-YFP vs. 24:Wt-MRT1-YFP+miR319	-0.1505	-0,1658 to -0,1352	Yes	****	<0,0001
12:Mut-MRT1-YFP vs. 24:Wt-MRT1-YFP +miR825-5p	0.224	0,2087 to 0,2393	Yes	****	<0,0001
12:Mut-MRT1-YFP vs. 24:Mut-MRT1-YFP	-0.0365	-0,05178 to -0,02122	Yes	****	<0,0001
12:Mut-MRT1-YFP vs. 24:Mut-MRT1-YFP + miR825-5p	-0.1165	-0,1318 to -0,1012	Yes	****	<0,0001
12:Mut-MRT1-YFP vs. 36:Wt-MRT1-YFP	-0.3015	-0,3168 to -0,2862	Yes	****	<0,0001
12:Mut-MRT1-YFP vs. 36:Wt-MRT1-YFP+miR319	-0.3465	-0,3618 to -0,3312	Yes	****	<0,0001
12:Mut-MRT1-YFP vs. 36:Wt-MRT1-YFP +miR825-5p	0.3245	0,3092 to 0,3398	Yes	****	<0,0001
12:Mut-MRT1-YFP vs. 36:Mut-MRT1-YFP	-0.1395	-0,1548 to -0,1242	Yes	****	<0,0001
12:Mut-MRT1-YFP vs. 36:Mut-MRT1-YFP + miR825-5p	-0.1375	-0,1528 to -0,1222	Yes	****	<0,0001
12:Mut-MRT1-YFP vs. 48:Wt-MRT1-YFP	-0.3215	-0,3368 to -0,3062	Yes	****	<0,0001
12:Mut-MRT1-YFP vs. 48:Wt-MRT1-YFP+miR319	-0.3205	-0,3358 to -0,3052	Yes	****	<0,0001
12:Mut-MRT1-YFP vs. 48:Wt-MRT1-YFP +miR825-5p	0.4915	0,4762 to 0,5068	Yes	****	<0,0001
12:Mut-MRT1-YFP vs. 48:Mut-MRT1-YFP	-0.111	-0,1263 to -0,09572	Yes	****	<0,0001
12:Mut-MRT1-YFP vs. 48:Mut-MRT1-YFP + miR825-5p	-0.1075	-0,1228 to -0,09222	Yes	****	<0,0001
12:Mut-MRT1-YFP + miR825-5p vs. 24:Wt-MRT1-YFP	0.0025	-0,01278 to 0,01778	No	ns	>0,9999
12:Mut-MRT1-YFP + miR825-5p vs. 24:Wt-MRT1-YFP+miR319	-0.0365	-0,05178 to -0,02122	Yes	****	<0,0001

12:Mut-MRT1-YFP + miR825-5p vs. 24:Wt-MRT1-YFP +miR825-5p	0.338	0,3227 to 0,3533	Yes	****	<0,0001
12:Mut-MRT1-YFP + miR825-5p vs. 24:Mut-MRT1-YFP	0.0775	0,06222 to 0,09278	Yes	****	<0,0001
12:Mut-MRT1-YFP + miR825-5p vs. 24:Mut-MRT1-YFP + miR825-5p	-0.0025	-0,01778 to 0,01278	No	ns	>0,9999
12:Mut-MRT1-YFP + miR825-5p vs. 36:Wt-MRT1-YFP	-0.1875	-0,2028 to -0,1722	Yes	****	<0,0001
12:Mut-MRT1-YFP + miR825-5p vs. 36:Wt-MRT1-YFP+miR319	-0.2325	-0,2478 to -0,2172	Yes	****	<0,0001
12:Mut-MRT1-YFP + miR825-5p vs. 36:Wt-MRT1-YFP +miR825-5p	0.4385	0,4232 to 0,4538	Yes	****	<0,0001
12:Mut-MRT1-YFP + miR825-5p vs. 36:Mut-MRT1-YFP	-0.0255	-0,04078 to -0,01022	Yes	***	0.0002
12:Mut-MRT1-YFP + miR825-5p vs. 36:Mut-MRT1-YFP + miR825-5p	-0.0235	-0,03878 to -0,008222	Yes	***	0.0005
12:Mut-MRT1-YFP + miR825-5p vs. 48:Wt-MRT1-YFP	-0.2075	-0,2228 to -0,1922	Yes	****	<0,0001
12:Mut-MRT1-YFP + miR825-5p vs. 48:Wt-MRT1-YFP+miR319	-0.2065	-0,2218 to -0,1912	Yes	****	<0,0001
12:Mut-MRT1-YFP + miR825-5p vs. 48:Wt-MRT1-YFP +miR825-5p	0.6055	0,5902 to 0,6208	Yes	****	<0,0001
12:Mut-MRT1-YFP + miR825-5p vs. 48:Mut-MRT1-YFP	0.003	-0,01228 to 0,01828	No	ns	>0,9999
12:Mut-MRT1-YFP + miR825-5p vs. 48:Mut-MRT1-YFP + miR825-5p	0.0065	-0,008778 to 0,02178	No	ns	0.9563
24:Wt-MRT1-YFP vs. 24:Wt-MRT1-YFP+miR319	-0.039	-0,05428 to -0,02372	Yes	****	<0,0001
24:Wt-MRT1-YFP vs. 24:Wt-MRT1-YFP +miR825-5p	0.3355	0,3202 to 0,3508	Yes	****	<0,0001
24:Wt-MRT1-YFP vs. 24:Mut-MRT1-YFP	0.075	0,05972 to 0,09028	Yes	****	<0,0001
24:Wt-MRT1-YFP vs. 24:Mut-MRT1-YFP + miR825-5p	-0.005	-0,02028 to 0,01028	No	ns	0.9966
24:Wt-MRT1-YFP vs. 36:Wt-MRT1-YFP	-0.19	-0,2053 to -0,1747	Yes	****	<0,0001
24:Wt-MRT1-YFP vs. 36:Wt-MRT1-YFP+miR319	-0.235	-0,2503 to -0,2197	Yes	****	<0,0001
24:Wt-MRT1-YFP vs. 36:Wt-MRT1-YFP +miR825-5p	0.436	0,4207 to 0,4513	Yes	****	<0,0001
24:Wt-MRT1-YFP vs. 36:Mut-MRT1-YFP	-0.028	-0,04328 to -0,01272	Yes	****	<0,0001
24:Wt-MRT1-YFP vs. 36:Mut-MRT1-YFP + miR825-5p	-0.026	-0,04128 to -0,01072	Yes	***	0.0001
24:Wt-MRT1-YFP vs. 48:Wt-MRT1-YFP	-0.21	-0,2253 to -0,1947	Yes	****	<0,0001
24:Wt-MRT1-YFP vs. 48:Wt-MRT1-YFP+miR319	-0.209	-0,2243 to -0,1937	Yes	****	<0,0001

24:Wt-MRT1-YFP vs. 48:Wt-MRT1-YFP +miR825-5p	0.603	0,5877 to 0,6183	Yes	****	<0,0001
24:Wt-MRT1-YFP vs. 48:Mut-MRT1-YFP	0.0005	-0,01478 to 0,01578	No	ns	>0,9999
24:Wt-MRT1-YFP vs. 48:Mut-MRT1-YFP + miR825-5p	0.004	-0,01128 to 0,01928	No	ns	0.9998
24:Wt-MRT1-YFP+miR319 vs. 24:Wt-MRT1-YFP +miR825-5p	0.3745	0,3592 to 0,3898	Yes	****	<0,0001
24:Wt-MRT1-YFP+miR319 vs. 24:Mut-MRT1-YFP	0.114	0,09872 to 0,1293	Yes	****	<0,0001
24:Wt-MRT1-YFP+miR319 vs. 24:Mut-MRT1-YFP + miR825-5p	0.034	0,01872 to 0,04928	Yes	****	<0,0001
24:Wt-MRT1-YFP+miR319 vs. 36:Wt-MRT1-YFP	-0.151	-0,1663 to -0,1357	Yes	****	<0,0001
24:Wt-MRT1-YFP+miR319 vs. 36:Wt-MRT1-YFP+miR319	-0.196	-0,2113 to -0,1807	Yes	****	<0,0001
24:Wt-MRT1-YFP+miR319 vs. 36:Wt-MRT1-YFP +miR825-5p	0.475	0,4597 to 0,4903	Yes	****	<0,0001
24:Wt-MRT1-YFP+miR319 vs. 36:Mut-MRT1-YFP	0.011	-0,004278 to 0,02628	No	ns	0.3607
24:Wt-MRT1-YFP+miR319 vs. 36:Mut-MRT1-YFP + miR825-5p	0.013	-0,002278 to 0,02828	No	ns	0.1551
24:Wt-MRT1-YFP+miR319 vs. 48:Wt-MRT1-YFP	-0.171	-0,1863 to -0,1557	Yes	****	<0,0001
24:Wt-MRT1-YFP+miR319 vs. 48:Wt-MRT1-YFP+miR319	-0.17	-0,1853 to -0,1547	Yes	****	<0,0001
24:Wt-MRT1-YFP+miR319 vs. 48:Wt-MRT1-YFP +miR825-5p	0.642	0,6267 to 0,6573	Yes	****	<0,0001
24:Wt-MRT1-YFP+miR319 vs. 48:Mut-MRT1-YFP	0.0395	0,02422 to 0,05478	Yes	****	<0,0001
24:Wt-MRT1-YFP+miR319 vs. 48:Mut-MRT1-YFP + miR825-5p	0.043	0,02772 to 0,05828	Yes	****	<0,0001
24:Wt-MRT1-YFP +miR825-5p vs. 24:Mut-MRT1-YFP	-0.2605	-0,2758 to -0,2452	Yes	****	<0,0001
24:Wt-MRT1-YFP +miR825-5p vs. 24:Mut-MRT1-YFP + miR825-5p	-0.3405	-0,3558 to -0,3252	Yes	****	<0,0001
24:Wt-MRT1-YFP +miR825-5p vs. 36:Wt-MRT1-YFP	-0.5255	-0,5408 to -0,5102	Yes	****	<0,0001
24:Wt-MRT1-YFP +miR825-5p vs. 36:Wt-MRT1-YFP+miR319	-0.5705	-0,5858 to -0,5552	Yes	****	<0,0001
24:Wt-MRT1-YFP +miR825-5p vs. 36:Wt-MRT1-YFP +miR825-5p	0.1005	0,08522 to 0,1158	Yes	****	<0,0001
24:Wt-MRT1-YFP +miR825-5p vs. 36:Mut-MRT1-YFP	-0.3635	-0,3788 to -0,3482	Yes	****	<0,0001
24:Wt-MRT1-YFP +miR825-5p vs. 36:Mut-MRT1-YFP + miR825-5p	-0.3615	-0,3768 to -0,3462	Yes	****	<0,0001
24:Wt-MRT1-YFP +miR825-5p vs. 48:Wt-MRT1-YFP	-0.5455	-0,5608 to -0,5302	Yes	****	<0,0001

24:Wt-MRT1-YFP +miR825-5p vs. 48:Wt-MRT1-YFP+miR319	-0.5445	-0,5598 to -0,5292	Yes	****	<0,0001
24:Wt-MRT1-YFP +miR825-5p vs. 48:Wt-MRT1-YFP +miR825-5p	0.2675	0,2522 to 0,2828	Yes	****	<0,0001
24:Wt-MRT1-YFP +miR825-5p vs. 48:Mut-MRT1-YFP	-0.335	-0,3503 to -0,3197	Yes	****	<0,0001
24:Wt-MRT1-YFP +miR825-5p vs. 48:Mut-MRT1-YFP + miR825-5p	-0.3315	-0,3468 to -0,3162	Yes	****	<0,0001
24:Mut-MRT1-YFP vs. 24:Mut-MRT1-YFP + miR825-5p	-0.08	-0,09528 to -0,06472	Yes	****	<0,0001
24:Mut-MRT1-YFP vs. 36:Wt-MRT1-YFP	-0.265	-0,2803 to -0,2497	Yes	****	<0,0001
24:Mut-MRT1-YFP vs. 36:Wt-MRT1-YFP+miR319	-0.31	-0,3253 to -0,2947	Yes	****	<0,0001
24:Mut-MRT1-YFP vs. 36:Wt-MRT1-YFP +miR825-5p	0.361	0,3457 to 0,3763	Yes	****	<0,0001
24:Mut-MRT1-YFP vs. 36:Mut-MRT1-YFP	-0.103	-0,1183 to -0,08772	Yes	****	<0,0001
24:Mut-MRT1-YFP vs. 36:Mut-MRT1-YFP + miR825-5p	-0.101	-0,1163 to -0,08572	Yes	****	<0,0001
24:Mut-MRT1-YFP vs. 48:Wt-MRT1-YFP	-0.285	-0,3003 to -0,2697	Yes	****	<0,0001
24:Mut-MRT1-YFP vs. 48:Wt-MRT1-YFP+miR319	-0.284	-0,2993 to -0,2687	Yes	****	<0,0001
24:Mut-MRT1-YFP vs. 48:Wt-MRT1-YFP +miR825-5p	0.528	0,5127 to 0,5433	Yes	****	<0,0001
24:Mut-MRT1-YFP vs. 48:Mut-MRT1-YFP	-0.0745	-0,08978 to -0,05922	Yes	****	<0,0001
24:Mut-MRT1-YFP vs. 48:Mut-MRT1-YFP + miR825-5p	-0.071	-0,08628 to -0,05572	Yes	****	<0,0001
24:Mut-MRT1-YFP + miR825-5p vs. 36:Wt-MRT1-YFP	-0.185	-0,2003 to -0,1697	Yes	****	<0,0001
24:Mut-MRT1-YFP + miR825-5p vs. 36:Wt-MRT1-YFP+miR319	-0.23	-0,2453 to -0,2147	Yes	****	<0,0001
24:Mut-MRT1-YFP + miR825-5p vs. 36:Wt-MRT1-YFP +miR825-5p	0.441	0,4257 to 0,4563	Yes	****	<0,0001
24:Mut-MRT1-YFP + miR825-5p vs. 36:Mut-MRT1-YFP	-0.023	-0,03828 to -0,007722	Yes	***	0.0007
24:Mut-MRT1-YFP + miR825-5p vs. 36:Mut-MRT1-YFP + miR825-5p	-0.021	-0,03628 to -0,005722	Yes	**	0.0022
24:Mut-MRT1-YFP + miR825-5p vs. 48:Wt-MRT1-YFP	-0.205	-0,2203 to -0,1897	Yes	****	<0,0001
24:Mut-MRT1-YFP + miR825-5p vs. 48:Wt-MRT1-YFP+miR319	-0.204	-0,2193 to -0,1887	Yes	****	<0,0001
24:Mut-MRT1-YFP + miR825-5p vs. 48:Wt-MRT1-YFP +miR825-5p	0.608	0,5927 to 0,6233	Yes	****	<0,0001
24:Mut-MRT1-YFP + miR825-5p vs. 48:Mut-MRT1-YFP	0.0055	-0,009778 to 0,02078	No	ns	0.9905
24:Mut-MRT1-YFP + miR825-5p vs. 48:Mut-MRT1-YFP + miR825-5p	0.009	-0,006278 to 0,02428	No	ns	0.6687
36:Wt-MRT1-YFP vs. 36:Wt-MRT1-YFP+miR319	-0.045	-0,06028 to -0,02972	Yes	****	<0,0001

36:Wt-MRT1-YFP vs. 36:Wt-MRT1-YFP +miR825-5p	0.626	0,6107 to 0,6413	Yes	****	<0,0001
36:Wt-MRT1-YFP vs. 36:Mut-MRT1-YFP	0.162	0,1467 to 0,1773	Yes	****	<0,0001
36:Wt-MRT1-YFP vs. 36:Mut-MRT1-YFP + miR825-5p	0.164	0,1487 to 0,1793	Yes	****	<0,0001
36:Wt-MRT1-YFP vs. 48:Wt-MRT1-YFP	-0.02	-0,03528 to -0,004722	Yes	**	0.0038
36:Wt-MRT1-YFP vs. 48:Wt-MRT1-YFP+miR319	-0.019	-0,03428 to -0,003722	Yes	**	0.0066
36:Wt-MRT1-YFP vs. 48:Wt-MRT1-YFP +miR825-5p	0.793	0,7777 to 0,8083	Yes	****	<0,0001
36:Wt-MRT1-YFP vs. 48:Mut-MRT1-YFP	0.1905	0,1752 to 0,2058	Yes	****	<0,0001
36:Wt-MRT1-YFP vs. 48:Mut-MRT1-YFP + miR825-5p	0.194	0,1787 to 0,2093	Yes	****	<0,0001
36:Wt-MRT1-YFP+miR319 vs. 36:Wt-MRT1-YFP +miR825-5p	0.671	0,6557 to 0,6863	Yes	****	<0,0001
36:Wt-MRT1-YFP+miR319 vs. 36:Mut-MRT1-YFP	0.207	0,1917 to 0,2223	Yes	****	<0,0001
36:Wt-MRT1-YFP+miR319 vs. 36:Mut-MRT1-YFP + miR825-5p	0.209	0,1937 to 0,2243	Yes	****	<0,0001
36:Wt-MRT1-YFP+miR319 vs. 48:Wt-MRT1-YFP	0.025	0,009722 to 0,04028	Yes	***	0.0002
36:Wt-MRT1-YFP+miR319 vs. 48:Wt-MRT1-YFP+miR319	0.026	0,01072 to 0,04128	Yes	***	0.0001
36:Wt-MRT1-YFP+miR319 vs. 48:Wt-MRT1-YFP +miR825-5p	0.838	0,8227 to 0,8533	Yes	****	<0,0001
36:Wt-MRT1-YFP+miR319 vs. 48:Mut-MRT1-YFP	0.2355	0,2202 to 0,2508	Yes	****	<0,0001
36:Wt-MRT1-YFP+miR319 vs. 48:Mut-MRT1-YFP + miR825-5p	0.239	0,2237 to 0,2543	Yes	****	<0,0001
36:Wt-MRT1-YFP +miR825-5p vs. 36:Mut-MRT1-YFP	-0.464	-0,4793 to -0,4487	Yes	****	<0,0001
36:Wt-MRT1-YFP +miR825-5p vs. 36:Mut-MRT1-YFP + miR825-5p	-0.462	-0,4773 to -0,4467	Yes	****	<0,0001
36:Wt-MRT1-YFP +miR825-5p vs. 48:Wt-MRT1-YFP	-0.646	-0,6613 to -0,6307	Yes	****	<0,0001
36:Wt-MRT1-YFP +miR825-5p vs. 48:Wt-MRT1-YFP+miR319	-0.645	-0,6603 to -0,6297	Yes	****	<0,0001
36:Wt-MRT1-YFP +miR825-5p vs. 48:Wt-MRT1-YFP +miR825-5p	0.167	0,1517 to 0,1823	Yes	****	<0,0001
36:Wt-MRT1-YFP +miR825-5p vs. 48:Mut-MRT1-YFP	-0.4355	-0,4508 to -0,4202	Yes	****	<0,0001
36:Wt-MRT1-YFP +miR825-5p vs. 48:Mut-MRT1-YFP + miR825-5p	-0.432	-0,4473 to -0,4167	Yes	****	<0,0001
36:Mut-MRT1-YFP vs. 36:Mut-MRT1-YFP + miR825-5p	0.002	-0,01328 to 0,01728	No	ns	>0,9999
36:Mut-MRT1-YFP vs. 48:Wt-MRT1-YFP	-0.182	-0,1973 to -0,1667	Yes	****	<0,0001
36:Mut-MRT1-YFP vs. 48:Wt-MRT1-YFP+miR319	-0.181	-0,1963 to -0,1657	Yes	****	<0,0001
36:Mut-MRT1-YFP vs. 48:Wt-MRT1-YFP +miR825-5p	0.631	0,6157 to 0,6463	Yes	****	<0,0001

36:Mut-MRT1-YFP vs. 48:Mut-MRT1-YFP	0.0285	0,01322 to 0,04378	Yes	****	<0,0001
36:Mut-MRT1-YFP vs. 48:Mut-MRT1-YFP + miR825-5p	0.032	0,01672 to 0,04728	Yes	****	<0,0001
36:Mut-MRT1-YFP + miR825-5p vs. 48:Wt-MRT1-YFP	-0.184	-0,1993 to -0,1687	Yes	****	<0,0001
36:Mut-MRT1-YFP + miR825-5p vs. 48:Wt-MRT1-YFP+miR319	-0.183	-0,1983 to -0,1677	Yes	****	<0,0001
36:Mut-MRT1-YFP + miR825-5p vs. 48:Wt-MRT1-YFP +miR825-5p	0.629	0,6137 to 0,6443	Yes	****	<0,0001
36:Mut-MRT1-YFP + miR825-5p vs. 48:Mut-MRT1-YFP	0.0265	0,01122 to 0,04178	Yes	***	0.0001
36:Mut-MRT1-YFP + miR825-5p vs. 48:Mut-MRT1-YFP + miR825-5p	0.03	0,01472 to 0,04528	Yes	****	<0,0001
48:Wt-MRT1-YFP vs. 48:Wt-MRT1-YFP+miR319	0.001	-0,01428 to 0,01628	No	ns	>0,9999
48:Wt-MRT1-YFP vs. 48:Wt-MRT1-YFP +miR825-5p	0.813	0,7977 to 0,8283	Yes	****	<0,0001
48:Wt-MRT1-YFP vs. 48:Mut-MRT1-YFP	0.2105	0,1952 to 0,2258	Yes	****	<0,0001
48:Wt-MRT1-YFP vs. 48:Mut-MRT1-YFP + miR825-5p	0.214	0,1987 to 0,2293	Yes	****	<0,0001
48:Wt-MRT1-YFP+miR319 vs. 48:Wt-MRT1-YFP +miR825-5p	0.812	0,7967 to 0,8273	Yes	****	<0,0001
48:Wt-MRT1-YFP+miR319 vs. 48:Mut-MRT1-YFP	0.2095	0,1942 to 0,2248	Yes	****	<0,0001
48:Wt-MRT1-YFP+miR319 vs. 48:Mut-MRT1-YFP + miR825-5p	0.213	0,1977 to 0,2283	Yes	****	<0,0001
48:Wt-MRT1-YFP +miR825-5p vs. 48:Mut-MRT1-YFP	-0.6025	-0,6178 to -0,5872	Yes	****	<0,0001
48:Wt-MRT1-YFP +miR825-5p vs. 48:Mut-MRT1-YFP + miR825-5p	-0.599	-0,6143 to -0,5837	Yes	****	<0,0001
48:Mut-MRT1-YFP vs. 48:Mut-MRT1-YFP + miR825-5p	0.0035	-0,01178 to 0,01878	No	ns	>0,9999

Annexed table 7. Statistics comparison of fluorescence constructs in *N. benthamiana* plants co-expressing them alone or with miR825. Data are mean ± SE.

Tukey's multiple comparisons test	Mean Diff,	95,00% CI of diff,	Significant?	Summary	Adjusted P Value	
12:Wt-MRT2-YFP vs. 12:Wt-MRT2-YFP + miR319	0.028	0,003161 to 0,05284	Yes	*	0.0176	
12:Wt-MRT2-YFP vs. 12:Wt-MRT2-YFP + miR825-5p	0.256	0,2312 to 0,2808	Yes	****	<0,0001	
12:Wt-MRT2-YFP vs. 12:Mut-MRT-YFP	0.0395	0,01466 to 0,06434	Yes	***	0.0003	
12:Wt-MRT2-YFP vs. 12:Mut-MRT-YFP + miR825-5p	-0.0745	-0,09934 to -0,04966	Yes	****	<0,0001	
12:Wt-MRT2-YFP vs. 24:Wt-MRT2-YFP	-0.072	-0,09684 to -0,04716	Yes	****	<0,0001	
12:Wt-MRT2-YFP vs. 24:Wt-MRT2-YFP + miR319	-0.116	-0,1408 to -0,09116	Yes	****	<0,0001	
12:Wt-MRT2-YFP vs. 24:Wt-MRT2-YFP + miR825-5p	0.2635	0,2387 to 0,2883	Yes	****	<0,0001	
12:Wt-MRT2-YFP vs. 24:Mut-MRT-YFP	0.003	-0,02184 to 0,02784	No	ns	>0,9999	
12:Wt-MRT2-YFP vs. 24:Mut-MRT-YFP + miR825-5p	-0.077	-0,1018 to -0,05216	Yes	****	<0,0001	
12:Wt-MRT2-YFP vs. 36:Wt-MRT2-YFP	-0.262	-0,2868 to -0,2372	Yes	****	<0,0001	
12:Wt-MRT2-YFP vs. 36:Wt-MRT2-YFP + miR319	-0.317	-0,3418 to -0,2922	Yes	****	<0,0001	
12:Wt-MRT2-YFP vs. 36:Wt-MRT2-YFP + miR825-5p	0.364	0,3392 to 0,3888	Yes	****	<0,0001	
12:Wt-MRT2-YFP vs. 36:Mut-MRT-YFP	-0.1	-0,1248 to -0,07516	Yes	****	<0,0001	
12:Wt-MRT2-YFP vs. 36:Mut-MRT-YFP + miR825-5p	-0.098	-0,1228 to -0,07316	Yes	****	<0,0001	
12:Wt-MRT2-YFP vs. 48:Wt-MRT2-YFP	-0.282	-0,3068 to -0,2572	Yes	****	<0,0001	
12:Wt-MRT2-YFP vs. 48:Wt-MRT2-YFP + miR319	-0.281	-0,3058 to -0,2562	Yes	****	<0,0001	
12:Wt-MRT2-YFP vs. 48:Wt-MRT2-YFP + miR825-5p	0.531	0,5062 to 0,5558	Yes	****	<0,0001	
12:Wt-MRT2-YFP vs. 48:Mut-MRT-YFP	-0.0715	-0,09634 to -0,04666	Yes	****	<0,0001	
12:Wt-MRT2-YFP vs. 48:Mut-MRT-YFP + miR825-5p	-0.068	-0,09284 to -0,04316	Yes	****	<0,0001	
12:Wt-MRT2-YFP + miR319 vs. 12:Wt-MRT2-YFP + miR825-5p	0.228	0,2032 to 0,2528	Yes	****	<0,0001	
12:Wt-MRT2-YFP + miR319 vs. 12:Mut-MRT-YFP	0.0115	-0,01334 to 0,03634	No	ns	0.9164	
12:Wt-MRT2-YFP + miR319 vs. 12:Mut-MRT-YFP + miR825-5p	-0.1025	-0,1273 to -0,07766	Yes	****	<0,0001	
12:Wt-MRT2-YFP + miR319 vs. 24:Wt-MRT2-YFP	-0.1	-0,1248 to -0,07516	Yes	****	<0,0001	
12:Wt-MRT2-YFP + miR319 vs. 24:Wt-MRT2-YFP + miR319	-0.144	-0,1688 to -0,1192	Yes	****	<0,0001	
12:Wt-MRT2-YFP + miR319 vs. 24:Wt-MRT2-YFP + miR825-5p	0.2355	0,2107 to 0,2603	Yes	****	<0,0001	

12:Wt-MRT2-YFP + miR319 vs. 24:Mut-MRT-YFP	-0.025	-0,04984 to -0,0001605	Yes	*	0.0475	
12:Wt-MRT2-YFP + miR319 vs. 24:Mut-MRT-YFP + miR825-5p	-0.105	-0,1298 to -0,08016	Yes	****	<0,0001	
12:Wt-MRT2-YFP + miR319 vs. 36:Wt-MRT2-YFP	-0.29	-0,3148 to -0,2652	Yes	****	<0,0001	
12:Wt-MRT2-YFP + miR319 vs. 36:Wt-MRT2-YFP + miR319	-0.345	-0,3698 to -0,3202	Yes	****	<0,0001	
12:Wt-MRT2-YFP + miR319 vs. 36:Wt-MRT2-YFP + miR825-5p	0.336	0,3112 to 0,3608	Yes	****	<0,0001	
12:Wt-MRT2-YFP + miR319 vs. 36:Mut-MRT-YFP	-0.128	-0,1528 to -0,1032	Yes	****	<0,0001	
12:Wt-MRT2-YFP + miR319 vs. 36:Mut-MRT-YFP + miR825-5p	-0.126	-0,1508 to -0,1012	Yes	****	<0,0001	
12:Wt-MRT2-YFP + miR319 vs. 48:Wt-MRT2-YFP	-0.31	-0,3348 to -0,2852	Yes	****	<0,0001	
12:Wt-MRT2-YFP + miR319 vs. 48:Wt-MRT2-YFP + miR319	-0.309	-0,3338 to -0,2842	Yes	****	<0,0001	
12:Wt-MRT2-YFP + miR319 vs. 48:Wt-MRT2-YFP + miR825-5p	0.503	0,4782 to 0,5278	Yes	****	<0,0001	
12:Wt-MRT2-YFP + miR319 vs. 48:Mut-MRT-YFP	-0.0995	-0,1243 to -0,07466	Yes	****	<0,0001	
12:Wt-MRT2-YFP + miR319 vs. 48:Mut-MRT-YFP + miR825-5p	-0.096	-0,1208 to -0,07116	Yes	****	<0,0001	
12:Wt-MRT2-YFP + miR825-5p vs. 12:Mut-MRT-YFP	-0.2165	-0,2413 to -0,1917	Yes	****	<0,0001	
12:Wt-MRT2-YFP + miR825-5p vs. 12:Mut-MRT-YFP + miR825-5p	-0.3305	-0,3553 to -0,3057	Yes	****	<0,0001	
12:Wt-MRT2-YFP + miR825-5p vs. 24:Wt-MRT2-YFP	-0.328	-0,3528 to -0,3032	Yes	****	<0,0001	
12:Wt-MRT2-YFP + miR825-5p vs. 24:Wt-MRT2-YFP + miR319	-0.372	-0,3968 to -0,3472	Yes	****	<0,0001	
12:Wt-MRT2-YFP + miR825-5p vs. 24:Wt-MRT2-YFP + miR825-5p	0.0075	-0,01734 to 0,03234	No	ns	0.9986	
12:Wt-MRT2-YFP + miR825-5p vs. 24:Mut-MRT-YFP	-0.253	-0,2778 to -0,2282	Yes	****	<0,0001	
12:Wt-MRT2-YFP + miR825-5p vs. 24:Mut-MRT-YFP + miR825-5p	-0.333	-0,3578 to -0,3082	Yes	****	<0,0001	
12:Wt-MRT2-YFP + miR825-5p vs. 36:Wt-MRT2-YFP	-0.518	-0,5428 to -0,4932	Yes	****	<0,0001	
12:Wt-MRT2-YFP + miR825-5p vs. 36:Wt-MRT2-YFP + miR319	-0.573	-0,5978 to -0,5482	Yes	****	<0,0001	
12:Wt-MRT2-YFP + miR825-5p vs. 36:Wt-MRT2-YFP + miR825-5p	0.108	0,08316 to 0,1328	Yes	****	<0,0001	
12:Wt-MRT2-YFP + miR825-5p vs. 36:Mut-MRT-YFP	-0.356	-0,3808 to -0,3312	Yes	****	<0,0001	
12:Wt-MRT2-YFP + miR825-5p vs. 36:Mut-MRT-YFP + miR825-5p	-0.354	-0,3788 to -0,3292	Yes	****	<0,0001	
12:Wt-MRT2-YFP + miR825-5p vs. 48:Wt-MRT2-YFP	-0.538	-0,5628 to -0,5132	Yes	****	<0,0001	
12:Wt-MRT2-YFP + miR825-5p vs. 48:Wt-MRT2-YFP + miR319	-0.537	-0,5618 to -0,5122	Yes	****	<0,0001	

12:Wt-MRT2-YFP + miR825-5p vs. 48:Wt-MRT2-YFP + miR825-5p	0.275	0,2502 to 0,2998	Yes	****	<0,0001	
12:Wt-MRT2-YFP + miR825-5p vs. 48:Mut-MRT-YFP	-0.3275	-0,3523 to -0,3027	Yes	****	<0,0001	
12:Wt-MRT2-YFP + miR825-5p vs. 48:Mut-MRT-YFP + miR825-5p	-0.324	-0,3488 to -0,2992	Yes	****	<0,0001	
12:Mut-MRT-YFP vs. 12:Mut-MRT-YFP + miR825-5p	-0.114	-0,1388 to -0,08916	Yes	****	<0,0001	
12:Mut-MRT-YFP vs. 24:Wt-MRT2-YFP	-0.1115	-0,1363 to -0,08666	Yes	****	<0,0001	
12:Mut-MRT-YFP vs. 24:Wt-MRT2-YFP + miR319	-0.1555	-0,1803 to -0,1307	Yes	****	<0,0001	
12:Mut-MRT-YFP vs. 24:Wt-MRT2-YFP + miR825-5p	0.224	0,1992 to 0,2488	Yes	****	<0,0001	
12:Mut-MRT-YFP vs. 24:Mut-MRT-YFP	-0.0365	-0,06134 to -0,01166	Yes	***	0.001	
12:Mut-MRT-YFP vs. 24:Mut-MRT-YFP + miR825-5p	-0.1165	-0,1413 to -0,09166	Yes	****	<0,0001	
12:Mut-MRT-YFP vs. 36:Wt-MRT2-YFP	-0.3015	-0,3263 to -0,2767	Yes	****	<0,0001	
12:Mut-MRT-YFP vs. 36:Wt-MRT2-YFP + miR319	-0.3565	-0,3813 to -0,3317	Yes	****	<0,0001	
12:Mut-MRT-YFP vs. 36:Wt-MRT2-YFP + miR825-5p	0.3245	0,2997 to 0,3493	Yes	****	<0,0001	
12:Mut-MRT-YFP vs. 36:Mut-MRT-YFP	-0.1395	-0,1643 to -0,1147	Yes	****	<0,0001	
12:Mut-MRT-YFP vs. 36:Mut-MRT-YFP + miR825-5p	-0.1375	-0,1623 to -0,1127	Yes	****	<0,0001	
12:Mut-MRT-YFP vs. 48:Wt-MRT2-YFP	-0.3215	-0,3463 to -0,2967	Yes	****	<0,0001	
12:Mut-MRT-YFP vs. 48:Wt-MRT2-YFP + miR319	-0.3205	-0,3453 to -0,2957	Yes	****	<0,0001	
12:Mut-MRT-YFP vs. 48:Wt-MRT2-YFP + miR825-5p	0.4915	0,4667 to 0,5163	Yes	****	<0,0001	
12:Mut-MRT-YFP vs. 48:Mut-MRT-YFP	-0.111	-0,1358 to -0,08616	Yes	****	<0,0001	
12:Mut-MRT-YFP vs. 48:Mut-MRT-YFP + miR825-5p	-0.1075	-0,1323 to -0,08266	Yes	****	<0,0001	
12:Mut-MRT-YFP + miR825-5p vs. 24:Wt-MRT2-YFP	0.0025	-0,02234 to 0,02734	No	ns	>0,9999	
12:Mut-MRT-YFP + miR825-5p vs. 24:Wt-MRT2-YFP + miR319	-0.0415	-0,06634 to -0,01666	Yes	***	0.0002	

12:Mut-MRT-YFP + miR825-5p vs. 24:Wt-MRT2-YFP + miR825-5p	0.338	0,3132 to 0,3628	Yes	****	<0,0001	
12:Mut-MRT-YFP + miR825-5p vs. 24:Mut-MRT-YFP	0.0775	0,05266 to 0,1023	Yes	****	<0,0001	
12:Mut-MRT-YFP + miR825-5p vs. 24:Mut-MRT-YFP + miR825-5p	-0.0025	-0,02734 to 0,02234	No	ns	>0,9999	
12:Mut-MRT-YFP + miR825-5p vs. 36:Wt-MRT2-YFP	-0.1875	-0,2123 to -0,1627	Yes	****	<0,0001	
12:Mut-MRT-YFP + miR825-5p vs. 36:Wt-MRT2-YFP + miR319	-0.2425	-0,2673 to -0,2177	Yes	****	<0,0001	
12:Mut-MRT-YFP + miR825-5p vs. 36:Wt-MRT2-YFP + miR825-5p	0.4385	0,4137 to 0,4633	Yes	****	<0,0001	
12:Mut-MRT-YFP + miR825-5p vs. 36:Mut-MRT-YFP	-0.0255	-0,05034 to -0,0006605	Yes	*	0.0404	
12:Mut-MRT-YFP + miR825-5p vs. 36:Mut-MRT-YFP + miR825-5p	-0.0235	-0,04834 to 0,001339	No	ns	0.0764	
12:Mut-MRT-YFP + miR825-5p vs. 48:Wt-MRT2-YFP	-0.2075	-0,2323 to -0,1827	Yes	****	<0,0001	
12:Mut-MRT-YFP + miR825-5p vs. 48:Wt-MRT2-YFP + miR319	-0.2065	-0,2313 to -0,1817	Yes	****	<0,0001	
12:Mut-MRT-YFP + miR825-5p vs. 48:Wt-MRT2-YFP + miR825-5p	0.6055	0,5807 to 0,6303	Yes	****	<0,0001	
12:Mut-MRT-YFP + miR825-5p vs. 48:Mut-MRT-YFP	0.003	-0,02184 to 0,02784	No	ns	>0,9999	
12:Mut-MRT-YFP + miR825-5p vs. 48:Mut-MRT-YFP + miR825-5p	0.0065	-0,01834 to 0,03134	No	ns	0.9998	
24:Wt-MRT2-YFP vs. 24:Wt-MRT2-YFP + miR319	-0.044	-0,06884 to -0,01916	Yes	****	<0,0001	
24:Wt-MRT2-YFP vs. 24:Wt-MRT2-YFP + miR825-5p	0.3355	0,3107 to 0,3603	Yes	****	<0,0001	
24:Wt-MRT2-YFP vs. 24:Mut-MRT-YFP	0.075	0,05016 to 0,09984	Yes	****	<0,0001	
24:Wt-MRT2-YFP vs. 24:Mut-MRT-YFP + miR825-5p	-0.005	-0,02984 to 0,01984	No	ns	>0,9999	
24:Wt-MRT2-YFP vs. 36:Wt-MRT2-YFP	-0.19	-0,2148 to -0,1652	Yes	****	<0,0001	
24:Wt-MRT2-YFP vs. 36:Wt-MRT2-YFP + miR319	-0.245	-0,2698 to -0,2202	Yes	****	<0,0001	
24:Wt-MRT2-YFP vs. 36:Wt-MRT2-YFP + miR825-5p	0.436	0,4112 to 0,4608	Yes	****	<0,0001	
24:Wt-MRT2-YFP vs. 36:Mut-MRT-YFP	-0.028	-0,05284 to -0,003161	Yes	*	0.0176	
24:Wt-MRT2-YFP vs. 36:Mut-MRT-YFP + miR825-5p	-0.026	-0,05084 to -0,001161	Yes	*	0.0343	
24:Wt-MRT2-YFP vs. 48:Wt-MRT2-YFP	-0.21	-0,2348 to -0,1852	Yes	****	<0,0001	
24:Wt-MRT2-YFP vs. 48:Wt-MRT2-YFP + miR319	-0.209	-0,2338 to -0,1842	Yes	****	<0,0001	

24:Wt-MRT2-YFP vs. 48:Wt-MRT2-YFP + miR825-5p	0.603	0,5782 to 0,6278	Yes	****	<0,0001	
24:Wt-MRT2-YFP vs. 48:Mut-MRT-YFP	0.0005	-0,02434 to 0,02534	No	ns	>0,9999	
24:Wt-MRT2-YFP vs. 48:Mut-MRT-YFP + miR825-5p	0.004	-0,02084 to 0,02884	No	ns	>0,9999	
24:Wt-MRT2-YFP + miR319 vs. 24:Wt-MRT2-YFP + miR825-5p	0.3795	0,3547 to 0,4043	Yes	****	<0,0001	
24:Wt-MRT2-YFP + miR319 vs. 24:Mut-MRT-YFP	0.119	0,09416 to 0,1438	Yes	****	<0,0001	
24:Wt-MRT2-YFP + miR319 vs. 24:Mut-MRT-YFP + miR825-5p	0.039	0,01416 to 0,06384	Yes	***	0.0004	
24:Wt-MRT2-YFP + miR319 vs. 36:Wt-MRT2-YFP	-0.146	-0,1708 to -0,1212	Yes	****	<0,0001	
24:Wt-MRT2-YFP + miR319 vs. 36:Wt-MRT2-YFP + miR319	-0.201	-0,2258 to -0,1762	Yes	****	<0,0001	
24:Wt-MRT2-YFP + miR319 vs. 36:Wt-MRT2-YFP + miR825-5p	0.48	0,4552 to 0,5048	Yes	****	<0,0001	
24:Wt-MRT2-YFP + miR319 vs. 36:Mut-MRT-YFP	0.016	-0,008839 to 0,04084	No	ns	0.5333	
24:Wt-MRT2-YFP + miR319 vs. 36:Mut-MRT-YFP + miR825-5p	0.018	-0,006839 to 0,04284	No	ns	0.3512	
24:Wt-MRT2-YFP + miR319 vs. 48:Wt-MRT2-YFP	-0.166	-0,1908 to -0,1412	Yes	****	<0,0001	
24:Wt-MRT2-YFP + miR319 vs. 48:Wt-MRT2-YFP + miR319	-0.165	-0,1898 to -0,1402	Yes	****	<0,0001	
24:Wt-MRT2-YFP + miR319 vs. 48:Wt-MRT2-YFP + miR825-5p	0.647	0,6222 to 0,6718	Yes	****	<0,0001	
24:Wt-MRT2-YFP + miR319 vs. 48:Mut-MRT-YFP	0.0445	0,01966 to 0,06934	Yes	****	<0,0001	
24:Wt-MRT2-YFP + miR319 vs. 48:Mut-MRT-YFP + miR825-5p	0.048	0,02316 to 0,07284	Yes	****	<0,0001	
24:Wt-MRT2-YFP + miR825-5p vs. 24:Mut-MRT-YFP	-0.2605	-0,2853 to -0,2357	Yes	****	<0,0001	
24:Wt-MRT2-YFP + miR825-5p vs. 24:Mut-MRT-YFP + miR825-5p	-0.3405	-0,3653 to -0,3157	Yes	****	<0,0001	
24:Wt-MRT2-YFP + miR825-5p vs. 36:Wt-MRT2-YFP	-0.5255	-0,5503 to -0,5007	Yes	****	<0,0001	
24:Wt-MRT2-YFP + miR825-5p vs. 36:Wt-MRT2-YFP + miR319	-0.5805	-0,6053 to -0,5557	Yes	****	<0,0001	
24:Wt-MRT2-YFP + miR825-5p vs. 36:Wt-MRT2-YFP + miR825-5p	0.1005	0,07566 to 0,1253	Yes	****	<0,0001	
24:Wt-MRT2-YFP + miR825-5p vs. 36:Mut-MRT-YFP	-0.3635	-0,3883 to -0,3387	Yes	****	<0,0001	
24:Wt-MRT2-YFP + miR825-5p vs. 36:Mut-MRT-YFP + miR825-5p	-0.3615	-0,3863 to -0,3367	Yes	****	<0,0001	
24:Wt-MRT2-YFP + miR825-5p vs. 48:Wt-MRT2-YFP	-0.5455	-0,5703 to -0,5207	Yes	****	<0,0001	

24:Wt-MRT2-YFP + miR825-5p vs. 48:Wt-MRT2-YFP + miR319	-0.5445	-0,5693 to -0,5197	Yes	****	<0,0001	
24:Wt-MRT2-YFP + miR825-5p vs. 48:Wt-MRT2-YFP + miR825-5p	0.2675	0,2427 to 0,2923	Yes	****	<0,0001	
24:Wt-MRT2-YFP + miR825-5p vs. 48:Mut-MRT-YFP	-0.335	-0,3598 to -0,3102	Yes	****	<0,0001	
24:Wt-MRT2-YFP + miR825-5p vs. 48:Mut-MRT-YFP + miR825-5p	-0.3315	-0,3563 to -0,3067	Yes	****	<0,0001	
24:Mut-MRT-YFP vs. 24:Mut-MRT-YFP + miR825-5p	-0.08	-0,1048 to -0,05516	Yes	****	<0,0001	
24:Mut-MRT-YFP vs. 36:Wt-MRT2-YFP	-0.265	-0,2898 to -0,2402	Yes	****	<0,0001	
24:Mut-MRT-YFP vs. 36:Wt-MRT2-YFP + miR319	-0.32	-0,3448 to -0,2952	Yes	****	<0,0001	
24:Mut-MRT-YFP vs. 36:Wt-MRT2-YFP + miR825-5p	0.361	0,3362 to 0,3858	Yes	****	<0,0001	
24:Mut-MRT-YFP vs. 36:Mut-MRT-YFP	-0.103	-0,1278 to -0,07816	Yes	****	<0,0001	
24:Mut-MRT-YFP vs. 36:Mut-MRT-YFP + miR825-5p	-0.101	-0,1258 to -0,07616	Yes	****	<0,0001	
24:Mut-MRT-YFP vs. 48:Wt-MRT2-YFP	-0.285	-0,3098 to -0,2602	Yes	****	<0,0001	
24:Mut-MRT-YFP vs. 48:Wt-MRT2-YFP + miR319	-0.284	-0,3088 to -0,2592	Yes	****	<0,0001	
24:Mut-MRT-YFP vs. 48:Wt-MRT2-YFP + miR825-5p	0.528	0,5032 to 0,5528	Yes	****	<0,0001	
24:Mut-MRT-YFP vs. 48:Mut-MRT-YFP	-0.0745	-0,09934 to -0,04966	Yes	****	<0,0001	
24:Mut-MRT-YFP vs. 48:Mut-MRT-YFP + miR825-5p	-0.071	-0,09584 to -0,04616	Yes	****	<0,0001	
24:Mut-MRT-YFP + miR825-5p vs. 36:Wt-MRT2-YFP	-0.185	-0,2098 to -0,1602	Yes	****	<0,0001	
24:Mut-MRT-YFP + miR825-5p vs. 36:Wt-MRT2-YFP + miR319	-0.24	-0,2648 to -0,2152	Yes	****	<0,0001	
24:Mut-MRT-YFP + miR825-5p vs. 36:Wt-MRT2-YFP + miR825-5p	0.441	0,4162 to 0,4658	Yes	****	<0,0001	
24:Mut-MRT-YFP + miR825-5p vs. 36:Mut-MRT-YFP	-0.023	-0,04784 to 0,001839	No	ns	0.0892	
24:Mut-MRT-YFP + miR825-5p vs. 36:Mut-MRT-YFP + miR825-5p	-0.021	-0,04584 to 0,003839	No	ns	0.1612	
24:Mut-MRT-YFP + miR825-5p vs. 48:Wt-MRT2-YFP	-0.205	-0,2298 to -0,1802	Yes	****	<0,0001	
24:Mut-MRT-YFP + miR825-5p vs. 48:Wt-MRT2-YFP + miR319	-0.204	-0,2288 to -0,1792	Yes	****	<0,0001	
24:Mut-MRT-YFP + miR825-5p vs. 48:Wt-MRT2-YFP + miR825-5p	0.608	0,5832 to 0,6328	Yes	****	<0,0001	
24:Mut-MRT-YFP + miR825-5p vs. 48:Mut-MRT-YFP	0.0055	-0,01934 to 0,03034	No	ns	>0,9999	
24:Mut-MRT-YFP + miR825-5p vs. 48:Mut-MRT-YFP + miR825-5p	0.009	-0,01584 to 0,03384	No	ns	0.9899	
36:Wt-MRT2-YFP vs. 36:Wt-MRT2-YFP + miR319	-0.055	-0,07984 to -0,03016	Yes	****	<0,0001	

36:Wt-MRT2-YFP vs. 36:Wt-MRT2-YFP + miR825-5p	0.626	0,6012 to 0,6508	Yes	****	<0,0001	
36:Wt-MRT2-YFP vs. 36:Mut-MRT-YFP	0.162	0,1372 to 0,1868	Yes	****	<0,0001	
36:Wt-MRT2-YFP vs. 36:Mut-MRT-YFP + miR825-5p	0.164	0,1392 to 0,1888	Yes	****	<0,0001	
36:Wt-MRT2-YFP vs. 48:Wt-MRT2-YFP	-0.02	-0,04484 to 0,004839	No	ns	0.2126	
36:Wt-MRT2-YFP vs. 48:Wt-MRT2-YFP + miR319	-0.019	-0,04384 to 0,005839	No	ns	0.2758	
36:Wt-MRT2-YFP vs. 48:Wt-MRT2-YFP + miR825-5p	0.793	0,7682 to 0,8178	Yes	****	<0,0001	
36:Wt-MRT2-YFP vs. 48:Mut-MRT-YFP	0.1905	0,1657 to 0,2153	Yes	****	<0,0001	
36:Wt-MRT2-YFP vs. 48:Mut-MRT-YFP + miR825-5p	0.194	0,1692 to 0,2188	Yes	****	<0,0001	
36:Wt-MRT2-YFP + miR319 vs. 36:Wt-MRT2-YFP + miR825-5p	0.681	0,6562 to 0,7058	Yes	****	<0,0001	
36:Wt-MRT2-YFP + miR319 vs. 36:Mut-MRT-YFP	0.217	0,1922 to 0,2418	Yes	****	<0,0001	
36:Wt-MRT2-YFP + miR319 vs. 36:Mut-MRT-YFP + miR825-5p	0.219	0,1942 to 0,2438	Yes	****	<0,0001	
36:Wt-MRT2-YFP + miR319 vs. 48:Wt-MRT2-YFP	0.035	0,01016 to 0,05984	Yes	**	0.0016	
36:Wt-MRT2-YFP + miR319 vs. 48:Wt-MRT2-YFP + miR319	0.036	0,01116 to 0,06084	Yes	**	0.0011	
36:Wt-MRT2-YFP + miR319 vs. 48:Wt-MRT2-YFP + miR825-5p	0.848	0,8232 to 0,8728	Yes	****	<0,0001	
36:Wt-MRT2-YFP + miR319 vs. 48:Mut-MRT-YFP	0.2455	0,2207 to 0,2703	Yes	****	<0,0001	
36:Wt-MRT2-YFP + miR319 vs. 48:Mut-MRT-YFP + miR825-5p	0.249	0,2242 to 0,2738	Yes	****	<0,0001	
36:Wt-MRT2-YFP + miR825-5p vs. 36:Mut-MRT-YFP	-0.464	-0,4888 to -0,4392	Yes	****	<0,0001	
36:Wt-MRT2-YFP + miR825-5p vs. 36:Mut-MRT-YFP + miR825-5p	-0.462	-0,4868 to -0,4372	Yes	****	<0,0001	
36:Wt-MRT2-YFP + miR825-5p vs. 48:Wt-MRT2-YFP	-0.646	-0,6708 to -0,6212	Yes	****	<0,0001	
36:Wt-MRT2-YFP + miR825-5p vs. 48:Wt-MRT2-YFP + miR319	-0.645	-0,6698 to -0,6202	Yes	****	<0,0001	
36:Wt-MRT2-YFP + miR825-5p vs. 48:Wt-MRT2-YFP + miR825-5p	0.167	0,1422 to 0,1918	Yes	****	<0,0001	
36:Wt-MRT2-YFP + miR825-5p vs. 48:Mut-MRT-YFP	-0.4355	-0,4603 to -0,4107	Yes	****	<0,0001	
36:Wt-MRT2-YFP + miR825-5p vs. 48:Mut-MRT-YFP + miR825-5p	-0.432	-0,4568 to -0,4072	Yes	****	<0,0001	
36:Mut-MRT-YFP vs. 36:Mut-MRT-YFP + miR825-5p	0.002	-0,02284 to 0,02684	No	ns	>0,9999	
36:Mut-MRT-YFP vs. 48:Wt-MRT2-YFP	-0.182	-0,2068 to -0,1572	Yes	****	<0,0001	
36:Mut-MRT-YFP vs. 48:Wt-MRT2-YFP + miR319	-0.181	-0,2058 to -0,1562	Yes	****	<0,0001	
36:Mut-MRT-YFP vs. 48:Wt-MRT2-YFP + miR825-5p	0.631	0,6062 to 0,6558	Yes	****	<0,0001	

36:Mut-MRT-YFP vs. 48:Mut-MRT-YFP	0.0285	0,003661 to 0,05334	Yes	*	0.0149	
36:Mut-MRT-YFP vs. 48:Mut-MRT-YFP + miR825-5p	0.032	0,007161 to 0,05684	Yes	**	0.0045	
36:Mut-MRT-YFP + miR825-5p vs. 48:Wt-MRT2-YFP	-0.184	-0,2088 to -0,1592	Yes	****	<0,0001	
36:Mut-MRT-YFP + miR825-5p vs. 48:Wt-MRT2-YFP + miR319	-0.183	-0,2078 to -0,1582	Yes	****	<0,0001	
36:Mut-MRT-YFP + miR825-5p vs. 48:Wt-MRT2-YFP + miR825-5p	0.629	0,6042 to 0,6538	Yes	****	<0,0001	
36:Mut-MRT-YFP + miR825-5p vs. 48:Mut-MRT-YFP	0.0265	0,001661 to 0,05134	Yes	*	0.0291	
36:Mut-MRT-YFP + miR825-5p vs. 48:Mut-MRT-YFP + miR825-5p	0.03	0,005161 to 0,05484	Yes	**	0.0089	
48:Wt-MRT2-YFP vs. 48:Wt-MRT2-YFP + miR319	0.001	-0,02384 to 0,02584	No	ns	>0,9999	
48:Wt-MRT2-YFP vs. 48:Wt-MRT2-YFP + miR825-5p	0.813	0,7882 to 0,8378	Yes	****	<0,0001	
48:Wt-MRT2-YFP vs. 48:Mut-MRT-YFP	0.2105	0,1857 to 0,2353	Yes	****	<0,0001	
48:Wt-MRT2-YFP vs. 48:Mut-MRT-YFP + miR825-5p	0.214	0,1892 to 0,2388	Yes	****	<0,0001	
48:Wt-MRT2-YFP + miR319 vs. 48:Wt-MRT2-YFP + miR825-5p	0.812	0,7872 to 0,8368	Yes	****	<0,0001	
48:Wt-MRT2-YFP + miR319 vs. 48:Mut-MRT-YFP	0.2095	0,1847 to 0,2343	Yes	****	<0,0001	
48:Wt-MRT2-YFP + miR319 vs. 48:Mut-MRT-YFP + miR825-5p	0.213	0,1882 to 0,2378	Yes	****	<0,0001	
48:Wt-MRT2-YFP + miR825-5p vs. 48:Mut-MRT-YFP	-0.6025	-0,6273 to -0,5777	Yes	****	<0,0001	
48:Wt-MRT2-YFP + miR825-5p vs. 48:Mut-MRT-YFP + miR825-5p	-0.599	-0,6238 to -0,5742	Yes	****	<0,0001	
48:Mut-MRT-YFP vs. 48:Mut-MRT-YFP + miR825-5p	0.0035	-0,02134 to 0,02834	No	ns	>0,9999	

Annexed table 8. Statistics comparison of fluorescence constructs in *N. benthamiana* plants co-expressing them alone or with miR825. Data are mean ± SE.

Tukey's multiple comparisons test	Mean Diff,	95,00% CI of diff,	Significant?	Summary	Adjusted P Value	
12:Wt-MRT1-YFP +miR319 vs. 12:Wt-MRT1-YFP + phasiR263-1	0.1805	-0,07505 to 0,4360	No	ns	0.3582	
12:Wt-MRT1-YFP +miR319 vs. 12:Wt-MRT1-YFP + phasiR263-2	0.1239	-0,1316 to 0,3794	No	ns	0.8621	
12:Wt-MRT1-YFP +miR319 vs. 12:phMut-MRT1-YFP + phasiR263-1	0.149	-0,1065 to 0,4045	No	ns	0.6449	
12:Wt-MRT1-YFP +miR319 vs. 12:phMut-MRT1-YFP + phasiR263-2	0.1125	-0,1430 to 0,3680	No	ns	0.929	
12:Wt-MRT1-YFP +miR319 vs. 12:phMut-MRT1-YFP + miR825-5p	0.0535	-0,2020 to 0,3090	No	ns	>0,9999	
12:Wt-MRT1-YFP +miR319 vs. 24:Wt-MRT1-YFP +miR319	-0.07142	-0,2801 to 0,1372	No	ns	0.9929	
12:Wt-MRT1-YFP +miR319 vs. 24:Wt-MRT1-YFP + phasiR263-1	0.1091	-0,2208 to 0,4390	No	ns	0.9952	
12:Wt-MRT1-YFP +miR319 vs. 24:Wt-MRT1-YFP + phasiR263-2	0.05248	-0,2774 to 0,3824	No	ns	>0,9999	
12:Wt-MRT1-YFP +miR319 vs. 24:phMut-MRT1-YFP + phasiR263-1	0.07758	-0,2523 to 0,4075	No	ns	>0,9999	
12:Wt-MRT1-YFP +miR319 vs. 24:phMut-MRT1-YFP + phasiR263-2	0.04108	-0,2888 to 0,3710	No	ns	>0,9999	
12:Wt-MRT1-YFP +miR319 vs. 24:phMut-MRT1-YFP + miR825-5p	-0.01792	-0,3478 to 0,3120	No	ns	>0,9999	
12:Wt-MRT1-YFP +miR319 vs. 36:Wt-MRT1-YFP +miR319	-0.118	-0,3266 to 0,09070	No	ns	0.6884	
12:Wt-MRT1-YFP +miR319 vs. 36:Wt-MRT1-YFP + phasiR263-1	0.06255	-0,2674 to 0,3925	No	ns	>0,9999	
12:Wt-MRT1-YFP +miR319 vs. 36:Wt-MRT1-YFP + phasiR263-2	0.00595	-0,3240 to 0,3359	No	ns	>0,9999	
12:Wt-MRT1-YFP +miR319 vs. 36:phMut-MRT1-YFP + phasiR263-1	0.03105	-0,2989 to 0,3610	No	ns	>0,9999	
12:Wt-MRT1-YFP +miR319 vs. 36:phMut-MRT1-YFP + phasiR263-2	-0.00545	-0,3354 to 0,3245	No	ns	>0,9999	
12:Wt-MRT1-YFP +miR319 vs. 36:phMut-MRT1-YFP + miR825-5p	-0.06445	-0,3944 to 0,2655	No	ns	>0,9999	
12:Wt-MRT1-YFP +miR319 vs. 48:Wt-MRT1-YFP +miR319	-0.08963	-0,2983 to 0,1190	No	ns	0.9412	
12:Wt-MRT1-YFP +miR319 vs. 48:Wt-MRT1-YFP + phasiR263-1	0.09087	-0,2390 to 0,4208	No	ns	0.9995	
12:Wt-MRT1-YFP +miR319 vs. 48:Wt-MRT1-YFP + phasiR263-2	0.03427	-0,2956 to 0,3642	No	ns	>0,9999	
12:Wt-MRT1-YFP +miR319 vs. 48:phMut-MRT1-YFP + phasiR263-1	0.05937	-0,2705 to 0,3893	No	ns	>0,9999	
12:Wt-MRT1-YFP +miR319 vs. 48:phMut-MRT1-YFP + phasiR263-2	0.02287	-0,3070 to 0,3528	No	ns	>0,9999	
12:Wt-MRT1-YFP +miR319 vs. 48:phMut-MRT1-YFP + miR825-5p	-0.03613	-0,3660 to 0,2938	No	ns	>0,9999	

12:Wt-MRT1-YFP + phasiR263-1 vs. 12:Wt-MRT1-YFP + phasiR263-2	-0.0566	-0,3121 to 0,1989	No	ns	>0,9999	
12:Wt-MRT1-YFP + phasiR263-1 vs. 12:phMut-MRT1-YFP + phasiR263-1	-0.0315	-0,2870 to 0,2240	No	ns	>0,9999	
12:Wt-MRT1-YFP + phasiR263-1 vs. 12:phMut-MRT1-YFP + phasiR263-2	-0.068	-0,3235 to 0,1875	No	ns	0.9997	
12:Wt-MRT1-YFP + phasiR263-1 vs. 12:phMut-MRT1-YFP + miR825-5p	-0.127	-0,3825 to 0,1285	No	ns	0.8397	
12:Wt-MRT1-YFP + phasiR263-1 vs. 24:Wt-MRT1-YFP +miR319	-0.2519	-0,5818 to 0,07799	No	ns	0.2556	
12:Wt-MRT1-YFP + phasiR263-1 vs. 24:Wt-MRT1-YFP + phasiR263-1	-0.07142	-0,2801 to 0,1372	No	ns	0.9929	
12:Wt-MRT1-YFP + phasiR263-1 vs. 24:Wt-MRT1-YFP + phasiR263-2	-0.128	-0,4579 to 0,2019	No	ns	0.9752	
12:Wt-MRT1-YFP + phasiR263-1 vs. 24:phMut-MRT1-YFP + phasiR263-1	-0.1029	-0,4328 to 0,2270	No	ns	0.9976	
12:Wt-MRT1-YFP + phasiR263-1 vs. 24:phMut-MRT1-YFP + phasiR263-2	-0.1394	-0,4693 to 0,1905	No	ns	0.9483	
12:Wt-MRT1-YFP + phasiR263-1 vs. 24:phMut-MRT1-YFP + miR825-5p	-0.1984	-0,5283 to 0,1315	No	ns	0.5993	
12:Wt-MRT1-YFP + phasiR263-1 vs. 36:Wt-MRT1-YFP +miR319	-0.2985	-0,6284 to 0,03146	No	ns	0.0997	
12:Wt-MRT1-YFP + phasiR263-1 vs. 36:Wt-MRT1-YFP + phasiR263-1	-0.118	-0,3266 to 0,09070	No	ns	0.6884	
12:Wt-MRT1-YFP + phasiR263-1 vs. 36:Wt-MRT1-YFP + phasiR263-2	-0.1746	-0,5045 to 0,1554	No	ns	0.773	
12:Wt-MRT1-YFP + phasiR263-1 vs. 36:phMut-MRT1-YFP + phasiR263-1	-0.1495	-0,4794 to 0,1805	No	ns	0.9125	
12:Wt-MRT1-YFP + phasiR263-1 vs. 36:phMut-MRT1-YFP + phasiR263-2	-0.186	-0,5159 to 0,1440	No	ns	0.6924	
12:Wt-MRT1-YFP + phasiR263-1 vs. 36:phMut-MRT1-YFP + miR825-5p	-0.245	-0,5749 to 0,08496	No	ns	0.2905	
12:Wt-MRT1-YFP + phasiR263-1 vs. 48:Wt-MRT1-YFP +miR319	-0.2701	-0,6000 to 0,05977	No	ns	0.1795	
12:Wt-MRT1-YFP + phasiR263-1 vs. 48:Wt-MRT1-YFP + phasiR263-1	-0.08963	-0,2983 to 0,1190	No	ns	0.9412	
12:Wt-MRT1-YFP + phasiR263-1 vs. 48:Wt-MRT1-YFP + phasiR263-2	-0.1462	-0,4761 to 0,1837	No	ns	0.9253	
12:Wt-MRT1-YFP + phasiR263-1 vs. 48:phMut-MRT1-YFP + phasiR263-1	-0.1211	-0,4510 to 0,2088	No	ns	0.9854	

12:Wt-MRT1-YFP + phasiR263-1 vs. 48:phMut-MRT1-YFP + phasiR263-2	-0.1576	-0,4875 to 0,1723	No	ns	0.8744	
12:Wt-MRT1-YFP + phasiR263-1 vs. 48:phMut-MRT1-YFP + miR825-5p	-0.2166	-0,5465 to 0,1133	No	ns	0.4658	
12:Wt-MRT1-YFP + phasiR263-2 vs. 12:phMut-MRT1-YFP + phasiR263-1	0.0251	-0,2304 to 0,2806	No	ns	>0,9999	
12:Wt-MRT1-YFP + phasiR263-2 vs. 12:phMut-MRT1-YFP + phasiR263-2	-0.0114	-0,2669 to 0,2441	No	ns	>0,9999	
12:Wt-MRT1-YFP + phasiR263-2 vs. 12:phMut-MRT1-YFP + miR825-5p	-0.0704	-0,3259 to 0,1851	No	ns	0.9995	
12:Wt-MRT1-YFP + phasiR263-2 vs. 24:Wt-MRT1-YFP +miR319	-0.1953	-0,5252 to 0,1346	No	ns	0.6227	
12:Wt-MRT1-YFP + phasiR263-2 vs. 24:Wt-MRT1-YFP + phasiR263-1	-0.01482	-0,3447 to 0,3151	No	ns	>0,9999	
12:Wt-MRT1-YFP + phasiR263-2 vs. 24:Wt-MRT1-YFP + phasiR263-2	-0.07142	-0,2801 to 0,1372	No	ns	0.9929	
12:Wt-MRT1-YFP + phasiR263-2 vs. 24:phMut-MRT1-YFP + phasiR263-1	-0.04632	-0,3762 to 0,2836	No	ns	>0,9999	
12:Wt-MRT1-YFP + phasiR263-2 vs. 24:phMut-MRT1-YFP + phasiR263-2	-0.08282	-0,4127 to 0,2471	No	ns	0.9999	
12:Wt-MRT1-YFP + phasiR263-2 vs. 24:phMut-MRT1-YFP + miR825-5p	-0.1418	-0,4717 to 0,1881	No	ns	0.9408	
12:Wt-MRT1-YFP + phasiR263-2 vs. 36:Wt-MRT1-YFP +miR319	-0.2419	-0,5718 to 0,08806	No	ns	0.3072	
12:Wt-MRT1-YFP + phasiR263-2 vs. 36:Wt-MRT1-YFP + phasiR263-1	-0.06135	-0,3913 to 0,2686	No	ns	>0,9999	
12:Wt-MRT1-YFP + phasiR263-2 vs. 36:Wt-MRT1-YFP + phasiR263-2	-0.118	-0,3266 to 0,09070	No	ns	0.6884	
12:Wt-MRT1-YFP + phasiR263-2 vs. 36:phMut-MRT1-YFP + phasiR263-1	-0.09285	-0,4228 to 0,2371	No	ns	0.9993	
12:Wt-MRT1-YFP + phasiR263-2 vs. 36:phMut-MRT1-YFP + phasiR263-2	-0.1294	-0,4593 to 0,2006	No	ns	0.9728	
12:Wt-MRT1-YFP + phasiR263-2 vs. 36:phMut-MRT1-YFP + miR825-5p	-0.1884	-0,5183 to 0,1416	No	ns	0.6747	
12:Wt-MRT1-YFP + phasiR263-2 vs. 48:Wt-MRT1-YFP +miR319	-0.2135	-0,5434 to 0,1164	No	ns	0.4878	
12:Wt-MRT1-YFP + phasiR263-2 vs. 48:Wt-MRT1-YFP + phasiR263-1	-0.03303	-0,3629 to 0,2969	No	ns	>0,9999	

12:Wt-MRT1-YFP + phasiR263-2 vs. 48:Wt-MRT1-YFP + phasiR263-2	-0.08963	-0,2983 to 0,1190	No	ns	0.9412	
12:Wt-MRT1-YFP + phasiR263-2 vs. 48:phMut-MRT1-YFP + phasiR263-1	-0.06453	-0,3944 to 0,2654	No	ns	>0,9999	
12:Wt-MRT1-YFP + phasiR263-2 vs. 48:phMut-MRT1-YFP + phasiR263-2	-0.101	-0,4309 to 0,2289	No	ns	0.9981	
12:Wt-MRT1-YFP + phasiR263-2 vs. 48:phMut-MRT1-YFP + miR825-5p	-0.16	-0,4899 to 0,1699	No	ns	0.8617	
12:phMut-MRT1-YFP + phasiR263-1 vs. 12:phMut-MRT1-YFP + phasiR263-2	-0.0365	-0,2920 to 0,2190	No	ns	>0,9999	
12:phMut-MRT1-YFP + phasiR263-1 vs. 12:phMut-MRT1-YFP + miR825-5p	-0.0955	-0,3510 to 0,1600	No	ns	0.9826	
12:phMut-MRT1-YFP + phasiR263-1 vs. 24:Wt-MRT1-YFP +miR319	-0.2204	-0,5503 to 0,1095	No	ns	0.4396	
12:phMut-MRT1-YFP + phasiR263-1 vs. 24:Wt-MRT1-YFP + phasiR263-1	-0.03992	-0,3698 to 0,2900	No	ns	>0,9999	
12:phMut-MRT1-YFP + phasiR263-1 vs. 24:Wt-MRT1-YFP + phasiR263-2	-0.09652	-0,4264 to 0,2334	No	ns	0.9989	
12:phMut-MRT1-YFP + phasiR263-1 vs. 24:phMut-MRT1-YFP + phasiR263-1	-0.07142	-0,2801 to 0,1372	No	ns	0.9929	
12:phMut-MRT1-YFP + phasiR263-1 vs. 24:phMut-MRT1-YFP + phasiR263-2	-0.1079	-0,4378 to 0,2220	No	ns	0.9957	
12:phMut-MRT1-YFP + phasiR263-1 vs. 24:phMut-MRT1-YFP + miR825-5p	-0.1669	-0,4968 to 0,1630	No	ns	0.8221	
12:phMut-MRT1-YFP + phasiR263-1 vs. 36:Wt-MRT1-YFP +miR319	-0.267	-0,5969 to 0,06296	No	ns	0.1913	
12:phMut-MRT1-YFP + phasiR263-1 vs. 36:Wt-MRT1-YFP + phasiR263-1	-0.08645	-0,4164 to 0,2435	No	ns	0.9998	
12:phMut-MRT1-YFP + phasiR263-1 vs. 36:Wt-MRT1-YFP + phasiR263-2	-0.1431	-0,4730 to 0,1869	No	ns	0.9367	
12:phMut-MRT1-YFP + phasiR263-1 vs. 36:phMut-MRT1-YFP + phasiR263-1	-0.118	-0,3266 to 0,09070	No	ns	0.6884	
12:phMut-MRT1-YFP + phasiR263-1 vs. 36:phMut-MRT1-YFP + phasiR263-2	-0.1545	-0,4844 to 0,1755	No	ns	0.8901	
12:phMut-MRT1-YFP + phasiR263-1 vs. 36:phMut-MRT1-YFP + miR825-5p	-0.2135	-0,5434 to 0,1165	No	ns	0.4884	
12:phMut-MRT1-YFP + phasiR263-1 vs. 48:Wt-MRT1-YFP +miR319	-0.2386	-0,5685 to 0,09127	No	ns	0.3252	
12:phMut-MRT1-YFP + phasiR263-1 vs. 48:Wt-MRT1-YFP + phasiR263-1	-0.05813	-0,3880 to 0,2718	No	ns	>0,9999	

12:phMut-MRT1-YFP + phasiR263-1 vs. 48:Wt-MRT1-YFP + phasiR263-2	-0.1147	-0,4446 to 0,2152	No	ns	0.9916	
12:phMut-MRT1-YFP + phasiR263-1 vs. 48:phMut-MRT1-YFP + phasiR263-1	-0.08963	-0,2983 to 0,1190	No	ns	0.9412	
12:phMut-MRT1-YFP + phasiR263-1 vs. 48:phMut-MRT1-YFP + phasiR263-2	-0.1261	-0,4560 to 0,2038	No	ns	0.9784	
12:phMut-MRT1-YFP + phasiR263-1 vs. 48:phMut-MRT1-YFP + miR825-5p	-0.1851	-0,5150 to 0,1448	No	ns	0.6984	
12:phMut-MRT1-YFP + phasiR263-2 vs. 12:phMut-MRT1-YFP + miR825-5p	-0.059	-0,3145 to 0,1965	No	ns	>0,9999	
12:phMut-MRT1-YFP + phasiR263-2 vs. 24:Wt-MRT1-YFP +miR319	-0.1839	-0,5138 to 0,1460	No	ns	0.7073	
12:phMut-MRT1-YFP + phasiR263-2 vs. 24:Wt-MRT1-YFP + phasiR263-1	-0.003417	-0,3333 to 0,3265	No	ns	>0,9999	
12:phMut-MRT1-YFP + phasiR263-2 vs. 24:Wt-MRT1-YFP + phasiR263-2	-0.06002	-0,3899 to 0,2699	No	ns	>0,9999	
12:phMut-MRT1-YFP + phasiR263-2 vs. 24:phMut-MRT1-YFP + phasiR263-1	-0.03492	-0,3648 to 0,2950	No	ns	>0,9999	
12:phMut-MRT1-YFP + phasiR263-2 vs. 24:phMut-MRT1-YFP + phasiR263-2	-0.07142	-0,2801 to 0,1372	No	ns	0.9929	
12:phMut-MRT1-YFP + phasiR263-2 vs. 24:phMut-MRT1-YFP + miR825-5p	-0.1304	-0,4603 to 0,1995	No	ns	0.9707	
12:phMut-MRT1-YFP + phasiR263-2 vs. 36:Wt-MRT1-YFP +miR319	-0.2305	-0,5604 to 0,09946	No	ns	0.374	
12:phMut-MRT1-YFP + phasiR263-2 vs. 36:Wt-MRT1-YFP + phasiR263-1	-0.04995	-0,3799 to 0,2800	No	ns	>0,9999	
12:phMut-MRT1-YFP + phasiR263-2 vs. 36:Wt-MRT1-YFP + phasiR263-2	-0.1066	-0,4365 to 0,2234	No	ns	0.9963	
12:phMut-MRT1-YFP + phasiR263-2 vs. 36:phMut-MRT1-YFP + phasiR263-1	-0.08145	-0,4114 to 0,2485	No	ns	0.9999	
12:phMut-MRT1-YFP + phasiR263-2 vs. 36:phMut-MRT1-YFP + phasiR263-2	-0.118	-0,3266 to 0,09070	No	ns	0.6884	
12:phMut-MRT1-YFP + phasiR263-2 vs. 36:phMut-MRT1-YFP + miR825-5p	-0.177	-0,5069 to 0,1530	No	ns	0.7567	
12:phMut-MRT1-YFP + phasiR263-2 vs. 48:Wt-MRT1-YFP +miR319	-0.2021	-0,5320 to 0,1278	No	ns	0.5715	
12:phMut-MRT1-YFP + phasiR263-2 vs. 48:Wt-MRT1-YFP + phasiR263-1	-0.02163	-0,3515 to 0,3083	No	ns	>0,9999	

12:phMut-MRT1-YFP + phasiR263-2 vs. 48:Wt-MRT1-YFP + phasiR263-2	-0.07823	-0,4081 to 0,2517	No	ns	>0,9999	
12:phMut-MRT1-YFP + phasiR263-2 vs. 48:phMut-MRT1-YFP + phasiR263-1	-0.05313	-0,3830 to 0,2768	No	ns	>0,9999	
12:phMut-MRT1-YFP + phasiR263-2 vs. 48:phMut-MRT1-YFP + phasiR263-2	-0.08963	-0,2983 to 0,1190	No	ns	0.9412	
12:phMut-MRT1-YFP + phasiR263-2 vs. 48:phMut-MRT1-YFP + miR825-5p	-0.1486	-0,4785 to 0,1813	No	ns	0.9158	
12:phMut-MRT1-YFP + miR825-5p vs. 24:Wt-MRT1-YFP +miR319	-0.1249	-0,4548 to 0,2050	No	ns	0.9803	
12:phMut-MRT1-YFP + miR825-5p vs. 24:Wt-MRT1-YFP + phasiR263-1	0.05558	-0,2743 to 0,3855	No	ns	>0,9999	
12:phMut-MRT1-YFP + miR825-5p vs. 24:Wt-MRT1-YFP + phasiR263-2	-0.001017	-0,3309 to 0,3289	No	ns	>0,9999	
12:phMut-MRT1-YFP + miR825-5p vs. 24:phMut-MRT1-YFP + phasiR263-1	0.02408	-0,3058 to 0,3540	No	ns	>0,9999	
12:phMut-MRT1-YFP + miR825-5p vs. 24:phMut-MRT1-YFP + phasiR263-2	-0.01242	-0,3423 to 0,3175	No	ns	>0,9999	
12:phMut-MRT1-YFP + miR825-5p vs. 24:phMut-MRT1-YFP + miR825-5p	-0.07142	-0,2801 to 0,1372	No	ns	0.9929	
12:phMut-MRT1-YFP + miR825-5p vs. 36:Wt-MRT1-YFP +miR319	-0.1715	-0,5014 to 0,1585	No	ns	0.7935	
12:phMut-MRT1-YFP + miR825-5p vs. 36:Wt-MRT1-YFP + phasiR263-1	0.00905	-0,3209 to 0,3390	No	ns	>0,9999	
12:phMut-MRT1-YFP + miR825-5p vs. 36:Wt-MRT1-YFP + phasiR263-2	-0.04755	-0,3775 to 0,2824	No	ns	>0,9999	
12:phMut-MRT1-YFP + miR825-5p vs. 36:phMut-MRT1-YFP + phasiR263-1	-0.02245	-0,3524 to 0,3075	No	ns	>0,9999	
12:phMut-MRT1-YFP + miR825-5p vs. 36:phMut-MRT1-YFP + phasiR263-2	-0.05895	-0,3889 to 0,2710	No	ns	>0,9999	
12:phMut-MRT1-YFP + miR825-5p vs. 36:phMut-MRT1-YFP + miR825-5p	-0.118	-0,3266 to 0,09070	No	ns	0.6884	
12:phMut-MRT1-YFP + miR825-5p vs. 48:Wt-MRT1-YFP +miR319	-0.1431	-0,4730 to 0,1868	No	ns	0.9365	
12:phMut-MRT1-YFP + miR825-5p vs. 48:Wt-MRT1-YFP + phasiR263-1	0.03737	-0,2925 to 0,3673	No	ns	>0,9999	
12:phMut-MRT1-YFP + miR825-5p vs. 48:Wt-MRT1-YFP + phasiR263-2	-0.01923	-0,3491 to 0,3107	No	ns	>0,9999	
12:phMut-MRT1-YFP + miR825-5p vs. 48:phMut-MRT1-YFP + phasiR263-1	0.005867	-0,3240 to 0,3358	No	ns	>0,9999	

12:phMut-MRT1-YFP + miR825-5p vs. 48:phMut-MRT1-YFP + phasiR263-2	-0.03063	-0,3605 to 0,2993	No	ns	>0,9999	
12:phMut-MRT1-YFP + miR825-5p vs. 48:phMut-MRT1-YFP + miR825-5p	-0.08963	-0,2983 to 0,1190	No	ns	0.9412	
24:Wt-MRT1-YFP +miR319 vs. 24:Wt-MRT1-YFP + phasiR263-1	0.1805	-0,07505 to 0,4360	No	ns	0.3582	
24:Wt-MRT1-YFP +miR319 vs. 24:Wt-MRT1-YFP + phasiR263-2	0.1239	-0,1316 to 0,3794	No	ns	0.8621	
24:Wt-MRT1-YFP +miR319 vs. 24:phMut-MRT1-YFP + phasiR263-1	0.149	-0,1065 to 0,4045	No	ns	0.6449	
24:Wt-MRT1-YFP +miR319 vs. 24:phMut-MRT1-YFP + phasiR263-2	0.1125	-0,1430 to 0,3680	No	ns	0.929	
24:Wt-MRT1-YFP +miR319 vs. 24:phMut-MRT1-YFP + miR825-5p	0.0535	-0,2020 to 0,3090	No	ns	>0,9999	
24:Wt-MRT1-YFP +miR319 vs. 36:Wt-MRT1-YFP +miR319	-0.04653	-0,2552 to 0,1621	No	ns	>0,9999	
24:Wt-MRT1-YFP +miR319 vs. 36:Wt-MRT1-YFP + phasiR263-1	0.134	-0,1959 to 0,4639	No	ns	0.9629	
24:Wt-MRT1-YFP +miR319 vs. 36:Wt-MRT1-YFP + phasiR263-2	0.07737	-0,2525 to 0,4073	No	ns	>0,9999	
24:Wt-MRT1-YFP +miR319 vs. 36:phMut-MRT1-YFP + phasiR263-1	0.1025	-0,2274 to 0,4324	No	ns	0.9977	
24:Wt-MRT1-YFP +miR319 vs. 36:phMut-MRT1-YFP + phasiR263-2	0.06597	-0,2639 to 0,3959	No	ns	>0,9999	
24:Wt-MRT1-YFP +miR319 vs. 36:phMut-MRT1-YFP + miR825-5p	0.006967	-0,3229 to 0,3369	No	ns	>0,9999	
24:Wt-MRT1-YFP +miR319 vs. 48:Wt-MRT1-YFP +miR319	-0.01822	-0,2269 to 0,1904	No	ns	>0,9999	
24:Wt-MRT1-YFP +miR319 vs. 48:Wt-MRT1-YFP + phasiR263-1	0.1623	-0,1676 to 0,4922	No	ns	0.8493	
24:Wt-MRT1-YFP +miR319 vs. 48:Wt-MRT1-YFP + phasiR263-2	0.1057	-0,2242 to 0,4356	No	ns	0.9967	
24:Wt-MRT1-YFP +miR319 vs. 48:phMut-MRT1-YFP + phasiR263-1	0.1308	-0,1991 to 0,4607	No	ns	0.9699	
24:Wt-MRT1-YFP +miR319 vs. 48:phMut-MRT1-YFP + phasiR263-2	0.09428	-0,2356 to 0,4242	No	ns	0.9992	
24:Wt-MRT1-YFP +miR319 vs. 48:phMut-MRT1-YFP + miR825-5p	0.03528	-0,2946 to 0,3652	No	ns	>0,9999	
24:Wt-MRT1-YFP + phasiR263-1 vs. 24:Wt-MRT1-YFP + phasiR263-2	-0.0566	-0,3121 to 0,1989	No	ns	>0,9999	
24:Wt-MRT1-YFP + phasiR263-1 vs. 24:phMut-MRT1-YFP + phasiR263-1	-0.0315	-0,2870 to 0,2240	No	ns	>0,9999	
24:Wt-MRT1-YFP + phasiR263-1 vs. 24:phMut-MRT1-YFP + phasiR263-2	-0.068	-0,3235 to 0,1875	No	ns	0.9997	
24:Wt-MRT1-YFP + phasiR263-1 vs. 24:phMut-MRT1-YFP + miR825-5p	-0.127	-0,3825 to 0,1285	No	ns	0.8397	
24:Wt-MRT1-YFP + phasiR263-1 vs. 36:Wt-MRT1-YFP +miR319	-0.227	-0,5569 to 0,1029	No	ns	0.3957	

24:Wt-MRT1-YFP + phasiR263-1 vs. 36:Wt-MRT1-YFP + phasiR263-1	-0.04653	-0,2552 to 0,1621	No	ns	>0,9999	
24:Wt-MRT1-YFP + phasiR263-1 vs. 36:Wt-MRT1-YFP + phasiR263-2	-0.1031	-0,4330 to 0,2268	No	ns	0.9975	
24:Wt-MRT1-YFP + phasiR263-1 vs. 36:phMut-MRT1-YFP + phasiR263-1	-0.07803	-0,4079 to 0,2519	No	ns	>0,9999	
24:Wt-MRT1-YFP + phasiR263-1 vs. 36:phMut-MRT1-YFP + phasiR263-2	-0.1145	-0,4444 to 0,2154	No	ns	0.9918	
24:Wt-MRT1-YFP + phasiR263-1 vs. 36:phMut-MRT1-YFP + miR825-5p	-0.1735	-0,5034 to 0,1564	No	ns	0.7798	
24:Wt-MRT1-YFP + phasiR263-1 vs. 48:Wt-MRT1-YFP +miR319	-0.1987	-0,5286 to 0,1312	No	ns	0.5971	
24:Wt-MRT1-YFP + phasiR263-1 vs. 48:Wt-MRT1-YFP + phasiR263-1	-0.01822	-0,2269 to 0,1904	No	ns	>0,9999	
24:Wt-MRT1-YFP + phasiR263-1 vs. 48:Wt-MRT1-YFP + phasiR263-2	-0.07482	-0,4047 to 0,2551	No	ns	>0,9999	
24:Wt-MRT1-YFP + phasiR263-1 vs. 48:phMut-MRT1-YFP + phasiR263-1	-0.04972	-0,3796 to 0,2802	No	ns	>0,9999	
24:Wt-MRT1-YFP + phasiR263-1 vs. 48:phMut-MRT1-YFP + phasiR263-2	-0.08622	-0,4161 to 0,2437	No	ns	0.9998	
24:Wt-MRT1-YFP + phasiR263-1 vs. 48:phMut-MRT1-YFP + miR825-5p	-0.1452	-0,4751 to 0,1847	No	ns	0.9291	
24:Wt-MRT1-YFP + phasiR263-2 vs. 24:phMut-MRT1-YFP + phasiR263-1	0.0251	-0,2304 to 0,2806	No	ns	>0,9999	
24:Wt-MRT1-YFP + phasiR263-2 vs. 24:phMut-MRT1-YFP + phasiR263-2	-0.0114	-0,2669 to 0,2441	No	ns	>0,9999	
24:Wt-MRT1-YFP + phasiR263-2 vs. 24:phMut-MRT1-YFP + miR825-5p	-0.0704	-0,3259 to 0,1851	No	ns	0.9995	
24:Wt-MRT1-YFP + phasiR263-2 vs. 36:Wt-MRT1-YFP +miR319	-0.1704	-0,5003 to 0,1595	No	ns	0.8001	
24:Wt-MRT1-YFP + phasiR263-2 vs. 36:Wt-MRT1-YFP + phasiR263-1	0.01007	-0,3198 to 0,3400	No	ns	>0,9999	
24:Wt-MRT1-YFP + phasiR263-2 vs. 36:Wt-MRT1-YFP + phasiR263-2	-0.04653	-0,2552 to 0,1621	No	ns	>0,9999	
24:Wt-MRT1-YFP + phasiR263-2 vs. 36:phMut-MRT1-YFP + phasiR263-1	-0.02143	-0,3513 to 0,3085	No	ns	>0,9999	
24:Wt-MRT1-YFP + phasiR263-2 vs. 36:phMut-MRT1-YFP + phasiR263-2	-0.05793	-0,3878 to 0,2720	No	ns	>0,9999	

24:Wt-MRT1-YFP + phasiR263-2 vs. 36:phMut-MRT1-YFP + miR825-5p	-0.1169	-0,4468 to 0,2130	No	ns	0.9898	
24:Wt-MRT1-YFP + phasiR263-2 vs. 48:Wt-MRT1-YFP +miR319	-0.1421	-0,4720 to 0,1878	No	ns	0.9399	
24:Wt-MRT1-YFP + phasiR263-2 vs. 48:Wt-MRT1-YFP + phasiR263-1	0.03838	-0,2915 to 0,3683	No	ns	>0,9999	
24:Wt-MRT1-YFP + phasiR263-2 vs. 48:Wt-MRT1-YFP + phasiR263-2	-0.01822	-0,2269 to 0,1904	No	ns	>0,9999	
24:Wt-MRT1-YFP + phasiR263-2 vs. 48:phMut-MRT1-YFP + phasiR263-1	0.006883	-0,3230 to 0,3368	No	ns	>0,9999	
24:Wt-MRT1-YFP + phasiR263-2 vs. 48:phMut-MRT1-YFP + phasiR263-2	-0.02962	-0,3595 to 0,3003	No	ns	>0,9999	
24:Wt-MRT1-YFP + phasiR263-2 vs. 48:phMut-MRT1-YFP + miR825-5p	-0.08862	-0,4185 to 0,2413	No	ns	0.9997	
24:phMut-MRT1-YFP + phasiR263-1 vs. 24:phMut-MRT1-YFP + phasiR263-2	-0.0365	-0,2920 to 0,2190	No	ns	>0,9999	
24:phMut-MRT1-YFP + phasiR263-1 vs. 24:phMut-MRT1-YFP + miR825-5p	-0.0955	-0,3510 to 0,1600	No	ns	0.9826	
24:phMut-MRT1-YFP + phasiR263-1 vs. 36:Wt-MRT1-YFP +miR319	-0.1955	-0,5254 to 0,1344	No	ns	0.621	
24:phMut-MRT1-YFP + phasiR263-1 vs. 36:Wt-MRT1-YFP + phasiR263-1	-0.01503	-0,3449 to 0,3149	No	ns	>0,9999	
24:phMut-MRT1-YFP + phasiR263-1 vs. 36:Wt-MRT1-YFP + phasiR263-2	-0.07163	-0,4015 to 0,2583	No	ns	>0,9999	
24:phMut-MRT1-YFP + phasiR263-1 vs. 36:phMut-MRT1-YFP + phasiR263-1	-0.04653	-0,2552 to 0,1621	No	ns	>0,9999	
24:phMut-MRT1-YFP + phasiR263-1 vs. 36:phMut-MRT1-YFP + phasiR263-2	-0.08303	-0,4129 to 0,2469	No	ns	0.9999	
24:phMut-MRT1-YFP + phasiR263-1 vs. 36:phMut-MRT1-YFP + miR825-5p	-0.142	-0,4719 to 0,1879	No	ns	0.9401	
24:phMut-MRT1-YFP + phasiR263-1 vs. 48:Wt-MRT1-YFP +miR319	-0.1672	-0,4971 to 0,1627	No	ns	0.8202	
24:phMut-MRT1-YFP + phasiR263-1 vs. 48:Wt-MRT1-YFP + phasiR263-1	0.01328	-0,3166 to 0,3432	No	ns	>0,9999	
24:phMut-MRT1-YFP + phasiR263-1 vs. 48:Wt-MRT1-YFP + phasiR263-2	-0.04332	-0,3732 to 0,2866	No	ns	>0,9999	
24:phMut-MRT1-YFP + phasiR263-1 vs. 48:phMut-MRT1-YFP + phasiR263-1	-0.01822	-0,2269 to 0,1904	No	ns	>0,9999	
24:phMut-MRT1-YFP + phasiR263-1 vs. 48:phMut-MRT1-YFP + phasiR263-2	-0.05472	-0,3846 to 0,2752	No	ns	>0,9999	

24:phMut-MRT1-YFP + phasiR263-1 vs. 48:phMut-MRT1-YFP + miR825-5p	-0.1137	-0,4436 to 0,2162	No	ns	0.9924	
24:phMut-MRT1-YFP + phasiR263-2 vs. 24:phMut-MRT1-YFP + miR825-5p	-0.059	-0,3145 to 0,1965	No	ns	>0,9999	
24:phMut-MRT1-YFP + phasiR263-2 vs. 36:Wt-MRT1-YFP +miR319	-0.159	-0,4889 to 0,1709	No	ns	0.8671	
24:phMut-MRT1-YFP + phasiR263-2 vs. 36:Wt-MRT1-YFP + phasiR263-1	0.02147	-0,3084 to 0,3514	No	ns	>0,9999	
24:phMut-MRT1-YFP + phasiR263-2 vs. 36:Wt-MRT1-YFP + phasiR263-2	-0.03513	-0,3650 to 0,2948	No	ns	>0,9999	
24:phMut-MRT1-YFP + phasiR263-2 vs. 36:phMut-MRT1-YFP + phasiR263-1	-0.01003	-0,3399 to 0,3199	No	ns	>0,9999	
24:phMut-MRT1-YFP + phasiR263-2 vs. 36:phMut-MRT1-YFP + phasiR263-2	-0.04653	-0,2552 to 0,1621	No	ns	>0,9999	
24:phMut-MRT1-YFP + phasiR263-2 vs. 36:phMut-MRT1-YFP + miR825-5p	-0.1055	-0,4354 to 0,2244	No	ns	0.9967	
24:phMut-MRT1-YFP + phasiR263-2 vs. 48:Wt-MRT1-YFP +miR319	-0.1307	-0,4606 to 0,1992	No	ns	0.9701	
24:phMut-MRT1-YFP + phasiR263-2 vs. 48:Wt-MRT1-YFP + phasiR263-1	0.04978	-0,2801 to 0,3797	No	ns	>0,9999	
24:phMut-MRT1-YFP + phasiR263-2 vs. 48:Wt-MRT1-YFP + phasiR263-2	-0.006817	-0,3367 to 0,3231	No	ns	>0,9999	
24:phMut-MRT1-YFP + phasiR263-2 vs. 48:phMut-MRT1-YFP + phasiR263-1	0.01828	-0,3116 to 0,3482	No	ns	>0,9999	
24:phMut-MRT1-YFP + phasiR263-2 vs. 48:phMut-MRT1-YFP + phasiR263-2	-0.01822	-0,2269 to 0,1904	No	ns	>0,9999	
24:phMut-MRT1-YFP + phasiR263-2 vs. 48:phMut-MRT1-YFP + miR825-5p	-0.07722	-0,4071 to 0,2527	No	ns	>0,9999	
24:phMut-MRT1-YFP + miR825-5p vs. 36:Wt-MRT1-YFP +miR319	-0.1	-0,4299 to 0,2299	No	ns	0.9983	
24:phMut-MRT1-YFP + miR825-5p vs. 36:Wt-MRT1-YFP + phasiR263-1	0.08047	-0,2494 to 0,4104	No	ns	>0,9999	
24:phMut-MRT1-YFP + miR825-5p vs. 36:Wt-MRT1-YFP + phasiR263-2	0.02387	-0,3060 to 0,3538	No	ns	>0,9999	
24:phMut-MRT1-YFP + miR825-5p vs. 36:phMut-MRT1-YFP + phasiR263-1	0.04897	-0,2809 to 0,3789	No	ns	>0,9999	
24:phMut-MRT1-YFP + miR825-5p vs. 36:phMut-MRT1-YFP + phasiR263-2	0.01247	-0,3174 to 0,3424	No	ns	>0,9999	
24:phMut-MRT1-YFP + miR825-5p vs. 36:phMut-MRT1-YFP + miR825-5p	-0.04653	-0,2552 to 0,1621	No	ns	>0,9999	
24:phMut-MRT1-YFP + miR825-5p vs. 48:Wt-MRT1-YFP +miR319	-0.07172	-0,4016 to 0,2582	No	ns	>0,9999	
24:phMut-MRT1-YFP + miR825-5p vs. 48:Wt-MRT1-YFP + phasiR263-1	0.1088	-0,2211 to 0,4387	No	ns	0.9953	

24:phMut-MRT1-YFP + miR825-5p vs. 48:Wt-MRT1-YFP + phasiR263-2	0.05218	-0,2777 to 0,3821	No	ns	>0,9999	
24:phMut-MRT1-YFP + miR825-5p vs. 48:phMut-MRT1-YFP + phasiR263-1	0.07728	-0,2526 to 0,4072	No	ns	>0,9999	
24:phMut-MRT1-YFP + miR825-5p vs. 48:phMut-MRT1-YFP + phasiR263-2	0.04078	-0,2891 to 0,3707	No	ns	>0,9999	
24:phMut-MRT1-YFP + miR825-5p vs. 48:phMut-MRT1-YFP + miR825-5p	-0.01822	-0,2269 to 0,1904	No	ns	>0,9999	
36:Wt-MRT1-YFP +miR319 vs. 36:Wt-MRT1-YFP + phasiR263-1	0.1805	-0,07505 to 0,4360	No	ns	0.3582	
36:Wt-MRT1-YFP +miR319 vs. 36:Wt-MRT1-YFP + phasiR263-2	0.1239	-0,1316 to 0,3794	No	ns	0.8621	
36:Wt-MRT1-YFP +miR319 vs. 36:phMut-MRT1-YFP + phasiR263-1	0.149	-0,1065 to 0,4045	No	ns	0.6449	
36:Wt-MRT1-YFP +miR319 vs. 36:phMut-MRT1-YFP + phasiR263-2	0.1125	-0,1430 to 0,3680	No	ns	0.929	
36:Wt-MRT1-YFP +miR319 vs. 36:phMut-MRT1-YFP + miR825-5p	0.0535	-0,2020 to 0,3090	No	ns	>0,9999	
36:Wt-MRT1-YFP +miR319 vs. 48:Wt-MRT1-YFP +miR319	0.02832	-0,1803 to 0,2370	No	ns	>0,9999	
36:Wt-MRT1-YFP +miR319 vs. 48:Wt-MRT1-YFP + phasiR263-1	0.2088	-0,1211 to 0,5387	No	ns	0.5219	
36:Wt-MRT1-YFP +miR319 vs. 48:Wt-MRT1-YFP + phasiR263-2	0.1522	-0,1777 to 0,4821	No	ns	0.9005	
36:Wt-MRT1-YFP +miR319 vs. 48:phMut-MRT1-YFP + phasiR263-1	0.1773	-0,1526 to 0,5072	No	ns	0.7541	
36:Wt-MRT1-YFP +miR319 vs. 48:phMut-MRT1-YFP + phasiR263-2	0.1408	-0,1891 to 0,4707	No	ns	0.944	
36:Wt-MRT1-YFP +miR319 vs. 48:phMut-MRT1-YFP + miR825-5p	0.08182	-0,2481 to 0,4117	No	ns	0.9999	
36:Wt-MRT1-YFP + phasiR263-1 vs. 36:Wt-MRT1-YFP + phasiR263-2	-0.0566	-0,3121 to 0,1989	No	ns	>0,9999	
36:Wt-MRT1-YFP + phasiR263-1 vs. 36:phMut-MRT1-YFP + phasiR263-1	-0.0315	-0,2870 to 0,2240	No	ns	>0,9999	
36:Wt-MRT1-YFP + phasiR263-1 vs. 36:phMut-MRT1-YFP + phasiR263-2	-0.068	-0,3235 to 0,1875	No	ns	0.9997	
36:Wt-MRT1-YFP + phasiR263-1 vs. 36:phMut-MRT1-YFP + miR825-5p	-0.127	-0,3825 to 0,1285	No	ns	0.8397	
36:Wt-MRT1-YFP + phasiR263-1 vs. 48:Wt-MRT1-YFP +miR319	-0.1522	-0,4821 to 0,1777	No	ns	0.9006	
36:Wt-MRT1-YFP + phasiR263-1 vs. 48:Wt-MRT1-YFP + phasiR263-1	0.02832	-0,1803 to 0,2370	No	ns	>0,9999	
36:Wt-MRT1-YFP + phasiR263-1 vs. 48:Wt-MRT1-YFP + phasiR263-2	-0.02828	-0,3582 to 0,3016	No	ns	>0,9999	
36:Wt-MRT1-YFP + phasiR263-1 vs. 48:phMut-MRT1-YFP + phasiR263-1	-0.003183	-0,3331 to 0,3267	No	ns	>0,9999	
36:Wt-MRT1-YFP + phasiR263-1 vs. 48:phMut-MRT1-YFP + phasiR263-2	-0.03968	-0,3696 to 0,2902	No	ns	>0,9999	

36:Wt-MRT1-YFP + phasiR263-1 vs. 48:phMut-MRT1-YFP + miR825-5p	-0.09868	-0,4286 to 0,2312	No	ns	0.9985
36:Wt-MRT1-YFP + phasiR263-2 vs. 36:phMut-MRT1-YFP + phasiR263-1	0.0251	-0,2304 to 0,2806	No	ns	>0,9999
36:Wt-MRT1-YFP + phasiR263-2 vs. 36:phMut-MRT1-YFP + phasiR263-2	-0.0114	-0,2669 to 0,2441	No	ns	>0,9999
36:Wt-MRT1-YFP + phasiR263-2 vs. 36:phMut-MRT1-YFP + miR825-5p	-0.0704	-0,3259 to 0,1851	No	ns	0.9995
36:Wt-MRT1-YFP + phasiR263-2 vs. 48:Wt-MRT1-YFP +miR319	-0.09558	-0,4255 to 0,2343	No	ns	0.999
36:Wt-MRT1-YFP + phasiR263-2 vs. 48:Wt-MRT1-YFP + phasiR263-1	0.08492	-0,2450 to 0,4148	No	ns	0.9998
36:Wt-MRT1-YFP + phasiR263-2 vs. 48:Wt-MRT1-YFP + phasiR263-2	0.02832	-0,1803 to 0,2370	No	ns	>0,9999
36:Wt-MRT1-YFP + phasiR263-2 vs. 48:phMut-MRT1-YFP + phasiR263-1	0.05342	-0,2765 to 0,3833	No	ns	>0,9999
36:Wt-MRT1-YFP + phasiR263-2 vs. 48:phMut-MRT1-YFP + phasiR263-2	0.01692	-0,3130 to 0,3468	No	ns	>0,9999
36:Wt-MRT1-YFP + phasiR263-2 vs. 48:phMut-MRT1-YFP + miR825-5p	-0.04208	-0,3720 to 0,2878	No	ns	>0,9999
36:phMut-MRT1-YFP + phasiR263-1 vs. 36:phMut-MRT1-YFP + phasiR263-2	-0.0365	-0,2920 to 0,2190	No	ns	>0,9999
36:phMut-MRT1-YFP + phasiR263-1 vs. 36:phMut-MRT1-YFP + miR825-5p	-0.0955	-0,3510 to 0,1600	No	ns	0.9826
36:phMut-MRT1-YFP + phasiR263-1 vs. 48:Wt-MRT1-YFP +miR319	-0.1207	-0,4506 to 0,2092	No	ns	0.9859
36:phMut-MRT1-YFP + phasiR263-1 vs. 48:Wt-MRT1-YFP + phasiR263-1	0.05982	-0,2701 to 0,3897	No	ns	>0,9999
36:phMut-MRT1-YFP + phasiR263-1 vs. 48:Wt-MRT1-YFP + phasiR263-2	0.003217	-0,3267 to 0,3331	No	ns	>0,9999
36:phMut-MRT1-YFP + phasiR263-1 vs. 48:phMut-MRT1-YFP + phasiR263-1	0.02832	-0,1803 to 0,2370	No	ns	>0,9999
36:phMut-MRT1-YFP + phasiR263-1 vs. 48:phMut-MRT1-YFP + phasiR263-2	-0.008183	-0,3381 to 0,3217	No	ns	>0,9999
36:phMut-MRT1-YFP + phasiR263-1 vs. 48:phMut-MRT1-YFP + miR825-5p	-0.06718	-0,3971 to 0,2627	No	ns	>0,9999
36:phMut-MRT1-YFP + phasiR263-2 vs. 36:phMut-MRT1-YFP + miR825-5p	-0.059	-0,3145 to 0,1965	No	ns	>0,9999
36:phMut-MRT1-YFP + phasiR263-2 vs. 48:Wt-MRT1-YFP +miR319	-0.08418	-0,4141 to 0,2457	No	ns	0.9998
36:phMut-MRT1-YFP + phasiR263-2 vs. 48:Wt-MRT1-YFP + phasiR263-1	0.09632	-0,2336 to 0,4262	No	ns	0.9989
36:phMut-MRT1-YFP + phasiR263-2 vs. 48:Wt-MRT1-YFP + phasiR263-2	0.03972	-0,2902 to 0,3696	No	ns	>0,9999

36:phMut-MRT1-YFP + phasiR263-2 vs. 48:phMut-MRT1-YFP + phasiR263-1	0.06482	-0,2651 to 0,3947	No	ns	>0,9999	
36:phMut-MRT1-YFP + phasiR263-2 vs. 48:phMut-MRT1-YFP + phasiR263-2	0.02832	-0,1803 to 0,2370	No	ns	>0,9999	
36:phMut-MRT1-YFP + phasiR263-2 vs. 48:phMut-MRT1-YFP + miR825-5p	-0.03068	-0,3606 to 0,2992	No	ns	>0,9999	
36:phMut-MRT1-YFP + miR825-5p vs. 48:Wt-MRT1-YFP +miR319	-0.02518	-0,3551 to 0,3047	No	ns	>0,9999	
36:phMut-MRT1-YFP + miR825-5p vs. 48:Wt-MRT1-YFP + phasiR263-1	0.1553	-0,1746 to 0,4852	No	ns	0.8859	
36:phMut-MRT1-YFP + miR825-5p vs. 48:Wt-MRT1-YFP + phasiR263-2	0.09872	-0,2312 to 0,4286	No	ns	0.9985	
36:phMut-MRT1-YFP + miR825-5p vs. 48:phMut-MRT1-YFP + phasiR263-1	0.1238	-0,2061 to 0,4537	No	ns	0.9819	
36:phMut-MRT1-YFP + miR825-5p vs. 48:phMut-MRT1-YFP + phasiR263-2	0.08732	-0,2426 to 0,4172	No	ns	0.9997	
36:phMut-MRT1-YFP + miR825-5p vs. 48:phMut-MRT1-YFP + miR825-5p	0.02832	-0,1803 to 0,2370	No	ns	>0,9999	
48:Wt-MRT1-YFP +miR319 vs. 48:Wt-MRT1-YFP + phasiR263-1	0.1805	-0,07505 to 0,4360	No	ns	0.3582	
48:Wt-MRT1-YFP +miR319 vs. 48:Wt-MRT1-YFP + phasiR263-2	0.1239	-0,1316 to 0,3794	No	ns	0.8621	
48:Wt-MRT1-YFP +miR319 vs. 48:phMut-MRT1-YFP + phasiR263-1	0.149	-0,1065 to 0,4045	No	ns	0.6449	
48:Wt-MRT1-YFP +miR319 vs. 48:phMut-MRT1-YFP + phasiR263-2	0.1125	-0,1430 to 0,3680	No	ns	0.929	
48:Wt-MRT1-YFP +miR319 vs. 48:phMut-MRT1-YFP + miR825-5p	0.0535	-0,2020 to 0,3090	No	ns	>0,9999	
48:Wt-MRT1-YFP + phasiR263-1 vs. 48:Wt-MRT1-YFP + phasiR263-2	-0.0566	-0,3121 to 0,1989	No	ns	>0,9999	
48:Wt-MRT1-YFP + phasiR263-1 vs. 48:phMut-MRT1-YFP + phasiR263-1	-0.0315	-0,2870 to 0,2240	No	ns	>0,9999	
48:Wt-MRT1-YFP + phasiR263-1 vs. 48:phMut-MRT1-YFP + phasiR263-2	-0.068	-0,3235 to 0,1875	No	ns	0.9997	
48:Wt-MRT1-YFP + phasiR263-1 vs. 48:phMut-MRT1-YFP + miR825-5p	-0.127	-0,3825 to 0,1285	No	ns	0.8397	
48:Wt-MRT1-YFP + phasiR263-2 vs. 48:phMut-MRT1-YFP + phasiR263-1	0.0251	-0,2304 to 0,2806	No	ns	>0,9999	
48:Wt-MRT1-YFP + phasiR263-2 vs. 48:phMut-MRT1-YFP + phasiR263-2	-0.0114	-0,2669 to 0,2441	No	ns	>0,9999	
48:Wt-MRT1-YFP + phasiR263-2 vs. 48:phMut-MRT1-YFP + miR825-5p	-0.0704	-0,3259 to 0,1851	No	ns	0.9995	
48:phMut-MRT1-YFP + phasiR263-1 vs. 48:phMut-MRT1-YFP + phasiR263-2	-0.0365	-0,2920 to 0,2190	No	ns	>0,9999	
48:phMut-MRT1-YFP + phasiR263-1 vs. 48:phMut-MRT1-YFP + miR825-5p	-0.0955	-0,3510 to 0,1600	No	ns	0.9826	
48:phMut-MRT1-YFP + phasiR263-2 vs. 48:phMut-MRT1-YFP + miR825-5p	-0.059	-0,3145 to 0,1965	No	ns	>0,9999	

Annexed table 9. Statistics comparison of fluorescence constructs in *N. benthamiana* plants co-expressing them alone or with phasiRNAs. Data are mean ± SE.

Tukey's multiple comparisons test	Mean Diff,	95,00% CI of diff,	Significant?	Summary	Adjusted P Value	
12:MRT2-YFP + miR319 vs. 12:MRT2-YFP + phasiR263-9	0.1121	-0,07881 to 0,3029	No	ns	0.4654	
12:MRT2-YFP + miR319 vs. 12:phMut-MRT2-YFP + phasiR263-9	0.02974	-0,1611 to 0,2206	No	ns	>0,9999	
12:MRT2-YFP + miR319 vs. 12:phMut-MRT2-YFP + phasiR825-5p	0.112	-0,07888 to 0,3029	No	ns	0.4662	
12:MRT2-YFP + miR319 vs. 24:MRT2-YFP + miR319	0.01656	-0,1743 to 0,2074	No	ns	>0,9999	
12:MRT2-YFP + miR319 vs. 24:MRT2-YFP + phasiR263-9	0.1286	-0,1413 to 0,3986	No	ns	0.7139	
12:MRT2-YFP + miR319 vs. 24:phMut-MRT2-YFP + phasiR263-9	0.0463	-0,2236 to 0,3162	No	ns	>0,9999	
12:MRT2-YFP + miR319 vs. 24:phMut-MRT2-YFP + phasiR825-5p	0.1286	-0,1414 to 0,3985	No	ns	0.7145	
12:MRT2-YFP + miR319 vs. 36:MRT2-YFP + miR319	-0.07997	-0,2708 to 0,1109	No	ns	0.8346	
12:MRT2-YFP + miR319 vs. 36:MRT2-YFP + phasiR263-9	0.0321	-0,2378 to 0,3020	No	ns	>0,9999	
12:MRT2-YFP + miR319 vs. 36:phMut-MRT2-YFP + phasiR263-9	-0.05023	-0,3202 to 0,2197	No	ns	0.9998	
12:MRT2-YFP + miR319 vs. 36:phMut-MRT2-YFP + phasiR825-5p	0.03203	-0,2379 to 0,3020	No	ns	>0,9999	
12:MRT2-YFP + miR319 vs. 48:MRT2-YFP + miR319	-0.1222	-0,3131 to 0,06865	No	ns	0.3623	
12:MRT2-YFP + miR319 vs. 48:MRT2-YFP + phasiR263-9	-0.01016	-0,2801 to 0,2598	No	ns	>0,9999	
12:MRT2-YFP + miR319 vs. 48:phMut-MRT2-YFP + phasiR263-9	-0.09248	-0,3624 to 0,1775	No	ns	0.9466	
12:MRT2-YFP + miR319 vs. 48:phMut-MRT2-YFP + phasiR825-5p	-0.01023	-0,2802 to 0,2597	No	ns	>0,9999	
12:MRT2-YFP + phasiR263-9 vs. 12:phMut-MRT2-YFP + phasiR263-9	-0.08233	-0,2732 to 0,1085	No	ns	0.8106	
12:MRT2-YFP + phasiR263-9 vs. 12:phMut-MRT2-YFP + phasiR825-5p	-0.00007425	-0,1909 to 0,1908	No	ns	>0,9999	
12:MRT2-YFP + phasiR263-9 vs. 24:MRT2-YFP + miR319	-0.09551	-0,3654 to 0,1744	No	ns	0.9345	
12:MRT2-YFP + phasiR263-9 vs. 24:MRT2-YFP + phasiR263-9	0.01656	-0,1743 to 0,2074	No	ns	>0,9999	
12:MRT2-YFP + phasiR263-9 vs. 24:phMut-MRT2-YFP + phasiR263-9	-0.06577	-0,3357 to 0,2042	No	ns	0.9964	

12:MRT2-YFP + phasiR263-9 vs. 24:phMut-MRT2-YFP + phasiR825-5p	0.01648	-0,2535 to 0,2864	No	ns	>0,9999
12:MRT2-YFP + phasiR263-9 vs. 36:MRT2-YFP + miR319	-0.192	-0,4620 to 0,07790	No	ns	0.2517
12:MRT2-YFP + phasiR263-9 vs. 36:MRT2-YFP + phasiR263-9	-0.07997	-0,2708 to 0,1109	No	ns	0.8346
12:MRT2-YFP + phasiR263-9 vs. 36:phMut-MRT2-YFP + phasiR263-9	-0.1623	-0,4322 to 0,1076	No	ns	0.4365
12:MRT2-YFP + phasiR263-9 vs. 36:phMut-MRT2-YFP + phasiR825-5p	-0.08004	-0,3500 to 0,1899	No	ns	0.9808
12:MRT2-YFP + phasiR263-9 vs. 48:MRT2-YFP + miR319	-0.2343	-0,5042 to 0,03565	No	ns	0.1058
12:MRT2-YFP + phasiR263-9 vs. 48:MRT2-YFP + phasiR263-9	-0.1222	-0,3131 to 0,06865	No	ns	0.3623
12:MRT2-YFP + phasiR263-9 vs. 48:phMut-MRT2-YFP + phasiR263-9	-0.2045	-0,4745 to 0,06539	No	ns	0.196
12:MRT2-YFP + phasiR263-9 vs. 48:phMut-MRT2-YFP + phasiR825-5p	-0.1223	-0,3922 to 0,1476	No	ns	0.7655
12:phMut-MRT2-YFP + phasiR263-9 vs. 12:phMut-MRT2-YFP + phasiR825-5p	0.08225	-0,1086 to 0,2731	No	ns	0.8114
12:phMut-MRT2-YFP + phasiR263-9 vs. 24:MRT2-YFP + miR319	-0.01318	-0,2831 to 0,2568	No	ns	>0,9999
12:phMut-MRT2-YFP + phasiR263-9 vs. 24:MRT2-YFP + phasiR263-9	0.09889	-0,1711 to 0,3688	No	ns	0.9192
12:phMut-MRT2-YFP + phasiR263-9 vs. 24:phMut-MRT2-YFP + phasiR263-9	0.01656	-0,1743 to 0,2074	No	ns	>0,9999
12:phMut-MRT2-YFP + phasiR263-9 vs. 24:phMut-MRT2-YFP + phasiR825-5p	0.09881	-0,1711 to 0,3688	No	ns	0.9196
12:phMut-MRT2-YFP + phasiR263-9 vs. 36:MRT2-YFP + miR319	-0.1097	-0,3796 to 0,1602	No	ns	0.8575
12:phMut-MRT2-YFP + phasiR263-9 vs. 36:MRT2-YFP + phasiR263-9	0.002359	-0,2676 to 0,2723	No	ns	>0,9999
12:phMut-MRT2-YFP + phasiR263-9 vs. 36:phMut-MRT2-YFP + phasiR263-9	-0.07997	-0,2708 to 0,1109	No	ns	0.8346
12:phMut-MRT2-YFP + phasiR263-9 vs. 36:phMut-MRT2-YFP + phasiR825-5p	0.002285	-0,2677 to 0,2722	No	ns	>0,9999
12:phMut-MRT2-YFP + phasiR263-9 vs. 48:MRT2-YFP + miR319	-0.152	-0,4219 to 0,1180	No	ns	0.5171
12:phMut-MRT2-YFP + phasiR263-9 vs. 48:MRT2-YFP + phasiR263-9	-0.0399	-0,3098 to 0,2300	No	ns	>0,9999
12:phMut-MRT2-YFP + phasiR263-9 vs. 48:phMut-MRT2-YFP + phasiR263-9	-0.1222	-0,3131 to 0,06865	No	ns	0.3623
12:phMut-MRT2-YFP + phasiR263-9 vs. 48:phMut-MRT2-YFP + phasiR825-5p	-0.03997	-0,3099 to 0,2300	No	ns	>0,9999
12:phMut-MRT2-YFP + phasiR825-5p vs. 24:MRT2-YFP + miR319	-0.09543	-0,3654 to 0,1745	No	ns	0.9348
12:phMut-MRT2-YFP + phasiR825-5p vs. 24:MRT2-YFP + phasiR263-9	0.01663	-0,2533 to 0,2866	No	ns	>0,9999

12:phMut-MRT2-YFP + phasiR825-5p vs. 24:phMut-MRT2-YFP + phasiR263-9	-0.06569	-0,3356 to 0,2042	No	ns	0.9964
12:phMut-MRT2-YFP + phasiR825-5p vs. 24:phMut-MRT2-YFP + phasiR825-5p	0.01656	-0,1743 to 0,2074	No	ns	>0,9999
12:phMut-MRT2-YFP + phasiR825-5p vs. 36:MRT2-YFP + miR319	-0.192	-0,4619 to 0,07798	No	ns	0.2521
12:phMut-MRT2-YFP + phasiR825-5p vs. 36:MRT2-YFP + phasiR263-9	-0.07989	-0,3498 to 0,1900	No	ns	0.9811
12:phMut-MRT2-YFP + phasiR825-5p vs. 36:phMut-MRT2-YFP + phasiR263-9	-0.1622	-0,4322 to 0,1077	No	ns	0.437
12:phMut-MRT2-YFP + phasiR825-5p vs. 36:phMut-MRT2-YFP + phasiR825-5p	-0.07997	-0,2708 to 0,1109	No	ns	0.8346
12:phMut-MRT2-YFP + phasiR825-5p vs. 48:MRT2-YFP + miR319	-0.2342	-0,5042 to 0,03572	No	ns	0.106
12:phMut-MRT2-YFP + phasiR825-5p vs. 48:MRT2-YFP + phasiR263-9	-0.1221	-0,3921 to 0,1478	No	ns	0.7667
12:phMut-MRT2-YFP + phasiR825-5p vs. 48:phMut-MRT2-YFP + phasiR263-9	-0.2045	-0,4744 to 0,06546	No	ns	0.1963
12:phMut-MRT2-YFP + phasiR825-5p vs. 48:phMut-MRT2-YFP + phasiR825-5p	-0.1222	-0,3131 to 0,06865	No	ns	0.3623
24:MRT2-YFP + miR319 vs. 24:MRT2-YFP + phasiR263-9	0.1121	-0,07881 to 0,3029	No	ns	0.4654
24:MRT2-YFP + miR319 vs. 24:phMut-MRT2-YFP + phasiR263-9	0.02974	-0,1611 to 0,2206	No	ns	>0,9999
24:MRT2-YFP + miR319 vs. 24:phMut-MRT2-YFP + phasiR825-5p	0.112	-0,07888 to 0,3029	No	ns	0.4662
24:MRT2-YFP + miR319 vs. 36:MRT2-YFP + miR319	-0.09653	-0,2874 to 0,09435	No	ns	0.6471
24:MRT2-YFP + miR319 vs. 36:MRT2-YFP + phasiR263-9	0.01554	-0,2544 to 0,2855	No	ns	>0,9999
24:MRT2-YFP + miR319 vs. 36:phMut-MRT2-YFP + phasiR263-9	-0.06679	-0,3367 to 0,2032	No	ns	0.9958
24:MRT2-YFP + miR319 vs. 36:phMut-MRT2-YFP + phasiR825-5p	0.01547	-0,2545 to 0,2854	No	ns	>0,9999
24:MRT2-YFP + miR319 vs. 48:MRT2-YFP + miR319	-0.1388	-0,3297 to 0,05209	No	ns	0.2315
24:MRT2-YFP + miR319 vs. 48:MRT2-YFP + phasiR263-9	-0.02672	-0,2967 to 0,2432	No	ns	>0,9999
24:MRT2-YFP + miR319 vs. 48:phMut-MRT2-YFP + phasiR263-9	-0.109	-0,3790 to 0,1609	No	ns	0.8618
24:MRT2-YFP + miR319 vs. 48:phMut-MRT2-YFP + phasiR825-5p	-0.02679	-0,2967 to 0,2431	No	ns	>0,9999
24:MRT2-YFP + phasiR263-9 vs. 24:phMut-MRT2-YFP + phasiR263-9	-0.08233	-0,2732 to 0,1085	No	ns	0.8106
24:MRT2-YFP + phasiR263-9 vs. 24:phMut-MRT2-YFP + phasiR825-5p	-0.00007425	-0,1909 to 0,1908	No	ns	>0,9999

24:MRT2-YFP + phasiR263-9 vs. 36:MRT2-YFP + miR319	-0.2086	-0,4785 to 0,06135	No	ns	0.1805	
24:MRT2-YFP + phasiR263-9 vs. 36:MRT2-YFP + phasiR263-9	-0.09653	-0,2874 to 0,09435	No	ns	0.6471	
24:MRT2-YFP + phasiR263-9 vs. 36:phMut-MRT2-YFP + phasiR263-9	-0.1789	-0,4488 to 0,09109	No	ns	0.3243	
24:MRT2-YFP + phasiR263-9 vs. 36:phMut-MRT2-YFP + phasiR825-5p	-0.0966	-0,3665 to 0,1733	No	ns	0.9298	
24:MRT2-YFP + phasiR263-9 vs. 48:MRT2-YFP + miR319	-0.2508	-0,5208 to 0,01909	No	ns	0.0747	
24:MRT2-YFP + phasiR263-9 vs. 48:MRT2-YFP + phasiR263-9	-0.1388	-0,3297 to 0,05209	No	ns	0.2315	
24:MRT2-YFP + phasiR263-9 vs. 48:phMut-MRT2-YFP + phasiR263-9	-0.2211	-0,4910 to 0,04883	No	ns	0.1394	
24:MRT2-YFP + phasiR263-9 vs. 48:phMut-MRT2-YFP + phasiR825-5p	-0.1389	-0,4088 to 0,1311	No	ns	0.6271	
24:phMut-MRT2-YFP + phasiR263-9 vs. 24:phMut-MRT2-YFP + phasiR825-5p	0.08225	-0,1086 to 0,2731	No	ns	0.8114	
24:phMut-MRT2-YFP + phasiR263-9 vs. 36:MRT2-YFP + miR319	-0.1263	-0,3962 to 0,1437	No	ns	0.7334	
24:phMut-MRT2-YFP + phasiR263-9 vs. 36:MRT2-YFP + phasiR263-9	-0.0142	-0,2841 to 0,2557	No	ns	>0,9999	
24:phMut-MRT2-YFP + phasiR263-9 vs. 36:phMut-MRT2-YFP + phasiR263-9	-0.09653	-0,2874 to 0,09435	No	ns	0.6471	
24:phMut-MRT2-YFP + phasiR263-9 vs. 36:phMut-MRT2-YFP + phasiR825-5p	-0.01427	-0,2842 to 0,2557	No	ns	>0,9999	
24:phMut-MRT2-YFP + phasiR263-9 vs. 48:MRT2-YFP + miR319	-0.1685	-0,4385 to 0,1014	No	ns	0.3916	
24:phMut-MRT2-YFP + phasiR263-9 vs. 48:MRT2-YFP + phasiR263-9	-0.05646	-0,3264 to 0,2135	No	ns	0.9992	
24:phMut-MRT2-YFP + phasiR263-9 vs. 48:phMut-MRT2-YFP + phasiR263-9	-0.1388	-0,3297 to 0,05209	No	ns	0.2315	
24:phMut-MRT2-YFP + phasiR263-9 vs. 48:phMut-MRT2-YFP + phasiR825-5p	-0.05653	-0,3265 to 0,2134	No	ns	0.9992	
24:phMut-MRT2-YFP + phasiR825-5p vs. 36:MRT2-YFP + miR319	-0.2085	-0,4785 to 0,06142	No	ns	0.1808	
24:phMut-MRT2-YFP + phasiR825-5p vs. 36:MRT2-YFP + phasiR263-9	-0.09645	-0,3664 to 0,1735	No	ns	0.9304	
24:phMut-MRT2-YFP + phasiR825-5p vs. 36:phMut-MRT2-YFP + phasiR263-9	-0.1788	-0,4487 to 0,09116	No	ns	0.3247	
24:phMut-MRT2-YFP + phasiR825-5p vs. 36:phMut-MRT2-YFP + phasiR825-5p	-0.09653	-0,2874 to 0,09435	No	ns	0.6471	
24:phMut-MRT2-YFP + phasiR825-5p vs. 48:MRT2-YFP + miR319	-0.2508	-0,5207 to 0,01916	No	ns	0.0748	
24:phMut-MRT2-YFP + phasiR825-5p vs. 48:MRT2-YFP + phasiR263-9	-0.1387	-0,4086 to 0,1312	No	ns	0.6283	
24:phMut-MRT2-YFP + phasiR825-5p vs. 48:phMut-MRT2-YFP + phasiR263-9	-0.221	-0,4910 to 0,04890	No	ns	0.1396	

24:phMut-MRT2-YFP + phasiR825-5p vs. 48:phMut-MRT2-YFP + phasiR825-5p	-0.1388	-0,3297 to 0,05209	No	ns	0.2315	
36:MRT2-YFP + miR319 vs. 36:MRT2-YFP + phasiR263-9	0.1121	-0,07881 to 0,3029	No	ns	0.4654	
36:MRT2-YFP + miR319 vs. 36:phMut-MRT2-YFP + phasiR263-9	0.02974	-0,1611 to 0,2206	No	ns	>0,9999	
36:MRT2-YFP + miR319 vs. 36:phMut-MRT2-YFP + phasiR825-5p	0.112	-0,07888 to 0,3029	No	ns	0.4662	
36:MRT2-YFP + miR319 vs. 48:MRT2-YFP + miR319	-0.04225	-0,2331 to 0,1486	No	ns	0.9986	
36:MRT2-YFP + miR319 vs. 48:MRT2-YFP + phasiR263-9	0.06981	-0,2001 to 0,3398	No	ns	0.9938	
36:MRT2-YFP + miR319 vs. 48:phMut-MRT2-YFP + phasiR263-9	-0.01252	-0,2825 to 0,2574	No	ns	>0,9999	
36:MRT2-YFP + miR319 vs. 48:phMut-MRT2-YFP + phasiR825-5p	0.06974	-0,2002 to 0,3397	No	ns	0.9938	
36:MRT2-YFP + phasiR263-9 vs. 36:phMut-MRT2-YFP + phasiR263-9	-0.08233	-0,2732 to 0,1085	No	ns	0.8106	
36:MRT2-YFP + phasiR263-9 vs. 36:phMut-MRT2-YFP + phasiR825-5p	-0.00007425	-0,1909 to 0,1908	No	ns	>0,9999	
36:MRT2-YFP + phasiR263-9 vs. 48:MRT2-YFP + miR319	-0.1543	-0,4243 to 0,1156	No	ns	0.4981	
36:MRT2-YFP + phasiR263-9 vs. 48:MRT2-YFP + phasiR263-9	-0.04226	-0,2331 to 0,1486	No	ns	0.9986	
36:MRT2-YFP + phasiR263-9 vs. 48:phMut-MRT2-YFP + phasiR263-9	-0.1246	-0,3945 to 0,1454	No	ns	0.7472	
36:MRT2-YFP + phasiR263-9 vs. 48:phMut-MRT2-YFP + phasiR825-5p	-0.04233	-0,3123 to 0,2276	No	ns	>0,9999	
36:phMut-MRT2-YFP + phasiR263-9 vs. 36:phMut-MRT2-YFP + phasiR825-5p	0.08225	-0,1086 to 0,2731	No	ns	0.8114	
36:phMut-MRT2-YFP + phasiR263-9 vs. 48:MRT2-YFP + miR319	-0.072	-0,3419 to 0,1979	No	ns	0.9919	
36:phMut-MRT2-YFP + phasiR263-9 vs. 48:MRT2-YFP + phasiR263-9	0.04007	-0,2299 to 0,3100	No	ns	>0,9999	
36:phMut-MRT2-YFP + phasiR263-9 vs. 48:phMut-MRT2-YFP + phasiR263-9	-0.04226	-0,2331 to 0,1486	No	ns	0.9986	
36:phMut-MRT2-YFP + phasiR263-9 vs. 48:phMut-MRT2-YFP + phasiR825-5p	0.04	-0,2299 to 0,3099	No	ns	>0,9999	
36:phMut-MRT2-YFP + phasiR825-5p vs. 48:MRT2-YFP + miR319	-0.1542	-0,4242 to 0,1157	No	ns	0.4987	
36:phMut-MRT2-YFP + phasiR825-5p vs. 48:MRT2-YFP + phasiR263-9	-0.04218	-0,3121 to 0,2278	No	ns	>0,9999	
36:phMut-MRT2-YFP + phasiR825-5p vs. 48:phMut-MRT2-YFP + phasiR263-9	-0.1245	-0,3944 to 0,1454	No	ns	0.7478	
36:phMut-MRT2-YFP + phasiR825-5p vs. 48:phMut-MRT2-YFP + phasiR825-5p	-0.04226	-0,2331 to 0,1486	No	ns	0.9986	

48:MRT2-YFP + miR319 vs. 48:MRT2-YFP + phasiR263-9	0.1121	-0,07881 to 0,3029	No	ns	0.4654	
48:MRT2-YFP + miR319 vs. 48:phMut-MRT2-YFP + phasiR263-9	0.02974	-0,1611 to 0,2206	No	ns	>0,9999	
48:MRT2-YFP + miR319 vs. 48:phMut-MRT2-YFP + phasiR825-5p	0.112	-0,07888 to 0,3029	No	ns	0.4662	
48:MRT2-YFP + phasiR263-9 vs. 48:phMut-MRT2-YFP + phasiR263-9	-0.08233	-0,2732 to 0,1085	No	ns	0.8106	
48:MRT2-YFP + phasiR263-9 vs. 48:phMut-MRT2-YFP + phasiR825-5p	-0.00007425	-0,1909 to 0,1908	No	ns	>0,9999	
48:phMut-MRT2-YFP + phasiR263-9 vs. 48:phMut-MRT2-YFP + phasiR825-5p	0.08225	-0,1086 to 0,2731	No	ns	0.8114	

Annexed table 10. Statistics comparison of fluorescence constructs in *N. benthamiana* plants co-expressing them alone or with phasiRNAs. Data are mean ± SE.

Abdelmaksoud EM, El-Refai SA, Mahmoud KW, Ragab ME. **2020**. Susceptibility of some new strawberry genotypes to infestation by western flower thrips, *Frankliniella occidentalis* (Pergande) (Thysanoptera: Thripidae) in the nursery. *Annals of Agricultural Sciences* **65**: 144–148.

Acevedo FE, Rivera-Vega LJ, Chung SH, Ray S, Felton GW. **2015**. Cues from chewing insects - the intersection of DAMPs, HAMPs, MAMPs and effectors. *Current Opinion in Plant Biology* **26**: 80–86.

Adachi H, Contreras M, Harant A, Wu CH, Derevnina L, Sakai T, Duggan C, Moratto E, Bozkurt TO, Maqbool A, *et al.* 2019. An N-terminal motif in NLR immune receptors is functionally conserved across distantly related plant species. *eLife* **8**: 1–31.

Ågren GI, Stenberg JA, Björkman C. **2012**. Omnivores as plant bodyguards-A model of the importance of plant quality. *Basic and Applied Ecology* **13**: 441–448.

Agut B, Gamir J, Jacas JA, Hurtado M, Flors V. **2014**. Different metabolic and genetic responses in citrus may explain relative susceptibility to *Tetranychus urticae*. *Pest Management Science* **70**: 1728–1741.

Ahmad S, Veyrat N, Gordon-Weeks R, Zhang Y, Martin J, Smart L, Glauser G, Erb M, Flors V, Frey M, et al. 2011. Benzoxazinoid metabolites regulate innate immunity against aphids and fungi in maize. *Plant Physiology* **157**: 317–327.

Alderton WK, Cooper CE, Knowles RG. **2001**. Nitric oxide synthases: structure, function and inhibition. *Biochemical Journal* **357**: 593–615.

Ali R, Ma W, Lemtiri-Chlieh F, Tsaltas D, Leng Q, von Bodman S, Berkowitz GA. **2007**. Death don't Have no mercy and Neither does calcium: Arabidopsis CYCLIC NUCLEOTIDE GATED CHANNEL2 and innate immunity. *The Plant Cell* **19**: 1081–1095.

Ament K, Kant MR, Sabelis MW, Haring MA, Schuurink RC. **2004**. Jasmonic acid is a key regulator of spider mite-induced volatile terpenoid and methyl salicylate emission in tomato. *Plant Physiology* **135**: 2025–2037.

Arasimowicz-Jelonek M, Floryszak-Wieczorek J. **2019**. A physiological perspective on targets of nitration in NO-based signaling networks in plants. *Journal of Experimental Botany* **70**: 4379–4389.

Ariga H, Katori T, Tsuchimatsu T, Hirase T, Tajima Y, Parker JE, Alcázar R, Koornneef M, Hoekenga O, Lipka AE, *et al.* 2017. NLR locus-mediated trade-off between abiotic and biotic stress adaptation in Arabidopsis. *Nature Plants* **3**: 17072.

Arimura G, Köpke S, Kunert M, Volpe V, David A, Brand P, Dabrowska P, Maffei ME, Boland W. **2008**. Effects of feeding *Spodoptera littoralis* on lima bean leaves: Diurnal and nocturnal damage differentially initiate plant volatile emission. *Plant Physiology* **146**: 965–973.

Arnaiz A, Martinez M, Gonzalez-Melendi P, Grbic V, Diaz I, Santamaria ME. **2019**. Plant

defenses against pests driven by a bidirectional promoter. *Frontiers in Plant Science* **10**: 1–16.

Arnaiz A, Romero-Puertas MC, Santamaria ME, Rosa-Diaz I, Arbona V, Muñoz A, Grbic V, González-Melendi P, Mar Castellano M, Sandalio LM, *et al.* 2023. The Arabidopsis thioredoxin TRXh5 regulates the S-nitrosylation pattern of the TIRK receptor being both proteins essential in the modulation of defences to Tetranychus urticae. *Redox Biology* **67**: 102902

Arnaiz A, Rosa-Diaz I, Romero-Puertas MC, Sandalio LM, Diaz I. **2021**. Nitric oxide, an essential intermediate in the plant–herbivore interaction. *Frontiers in Plant Science* **11:** 620086.

Arnaiz A, Santamaria ME, Rosa-Diaz I, Garcia I, Dixit S, Vallejos S, Gotor C, Martinez M, Grbic V, Diaz I. **2022**. Hydroxynitrile lyase defends Arabidopsis against *Tetranychus urticae*. *Plant Physiology* **189**: 2244–2258.

Arnaiz A, Talavera-Mateo L, Gonzalez-Melendi P, Martinez M, Diaz I, Santamaria ME. **2018**. Arabidopsis kunitz trypsin inhibitors in defense against spider mites. *Frontiers in Plant Science* **9**: 1–16.

Aroca A, Gotor C, Romero LC. **2018**. Hydrogen sulfide signaling in plants: emerging roles of protein persulfidation. *Frontiers in Plant Science* **9**: 1–8.

Astier J, Gross I, Durner J. **2018**. Nitric oxide production in plants: an update. *Journal of Experimental Botany* **69**: 3401–3411.

Astier J, Mounier A, Santolini J, Jeandroz S, Wendehenne D. **2019**. The evolution of nitric oxide signalling diverges between animal and green lineages. *Journal of Experimental Botany* **70**: 4355–4364.

Ballaré CL. **2011**. Jasmonate-induced defenses: A tale of intelligence, collaborators and rascals. *Trends in Plant Science* **16**: 249–257.

Barah P, Bones AM. 2015. Multidimensional approaches for studying plant defence against insects: from ecology to omics and synthetic biology. *Journal of Experimental Botany* **66**: 479–493.

Baudin M, Hassan JA, Schreiber KJ, Lewis JD. **2017**. Analysis of the ZAR1 immune complex reveals determinants for immunity and molecular interactions. *Plant Physiology* **174**: 2038–2053.

Becana M, Yruela I, Sarath G, Catalán P, Hargrove MS. **2020**. Plant hemoglobins: a journey from unicellular green algae to vascular plants. *New Phytologist* **227**: 1618–1635.

Bensoussan N, Santamaria ME, Zhurov V, Diaz I, Grbić M, Grbić V. **2016**. Plant-herbivore interaction: dissection of the cellular pattern of *Tetranychus urticae* feeding on the host plant. *Frontiers in Plant Science* **7**: 1–13.

Bethke PC, Badger MR, Jones RL. **2004**. Apoplastic synthesis of nitric oxide by plant tissues. *The Plant Cell* **16**: 332–341.

Bi G, Su M, Li N, Liang Y, Dang S, Xu J, Hu M, Wang J, Zou M, Deng Y, *et al.* 2021. The ZAR1 resistosome is a calcium-permeable channel triggering plant immune signaling. *Cell* **184**: 3528-3541.e12.

Bi J, Wang YF. **2020**. The effect of the endosymbiont *Wolbachia* on the behavior of insect hosts. *Insect Science* **27**: 846–858.

Bigeard J, Colcombet J, Hirt H. **2015**. Signalling mechanisms in Pattern-Triggered Immunity (PTI). *Molecular Plant* **8**: 521–539.

Bjornson M, Pimprikar P, Nürnberger T, Zipfel C. **2021**. The transcriptional landscape of *Arabidopsis thaliana* pattern-triggered immunity. *Nature Plants* **7**: 579–586.

Bonaventure G. **2011**. The *Nicotiana attenuata* LECTIN RECEPTOR KINASE 1 is involved in the perception of insect feeding. *Plant Signaling and Behavior* **6**: 2060–2063.

Boutrot F, Zipfel C. **2017**. Function, discovery, and exploitation of plant pattern ecognition receptors for broad-spectrum disease resistance. *Annual Review of Phytopathology* **55**: 257–286.

Brant EJ, Budak H. **2018**. Plant small non-coding RNAs and their roles in biotic stresses. *Frontiers in Plant Science* **9:** 1038.

Bricchi I, Leitner M, Foti M, Mithöfer A, Boland W, Maffei ME. **2010**. Robotic mechanical wounding (MecWorm) versus herbivore-induced responses: early signaling and volatile emission in Lima bean (*Phaseolus lunatus L*.). *Planta* **232**: 719–729.

Bruckhoff V, Haroth S, Feussner K, König S, Brodhun F, Feussner I. **2016**. Functional characterization of CYP94-genes and identification of a novel jasmonate catabolite in flowers. *PLoS ONE* **11**: 1–26.

Brutus A, Sicilia F, Macone A, Cervone F, De Lorenzo G. **2010**. A domain swap approach reveals a role of the plant wall-associated kinase 1 (WAK1) as a receptor of oligogalacturonides. *Proceedings of the National Academy of Sciences of the United States of America* **107**: 9452–9457.

Burch-Smith TM, Dinesh-Kumar SP. **2007**. The functions of plant TIR domains. *Science's STKE* **2007**: 46-46.

Caarls L, Bassetti N, Verbaarschot P, Mumm R, van Loon JJA, Schranz ME, Fatouros NE. **2023**. Hypersensitive-like response in Brassica plants is specifically induced by molecules from egg-associated secretions of cabbage white butterflies . *Frontiers in Ecology and Evolution* **10:** 1070859.

Caarls L, Elberse J, Awwanah M, Ludwig NR, De Vries M, Zeilmaker T, Van Wees SCM, Schuurink RC, Van den Ackerveken G. **2017**. Arabidopsis JASMONATE-INDUCED OXYGENASES down-regulate plant immunity by hydroxylation and inactivation of the hormone jasmonic acid. *Proceedings of the National Academy of Sciences of the United States of America* **114**: 6388–6393.

Campbell SA, Vallano DM. **2018**. Plant defences mediate interactions between herbivory and the direct foliar uptake of atmospheric reactive nitrogen. *Nature*

Communications **9**: 4743.
Campbell WH. **2001**. Structure and function of eukaryotic NAD(P)H: Nitrate reductase. *Cellular and Molecular Life Sciences CMLS* **58**: 194–204.
Campos ML, De Almeida M, Rossi ML, Martinelli AP, Litholdo Junior CG, Figueira A, Rampelotti-Ferreira FT, Vendramim JD, Benedito VA, Pereira Peres LE. **2009**. Brassinosteroids interact negatively with jasmonates in the formation of anti-herbivory traits in tomato. *Journal of Experimental Botany* **60**: 4347–4361.
Cantu-Medellin N, Kelley EE. **2013**. Xanthine oxidoreductase-catalyzed reduction of nitrite to nitric oxide: Insights regarding where, when and how. *Nitric Oxide* **34**: 19–26.
Cejudo FJ, Sandalio LM, Van Breusegem F. **2021**. Understanding plant responses to stress conditions: Redox-based strategies. *Journal of Experimental Botany* **72**: 5785–5788.
Cesari S. **2018**. Multiple strategies for pathogen perception by plant immune receptors. *New Phytologist* **219**: 17–24.
Chen YH, Gols R, Benrey B. **2015**. Crop domestication and its impact on naturally selected trophic interactions. *Annual Review of Entomology* **60**: 35–58.
Cheng X, Wu Y, Guo J, Du B, Chen R, Zhu L, He G. **2013**. A rice lectin receptor-like kinase that is involved in innate immune responses also contributes to seed germination. *Plant Journal* **76**: 687–698.
Cheng YT, Li Y, Huang S, Huang Y, Dong X, Zhang Y, Li X. **2011**. Stability of plant immune-receptor resistance proteins is controlled by SKP1-CULLIN1-F-box (SCF)-mediated protein degradation. *Proceedings of the National Academy of Sciences of the United States of America* **108**: 14694–14699.
Chiang Y-H, Coaker G. 2015. Effector triggered mmunity: NLR immune perception and downstream defense responses. *The Arabidopsis Book 2015.*
Chinchilla D, Zipfel C, Robatzek S, Kemmerling B, Nürnberger T, Jones JDG, Felix G, Boller T. **2007**. A flagellin-induced complex of the receptor FLS2 and BAK1 initiates plant defence. *Nature* **448**: 497–500.
Choi J, Tanaka K, Cao Y, Qi Y, Qiu J, Liang Y, Lee SY, Stacey G. **2014**. Identification of a Plant Receptor for Extracellular ATP. *Science* **343**: 290–294.
Chowdhury MR, Ahamed MS, Mas-ud MA, Islam H, Fatamatuzzohora M, Hossain MF, Billah M, Hossain MS, Matin MN. **2021**. Stomatal development and genetic expression in *Arabidopsis thaliana* L. *Heliyon* **7**: e07889.
Clotuche G, Mailleux AC, Fernández Astudillo A, Deneubourg JL, Detrain C, Hance T. **2011**. The formation of collective silk balls in the spider mite *Tetranychus urticae* Koch. *PLoS ONE* **6:** 18854.
Contreras E, Martinez M. **2022**. Comparative and evolutionary analysis of Arabidopsis RIN4-like/NOI proteins induced by herbivory. *PLoS ONE* **17**: 1–18.
Corpas FJ, González-Gordo S, Palma JM. **2020**. Plant peroxisomes: A factory of reactive

species. *Frontiers in Plant Science* **11**: 1–12.

Correa-Aragunde N, Cejudo FJ, Lamattina L. **2015**. Nitric oxide is required for the auxin-induced activation of NADPH-dependent thioredoxin reductase and protein denitrosylation during root growth responses in arabidopsis. *Annals of Botany* **116**: 695–702.

Cui B, Pan Q, Clarke D, Villarreal MO, Umbreen S, Yuan B, Shan W, Jiang J, Loake GJ. **2018**. S-nitrosylation of the zinc finger protein SRG1 regulates plant immunity. *Nature Communications* **9**: 4226.

Dangl JL, Jones JDG. **2001**. Plant pathogens and integrated defence responses to infection. *Nature* **411**: 826–833.

De Ollas C, González-Guzmán M, Pitarch Z, Matus JT, Candela H, Rambla JL, Granell A, Gómez-Cadenas A, Arbona V. 2021. Identification of ABA-mediated genetic and metabolic responses to soil flooding in tomato (*Solanum lycopersicum L. Mill). Frontiers in Plant Science* **12**: 1–20.

DeClerck RA, Steeves TA. **1988**. Oviposition of the gall midge *Cystiphora sonchi* (Bremi) (Diptera: Cecidomyiidae) via the stomata of perennial sowthistle (*Sonchus arvensis L*.). *The Canadian Entomologist* **120**: 189–193.

Delgado C, Mora-Poblete F, Ahmar S, Chen J-T, Figueroa CR. **2021**. Jasmonates and plant salt stress: Molecular players, physiological effects, and improving tolerance by using genome-associated tools. *International Journal of Molecular Sciences* **22:** 3082.

Delledonne M. **2005**. NO news is good news for plants. *Current Opinion in Plant Biology* **8**: 390–396.

Dicke M, van Loon JJA. **2014**. Chemical ecology of phytohormones: How plants integrate responses to complex and dynamic environments. *Journal of Chemical Ecology* **40**: 653–656.

Dinh ST, Baldwin IT, Galis I. **2013**. The HERBIVORE ELICITOR-REGULATED1 gene enhances abscisic acid levels and defenses against herbivores in *Nicotiana attenuata* plants. *Plant Physiology* **162**: 2106–2124.

Dixit S, Widemann E, Bensoussan N, Salehipourshirazi G, Bruinsma K, Milojevic M, Shukla A, Romero LC, Zhurov V, Bernards MA, *et al.* 2022. β-Cyanoalanine synthase protects mites against Arabidopsis defenses. *Plant Physiology* **189**: 1961–1975.

Douglas AE. **2018**. Strategies for enhanced crop resistance to insect pests. *Annual Review of Plant Biology* **69**: 637–660.

Duan G, Walther D. **2015**. The roles of post-translational modifications in the context of protein interaction networks. *PLoS Computational Biology* **11**: 1–23.

Duxbury Z, Wu CH, DIng P. **2021**. A comparative overview of the intracellular guardians of plants and animals: NLRs in innate immunity and beyond. *Annual Review of Plant Biology* **72**: 155–184.

Eigenbrode SD, White C, Rohde M, Simon CJ. **1998**. Behavior and effectiveness of adult

Hippodamia convergens (Coleoptera: Coccinellidae) as a predator of *Acyrthosiphon pisum* (Homoptera: Aphididae) on a wax mutant of *Pisum sativum*. *Environmental Entomology* **27**: 902–909.

Endo A, Sawada Y, Takahashi H, Okamoto M, Ikegami K, Koiwai H, Seo M, Toyomasu T, Mitsuhashi W, Shinozaki K, *et al.* 2008. Drought induction of Arabidopsis 9-cis-epoxycarotenoid dioxygenase occurs in vascular parenchyma cells. *Plant Physiology* **147**: 1984–1993.

Erb M, Flors V, Karlen D, De Lange E, Planchamp C, D'Alessandro M, Turlings TCJ, Ton J. **2009**. Signal signature of aboveground-induced resistance upon belowground herbivory in maize. *Plant Journal* **59**: 292–302.

Erb M, Meldau S, Howe GA. **2012**. Role of phytohormones in insect-specific plant reactions. *Trends in Plant Science* **17**: 250–259.

Erb M, Reymond P. **2019**. Molecular interactions between plants and insect herbivores. *Annual Review of Plant Biology* **70**: 527–557.

Fan W, Dong X. **2002**. In Vivo interaction between NPR1 and transcription factor TGA2 leads to salicylic acid-mediated gene activation in arabidopsis. *The Plant Cell* **14**: 1377–1389.

Fancy NN, Bahlmann AK, Loake GJ. **2017**. Nitric oxide function in plant abiotic stress. *The Plant Cell and Environment* **40**: 462–472.

Figueiredo AST, Resende JTV, Morales RGF, Gonçalves APS, da Silva PR. **2013**. The role of glandular and non-glandular trichomes in the negative interactions between strawberry cultivars and spider mite. *Arthropod-Plant Interactions* **7**: 53–58.

Floris M, Mahgoub H, Lanet E, Robaglia C, Menand B. **2009**. Post-transcriptional regulation of gene expression in plants during abiotic stress. *International Journal of Molecular Sciences* **10**: 3168–3185.

Förderer A, Yu D, Li E, Chai J. **2022**. Resistosomes at the interface of pathogens and plants. *Current Opinion in Plant Biology* **67**: 102212.

Foresi N, Mayta ML, Lodeyro AF, Scuffi D, Correa-Aragunde N, García-Mata C, Casalongué C, Carrillo N, Lamattina L. **2015**. Expression of the tetrahydrofolate-dependent nitric oxide synthase from the green alga *Ostreococcus tauri* increases tolerance to abiotic stresses and influences stomatal development in Arabidopsis. *Plant Journal* **82**: 806–821.

Foyer CH, Noctor G. **2005**. Redox homeostasis and antioxidant signalling: A metabolic interface between stress perception and physiological responses. *The Plant Cell* **17**: 1866–1875.

Fujino M. **1967**. Role of adenosinetriphosphate and adenosinetriphosphatase in stomatal movement. *Sci. Bull. Fac. Educ. Nagasaki Univ.* **18:** 1

Fürstenberg-Hägg J, Zagrobelny M, Bak S. **2013**. Plant defense against insect herbivores. *International Journal of Molecular Sciences* **14**: 10242–10297.

Garcia A, Martinez M, Diaz I, Santamaria ME. **2021a**. The price of the induced defense against pests: A meta-analysis. *Frontiers in Plant Science* **11**: 1–15.
Garcia A, Santamaria ME, Diaz I, Martinez M. **2021b**. Disentangling transcriptional responses in plant defense against arthropod herbivores. *Scientific Reports* **11**: 1–15.
Garcia A, Talavera-Mateo L, Santamaria ME. **2022**. An automatic method to quantify trichomes in *Arabidopsis thaliana*. *Plant Science* **323**: 111391.
Ge Y, Han J, Zhou G, Xu Y, Ding Y, Shi M, Guo C, Wu G. **2018**. Silencing of miR156 confers enhanced resistance to brown planthopper in rice. *Planta* **248**: 813–826.
Gilardoni PA, Hettenhausen C, Baldwin IT, Gilardoni PA, Hettenhausen C, Baldwin IT, Bonaventure G. **2023**. Nicotiana attenuate LECTIN RECEPTOR KINASE1 suppresses the insect-mediated inhibition of induced defense responses during *Manduca sexta* herbivory. *The Plant Cell* **23**: 3512–3532.
Giles GI, Nasim MJ, Ali W, Jacob C. **2017**. The reactive sulfur species concept: 15 years on. *Antioxidants* **6**: 1–29.
Gilroy E, Breen S. **2022**. Interplay between phytohormone signalling pathways in plant defence other than salicylic acid and jasmonic acid. *Essays in Biochemistry* **66**: 657–671.
Gómez-Gómez L, Boller T. **2000**. FLS2: An LRR receptor-like kinase involved in the perception of the bacterial elicitor flagellin in Arabidopsis. *Molecular Cell* **5**: 1003–1011.
Gomez-Sanchez A, Gonzalez-Melendi P, Santamaria ME, Arbona V, Lopez-Gonzalvez A, Garcia A, Hensel G, Kumlehn J, Martinez M, Diaz I. **2019**. Repression of drought-induced cysteine-protease genes alters barley leaf structure and responses to abiotic and biotic stresses. *Journal of Experimental Botany* **70**: 2143–2155.
González-Guzmán M, Apostolova N, Bellés JM, Barrero JM, Piqueras P, Ponce MR, Micol JL, Serrano R, Rodríguez PL. **2002**. The short-chain alcohol dehydrogenase ABA2 catalyzes the conversion of xanthoxin to abscisic aldehyde. *The Plant Cell* **14**: 1833–1846.
Gonzalez-Guzman M, Pizzio GA, Antoni R, Vera-Sirera F, Merilo E, Bassel GW, Fernández MA, Holdsworth MJ, Perez-Amador MA, Kollist H, *et al.* 2012. Arabidopsis PYR/PYL/RCAR receptors play a major role in quantitative regulation of stomatal aperture and transcriptional response to abscisic acid. *The Plant Cell* **24**: 2483–2496.
Gotor C, García I, Aroca Á, Laureano-Marín AM, Arenas-Alfonseca L, Jurado-Flores A, Moreno I, Romero LC. 2019. Signalling by hydrogen sulfide and cyanide through post-translational modification. *Journal of Experimental Botany* **70**: 4251–4265.
Graham J, Hackett CA, Smith K, Karley AJ, Mitchell C, Roberts H, O'Neill T. **2014**. Genetic and environmental regulation of plant architectural traits and opportunities for pest control in raspberry. *Annals of Applied Biology* **165**: 318–328.
Grant MR, Godiard L, Straube E, Ashfield T, Lewald J, Sattler A, Innes RW, Dangl JL. **1995**. Structure of the Arabidopsis RPM1 gene enabling dual specificity disease resistance. *Science* **269**: 843–846.

Grbić M, Van Leeuwen T, Clark RM, Rombauts S, Rouzé P, Grbić V, Osborne EJ, Dermauw W, Ngoc PCT, Ortego F, *et al.* 2011. The genome of *Tetranychus urticae* reveals herbivorous pest adaptations. *Nature* **479**: 487–492.

Griebel A, Peters JMR, Metzen D, Maier C, Barton CVM, Speckman HN, Boer MM, Nolan RH, Choat B, Pendall E. **2022**. Tapping into the physiological responses to mistletoe infection during heat and drought stress. *Tree Physiology* **42**: 523–536.

Groux R, Stahl E, Gouhier-Darimont C, Kerdaffrec E, Jimenez-Sandoval P, Santiago J, Reymond P. **2021**. Arabidopsis natural variation in insect egg-induced cell death reveals a role for LECTIN RECEPTOR KINASE-I.1. *Plant Physiology* **185**: 240–255.

Gupta KJ, Fernie AR, Kaiser WM, van Dongen JT. **2011**. On the origins of nitric oxide. *Trends in Plant Science* **16**: 160–168.

Han WH, Wang JX, Zhang F Bin, Liu YX, Wu H, Wang XW. **2022**. Small RNA and degradome sequencing reveal important microRNA function in *Nicotiana tabacum* response to *Bemisia tabaci*. *Genes* **13:** 361.

Hancock JT. **2019**. Hydrogen sulfide and environmental stresses. *Environmental and Experimental Botany* **161**: 50–56.

Hara K, Yokoo T, Kajita R, Onishi T, Yahata S, Peterson KM, Torii KU, Kakimoto T. **2009**. Epidermal cell density is autoregulated via a secretory peptide, EPIDERMAL PATTERNING FACTOR 2 in arabidopsis leaves. *Plant and Cell Physiology* **50**: 1019–1031.

Heitz T, Widemann E, Lugan R, Miesch L, Ullmann P, Désaubry L, Holder E, Grausem B, Kandel S, Miesch M, *et al.* 2012. Cytochromes P450 CYP94C1 and CYP94B3 catalyze two successive oxidation steps of plant hormone jasmonoyl-isoleucine for catabolic turnover. *Journal of Biological Chemistry* **287**: 6296–6306.

Hepworth C, Doheny-Adams T, Hunt L, Cameron DD, Gray JE. **2015**. Manipulating stomatal density enhances drought tolerance without deleterious effect on nutrient uptake. *New Phytologist* **208**: 336–341.

Hilker M, Meiners T. **2010**. How do plants “notice” attack by herbivorous arthropods? *Biological Reviews* **85**: 267–280.

Hillwig MS, Chiozza M, Casteel CL, Lau ST, Hohenstein J, Hernández E, Jander G, Macintosh GC. **2016**. Abscisic acid deficiency increases defence responses against *Myzus persicae* in Arabidopsis. *Molecular Plant Pathology* **17**: 225–235.

Hooper CM, Castleden IR, Tanz SK, Aryamanesh N, Millar AH. **2017**. SUBA4: the interactive data analysis centre for Arabidopsis subcellular protein locations. *Nucleic Acids Research* **45**: D1064–D1074.

Hou S, Liu Z, Shen H, Wu D. **2019**. Damage-associated molecular pattern-triggered immunity in plants. *Frontiers in Plant Science* **10:** 00646.

Hu L, Ye M, Kuai P, Ye M, Erb M, Lou Y. **2018**. OsLRR-RLK1, an early responsive leucine-rich repeat receptor-like kinase, initiates rice defense responses against a chewing herbivore. *New Phytologist* **219**: 1097–1111.

Hunt L, Bailey KJ, Gray JE. **2010**. The signalling peptide EPFL9 is a positive regulator of stomatal development. *New Phytologist* **186**: 609–614.

Ischiropoulos H, Al-Mehdi AB. **1995**. Peroxynitrite-mediated oxidative protein modifications. *FEBS Letters* **364**: 279–282.

Jeandroz S, Wipf D, Stuehr DJ, Lamattina L, Melkonian M, Tian Z, Zhu Y, Carpenter EJ, Wong GK-S, Wendehenne D. **2016**. Occurrence, structure, and evolution of nitric oxide synthase–like proteins in the plant kingdom. *Science Signaling* **9**: re2–re2.

Ji C, Ji Z, Liu B, Cheng H, Liu H, Liu S, Yang B, Chen G. **2020**. Xa1 Allelic R genes activate rice blight resistance suppressed by interfering TAL effectors. *Plant Communications* **1**: 100087.

Jing T, Du W, Gao T, Wu Y, Zhang N, Zhao M, Jin J, Wang J, Schwab W, Wan X, *et al.* 2021. Herbivore-induced DMNT catalyzed by CYP82D47 plays an important role in the induction of JA-dependent herbivore resistance of neighboring tea plants. The *Plant Cell and Environment* **44**: 1178–1191.

Jing T, Du W, Gao T, Wu Y, Zhang N, Zhao M, Jin J, Wang J, Schwab W, Wan X, et al. 2021. Herbivore-induced DMNT catalyzed by CYP82D47 plays an important role in the induction of JA-dependent herbivore resistance of neighboring tea plants. *Plant Cell and Environment* **44**: 1178–1191.

Jones JDG, Dangl JL. **2006**. The plant immune system. *Nature* **444**: 323–329.

Jubic LM, Saile S, Furzer OJ, El Kasmi F, Dangl JL. **2019**. Help wanted: helper NLRs and plant immune responses. *Current Opinion in Plant Biology* **50**: 82–94.

Jung SC, Martinez-Medina A, Lopez-Raez JA, Pozo MJ. **2012**. Mycorrhiza-induced resistance and priming of plant defenses. *Journal of Chemical Ecology* **38**: 651–664.

Kant MR, Sabelis MW, Haring MA, Schuurink RC. **2008**. Intraspecific variation in a generalist herbivore accounts for differential induction and impact of host plant defences. *Proceedings of the Royal Society B: Biological Sciences* **275**: 443–452.

Kant MR, Schuurink RC. **2021**. Life stage-dependent genetic traits as drivers of plant–herbivore interactions. *Current Opinion in Biotechnology* **70**: 234–240.

Karasov TL, Chae E, Herman JJ, Bergelson J. **2017**. Mechanisms to mitigate the trade-off between growth and defense. *The Plant Cell* **29**: 666–680.

Karley AJ, Mitchell C, Brookes C, McNicol J, O'Neill T, Roberts H, Graham J, Johnson SN. **2016**. Exploiting physical defence traits for crop protection: Leaf trichomes of *Rubus idaeus* have deterrent effects on spider mites but not aphids. *Annals of Applied Biology* **168**: 159–172.

Kaur P, Handa N, Verma V, Bakshi P, Kalia R, Sareen S, Nagpal A, Vig AP, Mir BA, Bhardwaj R. **2019**. Cross talk among reactive oxygen, nitrogen and sulfur during abiotic stress in plants. *Reactive Oxygen, Nitrogen and Sulfur Species in Plants* **2**: 857–871.

Keisham M, Jain P, Singh N, von Toerne C, Bhatla SC, Lindermayr C. **2019**. Deciphering the nitric oxide, cyanide and iron-mediated actions of sodium nitroprusside in

cotyledons of salt stressed sunflower seedlings. *Nitric Oxide* **88**: 10–26.
Koo AJK, Cooke TF, Howe GA. **2011**. Cytochrome P450 CYP94B3 mediates catabolism and inactivation of the plant hormone jasmonoyl-L-isoleucine. *Proceedings of the National Academy of Sciences of the United States of America* **108**: 9298–9303.
Kumar K, Mandal SN, Neelam K, de los Reyes BG. **2022**. MicroRNA-mediated host defense mechanisms against pathogens and herbivores in rice: balancing gains from genetic resistance with trade-offs to productivity potential. *BMC Plant Biology* **22**: 351.
Kuo YW, Lin JS, Li YC, Jhu MY, King YC, Jeng ST. **2019**. MicroR408 regulates defense response upon wounding in sweet potato. *Journal of Experimental Botany* **70**: 469–483.
Kuromori T, Seo M, Shinozaki K. **2018a**. ABA transport and plant water stress responses. *Trends in Plant Science* **23**: 513–522.
Kuromori T, Seo M, Shinozaki K. **2018b**. ABA transport and plant water stress responses. *Trends in Plant Science* **23**: 513–522.
Kutschera A, Dawid C, Gisch N, Schmid C, Raasch L, Gerster T, Schäffer M, Smakowska-Luzan E, Belkhadir Y, Vlot AC, *et al.* 2019. Bacterial medium-chain 3-hydroxy fatty acid metabolites trigger immunity in Arabidopsis plants. *Science* **364**: 178–181.
Lai Y, Eulgem T. **2018**. Transcript-level expression control of plant NLR genes. *Molecular Plant Pathology* **19**: 1267–1281.
Lapin D, Kovacova V, Sun X, Dongus JA, Bhandari D, Von Born P, Bautor J, Guarneri N, Rzemieniewski J, Stuttmann J, *et al.* 2019. A coevolved EDS1-SAG101-NRG1 module mediates cell death signaling by TIR-domain immune receptors. *The Plant Cell* **31**: 2430–2455.
Lawrence SD, Novak NG, Ju CJT, Cooke JEK. **2008**. Potato, Solanum tuberosum, defense against Colorado potato beetle, *Leptinotarsa Decemlineata* (Say): Microarray gene expression profiling of potato by Colorado potato beetle regurgitant treatment of wounded leaves. *Journal of Chemical Ecology* **34**: 1013–1025.
Le Roux C, Huet G, Jauneau A, Camborde L, Trémousaygue D, Kraut A, Zhou B, Levaillant M, Adachi H, Yoshioka H, *et al.* 2015. A receptor pair with an integrated decoy converts pathogen disabling of transcription factors to immunity. *Cell* **161**: 1074–1088.
León J, Costa-Broseta Á. **2020**. Present knowledge and controversies, deficiencies, and misconceptions on nitric oxide synthesis, sensing, and signaling in plants. *The Plant Cell and Environment* **43**: 1–15.
Lewis JD, Wu R, Guttman DS, Desveaux D. **2010**. Allele-specific virulence attenuation of the *Pseudomonas syringae* HopZ1a type III effector via the Arabidopsis ZAR1 resistance protein. *PLoS Genetics* **6**: 1–13.
Li J, Huang H, Zhu M, Huang S, Zhang W, Dinesh-Kumar SP, Tao X. **2019a**. A plant immune receptor adopts a two-step recognition mechanism to enhance viral effector perception. *Molecular Plant* **12**: 248-262.
Li J, Liu X, Wang Q, Huangfu J, Schuman MC, Lou Y. **2019b**. A group D MAPK protects

plants from autotoxicity by suppressing herbivore-induced defense signaling. *Plant Physiology* **179**: 1386–1401.

Li S, Liu S, Zhang Q, Cui M, Zhao M, Li N, Wang S, Wu R, Zhang L, Cao Y, *et al.* 2022. The interaction of ABA and ROS in plant growth and stress resistances. *Frontiers in Plant Science* **13**: 1–16.

Lim CW, Baek W, Jung J, Kim JH, Lee SC. **2015**. Function of ABA in stomatal defense against biotic and drought stresses. *International Journal of Molecular Sciences* **16**: 15251–15270.

Lindermayr C, Rudolf EE, Durner J, Groth M. **2020**. Interactions between metabolism and chromatin in plant models. *Molecular Metabolism* **38**: 100951.

Liu L, Hausladen A, Zeng M, Que L, Heitman J, Stamler JS. **2001**. A metabolic enzyme for S-nitrosothiol conserved from bacteria to humans. *Nature* **410**: 490–494.

Liu Y, He J, Jiang L, Wu H, Xiao Y, Liu Y, Li G, Du Y, Liu C, Wan J. **2011**. Nitric oxide production is associated with response to brown planthopper infestation in rice. *Journal of Plant Physiology* **168**: 739–745.

Liu Y, Teng C, Xia R, Meyers BC. **2020**. PhasiRNAs in plants: Their biogenesis, genic sources, and roles in stress responses, development, and reproduction. *The Plant Cell* **32**: 3059–3080.

Liu Y, Wu H, Chen H, Liu Y, He J, Kang H, Sun Z, Pan G, Wang Q, Hu J, *et al.* 2015. A gene cluster encoding lectin receptor kinases confers broad-spectrum and durable insect resistance in rice. *Nature Biotechnology* **33**: 301–305.

Livak KJ, Schmittgen TD. **2001**. Analysis of relative gene expression data using real-time quantitative PCR and the 2-ΔΔCT method. *Methods* **25**: 402–408.

López-Márquez D, Del-Espino Á, López-Pagán N, Rodríguez-Negrete EA, Rubio-Somoza I, Ruiz-Albert J, Bejarano ER, Beuzón CR. **2021**. MiR825-5p targets the TIR-NBS-LRR gene MIST1 and down-regulates basal immunity against *Pseudomonas syringae* in Arabidopsis. *Journal of Experimental Botany* **72**: 7316–7334.

López-Márquez D, Del-Espino Á, Ruiz-Albert J, Bejarano ER, Brodersen P, Beuzón CR. **2023**. Regulation of plant immunity via small RNA-mediated control of NLR expression. *Journal of Experimental Botany* **74**: 6052–6068.

Lorenzo O, Piqueras R, Sánchez-Serrano JJ, Solano R. **2003**. ETHYLENE RESPONSE FACTOR1 integrates signals from ethylene and jasmonate pathways in plant defense. *The Plant Cell* **15**: 165–178.

Luna E, Bruce TJA, Roberts MR, Flors V, Ton J. **2012**. Next-generation systemic acquired resistance. *Plant Physiology* **158**: 844–853.

Ma S, Lapin D, Liu L, Sun Y, Song W, Zhang X, Logemann E, Yu D, Wang J, Jirschitzka J, *et al.* 2020. Direct pathogen-induced assembly of an NLR immune receptor complex to form a holoenzyme. *Science* **370**: 3069.

Machado RAR, Robert CAM, Arce CCM, Ferrieri AP, Xu S, Jimenez-Aleman GH, Baldwin

IT, Erb M. **2016**. Auxin is rapidly induced by herbivore attack and regulates a subset of systemic, jasmonate-dependent defenses. *Plant Physiology* **172**: 521–532.
Macho AP, Zipfel C. **2014**. Plant PRRs and the activation of innate immune signaling. *Molecular Cell* **54**: 263–272.
Macke E, Magalhães S, Khan HDT, Luciano A, Frantz A, Facon B, Olivieri I. **2011**. Sex allocation in haplodiploids is mediated by egg size: Evidence in the spider mite *Tetranychus urticae* Koch. *Proceedings of the Royal Society B: Biological Sciences* **278**: 1054–1063.
Mai VC, Drzewiecka K, Jeleń H, Narozna D, Rucińska-Sobkowiak R, Kesy J, Floryszak-Wieczorek J, Gabryś B, Morkunas I. **2014**. Differential induction of *Pisum sativum* defense signaling molecules in response to pea aphid infestation. *Plant Science* **221–222**: 1–12.
Malhotra EV, Jain R, Tyagi S, Raman KV, Bansal S, Aminedi R, Pattanayak D. **2022**. Comparative analysis of herbivory responsive miRNAs to delineate pod borer (*Helicoverpa armigera*) resistance mechanisms in *Cajanus cajan* and its wild relative *Cajanus scarabaeoides*. *Plant Cell Reports* **41**: 1147–1161.
Mangal V, Lal MK, Tiwari RK, Altaf MA, Sood S, Kumar D, Bharadwaj V, Singh B, Singh RK, Aftab T. **2023**. Molecular insights into the role of reactive oxygen, nitrogen and sulphur species in conferring salinity stress tolerance in plants. *Journal of Plant Growth Regulation* **42**: 554–574.
Mano J, Biswas MS, Sugimoto K. **2019**. Reactive carbonyl species: A missing link in ROS signaling. *Plants* **8**: 1–23.
Mano J. **2012**. Reactive carbonyl species: Their production from lipid peroxides, action in environmental stress, and the detoxification mechanism. *Plant Physiology and Biochemistry* **59**: 90–97.
Mantelin S, Peng HC, Li B, Atamian HS, Takken FLW, Kaloshian I. **2011**. The receptor-like kinase SlSERK1 is required for Mi-1-mediated resistance to potato aphids in tomato. *Plant Journal* **67**: 459–471.
Mao YB, Liu YQ, Chen DY, Chen FY, Fang X, Hong GJ, Wang LJ, Wang JW, Chen XY. **2017**. Jasmonate response decay and defense metabolite accumulation contributes to age-regulated dynamics of plant insect resistance. *Nature Communications* **8**: 1–13.
Mapes CC, Davies PJ. **2001**. Indole-3-acetic acid and ball gall development on *Solidago altissima. New Phytologist* **151**: 195–202.
Marquis V, Smirnova E, Graindorge S, Delcros P, Villette C, Zumsteg J, Heintz D, Heitz T. **2022**. Broad-spectrum stress tolerance conferred by suppressing jasmonate signaling attenuation in Arabidopsis JASMONIC ACID OXIDASE mutants. *Plant Journal* **109**: 856–872.
Martel C, Zhurov V, Navarro M, Martinez M, Cazaux M, Auger P, Migeon A, Santamaria ME, Wybouw N, Diaz I, *et al.* 2015. Tomato whole genome transcriptional response to

Tetranychus urticae Identifies divergence of spider mite-induced responses between tomato and Arabidopsis. *Molecular Plant-Microbe Interactions* **28**: 343–361.

Martin GB, Bogdanove AJ, Sessa G. **2003**. Understanding the functions of plant disease resistance proteins. *Annual Review of Plant Biology* **54**: 23–61.

Martin R, Qi T, Zhang H, Liu F, King M, Toth C, Nogales E, Staskawicz BJ. **2020**. Structure of the activated ROQ1 resistosome directly recognizing the pathogen effector XopQ. *Science* **370**: 1–21.

Martinez De Ilarduya O, Xie QG, Kaloshian I. **2003**. Aphid-induced defense responses in Mi-1-mediated compatible and incompatible tomato interactions. *Molecular Plant-Microbe Interactions* **16**: 699–708.

Martínez-Medina A, Pescador L, Terrón-Camero LC, Pozo MJ, Romero-Puertas MC. **2019**. Nitric oxide in plant–fungal interactions. *Journal of Experimental Botany* **70**: 4489–4503.

Martínez-Ruiz A, Araújo IM, Izquierdo-Álvarez A, Hernansanz-Agustín P, Lamas S, Serrador JM. **2013**. Specificity in S-nitrosylation: A short-range mechanism for NO signalling? *Antioxidants and Redox Signaling* **19**: 1220–1235.

Mata-Pérez C, Sánchez-Calvo B, Padilla MN, Begara-Morales JC, Valderrama R, Corpas FJ, Barroso JB. **2017**. Nitro-fatty acids in plant signaling: New key mediators of nitric oxide metabolism. *Redox Biology* **11**: 554–561.

Mathen K, Radhakrishnan Nair CP, Gunasekharan M, Govindankutty MP, Solomon JJ. **1988**. Stylet course of lace bug *Stephanitis typica* (Distant) in coconut leaf. *Proceedings of Indian Acad.: Animal Sciences* **97**: 539–544.

McNickle GG, Evans WD. **2018**. Toleration games: Compensatory growth by plants in response to enemy attack is an evolutionarily stable strategy. *AoB PLANTS* **10**: 1–14.

Melotto M, Zhang L, Oblessuc PR, He SY. **2017**. Stomatal defense a decade later. *Plant Physiology* **174**: 561–571.

Merchant AM, Pajerowska-Mukhtar KM. **2015**. *Arabidopsis thaliana* dynamic phenotype plasticity in response to enviromental conditions. *International Journal of Modern Botany* **5**: 23–28.

Misra AN, Misra M, Singh R. **2011**. Nitric oxide: A ubiquitous signaling molecule with diverse role in plants. *African Journal of Plant Science* **5**: 57–74.

Mithöfer A, Boland W. **2012**. Plant defense against herbivores: Chemical aspects. *Annual Review of Plant Biology* **63**: 431–450.

Mithöfer A, Wanner G, Boland W. **2005**. Effects of feeding *Spodoptera littoralis* on lima bean leaves. Continuous mechanical wounding resembling insect feeding is sufficient to elicit herbivory-related volatile emission. *Plant Physiology* **137**: 1160–1168.

Mittler R, Vanderauwera S, Suzuki N, Miller G, Tognetti VB, Vandepoele K, Gollery M, Shulaev V, Van Breusegem F. **2011**. ROS signaling: The new wave? *Trends in Plant Science* **16**: 300–309.

Mittler R. **2017**. ROS are good. *Trends in Plant Science* **22**: 11–19.
Molassiotis A, Job D, Ziogas V, Tanou G. **2016**. Citrus plants: A model system for unlocking the secrets of NO and ROS-inspired priming against salinity and drought. *Frontiers in Plant Science* **7:** 00229.
Moloi MJ, Van der Westhuizen AJ. **2009**. Involvement of nitric oxide during the Russian wheat aphid resistance. *South African Journal of Botany* **75**: 412.
Monteiro F, Nishimura MT. **2018**. Structural, functional, and genomic diversity of plant NLR proteins: An evolved resource for rational engineering of plant immunity. *Annual Review of Phytopathology* **56**: 243–267.
Moreau M, Lindermayr C, Durner J, Klessig DF. **2010**. NO synthesis and signaling in plants: where do we stand? *Physiologia Plantarum* **138**: 372–383.
Mostafa S, Wang Y, Zeng W, Jin B. **2022**. Plant Responses to Herbivory, Wounding, and Infection. *International Journal of Molecular Sciences* **23:** 7031.
Moustaka J, Meyling NV, Hauser TP. **2021**. Induction of a compensatory photosynthetic response mechanism in tomato leaves upon short time feeding by the chewing insect *spodoptera exigua*. *Insects* **12:** 562.
Munemasa S, Hossain MA, Nakamura Y, Mori IC, Murata Y. **2011**. The Arabidopsis calcium-dependent protein kinase, CPK6, functions as a positive regulator of methyl jasmonate signaling in guard cells. *Plant Physiology* **155**: 553–561.
Mur L, Prats E, Pierre S, Hall M, Hebelstrup KH. **2013**. Integrating nitric oxide into salicylic acid and jasmonic acid/ ethylene plant defense pathways. *Frontiers in Plant Science* **4:** 00215.
Mur LAJ, Carver TLW, Prats E. **2006**. NO way to live; the various roles of nitric oxide in plant–pathogen interactions. *Journal of Experimental Botany* **57**: 489–505.
Musser RO, Cipollini DF, Hum-Musser SM, Williams SA, Brown JK, Felton GW. **2005**. Evidence that the caterpillar salivary enzyme glucose oxidase provides herbivore offense in solanaceous plants. *Archives of Insect Biochemistry and Physiology* **58**: 128–137.
Mustilli A, Merlot S, Vavasseur A, Fenzi F, Giraudat J. **2002**. Arabidopsis OST1 protein kinase mediates the regulation of stomatal aperture by abscisic acid and acts upstream of reactive oxygen species production. *The Plant Cell* **14**: 3089–3099.
Nabi RBS, Tayade R, Hussain A, Kulkarni KP, Imran QM, Mun BG, Yun BW. **2019**. Nitric oxide regulates plant responses to drought, salinity, and heavy metal stress. *Environmental and Experimental Botany* **161**: 120–133.
Ng DWK, Abeysinghe JK, Kamali M. **2018**. Regulating the regulators: The control of transcription factors in plant defense signaling. *International Journal of Molecular Sciences* **19:** 3737.
Ngou BPM, Ahn H-K, Ding P, Jones JDG. **2021b**. Mutual potentiation of plant immunity by cell-surface and intracellular receptors. *Nature* **592**: 110–115.
Ngou BPM, Ding P, Jones JDG. **2022a**. Thirty years of resistance: Zig-zag through the

plant immune system. *The Plant Cell* **34**: 1447–1478.

Ngou BPM, Heal R, Wyler M, Schmid MW, Jones JDG. **2022b**. Concerted expansion and contraction of immune receptor gene repertoires in plant genomes. *Nature Plants* **8**: 1146–1152.

Noctor G, Mhamdi A, Chaouch S, Han Y, Neukermans J, Marquez-Garcia B, Queval G, Foyer CH. **2012**. Glutathione in plants: An integrated overview. *Plant, Cell and Environment* **35**: 454–484.

Ojeda-Martinez D, Diaz I, Santamaria ME. **2022**. Transcriptomic landscape of herbivore oviposition in Arabidopsis: A systematic review. *Frontiers in Plant Science* **12**: 1–14.

Ojeda-Martinez D, Martinez M, Diaz I, Estrella Santamaria ME. **2021**. Spider mite egg extract modifies Arabidopsis response to future infestations. *Scientific Reports* **11**: 1–17.

Ojeda-Martinez D, Martinez M, Diaz I, Santamaria ME. **2020**. Saving time maintaining reliability: A new method for quantification of *Tetranychus urticae* damage in Arabidopsis whole rosettes. *BMC Plant Biology* **20**: 1–19.

Okamoto M, Tanaka Y, Abrams SR, Kamiya Y, Seki M, Nambara E. **2009**. High humidity induces abscisic acid 8'-hydroxylase in stomata and vasculature to regulate local and systemic abscisic acid responses in Arabidopsis. *Plant Physiology* **149**: 825–834.

Oñate-Sánchez L, Vicente-Carbajosa J. **2008**. DNA-free RNA isolation protocols for *Arabidopsis thaliana*, including seeds and siliques. *BMC Research Notes* **1**: 1–7.

Pagán I, García-Arenal F. **2018**. Tolerance to plant pathogens: Theory and experimental evidence. *International Journal of Molecular Sciences* **19:** 810.

Palle SR, Campbell LM, Pandeya D, Puckhaber L, Tollack LK, Marcel S, Sundaram S, Stipanovic RD, Wedegaertner TC, Hinze L, *et al.* 2013. RNAi-mediated Ultra-low gossypol cottonseed trait: Performance of transgenic lines under field conditions. *Plant Biotechnology Journal* **11**: 296–304.

Paludan SR, Pradeu T, Masters SL, Mogensen TH. **2021**. Constitutive immune mechanisms: mediators of host defence and immune regulation. *Nature Reviews Immunology* **21**: 137–150.

Park CJ, Shin R. **2022**. Calcium channels and transporters: Roles in response to biotic and abiotic stresses. *Frontiers in Plant Science* **13**: 1–15.

Pattyn J, Vaughan-Hirsch J, Van de Poel B. **2021**. The regulation of ethylene biosynthesis: a complex multilevel control circuitry. *New Phytologist* **229**: 770–782.

Pentzold S, Zagrobelny M, Roelsgaard PS, Møller BL, Bak S. **2014**. The multiple strategies of an insect herbivore to overcome plant cyanogenic glucoside defence. *PLoS ONE* **9:** 91337.

Perazzolli M, Dominici P, Romero-Puertas MC, Zago E, Zeier J, Sonoda M, Lamb C, Delledonne M. **2004**. Arabidopsis nonsymbiotic hemoglobin AHb1 modulates nitric oxide bioactivity. *The Plant Cell* **16**: 2785–2794.

Perazzolli M, Romero-Puertas MC, Delledonne M. **2006**. Modulation of nitric oxide

bioactivity by plant haemoglobins. *Journal of Experimental Botany* **57**: 479–488.
Pham AQ, Cho S-H, Nguyen CT, Stacey G. **2020**. Arabidopsis lectin receptor kinase P2K2 Is a second plant receptor for extracellular ATP and contributes to innate immunity. *Plant Physiology* **183**: 1364–1375.
Pieterse CMJ, Van Der Does D, Zamioudis C, Leon-Reyes A, Van Wees SCM. **2012**. Hormonal modulation of plant immunity. *Annual Review of Cell and Developmental Biology* **28**: 489–521.
Pieterse CMJ, Van Loon LC. **2004**. NPR1: The spider in the web of induced resistance signaling pathways. *Current Opinion in Plant Biology* **7**: 456–464.
Pincebourde S, Casas J. **2006**. Multitrophic biophysical budgets: thermal ecology of an intimate herbivore insect-plant interaction. *Ecological Monographs* **76**: 175–194.
Poelman EH, Broekgaarden C, Van Loon JJA, Dicke M. **2008**. Early season herbivore differentially affects plant defence responses to subsequently colonizing herbivores and their abundance in the field. *Molecular Ecology* **17**: 3352–3365.
Poudel AN, Zhang T, Kwasniewski M, Nakabayashi R, Saito K, Koo AJ. **2016**. Mutations in jasmonoyl-L-isoleucine-12-hydroxylases suppress multiple JA-dependent wound responses in Arabidopsis thaliana. *Biochimica et Biophysica Acta (BBA): Molecular and Cell Biology of Lipids* **1861**: 1396–1408.
Pradhan M, Pandey P, Gase K, Sharaff M, Singh RK, Sethi A, Baldwin IT, Pandey SP. 2017. Argonaute 8 (AGO8) mediates the elicitation of direct defenses against herbivory. *Plant Physiology* **175**: 927–946.
Prakash V, Singh VP, Tripathi DK, Sharma S, Corpas FJ. **2019**. Crosstalk between nitric oxide (NO) and abscisic acid (ABA) signalling molecules in higher plants. *Environmental and Experimental Botany* **161**: 41–49.
Prince DC, Drurey C, Zipfel C, Hogenhout SA. **2014**. The Leucine-rich repeat receptor-like kinase BRASSINOSTEROID INSENSITIVE1-ASSOCIATED KINASE1 and the cytochrome P450 PHYTOALEXIN DEFICIENT3 contribute to innate immunity to aphids in Arabidopsis. *Plant Physiology* **164**: 2207–2219.
Queiroz EF, Marcourt L, Stahl E, Hilfiker O, Riezman I, Riezman H, Wolfender J, Reymond P. **2020**. Phosphatidylcholines from *Pieris brassicae* eggs activate an immune response in Arabidopsis. *eLife*: 1–21.
Radi R. **2004**. Nitric oxide, oxidants, and protein tyrosine nitration. *Proceedings of the National Academy of Sciences of the United States of America* **101**: 4003–4008.
Ramírez-Serrano B, Querejeta M, Minchev Z, Gamir J, Perdereau E, Pozo MJ, Dubreuil G, Giron D. **2022**. Mycorrhizal benefits on plant growth and protection against *Spodoptera exigua* depend on N availability. *Journal of Plant Interactions* **17**: 940–955.
Ren C, Han C, Peng W, Huang Y, Peng Z, Xiong X, Zhu Q, Gao B, Xie D. **2009**. A leaky mutation in DWARF4 reveals an antagonistic role of brassinosteroid in the inhibition of root growth by jasmonate in Arabidopsis. *Plant Physiology* **151**: 1412–1420.

Reymond P. **2013**. Perception, signaling and molecular basis of oviposition-mediated plant responses. *Planta* **238**: 247–258.

Rioja C, Zhurov V, Bruinsma K, Grbic M, Grbic V. **2017**. Plant-herbivore interactions: A case of an extreme generalist, the two-spotted spider mite *Tetranychus urticae*. *Molecular Plant-Microbe Interactions* **30**: 935–945.

Rivas-San Vicente M, Plasencia J. **2011**. Salicylic acid beyond defence: Its role in plant growth and development. *Journal of Experimental Botany* **62**: 3321–3338.

Rockel P, Strube F, Rockel A, Wildt J, Kaiser WM. **2002**. Regulation of nitric oxide (NO) production by plant nitrate reductase in vivo and in vitro. *Journal of Experimental Botany* **53**: 103–110.

Romero-Hernandez G, Martinez M. **2022**. Opposite roles of MAPKKK17 and MAPKKK21 against *Tetranychus urticae* in Arabidopsis. *Frontiers in Plant Science* **13:** 1038866.

Romero-Puertas MC, Sandalio LM. **2016**. Nitric oxide level is self-regulating and also regulates its ROS partners. *Frontiers in Plant Science* **7**: 1–5.

Rowe J, Grangé-Guermente M, Exposito-Rodriguez M, Wimalasekera R, Lenz MO, Shetty KN, Cutler SR, Jones AM. **2023**. Next-generation ABACUS biosensors reveal cellular ABA dynamics driving root growth at low aerial humidity. *Nature Plants* **9**:1103–1115.

Rowe JH, Rizza A, Jones AM. **2022**. Quantifying phytohormones in vivo with FRETFörster Resonance nergy Transfer (FRET) biosensors and the FRETENATOR analysis toolset BT: environmental responses in Plants: Methods and Protocols. In: Duque P, Szakonyi D, eds. New York, NY: Springer US, 239–253.

Rubbo H, Radi R. **2008**. Protein and lipid nitration: Role in redox signaling and injury. *Biochimica et Biophysica Acta (BBA): General Subjects* **1780**: 1318–1324.

Rubbo H. **2013**. Nitro-fatty acids: Novel anti-inflammatory lipid mediators. *Brazilian Journal of Medical and Biological Research* **46**: 728–734.

Ruther J, Kleier S. **2005**. Plant-plant signaling: Ethylene synergizes volatile emission in *Zea mays* induced by exposure to (Z)-3-hexen-1-ol. *Journal of Chemical Ecology* **31**: 2217–2222.

Sances F V, Wyman JA, Ting IP. **1979**. Morphological responses of strawberry leaves to infestations of two spotted spider mite. *Journal of Economic Entomology* **72**: 710–713.

Sánchez-Vallet A, López G, Ramos B, Delgado-Cerezo M, Riviere MP, Llorente F, Fernández PV, Miedes E, Estevez JM, Grant M, *et al.* 2012. Disruption of abscisic acid signaling constitutively activates Arabidopsis resistance to the necrotrophic fungus *Plectosphaerella cucumerina*. *Plant Physiology* **160**: 2109–2124.

Sánchez-Vallet A, Ramos B, Bednarek P, López G, Piślewska-Bednarek M, Schulze-Lefert P, Molina A. **2010**. Tryptophan-derived secondary metabolites in Arabidopsis thaliana confer non-host resistance to necrotrophic *Plectosphaerella cucumerina* fungi. *The Plant Journal* **63**: 115–127.

Sánchez-Vicente I, Fernández-Espinosa MG, Lorenzo O, Brouquisse R. **2019**. Nitric oxide molecular targets: Reprogramming plant development upon stress. *Journal of Experimental Botany* **70**: 4441–4460.

Sandalio LM, Gotor C, Romero LC, Romero-Puertas MC. **2019**. Multilevel regulation of peroxisomal proteome by post-translational modifications. *International Journal of Molecular Sciences* **20**: 4881.

Santamaria ME, Arnaiz A, Martinez M, Diaz I. **2018a**. Plant perception and short-term responses to phytophagous insects and mites. *International Journal of Molecular Sciences* **19:** 1356.

Santamaria ME, Arnaiz A, Rosa-Diaz I, González-Melendi P, Romero-Hernandez G, Ojeda-Martinez DA, Garcia A, Contreras E, Martinez M, Diaz I. **2020**. Plant defenses against tetranychus urticae: Mind the gaps. *Plants* **9**: 1–16.

Santamaria ME, Arnaiz A, Velasco-Arroyo B, Grbic V, Diaz I, Martinez M. **2018b**. Arabidopsis response to the spider mite *Tetranychus urticae* depends on the regulation of reactive oxygen species homeostasis. *Scientific Reports* **8**: 1–13.

Santamaria ME, Diaz I, Martinez M. **2018c**. Dehydration stress contributes to the enhancement of plant defense response and mite performance on barley. *Frontiers in Plant Science* **9:** 00458.

Santamaria ME, Garcia A, Arnaiz A, Rosa-Diaz I, Romero-Hernandez G, Diaz I, Martinez M. **2021**. Comparative transcriptomics reveals hidden issues in the plant response to arthropod herbivores. *Journal of Integrative Plant Biology* **63**: 312–326.

Santamaria ME, Hernández-Crespo P, Ortego F, Grbic V, Grbic M, Diaz I, Martinez M. **2012**. Cysteine peptidases and their inhibitors in *Tetranychus urticae*: a comparative genomic approach. *BMC Genomics* **13**: 307.

Santamaria ME, Martinez M, Arnaiz A, Ortego F, Grbic V, Diaz I. **2017a**. MATI, a novel protein involved in the regulation of herbivore-associated signaling pathways. *Frontiers in Plant Science* **8:** 00975.

Santamaria ME, Martínez M, Arnaiz A, Rioja C, Burow M, Grbic V, Diaz I. **2019**. An arabidopsis TIR-lectin two-domain protein confers defense properties against *Tetranychus urticae*. *Plant Physiology* **179**: 1298–1314.

Santamaria ME, Martínez M, Cambra I, Grbic V, Diaz I. **2013**. Understanding plant defence responses against herbivore attacks: An essential first step towards the development of sustainable resistance against pests. *Transgenic Research* **22**: 697–708.

Santolamazza-Carbone S, Sotelo T, Velasco P, Cartea ME. **2016**. Antibiotic properties of the glucosinolates of *Brassica oleracea* var. acephala similarly affect generalist and specialist larvae of two lepidopteran pests. *Journal of Pest Science* **89**: 195–206.

Sarmento RA, Lemos F, Bleeker PM, Schuurink RC, Pallini A, Oliveira MGA, Lima ER, Kant M, Sabelis MW, Janssen A. **2011**. A herbivore that manipulates plant defence. *Ecology Letters* **14**: 229–236.

Sarris PF, Duxbury Z, Huh SU, Ma Y, Segonzac C, Sklenar J, Derbyshire P, Cevik V, Rallapalli G, Saucet SB, *et al.* 2015. A plant immune receptor detects pathogen effectors that target WRKY transcription factors. *Cell* **161**: 1089–1100.

Sauge MH, Mus F, Lacroze JP, Pascal T, Kervella J, Poëssel JL. **2006**. Genotypic variation in induced resistance and induced susceptibility in the peach-*Myzus persicae* aphid system. *Oikos* **113**: 305–313.

Schäfer M, Fischer C, Meldau S, Seebald E, Oelmüller R, Baldwin IT. **2011**. Lipase activity in insect oral secretions mediates defense responses in arabidopsis. *Plant Physiology* **156**: 1520–1534.

Schindelin J, Arganda-Carreras I, Frise E, Kaynig V, Longair M, Pietzsch T, Preibisch S, Rueden C, Saalfeld S, Schmid B, *et al.* 2012. Fiji: An open-source platform for biological-image analysis. *Nature Methods* **9**: 676–682.

Schmelz EA, Kaplan F, Huffaker A, Dafoe NJ, Vaughan MM, Ni X, Rocca JR, Alborn HT, Teal PE. **2011**. Identity, regulation, and activity of inducible diterpenoid phytoalexins in maize. *Proceedings of the National Academy of Sciences of the United States of America* **108**: 5455–5460.

Schmidt L, Schurr U, Röse USR. **2009**. Local and systemic effects of two herbivores with different feeding mechanisms on primary metabolism of cotton leaves. *Plant, Cell and Environment* **32**: 893–903.

Sharma A, Gupta R. **2009**. Biological activity of some plant extracts against *Pieris brassicae* (Linn.). *Journal of Biopesticides* **2**: 26–31.

Shirano Y, Kachroo P, Shah J, Klessig DF. **2002**. A gain-of-function mutation in an Arabidopsis Toll Interleukin1 Receptor-Nucleotide Binding Site-Leucine-Rich Repeat type R gene triggers defense responses and results in enhanced disease resistance. *The Plant Cell* **14**: 3149–3162.

Smirnova E, Marquis V, Poirier L, Aubert Y, Zumsteg J, Ménard R, Miesch L, Heitz T. **2017**. Jasmonic acid oxidase 2 Hydroxylates jasmonic acid and represses basal defense and resistance responses against *Botrytis cinerea* infection. *Molecular Plant* **10**: 1159–1173.

Smith CM, Boyko E V. **2007**. The molecular bases of plant resistance and defense responses to aphid feeding: current status. *Entomologia Experimentalis et Applicata* **122**: 1–16.

Sperdouli I, Andreadis SS, Adamakis IDS, Moustaka J, Koutsogeorgiou EI, Moustakas M. **2022**. Reactive oxygen species initiate defence responses of PPotato Photosystem II to sap-sucking insect feeding. *Insects* **13**: 1–15.

Stahl E, Fernandez Martin A, Glauser G, Guillou MC, Aubourg S, Renou JP, Reymond P. **2022**. The MIK2/SCOOP Ssignalling system contributes to Arabidopsis resistance against herbivory by modulating jasmonate and indole glucosinolate biosynthesis. *Frontiers in Plant Science* **13**: 1–13.

Stahl E, Hilfiker O, Reymond P. **2018**. Plant–arthropod interactions: who is the winner? *The Plant Journal* **93**: 703–728.

Steinbrenner AD, Munoz-Amatriain M, Chaparro AF, Jessica Montserrat Aguilar-Venegas, Lo S, Okuda S, Glauser G, Dongiovanni J, Shi D, Hall M, *et al.* 2020. A receptor-like protein mediates plant immune responses to herbivore-associated molecular patterns. *Proceedings of the National Academy of Sciences of the United States of America* **117**: 31510–31518.

Stöhr C, Stremlau S. **2006**. Formation and possible roles of nitric oxide in plant roots. *Journal of Experimental Botany* **57**: 463–470.

Su J, Spears BJ, Kim SH, Gassmann W. **2018**. Constant vigilance: plant functions guarded by resistance proteins.*The Plant Journal* **93**: 637–650.

Sun LR, Yue CM, Hao FS. **2019**. Update on roles of nitric oxide in regulating stomatal closure. *Plant Signaling & Behavior* **14**: e1649569.

Sun Z, Zang Y, Zhou L, Song Y, Chen D, Zhang Q, Liu C, Yi Y, Zhu B, Fu D, *et al.* 2021. A tomato receptor-like cytoplasmic kinase, SlZRK1, acts as a negative regulator in wound-induced jasmonic acid accumulation and insect resistance. *Journal of Experimental Botany* **72**: 7285–7300.

Suzuki T, España MU, Nunes MA, Zhurov V, Dermauw W, Osakabe M, Van Leeuwen T V., Grbic M, Grbic V. **2017**. Protocols for the delivery of small molecules to the two-spotted spider mite, *Tetranychus urticae*. *PLoS ONE* **12**: 1–23.

Tallman G. **2004**. Are diurnal patterns of stomatal movement the result of alternating metabolism of endogenous guard cell ABA and accumulation of ABA delivered to the apoplast around guard cells by transpiration? *Journal of Experimental Botany* **55**: 1963–1976.

Tamiru A, Paliwal R, Manthi SJ, Odeny DA, Midega CAO, Khan ZR, Pickett JA, Bruce TJA. **2020**. Genome wide association analysis of a stemborer egg induced "call-for-help" defence trait in maize. *Scientific Reports* **10**: 1–12.

Tanaka S, Han X, Kahmann R. **2015**. Microbial effectors target multiple steps in the salicylic acid production and signaling pathway. *Frontiers in Plant Science* **6**: 1–10.

Tang J, Yang D, Wu J, Chen S, Wang L. **2020**. Silencing JA hydroxylases in *Nicotiana attenuata* enhances jasmonic acid-isoleucine-mediated defenses against Spodoptera litura. *Plant Diversity* **42**: 111–119.

Tanou G, Filippou P, Belghazi M, Job D, Diamantidis G, Fotopoulos V, Molassiotis A. **2012**. Oxidative and nitrosative-based signaling and associated post-translational modifications orchestrate the acclimation of citrus plants to salinity stress. *The Plant Journal* **72**: 585–599.

Tian D, Tooker J, Peiffer M, Chung SH, Felton GW. **2012**. Role of trichomes in defense against herbivores: Comparison of herbivore response to woolly and hairless trichome mutants in tomato (*Solanum lycopersicum*). *Planta* **236**: 1053–1066.

Tooker JF, de Moraes CM. **2011**. Feeding by a gall-inducing caterpillar species alters levels of indole-3-acetic and abscisic acid in *Solidago altissima* (Asteraceae) stems. *Arthropod-Plant Interactions* **5**: 115–124.

Tretner C, Huth U, Hause B. **2008**. Mechanostimulation of *Medicago truncatula* leads to enhanced levels of jasmonic acid. *Journal of Experimental Botany* **59**: 2847–2856.

Uemura T, Hachisu M, Desaki Y, Ito A, Hoshino R, Sano Y, Nozawa A, Mujiono K, Galis I, Yoshida A, *et al.* 2020. Soy and Arabidopsis receptor-like kinases respond to polysaccharide signals from Spodoptera species and mediate herbivore resistance. *Communications Biology* **3**: 1–11.

Ullah MI, Arshad M, Ali S, Iftikhar Y, Mahmood SU, Arshad M. **2016**. Effect of thiamethoxam and some botanical extracts on *Cotesia glomerata* L. (braconidae: Hymenoptera): An endoparasitoid of *Pieris brassicae* (L.) (pieridae: Lepidoptera). *Egyptian Journal of Biological Pest Control* **26**: 545–549.

Underwood N. **2012**. When herbivores come back: Effects of repeated damage on induced resistance. *Functional Ecology* **26**: 1441–1449.

Vacante V. **2016**. *The handbook of mites of economic plants: Identification, bio-ecology and control*. CABI International, Wallingford, UK.

Van de Weyer AL, Monteiro F, Furzer OJ, Nishimura MT, Cevik V, Witek K, Jones JDG, Dangl JL, Weigel D, Bemm F. **2019**. A species-wide Inventory of NLR genes and alleles in *Arabidopsis thaliana*. *Cell* **178**: 1260-1272.e14.

Van Loon LC, Geraats BPJ, Linthorst HJM. **2006**. Ethylene as a modulator of disease resistance in plants. *Trends in Plant Science* **11**: 184–191.

Varkonyi-Gasic E. 2017. Stem-Loop qRT-PCR for the Detection of Plant microRNAs. *Kovalchuk, I. (eds) Plant Epigenetics. Methods in Molecular Biology, Humana Press, Boston, MA* **1456**: 163–175.

Vert G. **2008**. Plant signalling: Brassinosteroids, immunity and effectors are BAK! *Current Biology* **18**: 963–965.

Vos IA, Verhage A, Schuurink RC, Watt LG, Pieterse CMJ, Van Wees SCM. **2013**. Onset of herbivore-induced resistance in systemic tissue primed for jasmonate-dependent defenses is activated by abscisic acid. *Frontiers in Plant Science* **4**: 1–10.

Wagner AR, Weindel CG, West KO, Scott HM, Watson RO, Patrick KL. 2022. SRSF6 balances mitochondrial-driven innate immune outcomes through alternative splicing of BAX. *eLife* **11**: 82244.

Walling LL. **2000**. The myriad plant responses to herbivores. *Journal of Plant Growth Regulation* **19**: 195–216.

Walling LL. **2008**. Avoiding effective defenses: Strategies employed by phloem-feeding insects. *Plant Physiology* **146**: 859–866.

Wan L, Essuman K, Anderson RG, Sasaki Y, Monteiro F, Chung E-H, Osborne Nishimura E, DiAntonio A, Milbrandt J, Dangl JL, *et al.* 2019. TIR domains of plant immune

receptors are NAD+-cleaving enzymes that promote cell death. *Science* **365**: 799–803.
Wang B-L, Shi L, Li Y-X, Zhang W-H. **2010**. Boron toxicity is alleviated by hydrogen sulfide in cucumber (*Cucumis sativus* L.) seedlings. *Planta* **231**: 1301–1309.
Wang C, Huang X, Li Q, Zhang Y, Li JL, Mou Z. **2019**. Extracellular pyridine nucleotides trigger plant systemic immunity through a lectin receptor kinase/BAK1 complex. *Nature Communications* **10:** 4810.
Wang C, Zhou M, Zhang X, Yao J, Zhang Y, Mou Z. **2017**. A lectin receptor kinase as a potential sensor for extracellular nicotinamide adenine dinucleotide in *Arabidopsis thaliana*. *eLife* **6**: 1–23.
Wang H, Shi S, Hua W. **2023**. Advances of herbivore-secreted elicitors and effectors in plant-insect interactions. *Frontiers in Plant Science* **14**: 1–12.
Wang L, Einig E, Almeida-Trapp M, Albert M, Fliegmann J, Mithöfer A, Kalbacher H, Felix G. **2018**. The systemin receptor SYR1 enhances resistance of tomato against herbivorous insects. *Nature Plants* **4**: 152–156.
Wang P, Du Y, Hou YJ, Zhao Y, Hsu CC, Yuan F, Zhu X, Tao WA, Song CP, Zhu JK. **2015**. Nitric oxide negatively regulates abscisic acid signaling in guard cells by S-nitrosylation of OST1. *Proceedings of the National Academy of Sciences of the United States of America* **112**: 613–618.
Wang X, Mao Z, Choi K, Park K. **2006**. Significance of the leaf epidermis fingerprint for taxonomy of genus Rhododendron. *Journal of Forestry Research* **17**: 171–176.
Wang Y, Mostafa S, Zeng W, Jin B. **2021**. Function and Mechanism of Jasmonic Acid in Plant Responses to Abiotic and Biotic Stresses. *International Journal of Molecular Sciences **22**: 8568*.
Wasternack C, Hause B. **2013**. Jasmonates: Biosynthesis, perception, signal transduction and action in plant stress response, growth and development. An update to the 2007 review in Annals of Botany. *Annals of Botany* **111**: 1021–1058.
Wei H, Jing Y, Zhang L, Kong D. **2021**. Phytohormones and their crosstalk in regulating stomatal development and patterning. *Journal of Experimental Botany* **72**: 2356–2370.
Wendehenne D, Pugin A, Klessig DF, Durner J. **2001**. Nitric oxide: Comparative synthesis and signaling in animal and plant cells. *Trends in Plant Science* **6**: 177–183.
Widemann E, Bruinsma K, Walshe-Roussel B, Rioja C, Arbona V, Saha RK, Letwin D, Zhurov V, Gómez-Cadenas A, Bernards MA, *et al.* 2021. Multiple indole glucosinolates and myrosinases defend Arabidopsis against *Tetranychus urticae* herbivory. *Plant Physiology* **187**: 116–132.
Woźniak A, Formela M, Bilman P, Grześkiewicz K, Bednarski W, Marczak Ł, Narożna D, Dancewicz K, Mai VC, Borowiak-Sobkowiak B, *et al.* 2017. The dynamics of the defense strategy of pea induced by exogenous nitric oxide in response to aphid infestation. *International Journal of Molecular Sciences* **18**: 329.
Wu F, Chi Y, Jiang Z, Xu Y, Xie L, Huang F, Wan D, Ni J, Yuan F, Wu X, *et al.* 2020.

Hydrogen peroxide sensor HPCA1 is an LRR receptor kinase in Arabidopsis. *Nature* **578**: 577–581.

Wu J, Baldwin IT. **2009**. Herbivory-induced signalling in plants: Perception and action. *Plant, Cell and Environment* **32**: 1161–1174.

Wu Y, Zhang D, Chu JY, Boyle P, Wang Y, Brindle ID, De Luca V, Després C. **2012**. The Arabidopsis NPR1 protein is a receptor for the plant defense hormone salicylic acid. *Cell Reports* **1**: 639–647.

Wu Z, Huang S, Zhang X, Wu D, Xia S, Li X. **2017**. Regulation of plant immune receptor accumulation through translational repression by a glycine-tyrosine-phenylalanine (GYF) domain protein. *eLife* **6:** 23684.

Wünsche H, Baldwin IT, Wu J. **2011a**. S-Nitrosoglutathione reductase (GSNOR) mediates the biosynthesis of jasmonic acid and ethylene induced by feeding of the insect herbivore *Manduca sexta* and is important for jasmonate-elicited responses in *Nicotiana attenuata*. *Journal of Experimental Botany* **62**: 4605–4616.

Wünsche H, Baldwin IT, Wu J. **2011b**. Silencing NOA1 elevates herbivory-induced jasmonic acid accumulation and compromises most of the carbon-based defense metabolites in *Nicotiana attenuata*. *Journal of Integrative Plant Biology* **53**: 619–631.

Xu S, Liao C-J, Jaiswal N, Lee S, Yun D-J, Lee SY, Garvey M, Kaplan I, Mengiste T. **2018**. Tomato PEPR1 ORTHOLOG RECEPTOR-LIKE KINASE1 regulates responses to systemin, necrotrophic fungi, and insect herbivory. *The Plant Cell* **30**: 2214–2229.

Xu Y, Qu C, Sun X, Jia Z, Xue M, Zhao H, Zhou X. **2020**. Nitric oxide boosts *Bemisia tabaci* performance through the suppression of jasmonic acid signaling pathway in Tobacco plants. *Frontiers in Physiology* **11:** 00847.

Xue N, Zhan C, Song J, Li Y, Zhang J, Qi J. **2022**. The glutamate receptor-like 3.3 and 3.6 mediate systemic resistance to insect herbivores in Arabidopsis. *Journal of Experimental Botany* **73**: 7611–7627.

Yamaguchi H, Tanaka H, Hasegawa M, Tokuda M, Asami T, Suzuki Y. **2012**. Phytohormones and willow gall induction by a gall-inducing sawfly. *New Phytologist* **196**: 586–595.

Yamaguchi Y, Huffaker A, Bryan AC, Tax FE, Ryan CA. **2010**. PEPR2 is a second receptor for the Pep1 and Pep2 peptides and contributes to defense responses in Arabidopsis. *The Plant Cell* **22**: 508–522.

Yamasaki H, Sakihama Y. 2000. Simultaneous production of nitric oxide and peroxynitrite by plant nitrate reductase: in vitro evidence for the NR-dependent formation of active nitrogen species. *FEBS Letters* **468:** 89–92.

Yan J, Qiu R, Wang K, Liu Y, Zhang W. **2023**. Enhancing alfalfa resistance to Spodoptera herbivory by sequestering microRNA396 expression. *Plant Cell Reports* **42**: 805–819.

Yang J, Duan G, Li C, Liu L, Han G, Zhang Y, Wang C. **2019**. The crosstalks between jasmonic acid and other plant hormone signaling highlight the involvement of jasmonic

acid as a core component in plant response to biotic and abiotic stresses. *Frontiers in Plant Science* **10**: 1–12.

Yang X, Zhang L, Yang Y, Schmid M, Wang Y. **2021**. miRNA mediated regulation and onteraction between plants and pathogens. *International Journal of Molecular Sciences* **22:** 2913 .

Ye M, Kuai P, Hu L, Ye M, Sun H, Erb M, Lou Y. **2020**. Suppression of a leucine-rich repeat receptor-like kinase enhances host plant resistance to a specialist herbivore. *Plant Cell and Environment* **43**: 2571–2585.

Younas M, Naeem M, Raquib A, Masud S. **2004**. Population dyanimcs of *Pieris brassicae* on five cultivar of cauliflower at Peshawar. *Asian Journal of Plant Science* **3**: 391–393.

Young D, Pedre B, Ezeriņa D, De Smet B, Lewandowska A, Tossounian M-A, Bodra N, Huang J, Astolfi Rosado L, Van Breusegem F, *et al.* 2018. Protein promiscuity in H_2O_2 signalling. *Antioxidants & Redox Signaling* **30**: 1285–1324.

Yu X, Zhang W, Zhang Y, Zhang X, Lang D, Zhang X. **2019**. The roles of methyl jasmonate to stress in plants. *Functional Plant Biology* **46**: 197–212.

Yu Y, Jia, Chen X. **2017**. The 'how' and 'where' of plant microRNAs HHS Public Access. *New Phytologist* **216**: 1002–1017.

Yuan M, Jiang Z, Bi G, Nomura K, Liu M, Wang Y, Cai B, Zhou JM, He SY, Xin XF. **2021**. Pattern-recognition receptors are required for NLR-mediated plant immunity. *Nature* **592**: 105–109.

Yun BW, Skelly MJ, Yin M, Yu M, Mun BG, Lee SU, Hussain A, Spoel SH, Loake GJ. **2016**. Nitric oxide and S-nitrosoglutathione function additively during plant immunity. *New phytologist* **211**: 516–526.

Zamora O, Schulze S, Azoulay-Shemer T, Parik H, Unt J, Brosché M, Schroeder JI, Yarmolinsky D, Kollist H. **2021**. Jasmonic acid and salicylic acid play minor roles in stomatal regulation by CO_2, abscisic acid, darkness, vapor pressure deficit and ozone. *The Plant Journal* **108**: 134–150.

Zarate SI, Kempema LA, Walling LL. **2007**. Silverleaf whitefly induces salicylic acid defenses and suppresses effectual jasmonic acid defenses. *Plant Physiology* **143**: 866–875.

Zeidler D, Zähringer U, Gerber I, Dubery I, Hartung T, Bors W, Hutzler P, Durner J. **2004**. Innate immunity in Arabidopsis thaliana: Lipopolysaccharides activate nitric oxide synthase (NOS) and induce defense genes. *Proceedings of the National Academy of Sciences of the United States of America* **101**: 15811–15816.

Zhai J, Jeong DH, de Paoli E, Park S, Rosen BD, Li Y, González AJ, Yan Z, Kitto SL, Grusak MA, *et al.* 2011. MicroRNAs as master regulators of the plant NB-LRR defense gene family via the production of phased, trans-acting siRNAs. *Genes and Development* **25**: 2540–2553.

Zhang B, Liu M, Wang Y, Yuan W, Zhang H. 2022. Plant NLRs: Evolving with pathogen effectors and engineerable to improve resistance. *Frontiers in Microbiology* **13:** 1018504.

Zhang B, Zhang H, Li F, Ouyang Y, Yuan M, Li X, Xiao J, Wang S. **2020**. Multiple alleles encoding atypical NLRs with unique central tandem repeats in rice confer resistance to *Xanthomonas oryzae* pv. oryzae. *Plant Communications* **1**: 100088.

Zhang Y, Li X. **2019**. Salicylic acid: biosynthesis, perception, and contributions to plant immunity. *Current Opinion in Plant Biology* **50**: 29–36.

Zhou J, Zhang N, Wang P, Zhang S, Li D, Liu K, Wang G, Wang X, Ai H. **2015**. Identification of host-plant volatiles and characterization of two novel general odorant-binding proteins from the legume pod borer, *Maruca vitrata fabricius* (lepidoptera: Crambidae). *PLoS ONE* **10**: 1–17.

Zhou X, Joshi S, Patil S, Khare T, Kumar V. **2022**. Reactive oxygen, nitrogen, carbonyl and sulfur species and their roles in plant abiotic stress responses and tolerance. *Journal of Plant Growth Regulation* **41**: 119–142.

Zhurov V, Navarro M, Bruinsma KA, Arbona V, Santamaria ME, Cazaux M, Wybouw N, Osborne EJ, Ens C, Rioja C, *et al.* 2014. Reciprocal responses in the interaction between Arabidopsis and the cell-content-feeding chelicerate herbivore spider mite. *Plant Physiology* **164**: 384–399.

Zúñiga GE, Corcuera LJ. **1986**. Effect of gramine in the resistance of barley seedlings to the aphid *Rhopalosiphum padi*. *Entomologia Experimentalis et Applicata* **40**: 259–262.

PUBLICATIONS

LIST OF PHD PUBLICATIONS

Rosa-Diaz I, Arnaiz A, Romero-Puertas MC, Sandalio LM, Diaz I. 2021. Nitric oxide, an essential intermediate in the plant–herbivore interaction. Frontiers in Plant Science 11. 620086

Rosa-Diaz I, Santamaria ME, Acien JM, Diaz I. 2023. Jasmonic acid catabolism in Arabidopsis defence against mites. Plant Science 334: 111784.

OTHER PUBLICATIONS

Santamaria ME, Arnaiz A, **Rosa-Diaz I**, González-Melendi P, Romero-Hernandez G, Ojeda-Martinez DA, Garcia A, Contreras E, Martinez M, Diaz I. 2020. Plant defences against *Tetranychus urticae*: Mind the gaps. Plants 9: 1–16.

Santamaria ME, Garcia A, Arnaiz A, **Rosa-Diaz I**, Romero-Hernandez G, Diaz I, Martinez M. 2021. Comparative transcriptomics reveals hidden issues in the plant response to arthropod herbivores. Journal of Integrative Plant Biology 63: 312–326.

Arnaiz A, Santamaria ME, **Rosa-Diaz I**, Garcia I, Dixit S, Vallejos S, Gotor C, Martinez M, Grbic V, Diaz I. 2022. Hydroxynitrile lyase defends Arabidopsis *against Tetranychus urticae*. Plant Physiology 189: 2244–2258.

Arnaiz A, Romero-Puertas MC, Santamaria ME, **Rosa-Diaz I**, Arbona V, Muñoz A, Grbic V, González-Melendi P, Castellano M.M, Sandalio LM, Martinez M, Diaz I. 2023 The Arabidopsis thioredoxin TRXh5 regulates the S-nitrosylation pattern of the TIRK receptor being both proteins essential in the modulation of defences to *Tetranychus urticae.* Redox Biology 67:102902.